

**The use of GIS and Remote Sensing to
Identify and Prioritise Anomalies for Gold
from a Regional Exploration Dataset
located within the Weathered Lateritic
Environment of Mali, West Africa.**

Thesis submitted for the degree of
Doctor of Philosophy
at the University of Leicester.

Alison Stewart (M.Sc. Leicester)
Department of Geography
University of Leicester.

April 2000.

UMI Number: U133420

All rights reserved

INFORMATION TO ALL USERS

The quality of this reproduction is dependent upon the quality of the copy submitted.

In the unlikely event that the author did not send a complete manuscript and there are missing pages, these will be noted. Also, if material had to be removed, a note will indicate the deletion.



UMI U133420

Published by ProQuest LLC 2013. Copyright in the Dissertation held by the Author.
Microform Edition © ProQuest LLC.

All rights reserved. This work is protected against
unauthorized copying under Title 17, United States Code.



ProQuest LLC
789 East Eisenhower Parkway
P.O. Box 1346
Ann Arbor, MI 48106-1346

The use of GIS and remote-sensing to identify and prioritise
anomalies for gold from a regional exploration dataset
located within the weathered lateritic environment
of Mali, West Africa.

Alison Stewart.

University of Leicester
Department of Geography.

ABSTRACT.

The work in this research has used a wide variety of spatial data taken from a regional mineral exploration program. The region of study lies in an area of known artisan gold mining, encompassing the Birimian volcano-sedimentary lithologies, in which the Syama mine is currently operating.

These various data sources of cartographic, airborne, satellite and surface sampling have all been presented in an unprocessed 'raw' state with a complex range of scales, area extents and formats. One of the initial aims of the research has been to construct a fully integrated spatially georeferenced database for their use within a GIS. A second aim has been to find the most suitable analysis for assisting in the identification of data anomalies, pertaining to possible gold mineralisation. The individual analysis of these datasets have in their own right produced interesting 'stand-alone' results. A Third aim has been to combine the individual results, along with knowledge gained from the study of landscape geochemistry as an additional layer, in an effort to prioritise potential gold areas, on the basis of collective anomalies, thereby reducing the risk decision. Through taking advantage of the spatial processing powers of GIS two contrasting methods are investigated with regard to data aggregation and anomaly prioritisation. The first examines the 'weights-of-evidence' approach, which operates through assessing the spatial association of 'known' gold occurrences to individual associate layers, and the second uses an 'expert-system' approach to assess the combined importance of the individual GIS layers to the identification and prioritisation of anomalies.

The value of each approach in this environment is discussed and compared, with final conclusions drawn from the entire study.

ACKNOWLEDGEMENTS.

The author would like to take this opportunity to thank both the geography and geology departments at Leicester University. Large gratitude goes out to my supervisors Professor Peter Fisher (geography) and Dr. Charlie Moon (geology), for their time and support of this research. Also BHP, the staff, are thanked, in particular Dr. D. Pohl and Dr. G Lipton, for the use of their data and the funded field trip, which was a wonderful memorable experience.

Within the department of geography Mr. Bill Hickin, our computer manager is whole heartily thanked. He has been quite fantastic at sorting out 'unexplained' computer software glitches, and a magician when it came to finding extra disc storage space.

My parents (Brenda and John) and Mitch deserve a round of applause for their unfaltering support and love, they have been truly wonderful even through the difficult times. Thank you just doesn't seem enough!

Finally a thank you to all family, friends and those within the geography department who have given encouragement and friendship and made my time at Leicester enjoyable, and my brother-in-law Jonathan for time spent on translating papers.

CONTENTS

Page No.

CHAPTER 1 INTRODUCTION.

1.1 Statement of the problem.	2
1.2 Aims and objectives.	2
1.3 Thesis structure.	3
1.4 The Malian environment and population.	5
1.4.1 Geographical overview.	5
1.4.2 Socio-economic overview.	7
1.4.3 The history of gold exploration.	9
1.5 Choice and description of the study area.	18
1.5.1 Climate and physiography.	18
1.5.2 Relief.	19
1.5.3 Urbanisation.	21

CHAPTER 2 THE GEOLOGICAL ENVIRONMENT.

2.1 Introduction.	26
2.2 The Precambrian of West Africa - A synthesis.	27
2.2.1 West African tectonics.	28
2.3 Stratigraphy of the research area.	31
2.4 Regional faulting.	37
2.5 Known mineralisation and deposits.	39
2.6 The Birimian volcano-sedimentary sequence and associated gold mineralisation.	39
2.6.1 Overview.	41
2.6.2 Host lithologies.	42
2.6.2.1 Basalt.	42
2.6.2.2 Greywacke-argillite.	44
2.6.2.3 Andesitic intrusions.	45

2.6.3 Alteration.	45
2.6.4 Silicification.	49
2.6.5 Primary gold and sulphide mineralogy.	49
2.6.6 Volcano-sedimentary structure.	52
2.7 Regional similarities - a summary.	54

CHAPTER 3 THE WEATHERED ENVIRONMENT.

3.1 Introduction.	56
3.2 Theories of laterite genesis.	57
3.3 A typical laterite profile.	61
3.4 The effects of past and present climate on laterite formation.	66
3.5 Topography and its effects on laterite formation.	68
3.6 Profile variations with regard to lithology.	70
3.6.1 Weathering processes.	71
3.6.1.1 Hydration.	71
3.6.1.2 Hydrolysis.	71
3.6.1.3 Oxidation.	72
3.6.1.4 Simple solution.	73
3.6.1.5 Transformation.	73
3.6.2 Mineral resistance.	73
3.6.3 Mineral decomposition: the resultant profile.	74
3.6.4 Element distribution within the profile.	78
3.6.5 Gold distribution within the laterite profile.	83
3.7 Laterite within the research area.	96
3.7.1 Description of the lateritic profile and its geochemistry.	96
3.7.2 Element mobility within the profile.	104
3.7.3 The distribution and mobility of gold within the profile.	112
3.8 Regolith geochemical dispersion models.	118
3.8.1 The savannah geochemical dispersion model.	121
3.9 Summary-The established problem.	130

CHAPTER 4 DATA ACQUISITION AND PRELIMINARY PROCESSING.

4.1 Introduction.	135
4.2 Data acquisition.	136
4.3 Computer and software specification.	136
4.4 Field data.	136
4.4.1 Fieldwork aims, objectives and logistics.	138
4.5 Data processing.	138
4.5.1 Remote sensed data.	139
4.5.1.1 Correcting line dropouts.	140
4.5.1.2 Atmospheric correction.	140
4.5.1.3 Atmospheric methodology.	141
4.5.1.4 Geometric rectification.	142
4.5.1.5 Image mosaicking.	146
4.5.1.6 ERS-1 data.	146
4.5.1.7 Speckle suppression methodology.	147
4.5.2 Geochemical data.	151
4.5.2.1 Data quality and verification.	152
4.5.2.2 Data solutions.	153
4.5.2.3 Geometric rectification.	153
4.5.2.4 Data interpolation.	155
4.5.2.5 Grid mosaicking.	156
4.5.3 Radiometric data.	156
4.5.3.1 Data processing and error corrections.	157
4.5.4 Magnetic data.	158
4.5.4.1 Data processing.	158
4.5.5 Digitising of published cartographic data.	158
4.5.5.1 Geological data input.	158
4.5.5.2 Published mineral localities.	159
4.5.5.3 Topographic data.	160
4.5.5.4 Lateritic escarpment data.	160
4.5.5.5 Hydrological data.	161
4.5.5.6 Attribute linkages.	161
4.5.6 The digitising of unpublished cartographic data.	161

4.5.7 Coverage rectification and warping.	162
4.5.8 Cartographic data quality assessment.	163
4.6 Geochemical statistical analysis.	165
4.6.1 Global geochemical data.	165
4.6.2 Statistics related to lithology: a GIS approach.	174
4.6.3 Data thresholding and anomaly recognition.	180
4.7 Global radiometric statistical analysis.	189
4.8 Summary.	195

CHAPTER 5 THE GIS DATABASE AND PROCESS DERIVED COVERAGES.

5.1 Introduction.	199
5.2 Terrain models.	200
5.2.1 Triangular irregular network surface (TIN).	200
5.2.2 TIN construction.	201
5.2.3 Quality assessment.	201
5.3 TIN derivations.	202
5.4 Vegetation mapping using remotely sensed data.	202
5.4.1 Methodology.	203
5.4.2 Results.	205
5.4.3 Problems of classification accuracy.	207
5.5 Mineral prospecting using remotely sensed TM data.	207
5.5.1 Aims and objectives for TM analysis.	208
5.5.2 Iron oxide and hydroxyl-bearing mapping.	209
5.5.3 Principal component analysis (PCA).	219
5.5.4 Combining and mapping coincidences.	226
5.5.5 Lineament mapping.	230
5.6 The use of airborne radiometric data to aid Lithology and alteration mapping.	232
5.6.1 Selecting the appropriate methodology.	233
5.6.2 The application of feature space mapping.	247
5.7 The use of airborne magnetic data.	260
5.7.1 Airborne magnetic interpretation.	261
5.8 Summary.	269

CHAPTER 6 GIS INTEGRATION AND MODELING.

6.1 Introduction.	271
6.2 GIS approaches in mineral exploration.	272
6.3 Weight-of-evidence: The methodology.	273
6.3.1 Implementation and results of the weight-of-evidence approach.	275
6.3.2 Weights of evidence: discussion of results.	286
6.4 The expert-system approach: the methodology.	291
6.4.1 Implementation of the expert-system approach.	293
6.4.2 The expert-system: discussion of results.	303

CHAPTER 7 CONCLUSIONS, ISSUES AND FUTURE WORK.

7.1 Research conclusions.	310
7.2 Final address of issues.	311
7.2.1 Source quality control.	312
7.2.2 Database improvements.	312
7.3 Future work.	314

REFERENCES.

APPENDIX.

LIST OF FIGURES.

Page No.

CHAPTER 1.

Figure 1	Introduction map of West Africa and the research area.	6
Figure 2	Sketch map illustrating the spatial location of current gold interests in Mali.	13
Figure 3	Topographic plan.	22

CHAPTER 2.

Figure 3a	Distribution of Birimian supracrustal belts in West Africa and Africa.	30
Figure 3b	Development of ensialic and ensimatic basins formed by rifting.	30
Figure 3c	Diagrammatic illustration of arc sites.	30
Figure 4	Research area geology.	32
Figure 5	Mineral workings and local structural interpretation.	40
Figure 6	Cross-section through the Birimian volcano-sedimentary unit at Syama.	43
Figure 7a	Chemical analysis of mafic igneous host rocks at Syama.	48
Figure 7b	Chemical analysis of mafic igneous host rocks at Syama.	48
Figure 8a	Gold concentration in the Syama mafic host rocks.	50
Figure 8b	Copper, Nickel, Zinc, Chrome and Lead concentrations in the Syama mafic host rocks.	50

CHAPTER 3.

Figure 9	Sketch of a typical lateritic iron crust profile.	63
Figure 10	Profile variation caused by lateritic weathering.	77
Figure 10a	Solubility of cations by hydrolysis as a function of pH	79

Figure 10b	Solubility of various anions by hydrolysis as a function of pH.	79
Figure 10c	Solubility of various oxides by hydrolysis as a function of pH.	79
Figure 11	Adsorption isotherms of divalent cations and anions onto goethite as a function of pH.	83
Figure 12	Gold distribution within the profile.	91
Figure 13	Gold distribution within the profile.	92
Figure 14	Typical southern Mali lateritic profiles.	98
Figure 15	Geochemical distribution within the unmineralised profile of Syama.	101
Figure 16	Geochemical distribution within the mineralised profile of Syama.	101
Figure 17	Geochemical distribution within the mineralised Pitangoma profile (pit 128).	102
Figure 18	Geochemical distribution within the mineralised Pitangoma profile (pit 128).	102
Figure 19	Geochemical distribution within the unmineralised profile of Syama.	103
Figure 20	Geochemical distribution within the mineralised profile of Syama.	103
Figure 21	Element distribution in the unmineralised profile of Syama.	106
Figure 22	Element distribution in the mineralised profile of Syama.	106
Figure 23	Element distribution in the mineralised Pitangoma profile (pit 128).	110
Figure 24	Element distribution in the mineralised Pitangoma profile (pit 130).	110
Figure 25	Element distribution in the mineralised Pitangoma profile (pit 130).	110
Figure 26	Gold (Au) distribution in the mineralised Syama profile.	113
Figure 27	Gold (Au) distribution in the mineralised Pitangoma profile (pit 128).	113

Figure 28	Gold (Au) distribution in the mineralised Pitiangoma profile (pit 130).	113
Figure 29	A generalised landscape cross-section illustrating the codes relative to truncation level.	123
Figure 30	The geochemical landscape of the Goren Cu-Mo prospect.	125
Figure 31	Idealised models of dispersion in preserved or truncated lateritic profiles.	129

CHAPTER 4.

Figure 32	Sketch map of aerial extent for remote-sensed imagery.	145
Figure 33	ERS1-SAR image.	148
Figure 34	ERS1-SAR image histogram.	147
Figure 35	Speckle suppression flow-diagram.	150
Figure 36	Sketch map of geochemical sample regions.	151
Figure 37	Box-plot diagram for all elements.	166
Figure 38	Box-plot diagram for all logged elements.	168
Figure 39	Dendrogram for R-Mode cluster analysis.	173
Figure 40	Geochemical thresholds.	183
Figure 41	Geochemical thresholds.	184
Figure 42	Geochemical thresholds.	185
Figure 43	Geochemical thresholds.	186
Figure 44	Geochemical composite Au-Cu-Zn (R,G,B).	188
Figure 45	Thorium histogram plot.	190
Figure 46	Uranium histogram plot.	190
Figure 47	Potassium histogram plot.	190
Figure 48	Total count histogram plot.	190
Figure 49	Airborne radiometric data – Thorium.	191
Figure 50	Airborne radiometric data – Uranium.	192
Figure 51	Airborne radiometric data – Potassium.	193
Figure 52	Airborne radiometric data – Total count.	194

CHAPTER 5.

Figure 53	TM spectral profiles for selected landsurface features.	204
Figure 54	NDVI classification of TM image.	206
Figure 55	Diagnostic spectra of iron, clay, carbonate and chlorophyll adsorption.	210
Figure 56	The use of decorrelation stretch with TM data.	212
Figure 57	TM ratio image 3/1 4/3 5/7 (R, G, B).	215
Figure 58	Vegetation contribution estimates.	217
Figure 59	Elvidge and Lyon 'clay' image.	218
Figure 60	Fraser's DPCA 'iron' image.	221
Figure 61	Fraser's DPCA 'clay' image.	222
Figure 62	Costa 'F' image (iron).	224
Figure 63	Costa 'H' image (clay).	225
Figure 64	Combined 'iron' images.	228
Figure 65	Combined 'clay' images.	229
Figure 66	Levels of significance from combined contributions of iron and clay.	231
Figure 67	Ternary radiometric image (K, U, Th).	235
Figure 68	Statistical spatial plot (K/Th) for sub-sampled lithologies of Table 49.	237
Figure 69	Statistical spatial plot (U/Th) for sub-sampled lithologies of Table 49.	238
Figure 70	Statistical spatial plot (K/U) for sub-sampled lithologies of Table 49.	239
Figure 71	Ratio Thorium / Uranium (Th/U).	242
Figure 72	Ratio Potassium / Uranium (K/U).	242
Figure 73	Ratio Thorium / Potassium (Th/K).	243
Figure 74	Classification of ratio Th/K.	243
Figure 75	Radiometric unsupervised classification (Th, U, K).	245
Figure 76	Th and K feature space image showing supervised classes (AOI).	249

Figure 77	Th and U feature space image showing supervised classes (AOI).	249
Figure 78	U and K feature space image showing supervised classes (AOI).	249
Figure 79	Radiometric supervised classification (Th vs K).	250
Figure 80	Radiometric supervised classification (Th vs U).	251
Figure 81	Radiometric supervised classification (U vs K).	252
Figure 82	Unsupervised Vs supervised class delimitations.	254
Figure 83	Combining feature space classes (Th vs K & U vs K) to identify basic-type signatures and alteration.	256
Figure 84	Combining feature space classes (Th vs K & U vs K) to prioritise levels of potential alteration within basic-type signatures.	257
Figure 85	Spatial comparison of potassic alteration within the Birimian volcano-sedimentary zone.	259
Figure 86	Magnetic image (data stretch).	262
Figure 87	Edge enhancement of magnetic data.	264
Figure 88	Classification of magnetic gradient intensities.	266
Figure 89	Structural directional filtering (NW-SE).	268
Figure 90	Structural directional filtering (NE-SW).	268

CHAPTER 6.

Figure 91	Stage 1. Process of selecting and masking coverage criteria to study area.	276
Figure 92	Stage 2. Process for computing the weights.	277
Figure 93	Stage 3. Calculation of the a posteriori, weights combined.	278
Figure 94	Weight result illustrations.	287
Figure 95	Continuous rating scale for use in the pairwise comparison matrix.	292
Figure 96	Sigmoidal membership function as applied to distance from faults.	298
Figure 97	Criteria scores as applied to landscape	299

Figure 98	Criteria scores as applied to faults.	299
Figure 99	MCE Results. The 'expert-system' approach.	304
Figure 100	MCE Results. The 'expert-system' approach.	305

LIST OF TABLES.

Page No.

CHAPTER 1.

Table 1a	Mines.	12
Table 1b	Prospects.	14
Table 1c	Interests.	17

CHAPTER 2.

Table 2	Alteration zoning in the basaltic host rocks.	46
---------	---	----

CHAPTER 3.

Table 3	Chemical effects of deep weathering – summary.	66
Table 4	Hydrolysis reactions and their characteristics.	72
Table 5	The relative stability of common rock forming silicates to chemical weathering (under humid temperate climates).	74
Table 6	Clay group minerals.	75
Table 7	Major common minerals and their chemical compositions.	76
Table 8	Examples of point zero charge (pzc) for minerals and soils.	81
Table 9	Clay exchange capacity.	82
Table 10	The relative affinity for adsorption of some cations.	83
Table 11	The chemical species of gold mobilisation.	86
Table 12a	% mean chemical composition (mineralised locations).	99
Table 12b	% mean chemical composition (unmineralised locations).	99
Table 13	Geochemistry of the unmineralised profile – Syama.	100
Table 14	Geochemistry of the mineralised profile – Syama.	100
Table 15	Geochemistry of the mineralised profile – Pitangoma (Pit 128).	100

Table 16	Elements of the unmineralised profile – Syama.	105
Table 17	Elements of the mineralised profile – Syama.	105
Table 18	Elements of the mineralised profile (ppm) – Pitiangoma (Pit 128).	105
Table 19	Elements of the mineralised profile (ppm) – Pitiangoma (Pit 130).	105
Table 20	Classification of geochemical dispersion models (tropically weathered).	121

CHAPTER 4.

Table 21	Data specifications.	137
Table 22	Imagery specifications.	139
Table 23	TM atmospheric correction.	142
Table 24	SPOT atmospheric correction.	142
Table 25	Image RMS errors.	144
Table 26	Geochemical RMS errors.	154
Table 27	Elements statistical characteristics.	166
Table 28	Elements statistical characteristics log-normal transformed.	168
Table 29	Mean and standard deviation comparisons – outliers removed.	169
Table 30	Element correlations.	170
Table 31	Lithology based statistical information for Gold.	176
Table 32	Lithology based statistical information for Copper.	176
Table 33	Lithology based statistical information for Zinc.	177
Table 34	Lithology based statistical information for Lead.	177
Table 35	Lithology based statistical information for Nickel.	178
Table 36	Lithology based statistical information for Molybdenum.	178
Table 37	Lithology based statistical information for Lithium.	179
Table 38	Lithology based statistical information for Chromium.	179
Table 39	Radiometric statistical characteristics.	189
Table 40	Correlation results.	195

Table 41	Data summary as derived from Chapter 4.	197
----------	---	-----

CHAPTER 5.

Table 42	Percentage class contribution in TM image.	207
Table 43	TM band correlation analysis.	210
Table 44	Colour resultant ratio contribution.	214
Table 45	Directed Principal Component Analysis, three ratio input.	220
Table 46	Directed Principal Component Analysis (Fraser).	220
Table 47	Iron-oxide mapping 'F- image'.	223
Table 48	Hydroxyl mapping 'H - image'.	223
Table 49	Subsampled lithologies and their radiometric character.	240
Table 50	Summary of available data layers from Chapter 5.	269

CHAPTER 6.

Table 51	Au deposits from geology map (1:200,000) only.	279
Table 52	Au deposits taken from geology map and BHP map.	280
Table 53	'Bj' weight calculation accounting for extended spatial extent.	281
Table 54	Weights for high structural magnetic activity.	282
Table 55	Fault buffering from different source data and combinations.	283
Table 56	Weights according to spatial location within the landscape.	285
Table 57	Assessing the comparative importance of input factors through the pairwise comparison matrix.	300

LIST OF PLATES.

Page No.

CHAPTER 1.

Plate 1	Vegetation.	20
Plate 2	The Syama to Dioumantene main road.	20
Plate 3	Crossing the Bafini river in a dugout canoe.	20
Plate 4	Termite hills.	24
Plate 5	A village.	24
Plate 6	Narrow footpaths linking village to village.	24

CHAPTER 1

INTRODUCTION.

Contents.

- 1.1 Statement of the problem.**
- 1.2 Aims and objectives.**
- 1.3 Thesis structure.**
- 1.4 The Malian environment and population.**
 - 1.4.1 Geographical overview.**
 - 1.4.2 Socio-economic overview.**
 - 1.4.3 The history of gold exploration.**
- 1.5 Choice and description of the study area.**
 - 1.5.1 Climate and physiography.**
 - 1.5.2 Relief.**
 - 1.5.3 Urbanisation.**

1.1 Statement of the problem.

Very few ore bodies lie exposed on the Earth's surface. Most are concealed beneath vegetation, soil, or a thick cap of weathered material. Consequently, mineral exploration uses various remote and contact methods to obtain signatures of possible mineralisation. However, the interpretation of these signatures is difficult in environments where prolonged weathering produces a thick laterised cover, or where there is dense vegetation. Both these situations are typical in Mali.

In landscape geochemistry there is a premise that factors such as profile truncation level and depositional environment have an intrinsic link with the retention or release of elements. It also suggests that elements may be obscured in the landscape due to the actions of sediment mixing.

This research will attempt to incorporate some of the theory of landscape geochemistry into a GIS database. Whilst combining individual results from each analysis, landscape is to be used as a factor in anomaly prioritisation.

1.2 Aim and Objectives.

The aim of this research is to use a regional reconnaissance exploration dataset to first identify and then prioritise anomalies thought to be representative of gold mineralisation.

This will be achieved using a GIS. both to analyse data and establish the most appropriate technique for combining individual results. The end result will allow anomaly prioritisation of gold.

1.3 Thesis structure.

This thesis is divided into seven chapters.

Chapter (1) has introduced the reader to the principal aims and objectives of the research work, and highlights the exploration problems regularly faced with work in a lateritic environment. The later part of this chapter enables an understanding as to the importance of current and future gold exploration upon helping to improve the socio-economic welfare of Mali. The chapter concludes by introducing the study area.

Chapter (2) begins with a holistic approach to the geology of West Africa. The chapter then describes in detail the geology of the research area, as discussed in current literature. Although the region provides evidence of a long history of small-scale artisanal gold mines, much of the detail discussed (mineralisation, alteration structure etc.) has come from one of the principal active gold mines, that of Syama.

Chapter (3) introduces the environment of lateritic weathering, which forms a blanket across the region. A lateritic profile, as described in the chapter, is composed of geochemically different horizons. These horizons (allied to pH/Eh and water table levels) have a major influence on the movement of elements, and control the distribution of elements reported in the research area. The lateritisation is central to appreciating the principles of the geochemical landscape theory. The landscape model discusses, amongst many things, the importance of differentiating between full and truncated weathered profiles and the nature of the depositional environment.

Chapter (4) describes the type and format of the data supplied for this study. Focus is then placed upon the necessary procedures required to enable the data to be checked for errors and geographically registered within the GIS. Creating a fully integrated GIS database is prone to multiplying errors within the component data layers, awareness is made to the fact that databases are

never error-free. The final part of the chapter analyses the geochemical and radiometric data. A number of techniques are explored in order to understand any inter-element relationships among the geochemical data and to identify threshold levels. Mapping element thresholds helps visualize their spatial location within the landscape and any spatial variability between elements.

Chapter (5) is concerned with deriving information from the landscape. This begins with the creation of a terrain surface which digitally models the research area, including information on slope. Combining these two data sources, the landscape can be coded in accordance with some of the principals discussed in the landscape dispersion model. The second approach uses a variety of remotely sensed data (Landsat TM, radiometric and magnetic data) to identify signals pertaining to mineralisation, structure and lithology.

Chapter (6) considers the data synergistically. The analyses in both Chapters 4 and 5 have produced results from individual datasets that could stand alone as individual pointers to mineralisation. However, exploration centres on lowering the 'risk factor' in decision making. One way of doing this is to combine the results from individual analysis. However two questions need answering: Which method is the most appropriate given the data and the environment? Can these combined results be prioritised into areas most likely to indicate mineralisation?

Chapter (7) is the concluding chapter. It attempts to address some of the problematic issues which have arisen from this research and discusses possible improvements. It also looks at the progression of this research with regard to future work.

1.4 The Malian environment and population.

To many Mali is a country about which they know little except for its location in West Africa. It often comes as a surprise to discover that the familiar place-name "Tombouctou" actually exists within its borders. However, Mali is a country that has suffered discord in its historical occupations and alliances. Even in independence, it is plagued by accusations of corruption and tribal fractionation. Fortunately, recent gold exploration by multinational mining companies could, if sustained and carefully managed, help Mali to achieve its aim of economic independence.

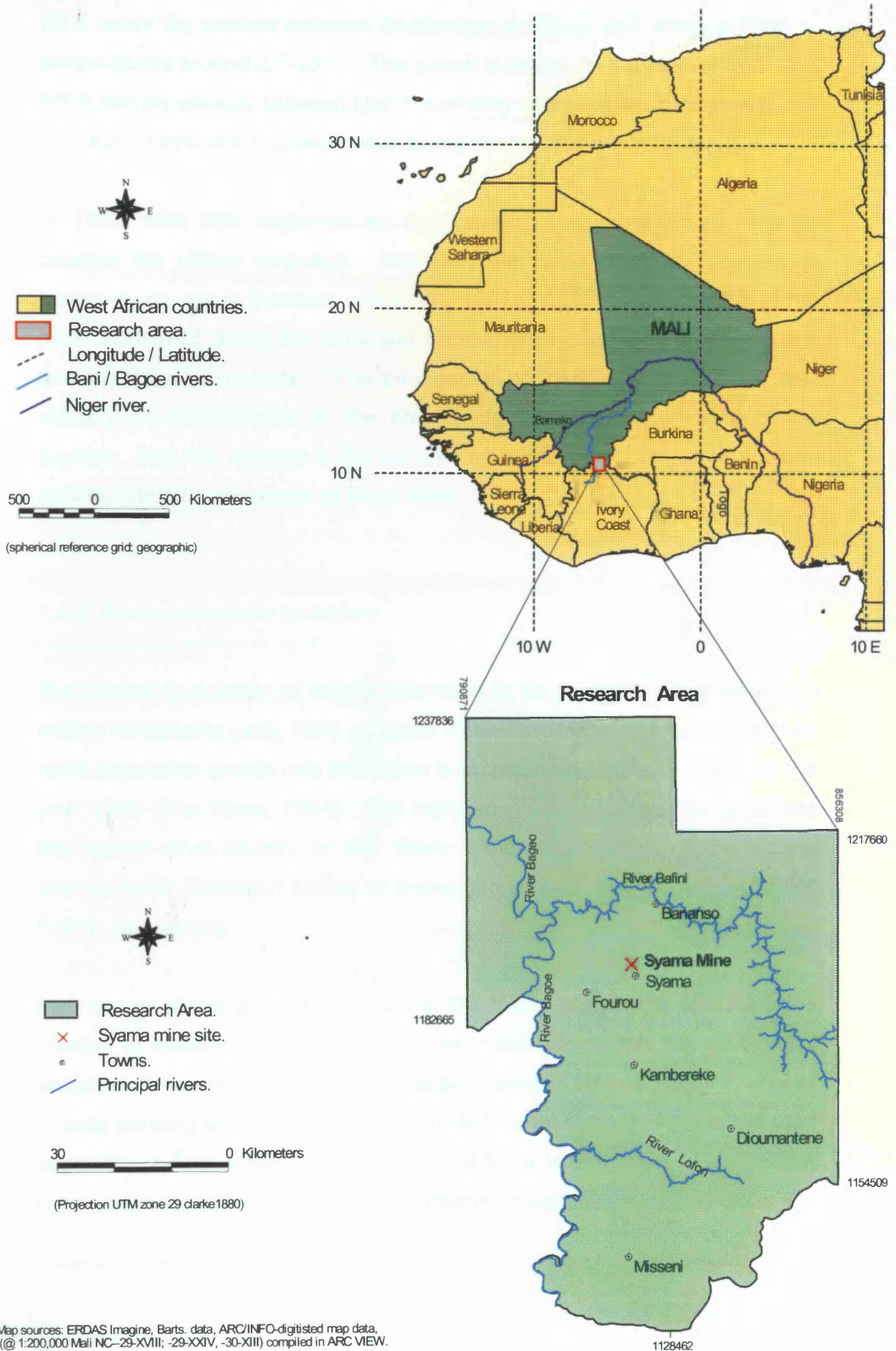
A brief résumé of Mali is now provided to familiarise the reader with the country's physical and socio-economic characteristics. A review is also undertaken of both historic and current gold prospectors and producers.

1.4.1 Geographical overview.

Mali is the largest country in West Africa, with an area in excess of 1.24 million km². It is land-locked and bordered by a total of seven countries (Fig.1). The country has relatively flat to rolling topography, with pockets of more rugged terrain, especially in the north-east. The climate and vegetation of Mali are determined by latitude. In the northern third of the country the presence of the Saharan Desert indicates a very hot and arid climate which ameliorates southward, grading eventually into a savannah landscape, (Anon., 1973). Within the savannah climatic regime there are three distinct seasons:

(i) A humid rainy season between the months of May and September, this period is also characterised by relatively mild temperatures.

Fig. 1 Introduction map of West Africa and the research area.



Map sources: ERDAS Imagine, Barts. data, ARC/INFO-digitised map data, (@ 1:200,000 Mali NC-29-XVII; -29-XXIV, -30-XIII) compiled in ARC VIEW.

- (ii) A warm dry season between September to March with average daytime temperatures around 22°-23° C. This period is known as the Harmattan[^].
- (iii) A hot dry season between March and May when maximum temperatures can reach highs of 40° C, especially during the hottest month of April.

In 1883, Mali was colonised by the French, and consequently, French became the official language. However, the most frequently and widely spoken language is Bambara, (W.W.W., 1997a; W.W.W., 1997b) thought to have developed along the important trans-Saharan trade routes during the ancient kingdom periods. The boundaries of these past kingdoms bear virtually no resemblance to the present day geo-political borders of the country. This has resulted in Bambara being the dominant language not only of Mali but of the remainder of West Africa.

1.4.2 Socio-economic overview.

The current population of Mali is estimated to be something in excess of 9 million inhabitants (July 1996 estimate W.W.W., 1997c). However, with its rapid population growth rate this figure is projected to reach 24 million by the year 2025 (The Times, 1994). The high birth rate and declining death rate are typical of a country in the "Early Expanding" phase of the classic *Demographic Transition Model* of population growth (see Jones, 1990, for further discussion).

Mali is one of the poorest countries in the World and this is reflected in a number of statistics and indices. For example, the current life expectancy stands at 46 years and only 17% of the population is believed to have access to safe drinking water. The literacy rate is thought to lie at 19% of the total population, whilst some 85% of the labour force is employed in agriculture, commonly subsistence farming. The intensity of agricultural activity gives rise

[^] Harmattan: An annual hot, dry dust-laden continental wind originating from the Sahara Desert

to great environmental concerns since the country has serious problems with both soil erosion and desertification. (Timiofeyev, 1989; W.W.W., 1997b; W.W.W., 1997c).

The general lack of infrastructure is another reflection of the country's overall poverty. Despite its size, Mali possesses only 642 km of narrow gauge railway linking it to the port of Dakar in Senegal. It has a total of 15,700 km of highway of which 1,600 km, (principally the road stretching between Bamako, Sikasso and Abidjan in the Ivory Coast) is tarmacked. Many of the other roads which link some of the larger villages and towns, are simple narrow strips of beaten earth which quickly become impassable in the southern region during the wet season. Although there are 33 recognised airport runways, only 17 of these are paved and 20 are less than 914 metres in length (W.W.W., 1997a). Telephone communications in Mali are also poorly developed with an estimated 11,000 connections (W.W.W., 1997c).

Mali has three main export commodities: cotton, livestock and gold. Unfortunately, since Mali's independence the country has been fraught by a series of economic fluctuations, many of which have been induced by prolonged and persistent droughts. These have damaged crops and livestock, driving rural workers into the towns, thus causing a further reduction in agricultural manpower and production. The economic crises have also been exacerbated in part, by political instability and through poor economic management (Hodgkinson, 1994). As a consequence, agriculture operating at the subsistence level often meets demand, but this contrasts, with the export market which regularly fails to meet its projected trade targets. As a nation, the agricultural volumes produced are insufficient to eliminate a negative trade balance between imports and exports (Hodgkinson, 1994; Thomas et al., 1994; W.W.W., 1997e; W.W.W., 1997c). This has resulted in Mali being a recipient of economic aid from many donors such as the United States of America, Western European countries and the Overseas Development Fund (Hodgkinson, 1994; Thomas et al., 1994; W.W.W.,

1997c). Mali is now placed amongst some 22 countries classified by the World Bank as “*debt-distressed*”. At the beginning of 1990 Mali’s official debt to France, \$240 million, was cancelled.

Taking all these factors into account the United Nations Development Program (U.N.D.P) ranks Mali as the fifth poorest country in the World, according to its Human Development Index (H.D.I.), (Thomas et al., 1994).

1.4.3 The History of Gold Exploration.

Mali’s ancient history of gold mining dates as far back as the 9th Century. In this and subsequent centuries, the kingdoms of Ghana and Mali gained wealth and became important regional forces due to the prolific exploitation and trading of their gold resources to buyers in the Middle East and Europe (Anon., 1973; Hodgkinson, 1994; WWW., 1997d). It has also been reported that within this era gold was traded pound-for-pound with salt, such was the value placed upon this scarce commodity!

Over the centuries Mali’s influence as a gold producer declined and continued to dwindle even during the French occupation which began in 1883. The scale of mining activity remained centred on the individual or village participation with artisanal mining and river washing.

The Republic of Mali gained independence from France on 22nd September 1960. Following independence, the Malian government became responsible for the exploration of natural mineral resources and their economic development. In an effort to better exploit its resources the state created a geological survey organisation called the Société Nationale de Recherche et d’Exploitation Minière (SONAREM). This was later to become the Direction National de la Géologie et des Mines (DNGM). These were really just extensions of the French Bureau de Recherches Géologiques et Minières,

(BRGM) an organisation introduced to Mali during the French occupation. The BRGM embarked on a program of geological mapping of the country in 1951, initiated by J.P. Spindler, at a scale of 1:500,000.

Mali's commitment to mapping and understanding its economic resource potential received assistance from the UNDP and also from a period of post-colonial allegiance with the former USSR. In 1964 with the assistance of the Soviet Union, SONAREM undertook an airborne magnetic survey over southern Mali, which was reported to have identified previously unknown basic and ultrabasic rocks (Kusnir et al., 1987). By 1972 Mali had commissioned the BRGM to undertake extensive exploration. This exercise resulted in the discovery of the copper/nickel deposit at Touban (Fig. 5). An opportunity was seized in the late 1970s to produce smaller scale maps, through the integrated use of Landsat imagery, as a result of which the 1:200,000 scale maps were derived. Kusnir et al. (1987) reports that unfortunately the maps made in this way had not been subjected to rigorous control on the ground. Although mapping had been performed by various organisations at various times, aided in part by the synoptic view afforded by Landsat imagery, there were inherent difficulties of traditional geological mapping in a terrain which is largely blanketed by thick lateritic deposits. This soon led to the adoption of large-scale geochemical exploration programs. One such successful program undertaken in the mid 1980s, assisted by UNDP funding, identified the Syama gold anomaly. The location of this in the south-east of Mali is a focus of study in this research. Other successes were at Medinandi, Kodieran, Morila, Kalana and Loulo. Many of these simply pinpointed, or rediscovered, sites of ancient artisanal mining.

In general the centrally planned economic systems employed by most West African countries in the early 1980s, which often went hand-in-hand with political instability, did not prove attractive to overseas private investment by the big mining houses (Bugeco^B, 1994; Anon., 1996a; Chaplin et al., 1997;

^B Bugeco, is an independent geology-mining consulting company.

Whyte, 1997). However, contrary to this general trend BHP-Utah, one of the largest mining houses in the world, decided to take a calculated gamble and risk investment in developing the Syama gold anomaly. After considerable negotiation an exploitation permit was granted to BHP-Utah (now BHP Minerals) at the end of the 1980s, and by 1990 gold was being mined.

The fall of communism and the break-up of the U.S.S.R (circa.1989/1990) prompted a political change within Africa from socialist policies to a more open capitalist-based system (as explained in Chaplin et al., 1997; Whyte, 1997; Gosselin 1997). As a consequence in 1991 Mali went about developing a new and more attractive mining code which it hoped would lead to greater private foreign investment. The scheme evolved into one whereby mines were categorised on the basis of size and then matched to a package of concessions and benefits in order to attract potential investors (Anon., 1995; Anon., 1996b; Chaplin et al., 1997; Duffett cited in Kootnikoff, 1997). This has resulted in a resurgence in gold exploration within its borders, (Chaplin et al., 1997; W.W.W., 1997e; W.W.W., 1997f; Gosselin, 1997) as illustrated in Tables 1a through to 1c.

Mali's 1996 gold production figure, excluding that arising from artisanal mining activity, was reported at ~6 tonnes per annum. This was derived mainly from the Syama mine which lies within the Kadiana (Tingrela) district and accounts for 4 tonnes of the total; the remainder comes from placer production (Anon., 1996c). However May 1997 saw the commencement of production at the Sadiola mine (Kayes district). This latter site, located upon remains of ancient artisanal activity is not only the largest and most important gold find within Mali to date, (International Finance Corporation (IFC), 1996, cited in lamgold 1996 annual report; W.W.W., 1997k) but is also reported to be one of the lowest cost mines in the world (lamgold, 1997; Brown, 1997; Thomas, 1997). Running at full production, it is expected to produce an average of 386,000 oz of gold per annum for the first 6 years of a planned 12 year life.

The discovery of the Sadiola deposit, coupled with the country's long history of artisanal gold mining, has brought an awareness that large scale exploration can be performed with the use of a variety of modern techniques (remote sensing, geophysics). This has undoubtedly increased interest in gold exploration by other mining houses (Chaplin et al., 1997), as shown in Tables 1a to 1c. Interests are typically focused on the Birimian lithologies around the Kéniéba, Kangaba and Kayes districts of West Mali (Fig. 2).

If gold tonnage continues to increase then foreign revenue arising from this export could surpass that generated from cotton and livestock, raising the prospect of reducing Mali's debt-servicing payments and possibly the country's future dependence on aid.

Table 1a: Mines.

Company	Location	Estimated annual production and reserves (1997)	Ownership
Randgold Resources. Formally owned by BHP-Utah, Mali Inc. (Sold October 1996)	Syama (and satellite ore bodies), SE Mali, Kadiana region.	190,000 oz/yr. ^o 2.2 moz reserve (4.35 moz resource) (Production increases planned, 270,000 oz by year 2000)	65% Randgold Resources. 20% Mali State. 15% IFC.
Semos. (Société d'exploration des Mines d'or de Sadiola, SA).	Sadiola Hill, W.Mali (90 km south of Kayes) Area 187 km ² .	386,000 oz/yr. 4.5 moz reserve (3.5 moz resource, giving an 8 moz resource base to date, 1997).	38% Anglo-American Corp. 38% lamgold. ^{HHH} 18% Mali State. 6% IFC. ^{HH}
(closed) Societe de Gestion et d'Exploration des mines d'Or de Kalana. (Sogemork)	Kalana mine 200 km South of Bamako.	Planned full capacity, 1,790 kg/yr. (Au) & 473 kg/yr. (Ag) However, in reality yielded <2.4 Mt.	Owned by the State: Sonarem. (technical assistance was given by USSR).

^o Estimate, production figure varies depending on source.

Fig. 2 Sketch map illustrating the spatial location of current Gold interests in Mali.

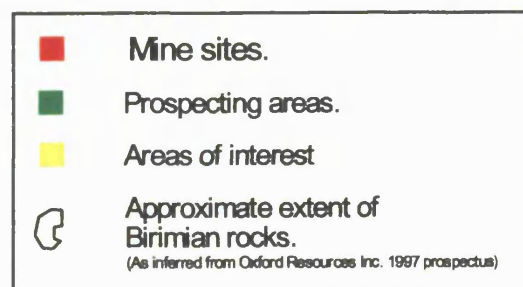
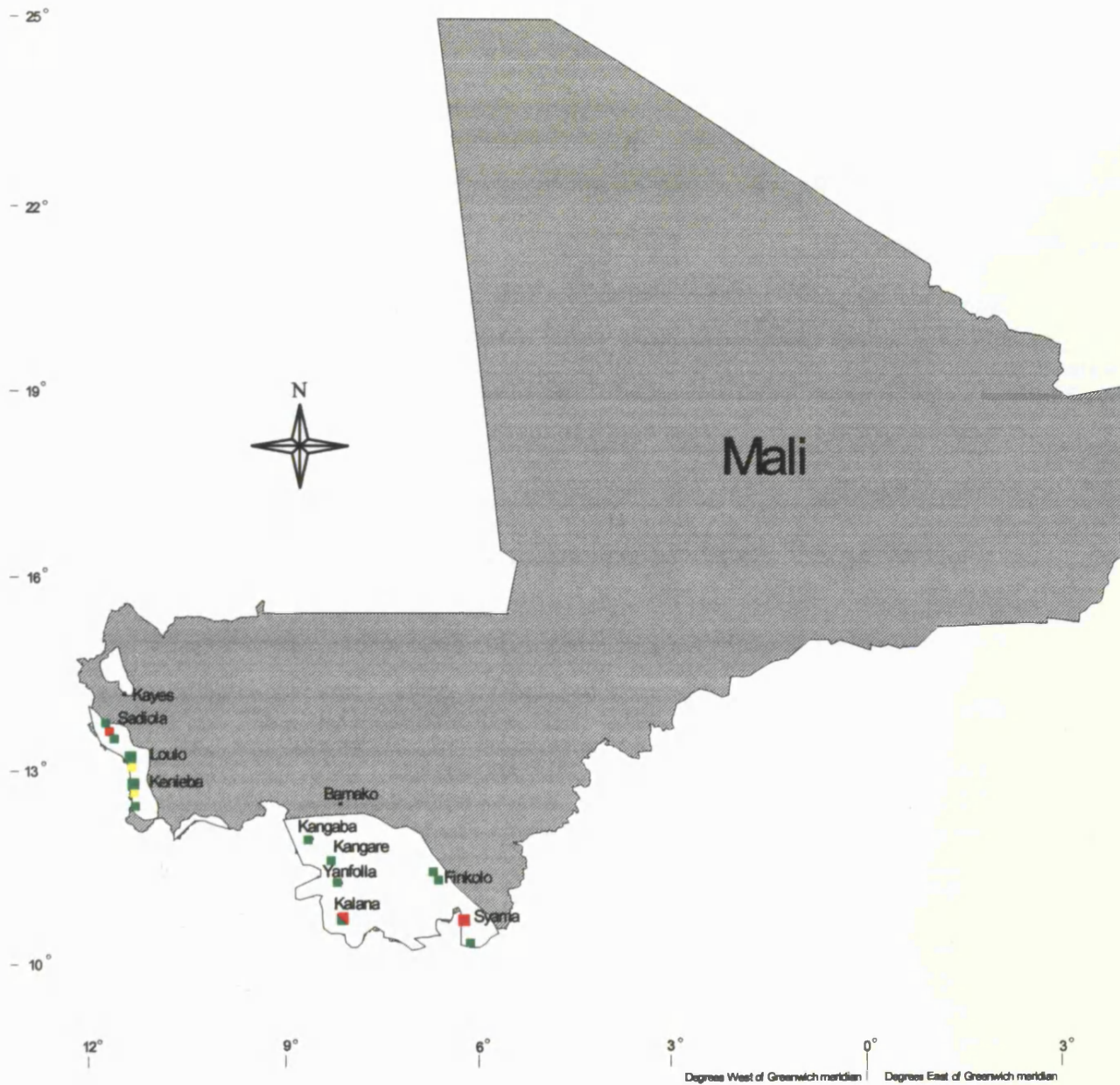


Table 1b: Prospects.

Companies	Permit Area	Ownership / info.
Ashanti Exploration & J.C.I.	Kalana (SW Mali) approx. area 388 km ² . (Aim to redevelop the Kalana mine see table 1a).	50% Ashanti Exploration. 30% J.C.I. 20% Mali state. (mine previously operated by former USSR).
Randgold Resources.	3 sites: Loulo 20 km from Kéniéba, area 300 km ² , plus further 300 km ² granted. Yalea 6 km south of Loulo. Morila approx. 90 km NE of Syama, (SE Mali).	Loulo: 49% Mali government & BRGM, (SOMILO). 51% (?) Randgold Resources. (resource calculations pre-feasibility) Loulo: 1.62 moz. Yalea: ~0.97 moz.
Barrick-gold.	Misseni approx. 50 km south of Syama (SE Mali).	Acquired concession areas immediately south of Syama.
AAC Anglo American Corp.	Kangaré, south of Bamako, (SW. Mali).	Permit acquired via Anmercosa ^{HHHH} , committed to spend \$3million over 3 years.
Sadiola Exploration Ltd. (SADEX).	Exploration surrounding the Sadiola Hill region approx. 398km ² (W. Mali). Alamoutala 13 km NE of Sadiola pit. Farabakouta 600 m north of Sadioloa pit. Dinguilou area 5.4 km ² .	50% Anglo-American. 50% lamgold. (SADEX is the exploration side for SEMOS). (Alamoutala inferred resource 200,000 oz). (Farabakouta inferred resource 173,833 oz). (Dinguilou announcement pending).
International Tournigan.	3 sites: Diangounte, 25 km from Sadiola Hill, (W. Mali). concession area 209 km ² Mogoyafara, 25 km south of Sadiola. Kolomba, 45 km south of Sadiola.	80% International Tournigan. (possible resource ~ 2 moz). International Tournigan joint venture SONAREM (Malian mining organisation).
Youngpoong Mining & Construction Corp. Of South Korea.	Region 250 km SW of Bamako (reserves estimated at 100 tonnes).	(intention to develop mine).
Nevsun Resources Ltd.	2 sites: Tabakoto Kéniéba region (W. Mali), area approx. 16 km ² . Kakadian, 20 km west of Sadiola mine (W. Mali), area approx. 200 km ² .	(Tabakoto inferred resource to date approx. 1.57 moz). (\$2.5 million to be spent in 3 years).

Table 1b continued.

West African Mining Co. (Wamco).	Region of Nénédiána and Sikorota in the Yanfolila area, (SW. Mali). Area approx. 300 km ² .	Represents North American and Malian investors, (\$1.5 million outlay over 3 years).
Pacific Galleon Mining in conjunction with Swiss based associate.	2 sites: Approx. 50 km north of Syama, (SE Mali). Finkolo 288 km ² . Niéna 274 km ² .	Finkolo 90% interest. Niéna option of 75% interest. (resource estimate pending).
Oliver Gold & (CMC) Trillion Resources.	3 sites: Ségala, Kéniéba area, (W. Mali). Two contiguous areas approx. 25 km ² Ségala & Keita, (W. Mali).	50% interest Oliver Gold. 50% interest Consolidated Mining Corp. (CMC), which is 51% held by Trillion Resources (Estimated resource 1 moz).
LEO Shield Exploration NL. (MAME - Mali Australian Mining Exploration SA).	4 sites: Moussala, 20 km SW Kéniéba 6 km east of Senegal. Area 79.15 km ² (W.Mali). Ouarala, Yanfoliolo-Kalana region. 20 km SW of Kalana deposit. Area 285 km ² . Diaban 100 km SW of Bamako (SW. Mali). Kouroufing 50 km SS of Kéniéba. Area approx 200 km ² (W.Mali).	Kouroufing: Occidental (wholly owned subsidiary. Of Leo Shield Exploration & Triangle D'Or (Triangle). 65% Occidental option of equity, may also require further 5% from Triangle. 35% Triangle.
BRGM.	Willi-Willi, 50 km SS Kéniéba, adjacent to Kouroufing of Leo Shield, (W. Mali).	
Mink International Resources Corp.	4 sites within the Kangaba region, (SW. Mali). Niaouléni Libre Plateau zone Kankou Moussa zone Goingoindougou Approx. area 400 km ² .	100% Mink interest. (Commissioning of an on-site gold preparation plant now in progress).
Pangea Goldfields Inc.	2 sites. Fodie, north of Sadiola. Area approx. 313 km ² (W. Mali). Foulaboula, (SW. Mali).	25-35% Pangea interest, joint venture partner?.
Oxford Resources Inc.	4 sites: Sélou 35 km south Loulo, 15 km SW Kéniéba Area approx. 150 km ² (W.Mali). Kéniéba group 15 km south of Loulo, approx. 12 km north of Kéniéba. Total area approx. 26 km ² (W.Mali). Dialafara-Rhama between Sadiola & Loulo. (W.Mali). Kangaba region Area approx. 650 km ² (SW. Mali).	Surveys in progress.

Table 1b continued.

Sanou Mining Corporation. (Azco Mining Inc.).	2 sites Medinandi & Dandoko, Kéniéba area, Area approx. 544 km ² (W. Mali).	Agreement between: Azco (51%), (WAG), Eagle River Inter. & Lion Holdings Ltd., forming joint venture. (Estimated resource of Medinandi >1moz).
Reunion Mining.	Sanoukou, Kéniéba area (W. Mali).	
Golden Star	Dioulafoundou Kéniéba area (W. Mali).	
Alpine Exploration Corp. & Joint Malian vendors (?). Emerging African Gold Inc. (EAG).	3 (?) sites: Metedia, & Kéniéba area Area 8 km ² each (W. Mali). Kalana area (SW. Mali). Koulo, 272 km ² . Kolomba-Mankouke 100 km ² (both located south of the Kéniéba region). Narena 173 km ² (located in the Kangaba basin).	Alpine can earn 63.75% of Yatia. Alpine can earn up to 85.5% of Metedia. Negotiated 85-100% project interests for Kalana area. 75% interest (gold & platinum). 65% interest (gold, silver & platinum). 70% interest (gold). (EAG is financed by St Genevieve Resources Ltd).
Barrick Gold.	Holds ground to the south of Sadiola mine, south of Kayes, (W. Mali).	
Resource Robex & Alpine Exploration.	Baroya, 15 km N Kéniéba, Area approx. 8 km ² (W. Mali).	Permit application state: 25%Resource Robex, 65% Alpine Exploration, 10% SOMEX-SARL, plus, 3% net-production royalty - original permit holders.

BHP-Utah Mali Inc.^H

I.F.C.^{H H}

Iamgold^{HHH}

Anmercosa^{HHHH}

Amgold^{HHHHH}

A wholly owned subsidiary of BHP Minerals.

International Finance Corporation.

A subsidiary of Canada's International African Gold Mining.

A subsidiary of Anglo-American Corporation.

A 50% subsidiary of Anglo American Corporation.

Table 1c: Interests.

Company	Interests
Pacific Galleon Mining & Swiss based associates.	Considering acquiring block claims near Loulo.(?) (W.Mali).
Consolidated Mining & Trillion Resources.	Considering funding exploration within Mali. (?)
Emerging African Gold Inc. (EAG).	Negotiations for Hafia, (SW. Mali); North Kayes; Ugico (SW. Mali); Kalana Est (S Mali) and Kekoro (NE of Kalana area).
Oxford Resources Inc.	Application claim pending for Sélou, Kéniéba region (W.Mali).

Information sources recorded in tables 1a to 1c are as follows:

Anon.,(1992); Anon.,(1993); Anon.,(1995); Anon.,(1996a); Anon.,(1996b); Anon.,(1996c); Anon.,(1996d); Anon.,(1996e); Anon.,(1996f); Anon., (1997a); Anon., (1997b); Bugeco (1994); Chaplin et al., (1997); W.W.W., (1997e); W.W.W., (1997f); W.W.W., (1997g); W.W.W., (1997h); W.W.W., (1997i); W.W.W., (1997j); W.W.W., (1997k); W.W.W., (1997l); W.W.W., (1997m); W.W.W., (1997n); W.W.W., (1997o); W.W.W., (1997p).

With respect to other mineral potential, Mali has considerable resources of salt, kaolin, bauxite, hematitic iron ore, manganese, limestone, and phosphates, as well as copper, nickel and uranium (Hodgkinson 1994; Ruffini 1997). Many of these have yet to be exploited due to lack of size and quality, and also through the lack of an adequate infrastructure to support their extraction and transportation to the World market. However, phosphate has been mined at Gao, marble quarried at Bajulabe, and salt on a limited scale has been extracted in the extreme north of the country near Taoudenni. Interest has also been shown in prospecting for petroleum deposits and tungsten (wolfram). In June 1995 a 36,000 km² diamond concession was granted in the Kéniéba region to Mink Minerals and Ashton Mining (WWW 1997j; WWW 1997q). This joint venture has discovered 24 kimberlite pipes, 8 of which are diamond bearing (July 1997 statistic, W.W.W., 1997j). Diamond exploration within this area has had a chequered history, with participation from the DFMG, the former French West African Department of Mines (1954-1957); Selection Trust (1960-1963); SONAREM with the Russian Geological Survey (1960-1963); and Syndicat Diamant-MALI, a joint venture between the Malian and French governments (1979-1983). The newly elected French

government of 1983 decided to terminate its involvement, resulting in the project lying dormant until 1995 (W.W.W., 1997). The number of known kimberlitic bodies, and the inference that more may still lie undiscovered has prompted reports that the Kéniéba region is the largest known kimberlite province in West Africa (W.W.W., 1997).

1.5 Choice and Description of the Study Area.

The research area (Fig. 1) is located in south-east Mali and is bordered on its southern and western margins by the Ivory Coast. It extends approximately 120 km from north to south, and 65 km from east to west. This area overlaps with the districts of Massigui (Sikasso), Kadiana (Tigrela) and Kadiola (Nellé). There was no personal involvement with respect to the selection of the study site. The site was chosen because BHP, the instigators of the research and suppliers of the raw data, were currently extracting gold at Syama, a mine, which is located within this region. The dimensions of the research study area were effectively imposed by the extents of the 1980 UNDP regional geochemical sample program.

1.5.1 Climate and Physiography.

This region classed under Soudanais type, experiences three climatic seasons as previously described in Section 1.4.1. To recap briefly, these are known as the Rainy Season, the Warm Season, and the Hot Season.

The Rainy Season brings most of the annual 900-1200 mm of precipitation. During this period the vegetation becomes lush and abundant, the land surface is predominantly covered by tall grasses, but there are also sporadic trees and small bushes. The density of trees increases markedly within topographic depressions, on the slopes of higher ground, and in the vicinity of watercourses, (Plate 1) resulting in gallery vegetation. Ephemeral streams

develop rapidly with the onset of the Rains and it is common for flooding to be experienced in low-lying areas and in local topographic depressions. Flooding often renders routes impassable and therefore travelling across the terrain is generally rather difficult, (Plate 2). Furthermore, most of the perennial rivers swell dramatically in the Rainy Season and often may only be crossed by dugout canoe since many of the wooden bridges become submerged (Plate 3).

The Hot Season, in contrast, brings scorching temperatures of 30° to 40°C which rapidly cause the tall wild grasses and small bushes to die back. It is common agricultural practice in this region to burn the grasses in order to fertilise the soil and revive pasturage, which reveals the characteristic red-brown tropical soils. The ephemeral streams dry up and the perennial streams become very narrow, thus exposing great expanses of cracked, hard, muddy banks.

Laterite forms a thick blanket across the topographic surface, which locally attain average depths of some 60 m (Chapter 3, section 3.7). Under these environmental conditions the laterite evolves both chemically and physically, culminating in the formation of a hard, iron-rich, and often impermeable surface cap.

1.5.2 Relief.

The surface topography of the study region is illustrated on the shaded elevation plan and cross-sectional maps presented in Fig. 3. Altitude varies from a low point of approximately 320 m to heights in excess of 650 m in the far north-east of the area. There appear to be four distinct plateau levels which correspond quite closely with the presence of different geological formations, (Fig. 4).

Plate 1 Vegetation.



Plate 2 The Syama to Dioumantene main road.

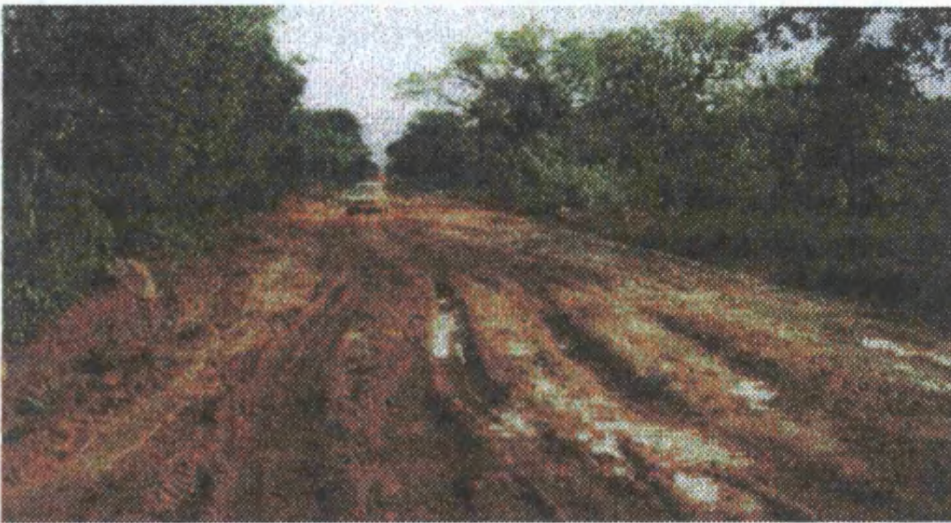


Plate 3 Crossing the Bafini river in a dug-out canoe.



The first level represents heights of ~ 320 m. This embodies all the low lying perennial rivers and some of the ephemeral streams, forming the ground base level.

The second level of 330 - 340 m is most characteristic of the eastern sector of the area, which incorporates the Proterozoic granite plateau. This area is of relatively constant altitude although there are some small superimposed local scale undulations. The one obvious exception is at Touban where an outcrop of ultrabasic rocks causes the altitude to rise to 429 m.

In contrast, the western sector, which encompasses the Birimian and Tarkwaian sequences, has a much greater fluctuation in height. In this area there are also numerous hills with laterite caps, which attain the third altitude level of 360 m. Also within the same region are a number of isolated peaks, which typically exceed 400 m. Overall these appear to display a regional north-south linear alignment which is concordant with the trace of the Birimian (Bj), volcano-sedimentary sequence (Chapter 2).

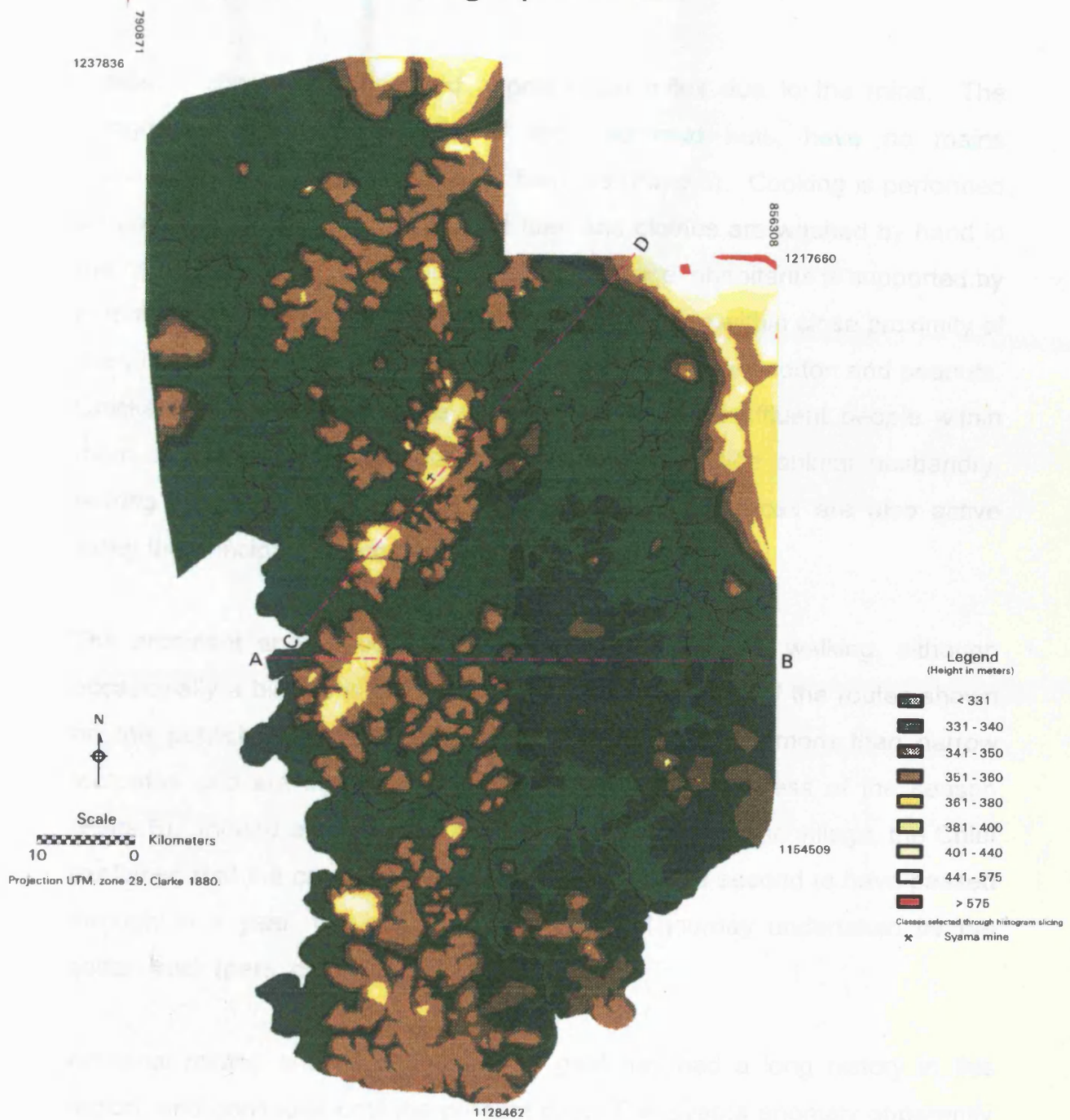
Finally, in the far north-east of the region the land rises quite sharply forming a cliff feature between the previously mentioned granite plateau (~ 330-340 m) and the Proterozoic sandstone (~ 400-500 m). This sandstone plateau is intruded by doleritic dykes and sills upon which local peaks attain altitudes of over 650 m.

An interesting phenomenon seen throughout the region is the development of sporadic termite hills. These mounds of excavated earth can reach 2 m or more in height, and thus they form quite prominent visual features in regions of relatively flat and otherwise rather featureless terrain (Plate 4).

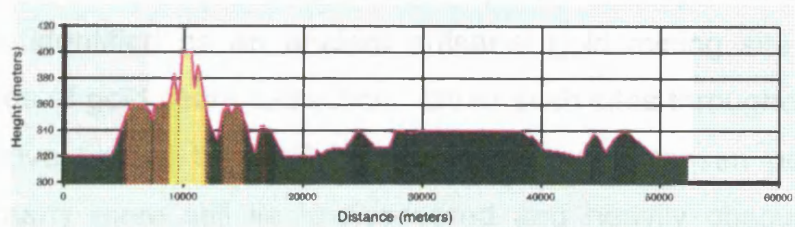
1.5.3 Urbanisation.

There are over one hundred villages scattered throughout the study region. Five of the largest urban centres are marked on Fig. 1 along with the Syama

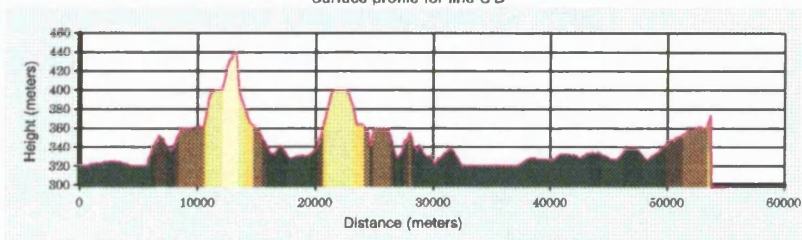
Fig. 3 Topographic Plan.



Surface profile for line A-B



Surface profile for line C-D



TIN, produced in ARC/INFO from digitised contour and spot height data - cartographic map sources: Feuille NC-29-XXIV(Massigui), NC-29-XXVIII(Kadiana), NC-30-XIII(Kadiolo) @ 1:200,000. Converted to an ARC/INFO GRID. Map composed in ERDAS Imagine.

village, which has experienced a population influx due to the mine. The villages, composed principally of assorted mud huts, have no mains electricity, running water or sewage facilities (Plate 5). Cooking is performed on open fires using harvested wood fuel, and clothes are washed by hand in the nearby streams. The livelihood of most village inhabitants is supported by communal subsistence farming practices, undertaken within close proximity of the village. Typical crops are rice, maize, millet, sorghum cotton and peanuts. Chickens are raised in all the villages but the more affluent people within them, and those wishing social prestige, also practice animal husbandry, rearing cattle and goats (Anon., 1973). Fishing practices are also active along the principal river courses.

The dominant and almost exclusive form of transport is walking, although occasionally a bicycle is available. Consequently, many of the routes shown on the published 1:200,000 scale maps are in fact no more than narrow footpaths and are impassable for motor vehicles regardless of the season (Plate 6). Indeed a car is such a rare sight here that in one village, the Chief explained that the car used for fieldwork was only the second to have passed through in a year, the other being the annual journey undertaken by the cotton truck (pers. comm.).

Artisanal mining and river washing for gold has had a long history in this region, and continues until the present day. The Syama anomaly apparently discovered by the 1980 UNDP regional geochemical survey was, upon further investigation, identified as an ancient artisanal gold mining site employing crude methods of gold seam extraction. Other such sites throughout the area have been investigated by BHP but it is believed (Hanssen pers. comm. 1995) that many more still lie undiscovered and heavily obscured by the vegetation.

Plate 4 Termite hills.



Plate 5 A village.



Plate 6 Narrow footpaths linking village to village.



CHAPTER 2

THE GEOLOGICAL ENVIRONMENT

Contents.

- 2.1 Introduction.
- 2.2 The Precambrian of West Africa - A synthesis.
 - 2.2.1 West African tectonics.
- 2.3 Stratigraphy of the research area.
- 2.4 Regional faulting.
- 2.5 Known mineralisation and deposits.
- 2.6 The Birimian volcano-sedimentary sequence and associated gold mineralisation.
 - 2.6.1 Overview.
 - 2.6.2 Host lithologies.
 - 2.6.2.1 Basalt.
 - 2.6.2.2 Greywacke-argillite.
 - 2.6.2.3 Andesitic intrusions.
 - 2.6.3 Alteration.
 - 2.6.4 Silicification.
 - 2.6.5 Primary gold and sulphide mineralogy.
 - 2.6.6 Volcano-sedimentary structure.
- 2.7 Regional similarities - a summary.

2.1 Introduction.

This chapter discusses and describes the geological environment of West Africa at a regional scale and details the lithology, structure, mineralisation and alteration observed within the research region.

The chapter begins by introducing the two important supracrustal sequences of the West African craton, the Birimian and Tarkwaian. Section 2.2 also highlights not only the dispute surrounding the stratigraphic relationship of these two rock sequences but the spatial differences in their distribution from east to west of the craton. Although these observed spatial differences referred to as Type I and Type II zones have caused conjecture with regard to tectonic models (subsection 2.2.1), there are nevertheless similarities between the craton regions as explained in Section 2.2. From Section 2.3 the research area becomes the focus for the remainder of the chapter. In this section the spatial distribution of each lithological unit is illustrated diagrammatically and the complex stratigraphy of the region is discussed. Regional faulting is described and discussed in Section 2.4. Mineralisation and known deposits are examined and reported upon in Section 2.5. The spatial location of the deposits are mapped with respect to underlying lithology, however, it is acknowledged that due to the region's long history of artisanal mining and lack of detailed mapping, many mineralised regions may still lie undiscovered. Section 2.6 and its subsections describe in detail the volcano-sedimentary sequence in which the Syama gold deposit lies. It describes the mineralogy for each of the host lithologies and discusses the type and pervasiveness of the alteration throughout the host basalt. Collated research from petrographic analysis (subsection 2.6.5) has shown that although pyrite is the principal host for gold it is not the only sulphide, for many others are observed in trace amounts. Finally the structural complexity of the volcano-sedimentary sequence is described and illustrated in subsection 2.6.6. This reviews recent new finds of suspected fault locations through the use of geophysical techniques and mine mapping. The chapter

concludes with a brief summary (Section 2.7), of the regional similarities observed throughout the geological environment of the research area.

2.2 The Precambrian of West Africa: A synthesis.

The West African craton is predominantly of Proterozoic age. In the eastern sector of this craton (occupying the areas of Ghana, Ivory Coast, Burkina Faso, southern Mali, south-east Senegal, northern Guinea, western Nigeria and south-east Liberia) there are Birimian and Tarkwaian supracrustal sequences. Although these lithologies are regarded as the oldest in this area (Wright et al., 1985), there is also speculation of a much older Archaean basement, (Wright et al., 1985; Kusnir et al., 1987). The suggestion that small pockets of Archaean crust might exist within the undifferentiated granite-gneiss and migmatite terrain, is as yet unproven. Although the Birimian and Tarkwaian are present throughout this sector of the craton, there are significant regional differences. These differences relate not only to the spatial distribution of the rocks, but also to the stratigraphic relationship between, and within, these two supracrustal sequences. This has led to a debate between the two schools of thought; namely theories developed from Ghana and those from the Ivory Coast (Wright et al., 1985).

The Ghanaian studies divide the Birimian into two distinct units. The lower unit is represented by metasediments and the upper unit by greenstone-type metavolcanics (Whitelaw, 1929; Wright et al., 1985; Appiah et al., 1991). The Tarkwaian is considered mainly as shallow-water derivatives, probably fluvial in origin possibly molasse (Oberthür et al., 1991). Nevertheless, the Tarkwaian is considered to lie unconformably on the Birimian (Kesse, 1985, cited in Appiah et al., 1991). In contrast, the Ivorian, see no obvious distinction within the two supracrustal sequences (Ledru et al., 1991). The metavolcanics, though subordinate to the metasediments, are regarded as either contemporaneous with, or older than, the metasediments. The complex inter-related folding and poor exposure of the Birimian and

Tarkwaian has hindered understanding of their relationship. As a result they are regarded as molasse-type but are often treated as lateral facies variants within the metasediments of the Birimian (Wright et al., 1985; Appiah et al., 1991).

Although the stratigraphic relationships are still in dispute, there are noticeable spatial differences throughout the West African craton. In the eastern region (known as Type I Belt), the Birimian metavolcanics dominate whilst in the western region of the craton (known as Type II Belt), Birimian metasediments prevail over metavolcanics Wright et al. 1985; Anon., 1993. Intruding the Birimian - Tarkwaian supracrustal sequences are large Proterozoic (syntectonic) batholithic granites. These are typically of two-mica type. Also present, though less abundant, are smaller sub-circular late-tectonic to post-tectonic stocks, of acid to intermediate composition. In some regions there are also basic stocks which intrude the larger granite masses.

Despite clear lithological differences between the eastern and western regions of the craton there also appear to be certain similarities. Major fractures, shear zones and the tight, steeply dipping folds and thrusts, are characteristic of both regions, (Wright et al., 1985; Bowell et al., 1991; Appiah et al., 1991; Oberthür et al., 1991; Liégeois et al., 1991; Olson et al., 1992; Dzigbodi-Adjimah, 1993; Anon., 1993). Furthermore, shear zones are typically NNE-SSW trending. Metamorphic grade is also generally consistent within each of the supracrustal sequences, regardless of region. The Birimian is characterised by greenschist to amphibolite grade, whilst the Tarkwaian, although described similarly, is mainly greenschist facies.

2.2.1 West African Tectonics.

The limited stratigraphic knowledge of this region has lent itself to somewhat circumspect tectonic models. If an older gneiss-granite-granulite Archaean basement exists beneath the Birimian supracrustal rocks then it would most

definitely have been affected by the Liberian tectonic event (c.2750 Ma) (Wright et al., 1985). However, if an older Archaean basement is not present, then the first period of deformation and metamorphism is the Eburnian event, which affected the Birimian and Tarkwaian supracrustal sequence (Wright et al., 1985; Kusnir et al., 1987; Oberthür et al., 1991). This thermotectonic event was believed to have been at its peak c.2100–2070 Ma, with earlier pulses theorised around c.2300 Ma. During this period, the emplacement of large syntectonic granites occurred, culminating in a later episode of reactivation resulting in post-tectonic intrusions.

The West African craton stabilised after the Eburnian event. Later post-Birimian sediments are essentially undeformed and unmetamorphosed, with only the far eastern section being influenced in part by the Pan African event (c.500 ± 50 Ma). There is an acceptance of the general concept that supracrustal belts can be split into Type I (Greenstone dominated) and Type II (metasediment dominated), which occupy east and west zones of the craton respectively (Fig. 3a). Two general tectonic hypotheses have evolved with regard to the evolution of these supracrustal belts:

- (i) The concepts of large oceanic basins or intracontinental rifts. In which Birimian supracrustal rocks were deposited in ensialic rift basins, as based upon geophysical data modelling (Hastings 1982) Fig.3b.
- (ii) The theory of small ensimatic and ensialic rift induced volcano-sedimentary basins which upon closure aggregated back-arc, inter-arc and continental blocks, as based upon paleomagnetic evidence and the metavolcanic assemblages present (Wright et al., 1985; Olson et al., 1992) Fig. 3c.

Accepting the later theory could help explain (as discussed in Wright et al., 1985) not only the spatial distribution of the Type I and Type II belts, (Type I ensimatic predominating in the east and Type II ensialic predominating in the west), but also the major NNE-SSW shear zones which are so characteristic

Fig. 3a Distribution of Birimian supracrustal belts in West Africa & Africa.

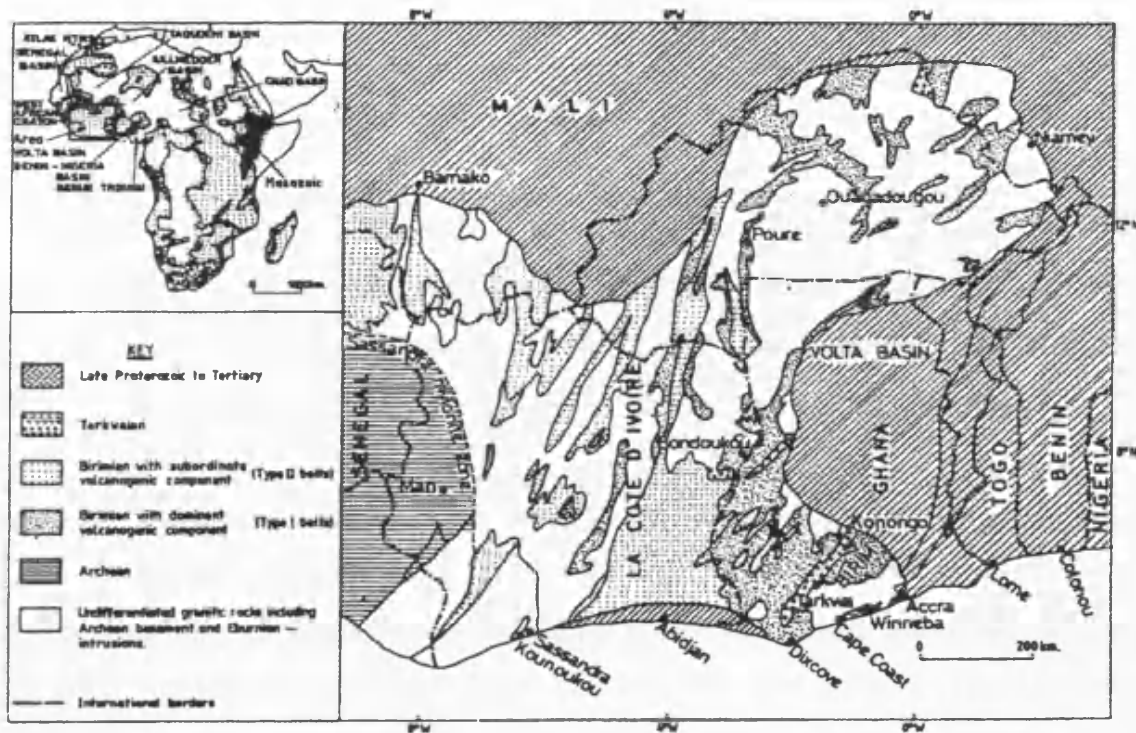


Fig. 3b Development of ensialic & ensimatic basins formed by rifting.



Fig. 3c Diagrammatic illustration of arc sites.

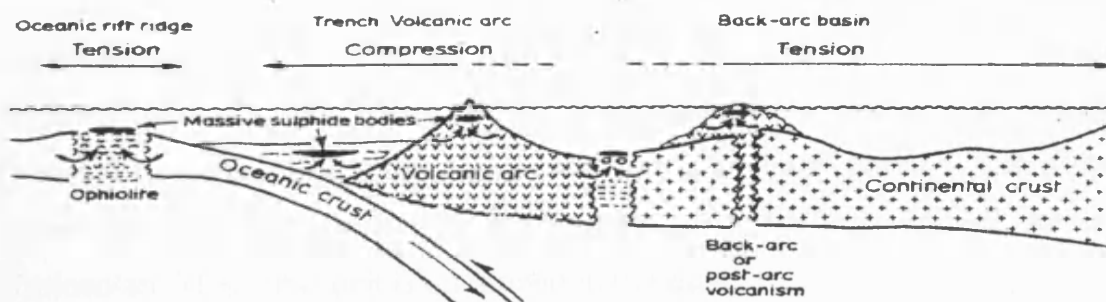


Fig.3a Taken from Dzigbodi-Adjimah, (1993). Fig.3b Taken from Wright et al., (1985)
 Fig.3c Taken from Edward & Atkinson, (1986).

of the region (Wright et al., 1985; Oberthür et al., 1991; Liégeois et al., 1991; Dzigbodi-Adjimah, 1992; Olson et al., 1992).

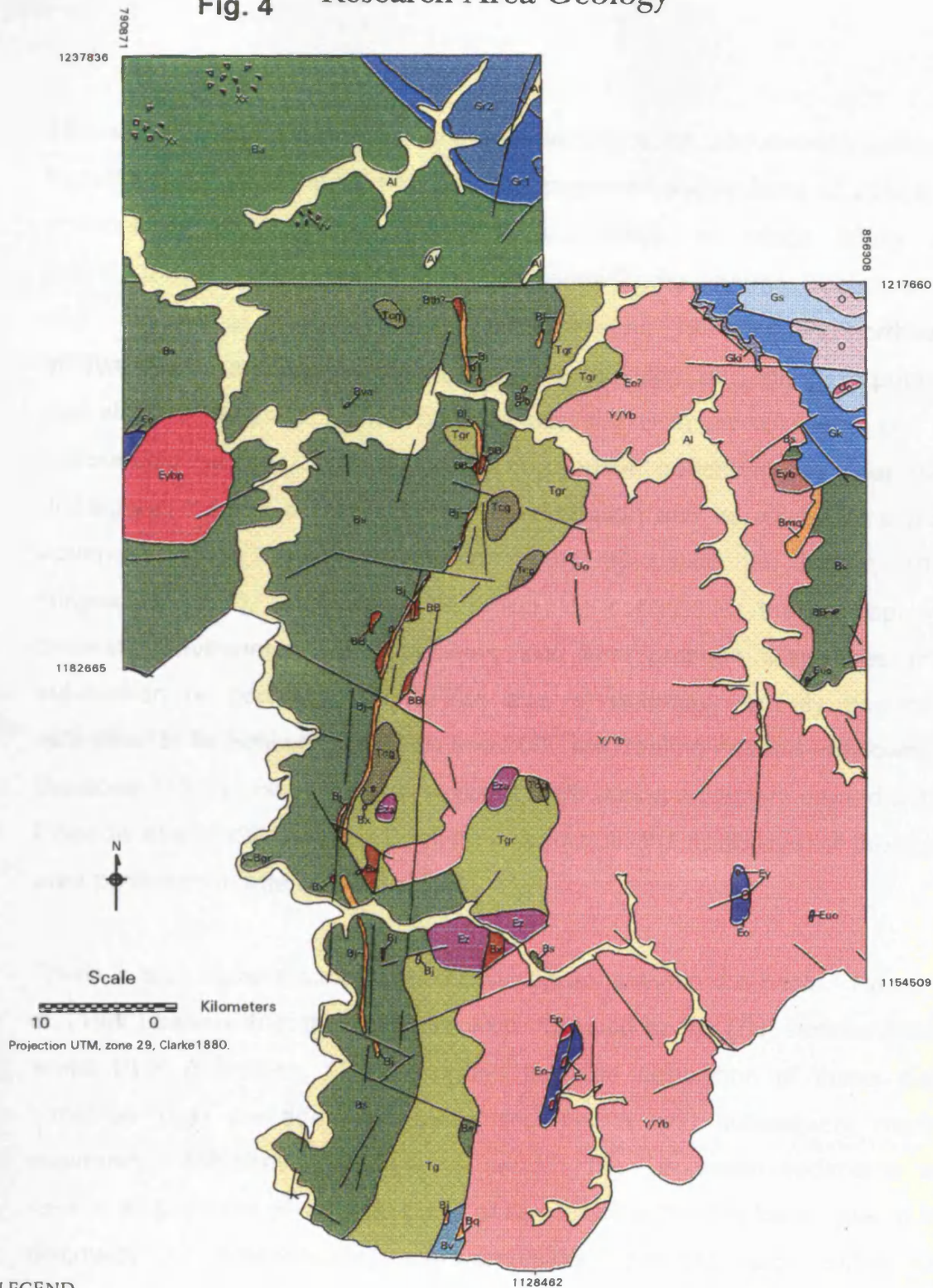
2.3 Stratigraphy of the research area.

A precise chronology of the region's geology (Fig. 4) is constrained by the lack of 'true' outcrops, as opposed to laterized soil or hardcap. Further complications arise due to limited mapping. Consequently, stratigraphic interpretations are tentative with respect to the precise timing of events.

There is some speculation as to the existence of an underlying Archaean basement within the extensive granite-gneiss massif (Kusnir et al., 1987), (Y/Yb, Fig. 4). The evidence to support this has been attributed to the sporadic identification of migmatites, amphibolites and gneiss. Their limited outcrop and the overprinting by the later Eburnian Orogeny reveals little support for this theory. If parallels are drawn with neighbouring areas, such as the amphibolite of Gaoura in Burkina Faso, then age determinants of between 2500 Ma and 2750 Ma would not be unrealistic (Bessoles, 1977).

In Fig. 4, the Birimian System is seen in two localities. The principal area is in the west of the region and is known as the Bagoé basin or syncline. It is flanked on its eastern margin by the Eburnian granite-gneiss massif (Y/Yb), and on its western margin by granite stocks in the neighbouring Ivory Coast. A smaller area is identified in the east, surrounded by the granite-gneiss and overlain by sandstone of the upper Proterozoic. The Bagoé syncline is comprised of three Birimian units. A narrow, elongate, north-south volcano-sedimentary unit, (Bj) (Section 2.6), bordered on its west by an argillite, greywacke schist (Bs), and to its east by a coarser grained greywacke, sandstone and (andesitic) conglomerate (Tgr/Tg/Tcg) known as the Tarkwaian. This latter unit is undefined in the east.

Fig. 4 Research Area Geology



LEGEND

SUPERFICIAL

Al Alluvium (Recent)

PROTEROZOIC-PERMIAN MAGMATISM

Uo Dolerite

O Gabbro

Vv Doleritic intrusions

UPPER-LOWER PROTEROZOIC (1000Ma)

Gs Sandstone, siltstone & clay

Gk Sandstone with glauconite

Gki Sandstone medium-coarse

Gr2 Predominantly dark grey sandstone
Gr1 Predominantly grey-white sandstone

LOWER PROTEROZOIC (2300-1900Ma)
(Eburnian intrusives)

Eyb Granite boitie Eybp, Granite biotite porphyry

Ez Diorite Eza, Quartziferous diorite & amphibole

Eo Gabbro Euo, Microgabbro

Ev Ultrabasic Ey, Peridotite Ep, Pyroxenes

Y Granite-gneiss Yb, Granite-boitite

Xx Granodiorite, monzodiorite & qtz-diorite

SYSTEM BIRIMIAN

Facies Tarkwaian (semi-metamorphosed)

Tgr Greywackes Tg, Sandstone

Tcg Polymict conglomerates

Formations Birimiannes (metamorphosed)

Bs Greywacke & arkose with schist

Ba. Volcano-sedimentary assemblage

Bgr Meta-greywacke & biotite

Bj Jasper Bq. Quartzite Bmq, Microquar (volcano-sedimentary assemblage)

Bva Acid volcanics & tuff

BB Basalt Bx, Andesites Btb, Basic tuff

Bv Undifferentiated volcano-sedimenta

Faults
exact stratigraphic position uncertain

¹Map digitised from cartographic map sources: Feuille NC-29-XXIV(Massigui), NC-29-XVIII(Kadiana), NC-30-XIII(Kadiolo) @ 1:200,000. Map composed in ERDAS Imagine.

The narrow outcrop of the volcano-sedimentary suite, and the dominance of tholeiitic over calc-alkaline magmas, has produced suggestions of a back-arc environment of deposition (Olson et al., 1992), in which rifting and graben formation occurred due to hot spot magma centres (Kusnir et al., 1987; Olson et al., 1992). However, Liégeois et al. (1991) working north-west of Syama in the Massigui region found no tholeiitic, but only high potassic calc-alkaline magmas. They propose that the Birimian volcanics and the surrounding plutons are of the same source geochemically, but have undergone magma differentiation or fractionation and so represent a more advanced stage of arc development (as discussed by Barker, 1968; Ringwood, 1974). Liégeois et al. (1991) do not dismiss the concept of a back-arc environment of deposition, but also propose similarities to a subduction or docking zone. The age of magmatic activity has been estimated to lie between 2300 Ma and 2000 Ma, (dating method unknown) by Bessoles (1977). However, more recent U/Pb dating on zircon, carried out by Liégeois et al. (1991) on the Birimian volcanics to the north-west of the study area produced a date of 2098 ± 5 Ma.

There is also some dispute over the stratigraphy within the basin. Kusnir et al. (1987) believe that the volcanics were followed by the (Bs) sedimentation, whilst BHP (Hanssen, 1995) propose that the deposition of these distal turbidites (Bs) preceded rift/graben tectonism and subsequent marine volcanism. Whichever of these is correct, the Tarkwaian sediments are viewed as products of the final stage of deposition within the basin, due to the discovery of metabasalts, meta-andesites, granites etc. within the conglomerates. Kusnir, (et al., 1987) reports a date therefore of c.1850 Ma.

Through time various degrees of uplift and erosion are believed to have occurred, especially along rift fault scarps. This erosion resulted in the local development of conglomerates along some fault scarps, for example, the conglomerates found in the east along the 'conglomerate shear' (Fig. 5), seen

outcropping at the Syama and Alpha mines, (Hanssen, 1995). Further examples occur near Finkolo and Banmbere.

It is highly likely that concurrent with the uplift and erosion the graben system was also undergoing compression. This compression, in a regime of dextral transpression (Hanssen, 1995), forced the closure of the complex graben structure, resulting in folding, faulting, shearing and metamorphism of the sediments and volcanics. It is also believed that it was at this time that andesitic dyke intrusions along with mineralisation and alteration took place (Pohl et al., 1991; Olson et al., 1991; Olson et al., 1992). A change is then believed to have occurred in the regional stress direction, from dextral to sinistral movement (Hanssen, 1995). However Liégeois et al. (1991) study of the shear in the Massigui region have identified three possible deformation events. Little is known of D_1 , however D_2 appears to indicate sinistral shear movement both of Eburnian orogenic age, whilst the post-Eburnian D_3 reactivation event, though separated by approximately 100 Ma (c. 1980 Ma), indicates a significant change in the regional shear stress direction from sinistral to dextral.

The composition and age of the granite-gneiss massif is uncertain, due to few outcrop exposures and imprinting of the Birimian orogeny, which helps to explain why there is no clear distinction made between Archaean and Birimian on the geological maps. The granite massif is believed to be indicative of Eburnian orogenic syn-tectonism, with commonly quoted radiometric dates lying between 2050 Ma and 1950 Ma (Kusnir et al., 1987). However, Lemoine and co-authors (1985) look within a broader context, and have postulated multiphase intrusive emplacement resulting from two principal orogenic periods. Firstly, a Burkinian cycle around 2250 Ma, and 2150 Ma; secondly, a more significant Eburnian cycle from 2100 Ma to 1950 Ma. Liégeois et al. (1991), working in the Massigui region of southern Mali, have found no evidence of events older than 2100 Ma, and believe the Eburnian orogenesis lie principally between 2100 and 2070 Ma. Evidence of later events are assumed to be the result of tectonic reactivation. Regardless

of these discrepancies, it is apparent from the examination of aeromagnetic data (chapter 5) that the subsurface extent of this massif beneath the Tarkwaian is far more extensive than that indicated on the published geological maps. The same can be said for the Ivorian granite lying to the west of the region, for that too appears to be present beneath the (Bs) sediments. The lower Proterozoic rocks constitute, volumetrically, the largest contribution to the study region. They encompass the Birimian System, the granitoids, and the basic/ultrabasic rocks, which were emplaced during the Eburnian Orogeny.

Rocks of the Birimian supracrustal sequences and the granite-gneiss massif were subsequently intruded by a variety of basic, intermediate and acid intrusions which were of varying size and which overlapped in time. In the east and south-east of the region two dolerite or microgabbro dykes (Euo, Fig. 4), cut both the granite-gneiss and Birimian. These are oriented NNE-SSW and are some 100 of meters long and 10s of meters wide. The exact age of these dykes is unknown, but Kusnir et al. (1987) have placed them within a Birimian age due to their level of metamorphism. In the south-east of the massif is the Touban complex, which extends across an area of approximately 6 x 2 km. It is composed of weakly metamorphosed gabbro, serpentinised dunite, and ultrabasic rocks (peridotite). Within this complex the BRGM discovered copper/nickel mineralisation (Fig. 5). The gabbro and peridotite at Touban have been dated by Rb-Sr, (whole rock) at 2067 ± 78 Ma (Kusnir et al., 1978), which is very similar to Liégeois date (by Sm-Nd) of 2049 ± 38 Ma. In the south of the granite-gneiss massif, and to the south-west of the Touban massif, is another slightly larger mafic complex at Zekoun. It is composed predominately of gabbro with smaller pockets described on the 1:200,000 scale geological map (Fig. 4), as undifferentiated ultrabasic and pyroxenites. No date has yet been determined for this complex. Of similar age and possibly temporally overlapping in part with the Touban intrusion is the intermediate diorite intrusion at Finkolo (Eza) dated at 2049 ± 38 Ma by Rb/Sr, (whole rock). Two other diorite stocks are found to the east and south-east of Finkolo, intruding the Birimian-Tarkwaian unit. These are partly

surrounded by the granite-gneiss massif. Probably one of the youngest Eburnian intrusions of the research area is that found to the west of the Bagoé river, within the Birimian unit (Bs). This large granite-biotite porphyry (Eybp), has a diameter of approximately 11 km and has been dated at 2036 Ma by the Rb method (Kusnir et al., 1987).

Around 1600 Ma small Post-Eburnian granitic intrusions were emplaced within the West African craton (Kusnir et al., 1987). One such small granite biotite stock (Eyb) in the east, is at the fringe of the granite-gneiss adjacent to the upper Proterozoic sandstone unit at Diourkasso. This post Eburnian intrusion is dated with reservation at 1603 Ma by Rb/Sr (whole rock), (see Kusnir et al., 1987 for further explanation).

By 1000 Ma the environment of deposition had changed dramatically, a fact that is reflected on the higher ground in the north-east of the region. Here the upper Proterozoic sediments, primarily the lower Kebeni (Gki), lie unconformably on the granite-gneiss platform. This north-eastern area represents a part of the large Taoudéni basin or syncline. It is believed that this basin began filling up prior to 1000 Ma (Bassot et al., 1981), culminating in some 400-450 m of sediments that are seen to be sourced mostly from the altered granitic-gneiss platform (Kusnir et al., 1978). These sedimentary units were deposited under coastal marine (littoral) conditions with varying sea depths. They comprise initially of coarse deltaic sandstones (Gr1, Gr2) and pebbles (Gki). These are then followed by very fine sandstones which have been described as having some glauconitic component (Gk). Deposition culminated with clayey siltstones and minor argillites (Gs). The age of this sedimentary assemblage has been determined by comparisons with sandstones near Bamako and with sandstones that are considered to be stratigraphic equivalents at nearby localities. Dates of 990 Ma by Bozhko and 1025 Ma by Clauer, (1976) have been suggested (cited in Kusnir et al., 1987). On rare exposure the sediments are described as being near-

horizontally bedded, dipping 2~3° to the north-east. They are reported as not having been affected by folding or metamorphism (Kusnir et al., 1987).

Finally, these sediments are cut by tholeiitic intrusives which are typically doleritic and gabbroic in nature. These formed dykes, laccoliths and, most commonly, sills, emplaced at the top of the Sorobilé Formation (GS) or at its base, in contact with the Kebeni Superior Formation (GK). Age determinations of the gabbro near Kai, using the Sm/Nd total rock method, have produced a date of 727 Ma (Liégeois, 1986, cited in Kusnir et al., 1987). Dating of a similar dolerite in Burkina Faso by the K/Ar total rock method has produced an age of 250 ± 13 Ma (Marcelin and Serre, 1971, cited in Kusnir et al., 1987).

The evolution of the region from the Tertiary to the present day has mostly been the product of an alternating climate. This is reflected in interspersed humid and arid periods, coupled with fluctuating water-table levels. These climatic conditions, which are on-going, have produced a thick weathered regolith referred loosely to as laterite which characteristically blankets the surface of the region (this is described in detail in chapter 3).

2.4 Regional faulting.

Little information exists regarding the nature and history of faulting within the region as a whole. The most significant contribution has come from BHP's investigation of the meta-volcano-sedimentary sequence, within their concession area. The complex faulting that was found within this area is explained in greater detail in Section 2.6.6. From an analysis of the 1:200,000 scale geological maps four principal fault orientations can be identified. These are as follows: (a) north-south, (b) east-west, (c) northeast-southwest and (d) northwest-southeast. Although faulting appears not to be restricted to any one lithology there is nevertheless a greater frequency within the Birimian system, and especially within the volcano-sedimentary

sequence. This sequence (Bj, Fig.4), is confined within a regional shear zone system (Olson et al., 1991; Hanssen et al., 1991; Olson et al., 1992) which was not identified on the 1:200,000 scale regional geological map. Within BHP's concession area an attempt has been made to map this complex zone through detailed studies performed at the scale of individual mines, and also at a sub-regional scale by ground very low frequency (VLF) electromagnetic survey work (Fig.5). This work has identified N010° to N030° oriented structures which are frequently cross cut by NE-SW to E-W trending faults (Hanssen, 1995), although on the 1:200,000 scale geological maps NW-SE faults are also seen crosscutting.

Unfortunately, structural mapping has been limited to the exploration permit area and consequently no regional map exists detailing the whole extent of the shear zone.

The chronology of regional faulting is difficult to ascertain. Some faults lie solely within a given lithology, some show multiple crosscutting relationships, and others imply angular double fault intersections. In general much of the faulting within the Birimian System is probably due to the closure of the rift system during the Eburnian tectonic event. The meta-volcano-sedimentary sequence was probably more susceptible to faulting and shearing due to the differences in competence between the volcanics and the sediments (Hanssen, 1995). Some of the crosscutting faults could represent possible reactivation, or the result of later tectonic pulses.

Faulting in the upper Proterozoic to lower Phanerozoic lithologies is likely to be related to Pan-African tectonism dated around 500 ± 50 Ma (Wright et al., 1985; Kusnir et al., 1987). However, the faults transgressing both lower Phanerozoic and lower Proterozoic lithologies may well represent reactivation along zones that have been previously structurally weakened.

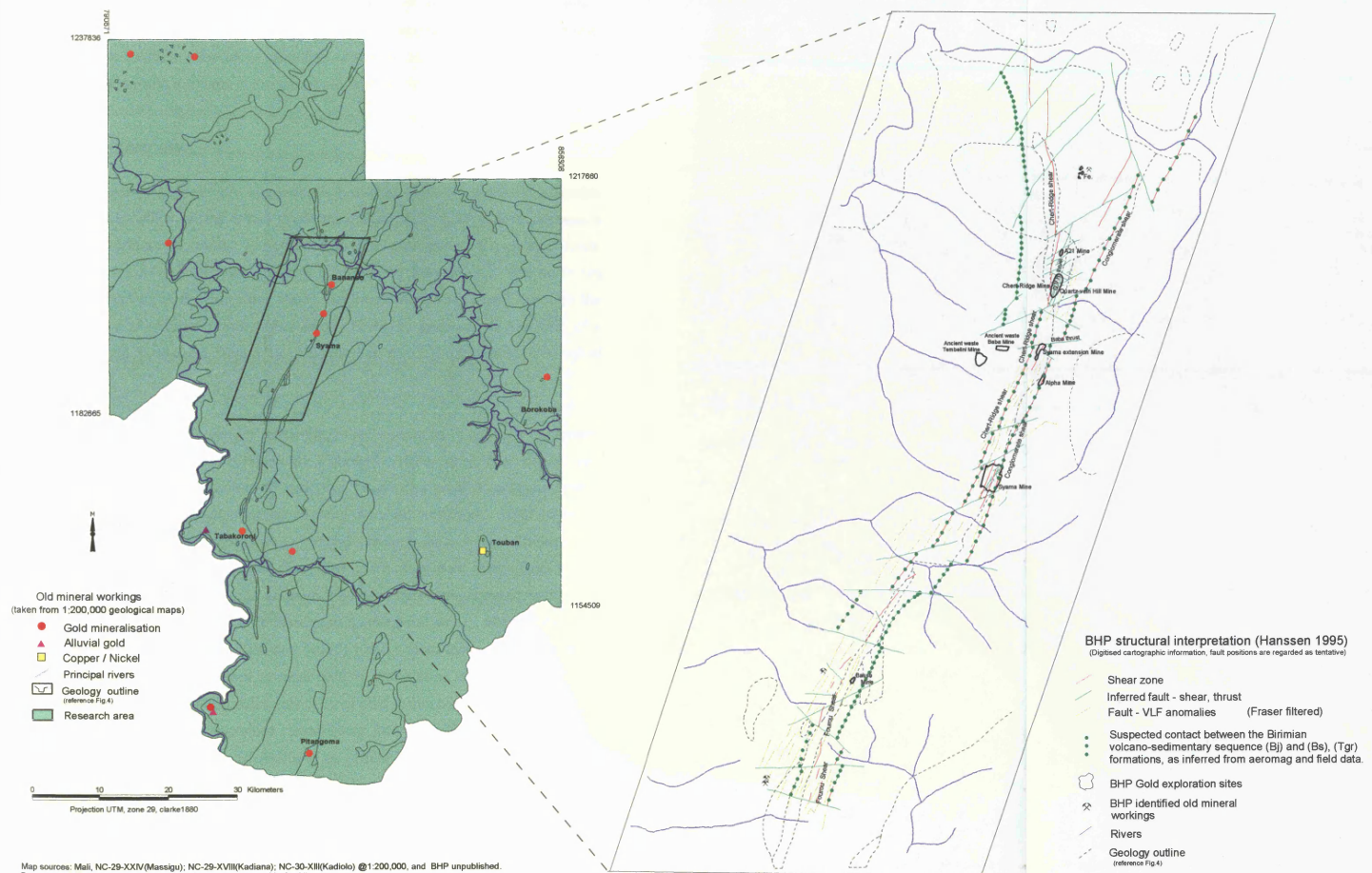
2.5 Known Mineralisation and Deposits.

As previously explained in Section 1.4.3, this region of Mali has had a long history of mineral exploration, especially for gold. Fig. 5 shows the ancient artisan (regolith) gold localities of the region, as identified on the published 1:200,000 geological maps, along with alluvial gold and a nickel/copper prospect at Touban. The latter was discovered through the work of the BRGM between 1972 and 1974. Kusnir et al. (1987) also report a Cr/Ni geochemical anomaly which is centred over the ultrabasic rocks of the small massif at Zekoun (not shown on Fig. 5). Fig. 5 also illustrates the BHP concession, the location of the Syama mine, and its satellite deposits, and a number of artisanal sites, unidentified on the 1:200,000 scale maps. Many of the satellite deposits showed evidence of artisanal mining prior to their contemporary development, a feature which has frequently been reported by companies prospecting for gold and establishing mines, within other regions of Mali (Fig. 2, W.W.W., 1997f; W.W.W., 1997i; lamgold, 1997; Chaplin et al., 1997). It is the author's contention, reinforced by personal communication with Hanssen, that given the long history of artisan mining and evidence gained from within the concession area, many minor artisan sites are omitted from the published 1:200,000 scale geological maps.

2.6 The Birimian volcano-sedimentary sequence and associated gold mineralisation.

There was very little published information regarding lithological relationships and mineralisation within the Birimian volcano-sedimentary sequence, prior to that published through BHP's own investigations or arising from collaborative work within the region. As a consequence, the majority of information recorded in this section is derived from open pit and drill hole data of the Syama mine. Some supplementary information is also drawn from several of the near operational satellite bodies, as well as the investigated Tabakoroni prospect in the south of the region.

Fig. 5 Mineral workings and local structural interpretation.



This section begins with a brief overview of the volcano-sedimentary sequence, followed by descriptions of the host lithologies, alteration patterns, and the sulphide mineralogy identified within the Syama sulphide ore zone. It concludes with a review of the structural complexity of this sequence.

2.6.1 Overview:

The volcano-sedimentary sequence is a narrow (500 m – 2000 m) ensemble of rocks, which reside within a complex shear fault system and possess a near north-south trend. Although regionally extensive and with near-linear form, it is in fact lens-like showing a 'Y-shaped' bifurcation in the north (as described by BHP, Hanssen, 1995). In the south it is believed, through the analysis of magnetic data (West et al., 1995), to terminate in the form of a stretched 'S-shaped' flexure, not identified on the 1:200,000 scale geological map.

In fresh section this weakly metamorphosed sequence is typically comprised of chloritic rich basalt (although Petersen, 1990, describes basalt and gabbro), varying thickness of graphitic greywacke-argillite horizons, minor andesitic (lamprophyric) intrusions, and silicified horizons. Gold is found within all these lithologies but in varying concentrations. Nevertheless, the green chloritic basalt is viewed as the main host of gold mineralisation. At Tabakoroni, however, gold is seen to be preferentially hosted within the graphitic siltstones of the metasediments (Hanssen et al., 1991). Work by Danti et al. (1989) and Petersen (1990) have shown pyrite to be the major gold host. Gold is reported to occur both on and around the margins of pyrite. Danti suggests that approximately 50% of gold within pyrite is less than 1 μm in diameter and are therefore classified as invisible. However, gold is also seen to occur as free gold (Danti et al., 1989; Petersen, 1990; Olson et al., 1992). In contrast, at Bananso and Tabakoroni, Hanssen et al. (1991) have reported finding gold within arsenopyrite. Lithological and ore contacts in most instances are faulted or sheared with dips that often parallel those of the

sequence as a whole, (approximately 55-60° west; Olson et al., 1992) although some deviations from this have been reported. Mineralogically, the sequence as a whole can be subdivided accordingly into a central mineralised sequence which is approximately 200-300 m thick, which is sandwiched between a basaltic, andesitic western hanging wall sequence and an eastern andesitic conglomeratic footwall.

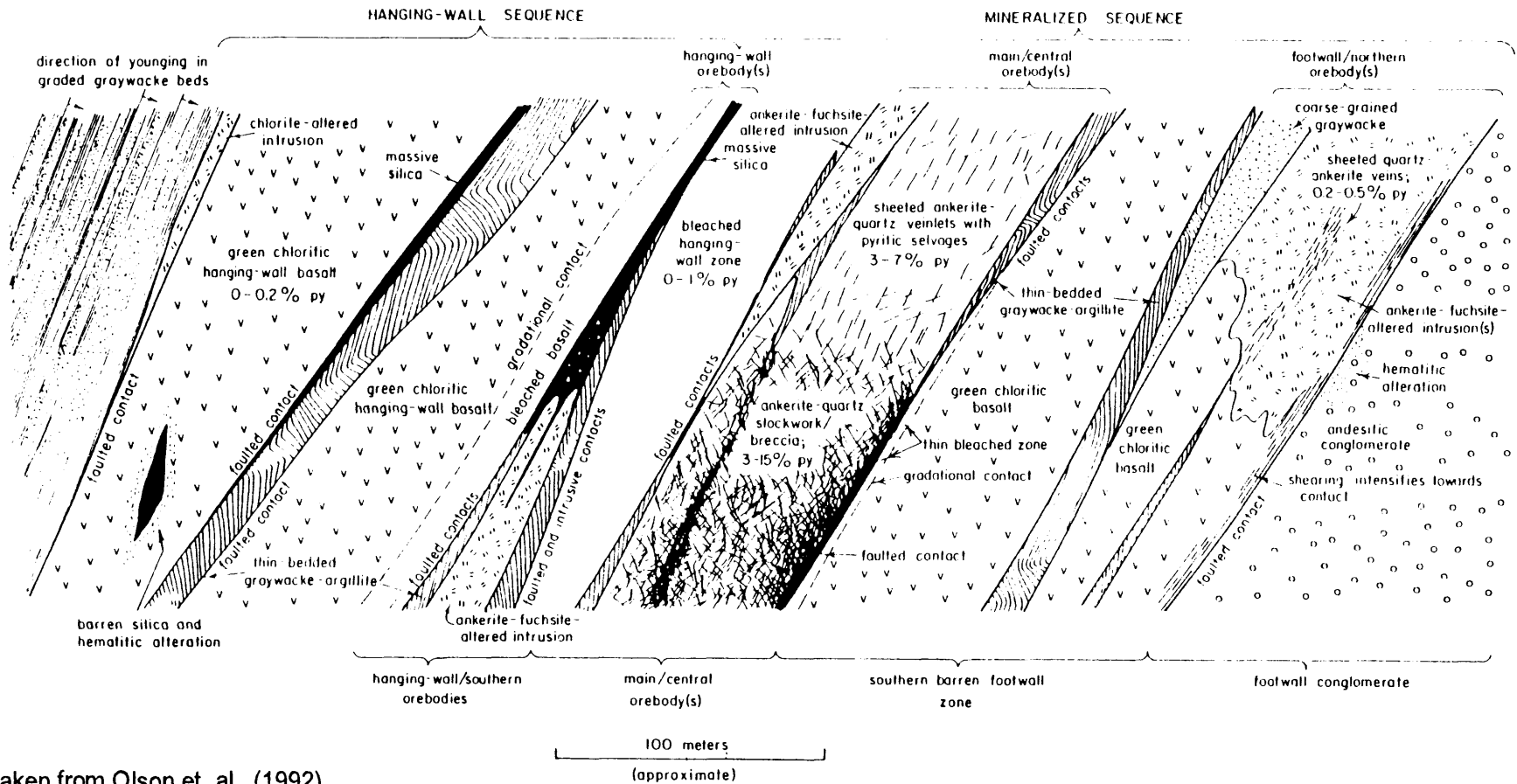
2.6.2 Host lithologies.

The main host lithology at Syama is green chloritic basalt. This shows progressive alteration, bleaching, and pyritization towards the central mineralisation zone. Other lithologies are greywacke, and andesitic intrusions. Their distribution throughout the hangingwall, footwall and central mineralised zone is illustrated in Fig. 6. The majority of the mineralisation is associated with ankerite-quartz veining. Gold concentration varies throughout these lithologies with respect to the pervasiveness of these veins.

2.6.2.1 Basalt.

Considered volumetrically, the basalt is the most prominent lithology present within the sequence. Within the weakly metamorphosed basalt of the hangingwall and footwall various forms of green chloritic basalt have been identified, some of which may contain extremely small concentrations of pyrite and gold; reportedly at less than 0.01 ppm (Petersen, 1990; Olson et al., 1992). Phenocrysts of magnetite ± ilmenite have altered to leucoxene. In the sheared diabasic basalt, typical of the hangingwall, alteration has been somewhat more pervasive, with plagioclase altered to a mixture of carbonate (calcite) and sericite, and with pyroxenes replaced by chlorite. The carbonates are reported as consisting essentially of calcite and dolomite (Colin et al., 1988). The degree of chemical and structural change to the chloritic basalt increases towards the central mineralised zone, until it is altered to bleached basalt. The bleached basalt, forming an encompassing halo to the main central basalt ore body, is distinguishable from its chloritic

Fig. 6 Cross-section through the Birimian volcano-sedimentary unit at Syama.



Taken from Olson et. al., (1992).

counterpart by sericite-ankerite groundmass, and by its ankerite-quartz veinlet mineralogy with accompanying pyrite (Table 2). The central (basalt) ore body is characterised by lenticular bodies of very intense ankerite-quartz stockworks, which blends into hydrothermal breccia of ankerite-quartz-albite and with regions of ankerite-quartz-(albite)-(pyrite) sheeted veinlets (Table 2). The invasive nature of the veinlets virtually obliterates the original texture of the host rock, except for the occasional occurrence of leucoxene minerals. Within the stockwork and breccia zones the veinlets can typically contain concentrations ranging from 3% to 15% disseminated pyrite, representing the highest ore grade (Au >4 ppm) within the deposit (Olson et al., 1992). The areas of sheeted veinlets often show strong pyritic halos and some bleached alteration halos. The average pyrite grade ranges between 3% and 7%, although higher grades similar to those of the stockwork and breccia are possible. Gold distribution throughout the various basalt lithologies shows a dramatic increase within the intense breccia and stockwork zones (Fig. 6).

2.6.2.2 Greywacke-argillite.

Greywacke-argillite lithologies are found in the hanging wall, footwall and the central mineralised zone (Fig. 6). There are two principal forms, as described by Olson et al. (1992):

- (i) thin bedded to laminated, fine grained greywacke and argillite
- (ii) coarse to medium grained, massive, and thickly bedded greywacke, containing mafic to intermediate igneous fragments, plagioclase and quartz.

Within the mineralised zones, strongly sheared thin-bedded greywacke and graphitic argillite, plus fine grained carbonaceous argillite are also present. These are accompanied with sericite, albite and ankerite alteration of the thin-bedded sequences. In all lithologies gold is disseminated within the invasive ankerite-albite pyritic veinlets, and is of lower grade than that found within the basalt.

2.6.2.3 Andesitic intrusions.

Although andesitic intrusions are found throughout the altered and mineralised sections of the sequence, there appears to be some affinity for the faulted and sheared zones within the greywacke-argillite. The width of intrusions varies from centimetres to meter scale, showing on occasions well defined chilled margins. Mineralogically, the least altered intrusions are those that lie furthest away from the central mineralised zone. Those found in the hangingwall (and at the Tabakoroni site) tend to be less altered, and more a andesitic in composition, consisting of plagioclase with minor biotite and amphibole, with green chloritic alteration (Olson et al., 1992). Towards the central zones the intrusions tend to contain more potassium and chrome, in the form of fuchsite. Phenocrysts of amphibole or biotite are altered to quartz, sericite, chlorite, ankerite and green fuchsite-like mica, with leucoxene, ankerite, sericite, quartz, albite and disseminated pyrite forms the groundmass (Olson et al., 1992). Mineralisation occurs in weak stockwork veins of ankerite-quartz where its pyrite concentration averages 0.5-1.0%, producing low gold grades. The inherent poor stockwork development and its complementary low gold grade, compared to its surrounding lithologies, has suggested to Olson et al. (1992) that these intrusions probably post-date the main phase of mineralisation.

2.6.3 Alteration.

Alteration of the protolith has been extensive and pervasive. Petersen (1990) and Hanssen et al. (1991) have described the global character of alteration as consisting of chloritization (chlorite), carbonation (ankerite, calcite), sericitisation (sericite, mariposite/fuchsite), albitisation (albite), carbonisation (carbon, graphite), sulfidation (pyrite) and silicification (quartz).

A cross-section through the Syama deposit (Fig. 6) highlights identifiable zones of increasing alteration towards the main central ore bodies. This zonation, although somewhat complicated by faulting, is best developed

within the basaltic unit, where the least altered peripheral basalts of the hanging wall and footwall are inwardly replaced by bleached basalt and subsequently by mineralised basalt (breccia, stockwork). These zones are typified by the progressive alteration or replacement of virtually all mafic minerals. Olivine and pyroxene are replaced by quartz, ankerite, ankerite-quartz, ankerite-chlorite, ankerite-sericite (\pm fuchsite) or sericite-quartz assemblages; whilst anorthic plagioclase is replaced by albite or by sericite or carbonate (Petersen, 1990). Therefore, taking into account rock, groundmass and veinlet mineralogy, it is not uncommon to find multiple alteration assemblages present within each rock. Of these alterations, Petersen (1990) reports ankerite as the most abundant and texture-destructive carbonate mineral, occupying from 20-80% of rock mass. These occur both as irregular patches disseminated throughout the rock and as selective replacement of feldspar, mafic minerals, and some of the groundmass. Table 2 illustrates the type of rock, groundmass and veinlet alteration recognised within each of the alteration zones of the basaltic host rocks.

Table 2 Alteration zoning in the basaltic host rocks.

	Unaltered basalt	Bleached basalt	Mineralised basalt	Silicification
Rock mineralogy	<i>Phenocrysts:</i> plagioclase, altered to sericite, albite, and calcite. Pyroxene, fresh and altered to chlorite. <i>Groundmass:</i> chlorite, calcite, quartz, leucoxene, altered magnetite and/or ilmenite (pyrite)	Sericite-ankerite-(albite), sericite-ankerite-(chlorite). Sericite, ankerite, (chlorite)	Ankerite, albite, quartz, (sericite), pyrite, leucoxene.	Quartz, pyrite, (leucoxene), (ankerite), (sericite).
Veinlet mineralogy	Calcite, quartz, chlorite. (separate veinlets)	Ankerite, quartz	Ankerite, quartz, albite, (pyrite)	Pyrite, graphitic and pyritic stylolites
Vein selvage	None	Ankerite, (sericite), (albite), (pyrite)	Pyrite, ankerite, albite, (sericite)	No discernible selvage.

Taken from Olson et al., 1992.

Assemblages typically characterise zones, thus the bleached basalt, representing a less intensive alteration, is characterised by sericite-ankerite, with minor chlorite and/or albite; whilst the mineralised basalt is altered to ankerite-albite and quartz.

The alteration pattern identified within the basaltic hosts can be characterised by the depletion and accumulation of elements with respect to zone. Fig. 7a and b are plots of the average chemistry obtained from five bore holes that cut the different alteration zones. Fe_2O_3 and Al_2O_3 show an overall decrease in concentration from 'fresh' to mineralised basalt, accompanied by a similar but less marked trend in MgO. BHP staff suggest that the decrease in these elements could be represented by the presence of hematite and talc-like mica present with the silica (Olson et al., 1992). Although the less striking reduction in MgO shadows in part a response to the alteration and weakening of the 'fresh' MgO rich minerals by subsequent chloritization, sericitisation and carbonation processes. In contrast, increases were identified in SiO_2 , Na_2O , S, and complementary CO_2 and C with respect to the initial 'fresh' basalt. These are indicative of the increasing contribution made by silicification, albitisation, carbonation, sulfidation and carbonisation as the highly altered breccia stockwork zone is approached.

The change from 'fresh' basalt to bleached basalt is marked by the presence of sericite alteration (Section 2.6.2.1, Table 2). Sericitisation, involving the addition of K^+ , H^+ and the removal of Na^+ ions (as described by Dizigbodi-Ajimah, 1992), can be identified on Fig. 7a by the increase in K_2O and reduction in Na_2O of the 'fresh' and bleached basalt.

The andesitic intrusions, which also show an increase in K_2O and a reduction of Na_2O , can be explained in part by sericitisation, and by the presence of fuchsite mica, producing an increase in potassium concentrations (Olson et al., 1992). BHP suggest derivation from surrounding wall rocks, leaching from

Fig. 7a.

Chemical analysis of the mafic igneous host rocks at Syama.

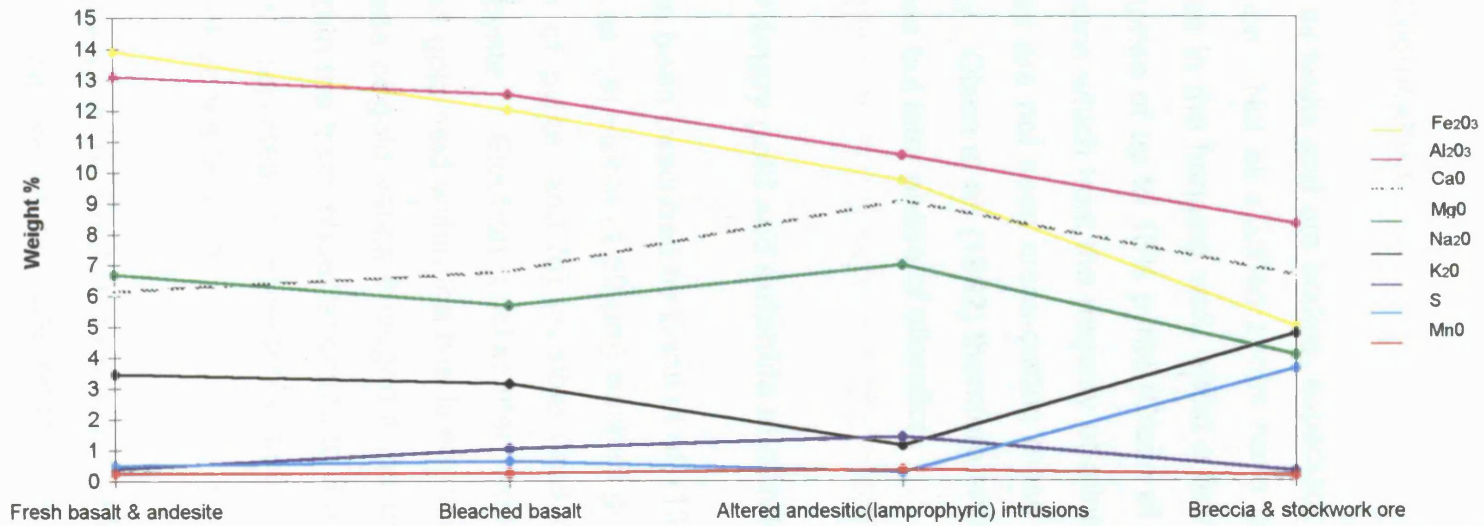
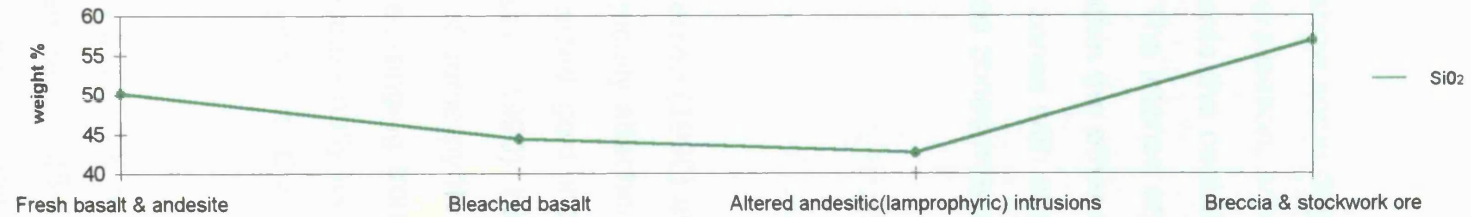


Fig. 7b.

Chemical analysis of the mafic igneous host rocks at Syama.



Data adapted from Olson et al. 1992.

Values represent averages, computed from wet chemical analysis of 5 drill hole datums.

bleached basalt and possible intrusions, with fluid migration via major (and now silicified) faults (Olson et al., 1992).

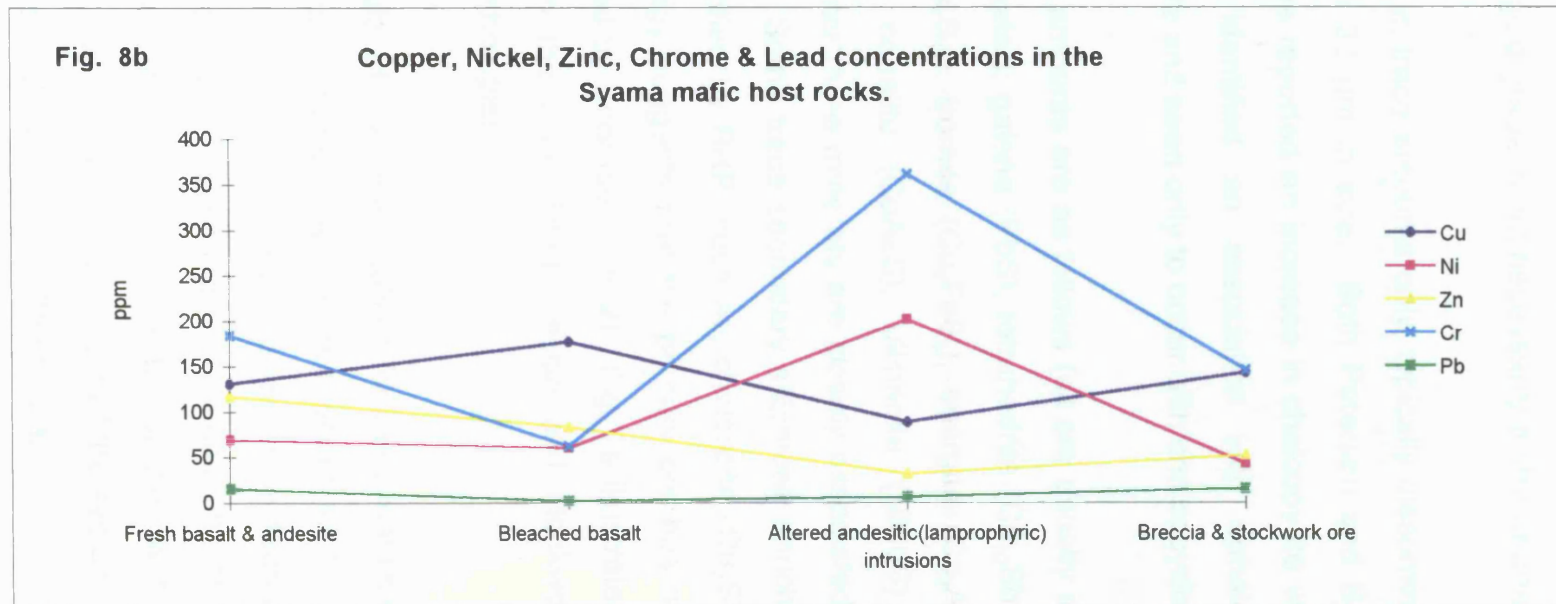
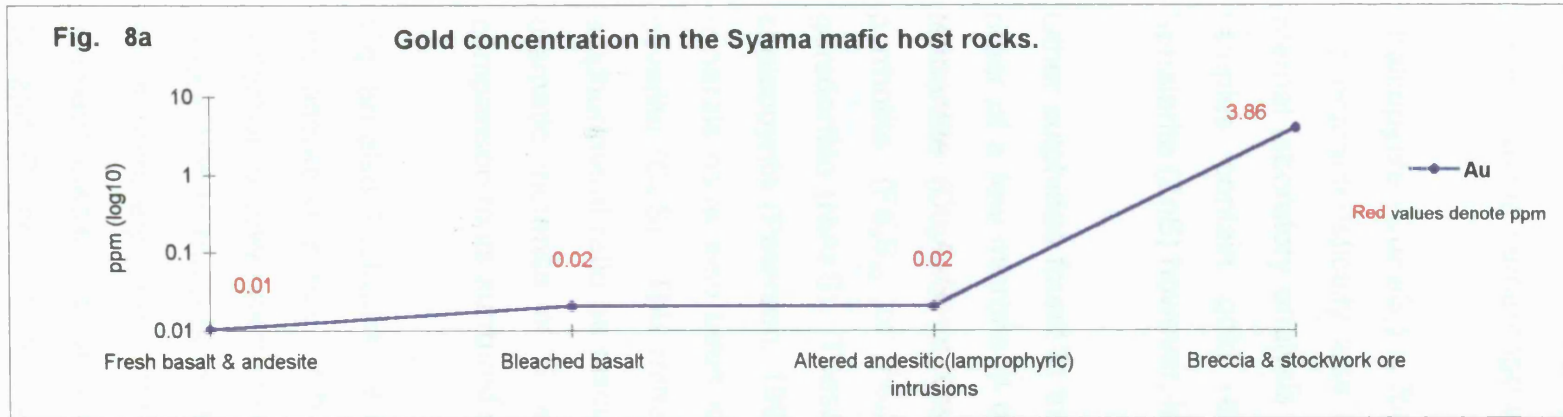
2.6.4 Silicification.

Virtually all faults and ore bodies, especially at Syama, show some degree of silicification. Not all silicified zones have sulphide mineralisation, some are barren, as in the hanging wall, whilst a few others towards the central zone can comprise of up to 15% pyrite (Olson et al., 1992). The intense ankerite-quartz veins which host the majority of mineralisation within the other named lithologies are not seen cross-cutting these silica-pyrite zones with any great regularity. Olson et al. (1992) therefore implies that these zones may well be an intense but later phase of alteration.

2.6.5 Primary gold and sulphide mineralogy.

Gold has been described by Danti et al. (1989) and Petersen (1990) as being present as: (a) visible (1-50 μm) isolated gold grains, typically attached to the margins of pyrite, and (b) invisible (less than 1 μm) sized gold inclusions within pyrite. Electron backscatter work by Petersen (1990) has also identified gold held within the fine linear microfractures of some pyrite grains. The grade of gold varies throughout the unoxidised ore, ranging from <0.01 ppm within the fresh basalt/andesite to 3-5 ppm (and occasionally as high as 24 ppm, reported in Petersen's petrographic analysis) in the breccia stockwork zones (Fig. 8a).

Pyrite (FeS_2) is the predominant sulphide and occupies from <1% to 20% of rock volume, whilst on rare occasions it may even reach 35-40%, as established by Petersen's petrographic analysis. Petersen believes that the majority of pyrite found is, in fact, the result of rock sulfidation. Pyrite is commonly found disseminated within the rock, though small clusters are not



uncommon. The crystals can range from 20-600 μm , often showing radial bladed quartz overgrowths. Although pyrite is the principal gold bearing sulphide, Petersen's petrographic analysis establishes that the relationship between pyrite percentage and gold grade is not necessarily a strong one.

Chalcopyrite (CuFeS_2) is found in trace amounts only, typically disseminated and characteristically less than 20 μm in size. Both Petersen and BHP's internal laboratory analysis have reported an increase in chalcopyrite where samples contain gold; and identified an association with sphalerite. Sphalerite (ZnS) however, is rare and seen only to occur with chalcopyrite.

Other sulphides found in trace amounts are as follows (all are usually in the order of a few microns in diameter): galena (PbS), tetrahedrite ($\text{Cu}_{12}\text{Sb}_4\text{S}_{13}$), tennantite (Cu_3AsS_3 or $\text{Cu}_{12}\text{As}_4\text{S}_{18}$), bornite (Cu_5FeS_2), enargite (Cu_3AsS_4), pyrrhotite (Fe_9S_{10} or Fe_7S_8), cobalite (CoAsS), ullmanite (NiSbS) and gersdorffite (NiAsS). These latter three minerals are closely associated with chalcopyrite (Petersen, 1990). Some trace secondary sulphides enrichment minerals have also been identified by BHP, such as; chalcocite (Cu_2S) and covellite (CuS). This mineralogy suggests that the primary ore has a high sulphur/metal ratio as discussed by Thornber, (1992). Fig. 7a illustrates this dramatic increase of S within the mineralised breccia and stockwork in comparison to its surrounding lithologies.

Fig. 8b also illustrates the results of chemical analysis for base metals within the alteration zones. Pb is characteristically low throughout all zones, a reflection of only galena being reported. Zn shows a progressive decrease in concentration towards the breccia and stockwork ore. This could be an effect of its relatively high mobility and its failing attempts to complex with other element species, consequently it is effectively moved out of the system. Both Ni and Cr concentrations are high within the 'fresh' basic rocks, which realistically would not be deemed atypical. An increase of Cr within the andesitic intrusions, however is likely to be the response to the presence of

the fuchsite mica (Section 2.6.2.3). Cu shows slight fluctuations, increasing in the bleached zone, but decreasing in the andesitic intrusions.

2.6.6 Volcano-sedimentary structure.

Although it is accepted that the Birimian volcano-sedimentary sequence resides within a north-south trending shear zone, a regional map detailing the complete structures has yet to be published.

BHP, however, have produced an unpublished structural map of their concession area, as illustrated by the enlargement on Fig. 5. This was developed from ground VLF work and open pit field observations. Consequently, the locations of some of the structures are still regarded as tentative interpretations rather than absolute. Their work has highlighted a 1000 m - 1500 m wide shear-bounded faulted zone, which strikes between N010° and N030°. This zone, along with its internal fault splays, is cut and displaced at regular intervals by northeast-southwest orientated faults, and, to a lesser degree by east-west and northwest-southeast faults respectively. The overall nature of the faulting throughout this area is shown to be a complex mixture of shears, thrusts, and normal and reverse faults. On a local scale faulting within the pits can be very complex, with duplexing, imbrication, anastomosing, and transverse jog faulting, intermixed with the larger scale thrusts and shears (Olson et al., 1991 and 1992; Hanssen et al., 1991; Hanssen, 1995). Many of these smaller scale structures can not easily be correlated with any accuracy within the sub-regional scene. Fault movement both at the sub-regional and pit scale has been identified to be both dextral or sinistral in nature, the former is proposed to represent the tectonic rifting phase allied to the main mineralisation event (Hanssen, 1995). Detailed descriptions for some of the identified regional faults shown in Fig. 5 are as follows:

1. The conglomeratic shear represents the eastern north-south shear, marking the boundary between the basal conglomerates of the greywackes (Tgr, Fig. 4) and the basaltic rocks of the volcano-sedimentary unit. This shear is seen in the pits at Syama, Alpha and also at the Syama extension to the north. BHP staff assume that it continues northwards forming the eastern limit of the Y bifurcation.
2. The Chert Ridge Shear (C.R.) represents the western flank of this north-south shear, a zone which is approximately 10-30 meters wide. This fault is also believed to extend northwards to the Banifin River, and forms the western area of the bifurcation. BHP staff believe this can be traced in part through the identification of intermittent silicified chert outcrops. In the north, this shear is presumed to be surrounded by the volcano-sedimentary sequence, which is cut and displaced most frequently by northeast-southwest trending faults.
3. The Quartz Vein Ridge Thrust (Q.V.R.), believed to be a duplex thrust, splays off from the Chert Ridge Shear at an angle of approximately N030°. This zone represents a complex, structural setting within which the Chert Ridge and Quartz Vein mines are located. The thrust has been traced northwards where it is identified within the A21 mine.
4. The Baba Thrust, which strikes N080° / 30° N, and which is identified along the northern wall of the Syama Extension Pit. It is believed to cross-cut and offset both the Chert Ridge and the Conglomerate Shears, resulting in a widening of the shear to the north and a reduction in width to the south of the thrust.
5. To the south of the study region, the Fourou Shear has been identified, and its trace implied by the surface expression of chert outcrops. It has a 4 km trace of varying width and exhibits a slight sigmoidal form, passing west of the Basso Mine before dissipating.

In conclusion, there is very little spatial correlation between the faults displayed on the published 1:200,000 Kadiana map and the corresponding structural map produced by BHP.

2.7 Regional similarities – A summary.

Subsequent to 1992, work by BHP revealed new data comprising six areas of explorative interest outside of Syama, but which lie within their current exploration permit. These areas, along with those previously described, are located on Fig. 5.

Slight differences of geology and mineralogy do exist between these areas. However, their differences are outweighed by the similarities, which are as follows:

1. The thin Birimian volcanic sequence houses all known gold prospects (Olson et al., 1992).
2. Known prospects are located within the highly faulted shear zone, or within offshoot splays, and show evidence of reverse faulting (Olson et al., 1992).
3. Faults are often complex, with lithological contacts steep and dipping typically 55-60° west.
4. The majority of high-grade gold is hosted by basalt.
5. Andesitic (lamporphyric) dykes intrude lithologies.
6. Silicification bounds most faults and ore bodies.
7. Alteration within the mineralised lithologies is characterised by sericite, carbonate and albite.

CHAPTER 3

THE WEATHERED ENVIRONMENT.

Contents.

- 3.1 Introduction.**
- 3.2 Theories of laterite genesis.**
- 3.3 A typical laterite profile.**
- 3.4 The effects of past and present climate on laterite formation.**
- 3.5 Topography and its effects on laterite formation.**
- 3.6 Profile variations with regard to lithology.**
 - 3.6.1 Weathering processes.**
 - 3.6.1.1 Hydration.**
 - 3.6.1.2 Hydrolysis.**
 - 3.6.1.3 Oxidation.**
 - 3.6.1.4 Simple solution.**
 - 3.6.1.5 Transformation.**
 - 3.6.2 Mineral resistance.**
 - 3.6.3 Mineral decomposition: the resultant profile.**
 - 3.6.4 Element distribution within the profile.**
 - 3.6.5 Gold distribution within the laterite profile.**
- 3.7 Laterite within the research area.**
 - 3.7.1 Description of the lateritic profile and its geochemistry.**
 - 3.7.2 Element mobility within the profile.**
 - 3.7.3 The distribution and mobility of gold within the profile.**
- 3.8 Regolith geochemical dispersion models.**
 - 3.8.1 The savannah geochemical dispersion model.**
- 3.9 Summary- The established problem.**

3.1 Introduction.

This chapter is concerned with describing the geochemical weathering environment of laterite within the savannah landscape. It discusses profile form, the mobility and distribution of elements within the laterite, and finally the implication of the latter with respect to landscape geochemistry.

The chapter begins by explaining some of the early theories of laterite formation (Section 3.2) and the inevitable controversy which surrounded these theories. This is followed by Section 3.3, which describes and illustrates a lateritic profile from bedrock to ground surface, highlighting the typical structure developed by prolonged weathering. Section 3.4 and 3.5 explain how a lateritic profile can be altered chemically and physiologically by both climate and erosion, factors which are important in governing the geochemical evolution of a landscape. Section 3.6 and its subsections begin by briefly describing the type of chemical weathering occurring under peritropical conditions. It also details, through the use of examples, how different bedrock material weathers progressively into aluminosilicates and oxyhydroxides in the upper portions of a profile irrespective of the source lithology. Subsection 3.6.4 explains in detail how certain elements possess affinities for particular horizons within the profile. The mobility and adsorption of elements are discussed with reference to Eh/pH conditions and the chemical composition of horizons. Subsection 3.6.5 examines through the work of leading geochemists the causes and controls of gold solubility and precipitation and discusses, with examples, the reasoning behind the spatial distribution of gold in lateritic profiles. Section 3.7 looks at the laterite from two regions within the research area. It discusses the structure and geochemical composition of each lateritic profile and examines element distributions throughout the profiles with respect to horizon composition, thereby providing a link to the processes previously described in Sections 3.6.4 and 3.6.5. The final part of this chapter (Section 3.8 and Subsection 3.8.1) introduces the important concept of landscape geochemistry. This is in

essence an acceptance that there exists an important link between geochemical dispersion, landscape evolution and regolith formation. This link is born out by the introduction of numerous models which seek to clarify and categorise geochemical information based upon type areas or climatic zones. Section 3.8.1 takes one such model that has been developed around a savannah climatic regime. It discusses, mostly through the use of examples, the implications that horizon geochemistry or the level of profile truncation has upon the geochemical signal received. The importance regarding the presence, absence and heterogeneity of overburden in the obscuring of geochemical signals is also addressed. A summary of the chapter is provided in Section 3.9.

3.2 Theories of laterite genesis.

Controversy has surrounded the genesis of laterite ever since the early work of Buchanan, published in 1807. He described laterite as having a distinctive colour and hardness, but also mistakenly classified it as a rock. This misclassification was recognised and corrected by subsequent workers such as Benza (1836), and by Clark (1838) who proceeded to describe laterite as a residuum; in other words a left-over from the in-situ weathering of an original rock mass. This re-classification resulted in the first theory of laterite genesis, known as the "residuum school of thought". This theory was developed further by Russell (1889), and later by Glinka (1914), emphasising that laterite formation was not only the product of weathering processes but also the result of chemical solutions which acted preferentially in the removal of material.

As a consequence of Glinka's work the process of precipitation was incorporated into the residuum theory. The formation of laterite was deemed to involve two stages. The first of these was responsible for the release and retention of the most resistant and least mobile elements from the parent rock. This was followed by a short-lived mobile phase, probably induced by

the actions of ground waters (Harrison and Reid, 1910). In this latter stage the normally immobile elements become mobilised through re-solution and are eventually precipitated. This basic concept was also used in an explanation of laterite formation developed by DuBois and Jeffery (1955). They emphasised the need for an overhead source of mineral enrichment which was coupled to the precipitation of iron solutions found in the soil once contact was made with ground waters.

Thus, one of the key issues surrounding the residuum theory is its requirement for an overhead source. This was always highly questionable since the source would have to be inordinately thick in order to account for the depth of some laterites that are found today. In view of this problem Maclaren forwarded an alternative theory for laterite formation in 1906. He suggested that laterite was not the product of in-situ rock decomposition, as had been previously suggested, but instead that it was the result of mineral precipitation arising from seasonally fluctuating ground waters. It was postulated that these ground waters derived their mineral source from underlying and nearby lithologies. Maclaren's proposition was reiterated by Campbell in 1917 and it gave rise to the second major theory of laterite genesis, known as the "precipitate school of thought". The precipitate model represented a fundamental shift in the theory of laterite genesis for it suggested a completely opposite source, with movement and enrichment being essentially upwards rather than downwards. The upwards movement was driven by seasonal fluctuations in ground water level further assisted by capillary action. In contrast, the residuum theory deduced that the movement of elements was always downwards and emanating from an overhead source.

One of the main foundations of support for the precipitate theory came from the identification of leached "pallid zones" within lateritic profiles (Maclaren, 1906; Simpson, 1912). Since the pallid zone was iron-depleted this was believed, in part, to represent the source of the iron found in upper horizons. Other features of the precipitate theory are that it requires the existence of a

planation surface, and that it dictates that the depth of a laterite is a direct reflection of its age. Quite simply, older laterites are expected to have a greater depth than younger ones.

Unfortunately, much of the evidence used to support the precipitate theory was circumstantial. On examination it was found that the pallid zone was not present in all laterite profiles, and neither was the presence of a planation surface (McFarlane, 1976). The mechanism for enrichment, namely an oscillating water table and capillary action, also came under scrutiny and criticism. Many later writers have discounted the concept of capillary action as a major contributing mechanism for laterite formation (e.g. Goudie, 1973). Furthermore, others (Prescott and Pendleton, 1952; Goudie, 1973; Trendall, 1962) have found the proposed dynamics of water table movement necessary for the existence of some laterites to be scientifically unsubstantiated, although they do acknowledge the involvement of the water table. Trendall (1962) has also queried the concept of the pallid zone being the original source area for the iron present in a laterite. He found that there was no correlation between pallid zone thickness and laterite thickness, and that the two were not mutually compatible. It has also been noted that the accumulation of iron can not be adequately explained in those situations where the pallid zone is not present within the profile (McFarlane, 1976).

The final outcome of this debate was that neither the residuum theory nor the precipitate theory could, when taken alone, adequately explain all cases of laterite formation and the variety of lateritic profiles. Furthermore, neither theory could account for the variation in topographic location of laterites whereby both high and low level formations are found. Because of these difficulties opinion has drifted towards a dual source. One such advocate was Trendall (1962) who sought both an overhead and underlying component for the mineral source that is needed for laterite formation. He did not reject the concept of enrichment coming from the pallid zone, due to the actions of a fluctuating water table, but incorporated a new and important notion that the

whole profile transgresses downwards due to erosion. The importance of this transgression, is that new material is always being entered into the system.

McFarlane (1971 and 1976), and subsequently Butt (1981 and 1987) regard laterite as a residual precipitate. They accept and work with the premise of land surface reduction with a downward movement of the profile, but reject the idea that the pallid zone is the iron source for the surface laterite. Instead, they believe that the pallid zone represents a path through which the oscillating water table has moved, and that it is the zone where iron is segregated from minerals through redox reactions. The re-mobilised iron and aluminium oxides are then precipitated, principally by Eh control (Maignien, 1978), as mineral replacements and as coatings and concretions, with enrichment coming both from above and laterally. With the continual downward movement of both the profile and the water table, hydration of the upper residuum eventually results in the formation of a hard, ferruginous, and impermeable surface deposit. This is known as a duricrust or cuirasse. The cuirasse is dominantly composed of highly stable and resistant minerals such as kaolinite, gibbsite, hematite and limonite.

Thus the current thinking within the literature (e.g. Butt and Nickel, 1981; Butt, 1981; Roquin et al., 1990; Nahon and Tardy, 1992) is that laterite is a weathering residuum that develops in-situ from the breakdown of original parent material. Horizon stratification evolves over time with clear visible and physical differentiation. It is believed that each horizon is derived from that which underlies it. Furthermore, the weathering process of element breakdown, the mechanics of leaching, and a redistribution and concentration of elements produces geochemical differences between regolith horizons.

Horizon II : Saprolite. this is often split into a
Lower coarse grained level (A), and
an upper fine grained level (B)

Horizon I : Parent lithology.

The characteristic of each horizon is now described briefly in turn, with reference to Fig. 9. It should be emphasised that gradational boundaries are generally expected between these units as opposed to discrete or abrupt changes.

Horizon I : Parent lithology.

This horizon has normally remained free from weathering although at its upper surface, where contact is made with Horizon II, it may show some secondary minerals in fissures.

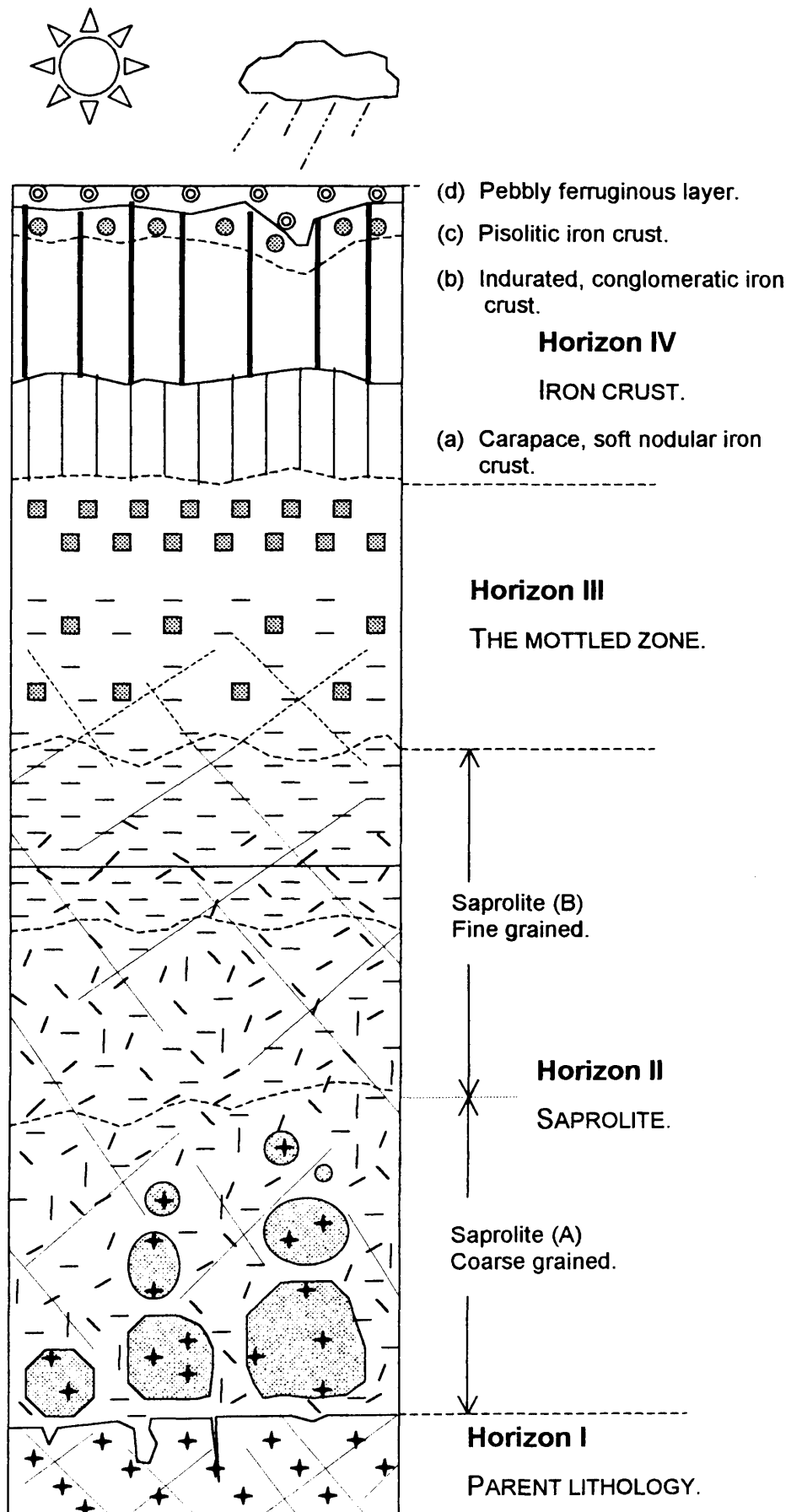
Horizon II : Saprolite (A).

Coarse grained region or "saprock". Horizon II(a) is characterised by varying sizes of dismantled parent lithology caused by the weathering process. Nahon and Tardy (1992) report that petrographic examination reveals primary minerals to be dislodged and replaced pseudomorphically by isovolumetric weathering products. At the upper limits of this horizon no primary minerals exist, rock porosity increases, and the overall colour changes from yellow nearer its base through to red. Mineralogically, some smectites and kaolinites form at the base of the horizon, iron hydroxides replace iron bearing primary minerals and Fe³⁺ bearing (ferric iron) minerals. Kaolinites develop from the breakdown of feldspars.

Horizon II : Saprolite (B).

Fine grained region. In this zone virtually all primary minerals have been altered to secondary minerals, i.e. kaolinite, goethite, or amorphous iron oxyhydroxides. Only the most resistant primary minerals remain, such as quartz, zircon, tourmaline and chromite. Although weathering is extensive in

Fig. 9 Sketch of a typical lateritic iron crust profile.



this zone the original rock fabric is perfectly preserved. The saprolite at the base of the zone is characteristically fine grained and slightly porous. However, it changes with height into a more massive clay dominated form, resulting from the secondary precipitation and accumulation of kaolinite from the breakup of primary minerals. Provided they are saturated below the water table both kaolinite and goethite exist in this horizon, forming from the breakdown of feldspars and ferromagnesian minerals. This fine saprolite zone is often referred to as the “pallid zone”.

Horizon III : The mottled zone.

The mottled zone is located above the water table in the unsaturated oxidising region. Two principal destructive processes operate within this region: Firstly, the vertical and lateral percolation of ground water leads to the formation of small voids. Secondly, mobilisation and re-precipitation of iron occurs. This latter process leads to the development of ferruginous spots, or mottles, ranging in size from 0.5 cm to 1 cm, and also to the development of indurated nodules. Indurated nodules are 1 cm to 3 cm in size and are a precursor to the presence of the concretions that increase in abundance towards the top of the horizon (Nahon and Tardy, 1992). Nahon and Tardy (1992) report that iron is mobilised, re-precipitated and becomes concentrated in the clay-rich areas of this horizon. Furthermore, kaolinite is replaced by hematite to form Al-hematite. As a result of this activity any pre-existing structure inherited from the parent rock is obliterated in the upper portions of this horizon as the indurated nodules accumulate.

Horizon IV : Iron crust.

This uppermost horizon lies above the mottled zone. It is believed to have developed as a result of the continuing coalescence of the hematite nodules present in the mottled zone, and through dehydration. Eventually these processes lead to an indurated cuirasse. On closer inspection the horizon is seen to be composed of further characteristic sub-horizons or layers. The

basal crust lying in contact with the mottled zone is soft and nodular but is gradually replaced by a more conglomeratic structure formed by the in-situ accumulation of iron oxides. Towards the top of this conglomeratic iron crust an outer coating of aluminous goethite develops on the nodules. Over time a pisolitic structure develops due to concentric growth by rehydration and also due to the replacement of Al-hematite by Al-goethite. Ultimately, cohesion diminishes in the indurated surface as pisolith size reduces and as cracks and dissolution features develop. Almost pure goethite and minor kaolinite form between the cracks and fissures of the pisoliths. Thus the final ferruginous and somewhat pebbly layer is regarded by Nahon and Tardy (1992) to be the result of geochemical degradation of the indurated cemented iron crust which underlies it.

With the onset of greater aridity and/or a lowering of the water table, leaching of the upper horizons continues. The dehydration and hardening of the iron oxides and siliceous horizons culminates in the formation of an oxidised cuirasse. The iron present in this horizon can take on numerous forms depending on the specific climatic environment. In dry or seasonally dry environments it is most likely that the dehydrated iron forms of hematite and boehmite will develop. In contrast, in a wetter environment hydrated goethite and gibbsite are likely to predominate. However, it is also not uncommon to find higher proportions of dehydrated Fe-oxides closer to the surface than the hydrated forms, or pisoliths with a goethite cortex and a hematite shell (as observed by Colin et al., 1988).

In summary, horizon boundaries in laterite are not sharp and discrete but gradational. The mass transfer between horizons is predominantly vertical. Only the most resistant elements, or those capable of complexing or being picked up by scavenging Fe-Mn-oxides, reach the upper horizons. Overall, there is an upward increase in Al and Fe within the profile and a loss of the most mobile constituents such as alkalis and alkaline earths (Table 3). A laterite developed in-situ and subjected over time to natural vertical descent

through the processes of landscape erosion should, through the actions of this process, have incorporated into its upper horizons some bedrock signatures. This has been the suggestion of both Roquin et al. (1990) working in Mali, and Matheis (1981) working in Nigeria. However, the geochemical signal derived from the bedrock or underlying mineralisation is progressively modified depending upon the horizon and degree of evolution present within the weathered landscape. These issues are discussed in some depth in this chapter.

Table 3 Chemical effects of deep weathering – summary.

i	Leaching of mobile elements (alkalis, alkaline earths, and components from oxidizing sulphides)
ii	Formation of stable secondary minerals (clays - principally kaolinite, Ti and Al oxides)
iii	Partial leaching of less mobile constituents (silica, alumina, titanium)
iv	Mobilisation and partial reprecipitation of redox-controlled constituents (iron, manganese), as hydrous oxides near the water table.
v	Retention and residual concentration of resistant minerals (zircon, chromite, magnetite, quartz)

Source: Butt, 1987; Butt and Zeegers, 1992.

3.4 The effects of past and present climate on laterite formation.

The climate, and most notably temperature and moisture availability, controls the development of both landform and regolith. In terms of the regolith, significant changes in climate can have considerable effects upon a profile (as described by Lucas and Chauvel, 1992). Climate can cause the rate of regolith development to alter, and may also change the chemical and mineralogical nature of the residuum. The climate can also alter the active dispersion processes at the subsurface and surface level (Butt, 1987; 1988a), and change or influence the mechanisms of erosion and sediment

transportation. These findings are the result of regolith-geochemical research performed in differing climatic regions funded by government assisted research organisations and exploration companies (McFarlane, 1976; Butt, 1987; Lucas and Chauvel, 1992; Thornber and Taylor, 1992; Smith, 1996).

The majority of the research has originated from Australia where the quest for new mineral deposits is confronted by the obstacle of deeply weathered regoliths of Tertiary age. Further difficulties arise from the fact that thick younger sediments or transported material often overlie these regoliths. Consequently, bodies have emerged such as the Laterite Geochemistry Research Group within CSIRO (Commonwealth Scientific Industrial Research Organisation), and more recently, CRC LEME (Co-operative Research Centre for Landscape Evolution and Mineral Exploration). Their research has resulted in a widespread acceptance that geochemistry is an integral component of, and responds to, changes in regolith-landscape evolution (Butt, 1987, Smith, 1996). This is a concept originally advanced by the Soviet scientist Polynov, in the 1930s and reiterated by both Bradshaw (1975) and Fortescue (1975; 1992) in their landscape geochemistry approach.

The generic link between climate, landscape-regolith evolution, and geochemical dispersion are important concepts when considering the movement of continents over geological time due to the actions of plate tectonics. Continents which have moved considerable distances and have been geologically stable (Australia and India, for example) are likely to have been subjected to a variety of climatic regimes during the passage. This will have resulted in the regoliths and dispersion patterns of some regions assimilating and retaining the effects of past climatic conditions, which may well have been in existence for longer and have been more extreme in nature than the current climate under which they are found. Understandably, this situation can lead to quite complex sequences and dispersion patterns (Butt, 1978; Smith, 1996). In contrast, those continents that have had little movement beyond the equatorial margin over the last 180 million years

(Central Africa and parts of South America, for example) will have experienced little in the way of climatic variation. Therefore, the effects of sub-aerial weathering on landform-regolith development and dispersion should have remained relatively constant and accumulative in nature. Budel's (1982) morphoclimatic zonation was devised around this premise, namely that similarities can be drawn between regions that have had similar weathering histories and landform development cycles (or palaeoclimates). Therefore, although the majority of deeply weathered regoliths reside between 25°N and 25°S of the equator, the morphoclimatic zone is of particular importance when assessing landscape-geochemical evolution within and between regions.

According to Budel's classification, Mali resides within the peritropical zone, which is represented by the seasonal tropics or savannahs. It is possible through plate reconstruction to observe the movements of Mali during the past 180 million years (Dietz and Holden, 1970). This shows a movement that has had no dramatic climatic implications, suffering only minor fluctuations of humidity during the Tertiary Period (Kusnir, 1987; Butt, 1987). These conditions have resulted in the formation of deeply weathered regoliths, which are highly characteristic of the region and exhibit typical chemical effects as portrayed in Table 3.

3.5 Topography and its effects on laterite formation.

In the peritropical zone the climate, aided by the processes of erosion, sediment transport and deposition, helps to sculpture the land surface producing the familiar topography of rounded hills, slopes and valleys. The topographic forming processes, through their actions, also modify the laterite with respect to the horizon that is exposed and its geochemical signal expressed at the surface (Ambrosi 1984; Butt, 1987; Roquin et al., 1989; Roquin et al., 1990; Zeegers and Lecomte, 1992; Smith, 1996), as discussed in Section 3.8.1.

The highest most elevated positions within a lateritic terrain are often the oldest and therefore are also the most highly evolved both physically and chemically (as discussed by Tardy et al., 1988; Roquin et al., 1990). As such these regions are often characterised by a full, well developed profile (as detailed in Section 3.3, Fig 29). The preservation of these profiles and their elevated position are largely attributable to the protection afforded by the surface indurated ferruginous cap (Butt, 1981). Since these regions become elevated with respect to their surroundings due to erosion, it would be reasonable to assume that the surficial materials have developed in-situ with no allochthonous contribution.

On slopes however, the situation is very different and profiles can vary depending upon the angle of repose. In regions of steep slopes, which characteristically occupy the upper portions of a slope profile, lateritic horizons are often eroded through. On the lower regions of a slope profile, where angles are generally much gentler, the potential surface area truncated through each horizon is far greater, often dissecting into the lower lateritic horizons (Section 3.8.1, Fig 29 and 30). However, the vertical movement of residual material downslope through surface wash and gravitational particle instability is somewhat complicated in comparison to hilltop processes. On high angle slopes little transported material is stable upon its surface, whereas on gentler slopes where kinetic energy can dissipate, deposition will occur. The deposited material will be somewhat heterogeneous in nature and will therefore be a combination of transported upper slope material, gravel-like material resulting from the break-up of the ferricrete (as described by Roquin et al., 1990), and in-situ material. In the wetter season however, the down slope movement of material may be impeded due to the greater presence of vegetation contrasted to the summer, when vegetation has burnt back.

Finally, the topographic lows are generally the valleys through which ephemeral rivers flow. These regions can often truncate into the lower lateritic horizons of the mottled zone or saprolite. The valleys act as terminal

depositional zones, accumulating materials derived from upslope and also that from in-situ weathering. The material within these regions maybe added to further by the actions of termites (as described by Roquin et al., 1990) which bring to the surface material that is derived from lower horizons. This is eventually accumulated as silty clay in the valley flats. Out of all the regions described so far, it is the topographic lows which have the greatest potential volume of allochthonous material present.

Topography may also cause geochemical conditions to change between upslope and downslope due to differing drainage conditions. Lucas and Chauvel (1992) explain that elements leached from the well-drained upslope areas can be transported and accumulated, causing enrichment within the water table zone of downslope regions.

The topography of a region plays an important role when attempting to understand and anticipate the spatial distribution of lateritic horizons, the potential contribution made to a site by allochthonous material and its general directional flow path. It can also help us to understand the geochemical distribution of elements across a surface by the extent of land surface erosion. The inter-twined nature of landscape evolution and topography often result in what has been described as a patchwork pattern of facies across a lateritic surface (Roquin et al., 1990).

3.6 Profile variations with regard to lithology.

Variations in profiles are believed to be due to the combined interactive effect of the current climate and palaeoclimate, topographic position, and the underlying parent lithology or protolith (Butt, 1981).

The parent lithology, although obscured by the overlying regolith, still emits signals into the regolith due to the in-situ development of laterites. In the lower horizons where the effects of weathering have been less intense, the mineralogical assemblages present are representative of the parent lithology.

Moving up the profile towards the upper near surface horizons leads to a progressive weakening of the similarity between the bedrock and the weathered sediment. The amount of weathering a given lithology incurs is in part governed by its microenvironment, as described by McFarlane (1976). This involves lithological parameters such as mineralogical composition, porosity, and permeability, and external parameters such as Eh and pH that govern element solubility. Butt (1981) has also acknowledged that lithological disintegration may be further enhanced by the presence of structural features such as shears and faults, which may act as deep conduits for the ingress of percolating ground waters.

3.6.1 Weathering processes.

Regolith formation under peritropical conditions is dominated by chemical weathering. The principal types of reactions associated with this form of weathering are as follows.

3.6.1.1 Hydration: The absorption of water molecules into the crystal structure of a mineral. This process can often occur alongside other weathering reactions. Two such hydration reactions are where aluminosilicates transform into clays, and iron minerals transform into hydrated ferric oxides

3.6.1.2 Hydrolysis: This causes the dissociation of water molecules, consumption of H^+ ions, and the production of OH^- ions, as described by Trescases (1992). This reaction typically operates within the pH range of 5.0 to 9.0. Rose et al. (1990) regard this reaction as the most important in terms of rock disintegration, particularly in silicate weathering. The hydrolysis reaction can produce clays or iron oxides from an initial silicate mineral bearing aluminium (Al) or iron (Fe). However, aluminium, which is incorporated in most primary silicates such as feldspars, micas, pyroxenes and amphiboles, is at its least soluble within the acting

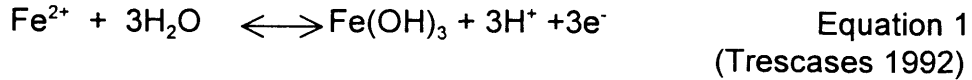
pH range of hydrolysis. As a consequence, aluminium released by hydrolysis is not easily removed from the weathering profile. The result is that the clay groups of kaolinite, montmorillonite and vermiculite, produced through the weathering of primary aluminosilicates, all retain Al. Perdo (1966) identified three types of hydrolysis reactions involving aluminosilicate minerals, each believed to characterise a particular climatic environment, as illustrated in Table 4. A bi-product of hydrolysis is an increase in pH.

Table 4 Hydrolysis reactions and their characteristics.

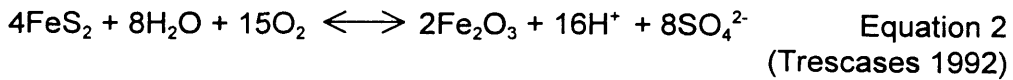
Hydrolysis	Secondary minerals	Soluble phase (major elements)	Soil	Climate
Allitization	gibbsite, goethite, hematite.	Si, Na, K, Ca, Mg.	Ferrallitic soils (laterites).	Tropical humid (rainforest).
Monosiallitization	kaolinite, goethite, hematite.	Si, Na, K, Ca, Mg.	Ferrallitic soils (laterites).	Tropical short dry season (wet savannah).
Bisiallitization	Al-Fe smectites.	Na, K, Ca, Mg.	Vertisols.	Tropical long dry season (dry savannah).

Source Trescses 1992 - (modified from Pedro,1984).

3.6.1.3 Oxidation: This process occurs most commonly in the aerating oxidising zone of a profile above the permanent saturation zone. Elements that are most likely to be affected by oxidation are Fe, Mn and S, all of which have multiple oxidation states. However, in the primary environment where the presence of oxygen is normally at a minimum, these elements are present and stable in their lowest oxidation state as either divalent cations or anions (i.e. Fe^{2+} , Mn^{2+} , and S^{2-}). Instability occurs in the weathering zone with the introduction of oxygen through air or liquid (or by increasing the pH) and oxidation then results. Consequently, ferrous iron as Fe^{2+} is oxidised to its ferric form Fe^{3+} , as illustrated in Equation 1 below.



With an iron sulphide, such as pyrite, oxidation affects both the iron and the sulphur, producing acidity as a bi-product, as illustrated in Equation 2.



3.6.1.4 Simple solutions: This is the dissolution of minerals by water in the surface environment. A typical example is the slow release of silica and the common cations of K^+ , Mg^+ , Na^+ and Ca^+ , during the hydrolysis of primary silicates (as illustrated in Table 4).

3.6.1.5 Transformation: Primary layer lattice minerals or phyllosilicates can behave or weather through what has been described as a simple solid-state transformation. For example;



3.6.2 Mineral resistance.

The susceptibility of a lithology to weathering reactions is largely controlled by its primary mineral composition. Minerals, whether they are primary or accessory, have different resistances to weathering depending upon their molecular structure and physical bonding. If internal bonds are weak, especially in the primary minerals, then weathering reactions can attack more easily and quickly causing rapid rock fabric disintegration. The silicates are the most widely distributed and diverse group of rock mineral compounds, occurring in olivines, pyroxenes, amphiboles, micas, talc, quartz, and feldspar. They occur in virtually all of the major rock forming groups (i.e. igneous, metamorphic and sedimentary) with the exception of those that have an organic origin. Consequently, the silicate group often constitutes the essential building blocks of rocks. However, it is the proportions of each silicate group and how these different silicates react to chemical weathering

that will determine both the overall susceptibility to weathering of the bedrock and the initial chemistry of the weathered residual products (Table 9 Section 3.6.3).

Goldich's work in 1938, and the Bowen Reaction Series demonstrated the relative chemical stability of one silicate mineral over another (Table 5). The general conclusion is that basic and ultrabasic rocks are more susceptible to chemical weathering than acid rocks due to their primary and accessory mineral assemblage.

Table 5 The relative stability of common rock forming silicates to chemical weathering (under humid temperate climates).

Increasing stability ↓	Olivine	Calcic plagioclase
	Augite (pxoyenes)	Calc-alkalic plagioclase
	Hornblende (amphiboles)	Alkali-calcic plagioclase
	Biotite	Alkalic plagioclase
	Potash	Feldspar
	Muscovite	
	Quartz	

Source: Rose et al. (1990), after Goldich (1938).

Regardless of the lithology, repeated and prolonged cycles of wetting and drying will eventually cause weathering to occur and this will result in the disintegration of the rock fabric. The resultant weathered material will, over time, evolve steadily diminishing any mineralogical similarities with the original source rock.

3.6.3 Mineral decomposition: the resultant profile.

The fate of elements released as a result of mineral breakdown is controlled by their ionic charge, their mobility, and the Eh and pH of the surrounding environment. Consequently, elements can be removed entirely from the system, although they are more likely to become adsorbed onto other minerals or incorporated into different chemical structures to create secondary minerals (Kühnel, 1987). Secondary minerals are a natural bi-product of the weathering process but they too can become chemically altered by further weathering, and so the weathered residuum becomes further evolved from its

original parent chemistry. The process of evolving chemical stability with weathering is illustrated through the work of Jackson and his colleagues in 1948. They showed the high instability of many of the primary calcium and silicate minerals and their evolution towards the more stable clay group and iron oxide minerals during multiple stages of weathering. This process is displayed well in lateritic profiles, where clays and iron oxides are the dominant products irrespective of source lithology.

Hydrous aluminosilicates or clay minerals are produced primarily through the weathering of silicate minerals. As this group constitutes the major group of rock forming minerals, it is not surprising that clays dominate lateritic profiles. There are five recognised clay groups (Table 6), and their development is determined by the chemical composition of the parent lithology, the drainage and climatic conditions, and finally by the intensity of weathering (Rose et al., 1990).

Table 6 Clay group minerals.

Clay group	Common chemical formula	Conditions of formation and general comments
Kaolinite	$Al_2Si_2O_5(OH)_4$	Normally the most common clay mineral in the weathering zone. Its formation favours an acid environment, free drainage, and though base ion leaching.
Illite	$K_{1-1.5}Al_4(Si_{1-6.5}Al_{1-1.5}O_{20})(OH)_4$	Known as hydrous mica, common in acid rocks
Montmorillonite	$(Na, Ca)_{0.33}-(Al, Mg)_2Si_4O_{10}(OH)_2 \cdot nH_2O$	Sometimes known as the smectite group. Formed from silicates high in Fe, Mg, Ca and low in K. Development also favoured where incomplete leaching of bases has occurred. Normally typical of basic / ultrabasic lithologies
Vermiculite	$(Mg, Fe, Al)_3(Al, Si)_4O_{10}(OH)_2 \cdot 4H_2O$	Related to the montmorillonite group and chlorites. Forms mainly from alteration of biotite and rarely chlorites and hornblends. Common in mafic rocks.
Palygorskite	$(Mg, Al)_2Si_4O_{10}(OH) \cdot 4H_2O$	A rare variety of chain structured rather than layered clay mineral

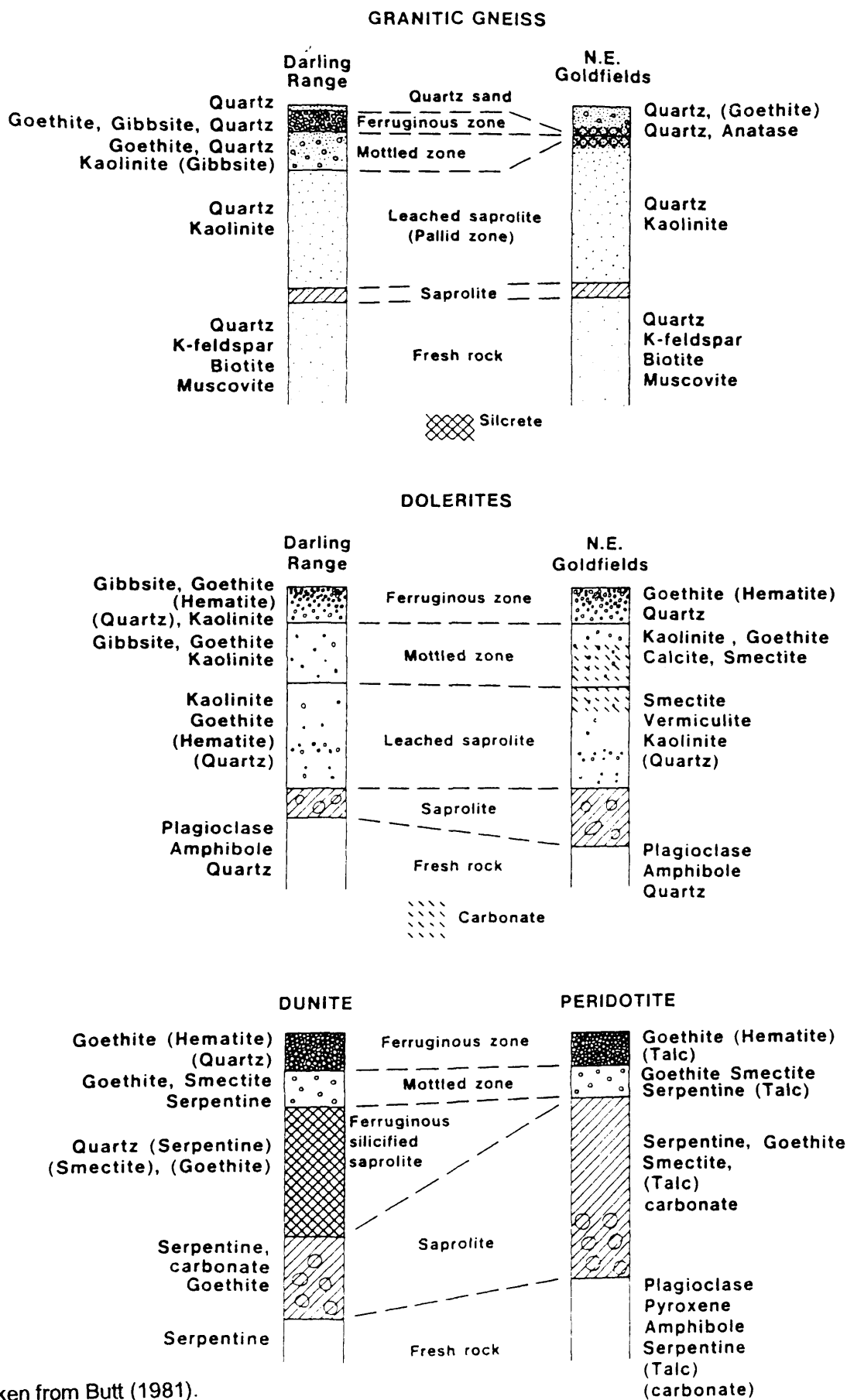
Source: Rose et al. (1990), Whitten and Brooks (1983) and O'Donoghue (1994).

Examples of chemical variations found in profiles through mineral decomposition are illustrated in Fig. 10. In this figure the three differing chemical compositions of the parent lithologies, described in Table 7, tend to predetermine the type of clay produced. However, some of these chemical changes are a result of varying climatic conditions as illustrated previously in Table 4.

Table 7 Major common minerals and their chemical compositions.

Peridotite		
40-75%	Olivine (essential)	$(\text{MgFe}^2)_2 \text{SiO}_4$
30-60%	Pyroxenes (augite)	$(\text{Ca, Mg, Fe, Al})_2 (\text{AlSi})_2 \text{O}_6$
<20%	Amphibole (hornblende)	$\text{NaCa}_2(\text{MgFe}^2)_4(\text{Al, Fe}^3)(\text{SiAl})_8 \text{O}_{22}(\text{OH, F})_2$
+/- <10%	Calci-plagioclase feldspar	$\text{Ca}(\text{AlSi}_3\text{O}_8)$
Some accessories which may be present are:		
	Mica (biotite)	$\text{K}(\text{MgFe})_3 \text{AlSi}_3\text{O}_{10} (\text{OHF})_2$
	Chromite	$(\text{Fe}^2\text{Cr}_2\text{O}_4)$
	Garnet	$\text{Mg}_3\text{Al}_2\text{Si}_3\text{O}_{12} / \text{Ca}_3\text{Cr}_2\text{Si}_3\text{O}_{12}$
Overall, the chemistry is characterised by very high ferromagnesian minerals. Major elements are Mg, Fe, Al, Ca, +/- with Cr and Ni		
Dolerite / Basalt		
40-60%	Plagioclase feldspar (Na) +/- (Ca) (common labradorite)	$(\text{NaCa})\text{Al}_{1-2}\text{Si}_{3-2}\text{O}_8$
20-35%	Pyroxenes (augite)	$(\text{Ca, Mg, Fe, Al})_2 (\text{AlSi})_2 \text{O}_6$
<15%	Amphibole (hornblende)	$\text{NaCa}_2(\text{MgFe}^2)_4(\text{Al, Fe}^3)(\text{SiAl})_8 \text{O}_{22}(\text{OH, F})_2$
<10%	Olivine	$(\text{MgFe}^2)_2 \text{SiO}_4$
The amount of olivine, pyroxene, and plagioclase depends upon the phenocrysts composition.		
Groundmass in dolerites sometimes have:		
	Quartz	SiO_2
	Mica (Biotite)	$\text{K}(\text{MgFe})_3 \text{AlSi}_3\text{O}_{10} (\text{OHF})_2$
Groundmass in basalts may also contain		
	Magnetite	Fe_3O_4
Overall, the chemistry is characterised by high Ca, Mg, Fe, with lower Na, SiO_2 and K.		
Granite		
30-50%	(K) alkaline feldspar	KAlSi_3O_8
25-30%	Quartz	SiO_2
10%	Mica (biotite & muscovite)	$\text{K}(\text{Mg Fe})_3 \text{AlSi}_3\text{O}_{10}(\text{OHF})_2$
		$\text{KAl}_2(\text{AlSi}_3\text{O}_{10})(\text{OHF})_2$
±10-20%	(Na) Sodic-plagioclase feldspar (albite)	$\text{NaAlSi}_3\text{O}_8$
±15%	Amphibole (hornblende)	$\text{NaCa}_2(\text{MgFe}^2)_4(\text{Al, Fe}^3)(\text{SiAl})_8 \text{O}_{22}(\text{OHF})_2$
Common accessories include:		
	Apatite	$\text{Ca}_5(\text{PO}_4)_3\text{F}$
	Sphene	CaTiSiO_5
	Zircon	ZrSiO_4
	Magnetite	Fe_3O_4
Overall, the chemistry is characterised by high K, Al, Na and silica (SiO_2), and by low Ca, Mg and Fe.		

Fig. 10 Profile variation caused by lateritic weathering.



Taken from Butt (1981).

Element distribution within the profile.

Although the underlying source lithology influences the geochemical character of the lower profile, its effect is observed to decrease with distance from the source rock. The uppermost evolved horizons are chemically altered to such an extent that they are dominated by the presence of clays and iron irrespective of the source lithology (Fig. 10).

In exploration geochemistry, importance lies in understanding how the distinctive chemistry of the laterite horizons effects the expression of elements. Field data and laboratory analysis have indicated that certain elements possess affinities for particular horizons (Ambrosi, 1984; Roquin et al., 1989; 1990; Zeegers and Lecomte, 1992). Acknowledging and understanding these phenomena has additional important implications to the surface geochemistry, with respect to the profile truncation level, the implications of which are further discussed in the Section 3.7 and 3.8.

The mobility of an element, whether reference is to its stability, adsorption, or its eventual precipitation, is controlled by the pH and Eh of the environment (Rose et al., 1990; Thornber, 1992). The oxidation state does however affect the solubility of an element, as reported by Rose et al. (1990) and Thornber (1992). Consequently, elements that possess variable oxidation states (valences) for example, Cu, Cr, Mo, Mn, Fe and Au have the potential for variable mobility depending on Eh. However, the valence alone does not determine solubility, for the pH of the surrounding environment is also a factor which influences an element's solution chemistry. Element pH studies depicted by U-shaped curves, have revealed antipathetic behaviour between the solubility of cations and anions with respect to pH. Fig. 10a, b & c illustrate some of the cation, anion and oxide responses. Cation solubility and mobility increases at low pH, whilst anion solubility and mobility increases at higher pH. The influence that pH exerts on element mobility has important implications regarding the composition of sulphide assemblages within a

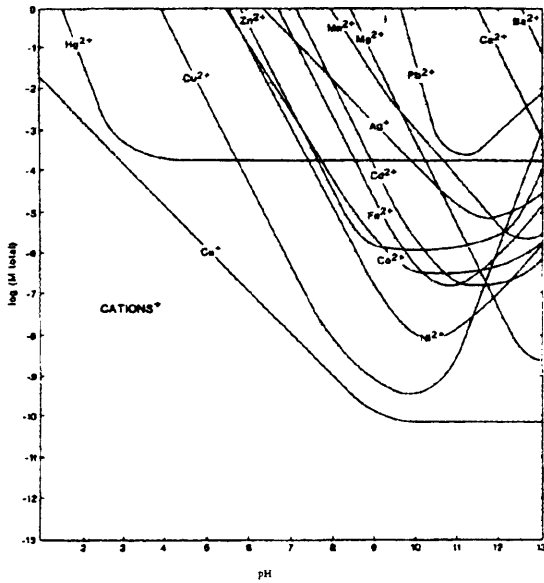


Fig. 10a Solubility of cations by hydrolysis as a function of pH.

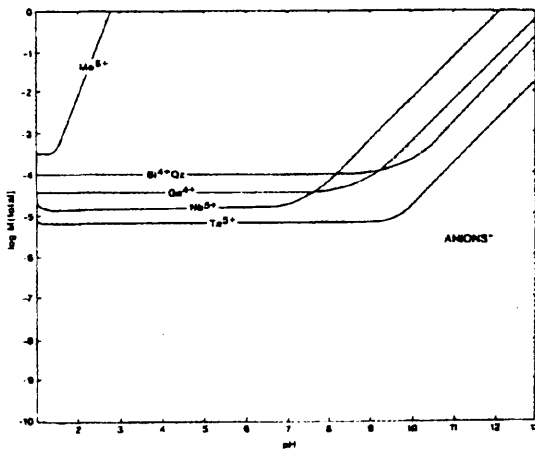


Fig. 10b Solubility of various anions by hydrolysis as a function of pH.

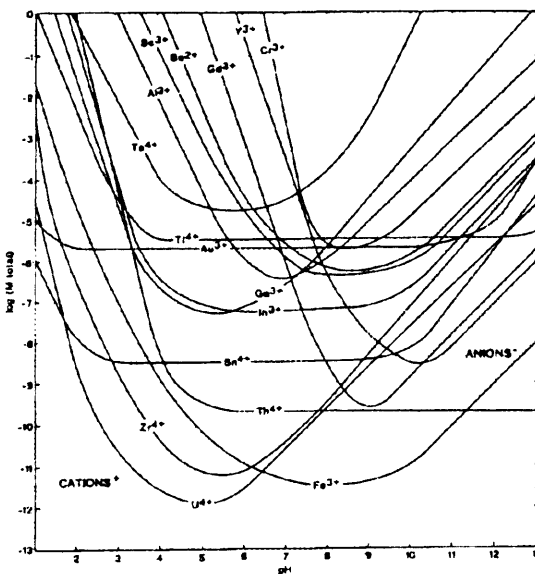


Fig. 10c Solubility of various oxides by hydrolysis as a function of pH.

Source: Thornber (1992)

mineralised zone. Thornber and Taylor (1992) have indicated that in assemblages that possess a high Fe sulphide content and/or a high sulphur to metal mineral ratio will, on oxidation and subsequent hydrolysis, produce acidic conditions within the environment (Equation 2, page 72). Under such acidic conditions, most base metal cations become soluble and hence more mobile. Their existence in the soluble state can be terminated by changes in Eh/pH resulting in precipitation, or migrate further up within the weathering profile through adsorption, complexing or co-precipitating with other elements. These scavenging type processes, though pH dependent, are a major contributor not only to element mobility but also to the collection, concentration and segregation of elements within the profile, as discussed by Kühnel (1987).

The most common scavenger minerals in laterites are Fe, Mn, and Al oxyhydroxides, amorphous silica and clays (Kühnel, 1987; Rose et al., 1990). The physical process of scavenging operates through the ionic charge, whereby like charges repel and opposites attract. However, scavenger charge is a function of pH. Hence minerals can change their surface charge based on whether their surrounding environment is acidic or alkaline. Hematite and goethite have a strong positive surface charge in acidic environments (Fig. 10c) and, as a result, will attract or scavenge negatively charged ions (i.e. Mo, Cr). On the other hand at higher pH these oxides possess a negative charge attracting cations such as Cu, Pb, and Zn. The pH at which minerals change from positively charged to negatively charged is referred to as the point of zero charge (pzc). Table 8 illustrates some pzc values for some minerals. Many of these are represented as a pH range implying that the absorption or release of ions within the specified range is likely to be a gradational process. However, predicting adsorption at the individual mineral level is reported as difficult and problematic by Thornber (1992), especially if organic matter resides within the system. For this reason it is often more simplistic to base adsorption prediction upon the pzc of the soil, as illustrated in Table 8.

Table 8 Examples of point zero charge (pzc) for minerals and soils.

pH below pzc means strong positive surface charge
 pH above pzc means strong negative surface charge

Mineral	pzc	Reference
Amorphous SiO ₂ / Quartz	1.8 – 3.5	1
Kaolinite / Illite Al ₄ Si ₄ O ₁₀ (OH) ₈	3.3 – 6.0	1, 2
Montmorillonite Na ₂ Mg ₂ Al ₁₀ Si ₂₄ O ₆₀ (OH) ₂₄	2.5 – 6.0	1, 2
Al ₂ O ₃	6.8 – 9.5	1
Calcite CaCO ₃	8.0 – 9.0	1
MgO	12.5	1
Gibbsite Al(OH) ₃	9.5	3
Hematite Fe ₂ O ₃	6.5 – 8.6	4
goethite FeOOH	7.6 – 8.1	3
Ferrihydrite Fe ₄ O ₅ (OH) ₂	6.9	3
Soil		
Oxisol (latosol or ferralisol of humid tropics)	4.0	3
Tropeptic Eutristoxox (latosol in dry savannahs)	3.75	5

Table adapted from Thomber (1992).

References: (1) Parks (1967), (2) Farrah and Pickering (1979), (3) Parfitt (1980),
 (4) Parks and DeBruyn (1962), (5) Stoop (1980).

The clay rich environment of the lower and upper saprolite, (and to a lesser degree the lower mottled zone), and the increasingly iron rich upper mottled zone and cuirasse act as scavengers which, through selective adsorption, vertically concentrate and partition elements based upon pH. Clay minerals, as shown in Table 8 have a relatively low pzc, and when this is allied with the slightly acidic savannah soils tends to bias the development of negatively charged clays. Consequently, dissolved base cations, for example Cu, Co, Pb, Zn and Ni are scavenged and concentrated by the clays (Ambrosi, 1984; Kühnel, 1987; Rose et al., 1990; Zeegers and Lecomte, 1992). However, it is the clay species, which determines the capacity to retain elements. As Rose et al. (1990) explain, vermiculite and smectite clays provide a much greater cation exchange site than kaolinite clays (Table 9).

Consequently, the transitions between smectite clays of the lower saprolite and the kaolinite of the upper saprolite and lower mottled zone (characteristic of basalt protoliths) would involve a physical release of cations due to the

lower exchange capacity of kaolinite. The implications of such a process are reflected in a reduced mineral signal compared to the higher capacity smectite clay.

Table 9 Clay exchange capacity.

Minerals / Soil	Cation exchange capacity (mEq/100g)
Kaolinite	3 - 15
Illite / Chlorite	10 - 40
Montmorillonite (smectite)	8 - 150
Vermiculite	100 - 150
Organic fraction of soil	150 - 500

Adapted from Rose et al. (1990).

Fe-oxides and oxy-hydroxides, typically hematite and goethite dominate the uppermost evolved portions of the profile. The pzc of such iron minerals indicate that any co-precipitation and absorption of base metals would require a high pH environment, considerably higher than that needed for clays (Table 8). Consequently in the slightly acidic savannah soils, or where acidity is caused by either an oxidising Fe-sulphide assemblage or the result of ferrolysis (Mann, 1984a,b), base cations are more likely repelled from the pH induced positive surface charge of Fe-oxide, whereas anions and oxy-anions are scavenged, such as Mo, As, Sb, Te, Cr (Roquin et al., 1989 and 1990; Thornber, 1992). The affinity some elements have for Fe-oxides often reflects itself in a concentration much greater than that observed within the underlying saprolite or protolith (Ambrosi, 1984; Zeegers and Lecomte, 1992). Of the base metals, Cu, and to a lesser degree Pb, are more likely to be retained within oxide horizons or surface gossanous material (Butt, 1987; Thornber et al., 1992), because these two cations have the greatest affinity for adsorption by oxy-hydroxides (Table 10, and Fig. 11).

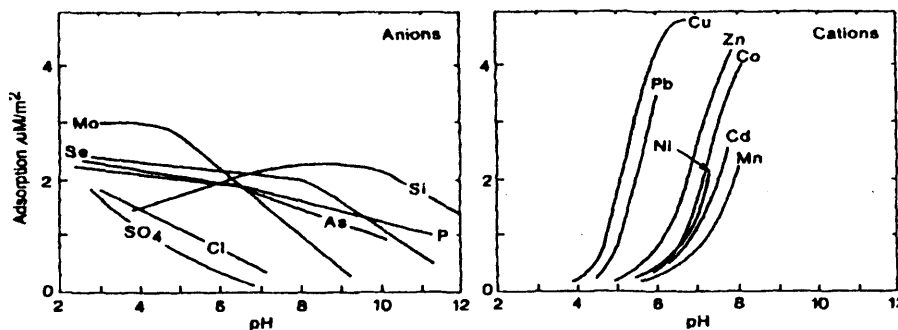
Table 10 The relative affinity for absorption of some cations.

Affinity for absorption	Mn oxides	Amorphous Fe-oxides	Goethite	Amorphous Al-oxides
Greatest	Cu ²⁺	Pb ²⁺	Cu ²⁺	Cu ²⁺
↓	Co ²⁺	Cu ²⁺	Pb ²⁺	Pb ²⁺
↓	Mn ²⁺	Zn ²⁺	Zn ²⁺	Zn ²⁺
↓	Zn ²⁺	Ni ²⁺	Co ²⁺	Ni ²⁺
Least	Ni ²⁺	Cd ²⁺	Cd ²⁺	Co ²⁺

Table adapted from Rose et al. (1990).

Sources: Mn-oxides Murray (1975).
 Amorphous Fe and Al oxides Kinniburgh et al. (1976).
 Goethite Forbes et al. (1976).

Fig. 11 Adsorption isotherms of divalent cations and anions onto goethite as a function of pH.



Source Thornber (1992).

3.6.5 Gold distribution within the laterite profile.

Evidence for the mobility of Au within the weathered regolith, by both physical and chemical processes, has been identified by:

- (i) Morphological changes of the primary Au grains.
 For example, these have been described as decreasing grain size, presence of sponge grains, corrosion (pitting, etching, and increased rounding of the grains), crystalline octahedral grains, flakes and dendritic forms (Mann 1984a; Webster and Mann 1984; Lawrance, 1988; Colin and Lecomte 1989; Freyssinet et al., 1989, 1990a, 1990b; Colin and Vieillard 1991; Bowell et al., 1991; 1995; Gray et al., 1992).

(ii) Chemical changes of the primary Au grains.

These can include increases in Au fineness, the presence of Ag depletion rims on Au grains, and Au coatings on iron grains (Mann 1984a, 1984b; Wilson, 1981; Freyssinet et al., 1989; Bowell et al., 1991; Gray et al., 1992; Bowell et al., 1995).

(iii) Lateral dispersion.

The size of the primary halo is often smaller and restricted to the lode, whereas the secondary halo is characteristically wider (Colin and Vieillard, 1991; Freyssinet et al., 1989; Bowell et al., 1995).

Gold is principally inert and immobile, therefore to be dissolved and mobilised the formation of an anion complex is necessary. However, controversy has surrounded the actual complex that is responsible. Theories and laboratory tests have proved differing complexes to be capable of dissolving Au. Krauskopf (1951) proposed the idea of a chloride complex which, under acid oxidising conditions, would dissolve Au. Cloke and Kelly (1964) agreed with Krauskopf proclaiming that Au in a chloride acid solution could be dissolved when the MnO₂ mineral pyrolusite was present. Mann (1984b) proceeded to test various solutions in an attempt to assess the most likely solutions for Au and Ag transport. His conclusions confirmed those of Krauskopf, and Cloke and Kelly, with respect to the MnO₂ additions, but also highlighted the critical role oxygen fugacity has on Au solubility. He stated that low down in the profile where Fe²⁺ availability is high and oxygen availability low, Au would likely have limited solubility compared to that near the water table or capillary fringe where oxygen fugacity is higher. His tests also acknowledged the role of thiosulphate which dissolved Au in non-saline fluids of neutral-alkaline pH range. Listova et al. (1968) and Goleva et al. (1970) had already identified the thiosulphate ion as an Au solubiliser. Webster (1984, 1986) on analysing the carbonate-rich sulphur lode at Wau, Papua New Guinea, proclaimed the thiosulphide ion as the likely Au mobilising complex, due to the presence of alkaline solutions. Thiosulphide was observed to be at its greatest stability at pH >7 and Eh 0.4 - 0.1V, therefore encompassing very mildly acidic to highly

alkaline pH conditions, and reduced to moderate oxidising conditions. Hence Webster viewed the phreatic zone of the weathered profile as a suitable environment for thiosulphate stability due to the reduced oxygen concentrations.

Lakin et al. (1974) suggested that there were a wide variety of ion complexes capable of dissolving Au. These included the aforementioned chloride halid and thio-complexes along with organic and cyanide solutions. He references cyanglycosides as a source of HCN which, when present in plants, could cause Au mobilisation. Cyanide producing bacteria have also been suggested as solubilisers of Au by Smith and Hunt (1985); cited in Gray et al., (1992). Although these experiments illustrate the mobility of gold under the release of cyanide from both plant and micro-organisms, Gray et al. (1992) query its validity with respect to the actual available concentration of cyanide in any given profile. Nevertheless, Howell et al. (1991) in their study of the Ghanaian Ashanti concession refer to cyanide complexing as one of a number of possible complexes for Au solubilisation.

Experiments conducted by Freise (1931), and later by Baker (1973, 1978), have indicated that humic acids, produced as a by-product of micro-organism action on decomposing vegetation, can dissolve gold in oxidising to near oxidising conditions. This is a process more characteristic of tropical conditions. Ong and Swanson (1969) proposed the colloidal transport of Au. Their experiments indicated that the presence of humic acid could cause not only gold chloride to be reduced to a colloid, but that humic acid could also act as a protective colloid. In fact, Butt (1988b) suggests Au precipitation from any of these aqueous solutions and organic complexes may be prone to colloidal mobilisation. Consequently, these experiments and observations have highlighted not only that Au can be dissolved and transported by inorganic or organic complexes, but also that its existence in such soluble complexes is tightly constrained within differing pH and Eh regimes. Any subsequent change in these conditions will cause Au precipitation. Table 11

illustrates the possible aqueous gold species and their conditions for solubility and precipitation.

Table 11 The chemical species of gold mobilisation.

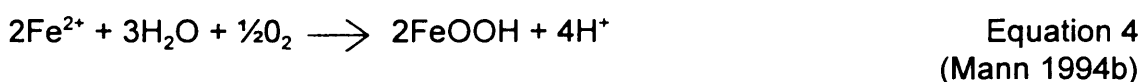
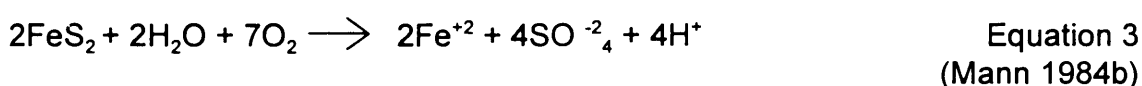
Species.	Possible origin.	Solubility conditions.	Product.	Precipitation conditions.
AuCl AuCl ⁻ ₄	Oxidative dissolution of gold under acid saline conditions. $Au + 2Cl^- \xrightarrow{(O)/(H^+)} AuCl_2^-$	Oxidized, saline, acidic. PH < 4.0 Cl > 35000 mg/L	High fineness gold (~ 1000). High fineness gold (~ 1000).	Dilution; reduction; alkalinity.
AuI ⁻ ₂	Dissolution of gold under moderately oxidative conditions. $Au + 2I^- \xrightarrow{(O)/(H^+)} AuI_2^-$	Enhanced where I ⁻ is released by decomposition of organic matter.	High fineness gold (~ 1000).	Reduction.
Au(HS) ⁻ ₂	Dissolution of gold by reduced waters during early supergene alteration, or by biological reduced solutions. $Au + 2SH^- \xrightarrow{(O)} Au(SH)_2^-$	Reduced /neutral.	Medium – high fineness gold (~ 998).	Dilution; acidification; oxidation.
Au(S ₂ O ₃) ³⁻ ₂	Weathering of gold / pyrite in neutral to alkaline solution. $Au + 2S_2O_3^{2-} \xrightarrow{(O)} Au(S_2O_3)_2^{3-}$	Alkaline to weakly acid (meta-stable) Reducing to mildly oxidising.	Medium fineness gold (~ 985).	Dilution; Reduction; Acidification; Oxidation.
Au(CN) ⁻ ₂	Interaction of cyanide with gold. $Au + 2CN^- \xrightarrow{(O)} Au(CN)_2^-$	Cyanide present (mildly acidic to oxidising pH).	Low fineness gold (~ 5).	
Au-organic matter	Interaction of organic matter with gold under oxidising conditions. $Au + OM \xrightarrow{(O)} Au^+-OM?$	Not certain, may depend on source of material (weakly acidic to oxidising conditions).	High fineness gold, fine grained.	Reduction.
Colloidal gold	May be formed during reduction of gold by organic matter. $Au^+ + OM^- \rightarrow Au^0$	Not confirmed for natural waters.	High fineness gold, fine grained.	

Source: Gray et al., 1992; supplements from Bowell et al., 1991; Butt 1988a.

The type of complexes formed, however, and the resultant distribution of Au within a profile, are a result of a number of factors. Parent lithology, the composition of the mineralisation, the climate (both past and present), and topographic position are all contributory factors (Webster and Mann, 1984;

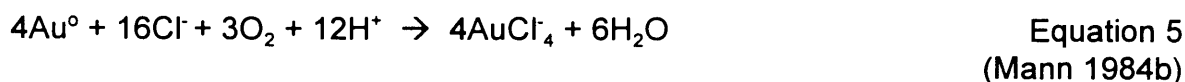
Butt, 1987, 1988; Gray et al., 1992). Parent lithology can influence ground water pH, with solutions becoming more alkaline with increasing carbonate content or more acidic where granite lithologies are present. However, within the vein system and adjacent wall rock, the pH of the ground water solution can be influenced by the percentage of Fe-bearing sulphides, as reported by Thornber and Taylor (1992). Alternatively, as Mann (1984a) has described, the sulphur/carbonate ratio (pyrite/calcite) of the mineralisation can have a similar influence. The iron sulphide, pyrite, is regarded as one of the most common mineral accessories (Mann 1984a; Trescases, 1992). When weathered this mineral is an important source of strong acidification primarily through the release of H⁺ ions (Trescases, 1992). This has already been illustrated in Equation 2, Section 3.6.1.3.

Pyrite oxidation is therefore an important contributor to acidity, provided that the carbonate content is not sufficient in quantity to neutralise the reaction. Mann (1984b) describes the oxidation of pyrite as possibly prescribing to two discrete reactions within a profile. The first represents the weathering of pyrite at the bedrock front (Equation 3) and the second is the oxidation of ferrous iron at or near the water table at a higher oxygen fugacity (Equation 4).

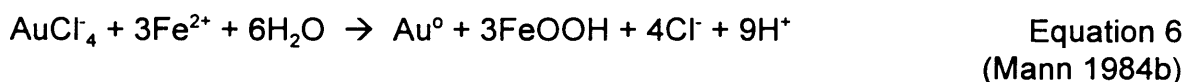


This later reaction represents ferrollysis, resulting in an increase in acidity within the profile. If the prevailing conditions allow ferrollysis to continue then the accumulation of oxy-hydroxides results in the development of a ferruginous horizon. Consequently an active weathering profile undergoing ferrollysis, as described by Mann (1984b), would show increasing Eh and reducing pH conditions from the weathered bedrock to the water table. Provided that there exists sufficient chloride concentration (Cl⁻), acid pH by H⁺ release and adequate oxygen fugacity (Krauskopf, 1951; Mann, 1984b) Au and Ag, can be dissolved by the following reaction (Equation 5). This type of gold

dissolution has been proposed by Mann (1984b) in the Yilgarn block of Western Australia.

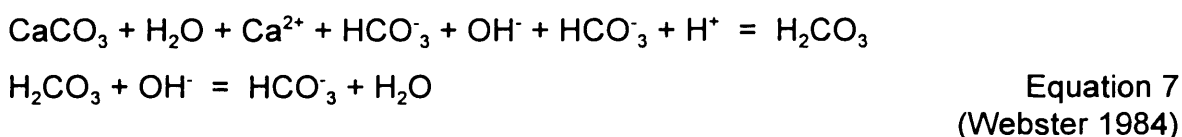


Gold in the AuCl_4^- complex can precipitate through an increase in pH, dilution or reduction of the complex with Fe^{2+} as shown in Equation 6.



Unlike gold, silver complexes do not reduce as easily with Fe^{2+} , as a consequence gold of high fineness is precipitated.

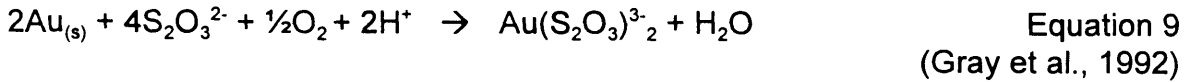
Veins which possess a higher proportion of carbonate minerals or a high metal to sulphur ratio, as described by Thornber and Taylor (1992), may neutralise any acidity produced, especially by pyrite oxidation (Mann 1984a). Webster (1984) describes such a carbonate neutralising process to be in operation at the Upper Ridges Mine in Papua New Guinea through the following reaction (Equation 7).



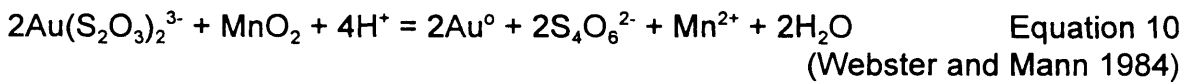
With a decrease in acidity and an increase in alkalinity Goldhaber (1983) identified the product of pyrite oxidation to change from ferrous iron and sulphate iron in acid pH through to thio-complexes e.g. tetrathionate (S_4O^{2-}) at pH 6.0-7.0 and thiosulphate ($\text{S}_2\text{O}_3^{3-}$) at pH > 7.0. Although there exist a number of other thio-complexes (hydrogen sulphide SH^- ; solid sulphur S ; sulphite SO^{2-}_3 ; and sulphate SO^{2-}_4) Webster (1984) reports thiosulphate as the most commonly occurring complex under neutral to alkaline pH. Pyrite oxidation within an alkaline pH > 7.0 would proceed through the following reaction (Equation 8).



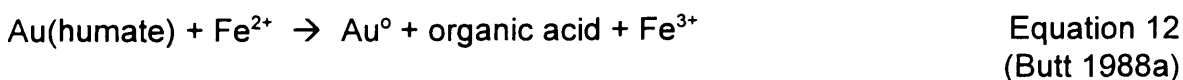
The thiosulphide complex is capable of dissolving Au (and similarly Ag) as is illustrated in the following reaction (Equation 9).



Thiosulphate Au (and Ag) complexes are stable within alkaline and reducing to mildly oxidising conditions but may become unstable with deviations from these pH/Eh conditions, possible at a redox (water table) boundary. Webster (1984) investigated a number of potential mineral precipitants (MnO_2 , Fe_2O_3 , FeSO_4 , etc) for the thiosulphate complex. His results indicated that in the presence of MnO_2 thiosulphate became unstable. Precipitation of the Au-thiosulphate by oxidation from manganese dioxide could be explained by the following redox reaction (Equation 10).



The degradation of organic matter in soils can cause gold to be mobilised and precipitated by organic complexes (Equation 11 and 12). This produces a fine-grained Au of high fineness located within the iron oxy-hydroxides of the surface ferruginous horizons. These complexes have been suggested as likely contributors to the increased solubility of Au within the near surface in areas of high humidity or seasonal humidity, typically tropical. Examples include: Dondo Mobi, Gabon (Colin and Vieillard, 1991); the Ashanti concession, Ghana (Bowell et al., 1991); Kangaba, SW Mali (Freysenet et al., 1990a); and Wau, Papua New Guinea (Webster and Mann, 1984).



As explained above the Eh/pH conditions, the carbonate-to-sulphur ratio of a mineralised vein, and the composition of the surrounding bedrock can all help

considerably in the determination of Au-complexing processes. Butt (1988a,b) however, has also proposed that the spatial distribution of the gold and the complexes involved are equally a response to climatic change. Many terrains have changed climatically from the seasonally humid climate that produced the deep weathered regoliths to dry or wetter environments through plate tectonic movement (Section 3.4). Butt (1988a,b) and Lawrance (1988b) suggest that the products of a complex weathering history can be reflected in the Au-distribution within the regolith. Essentially two types of regolith enrichment have been identified.

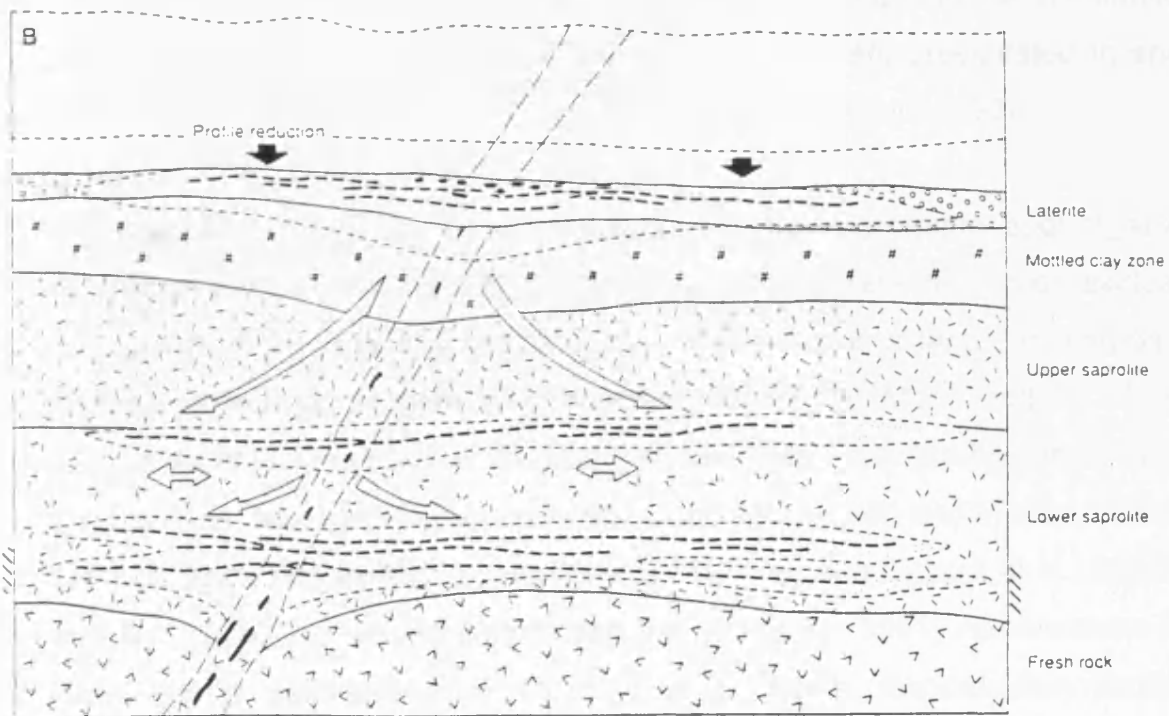
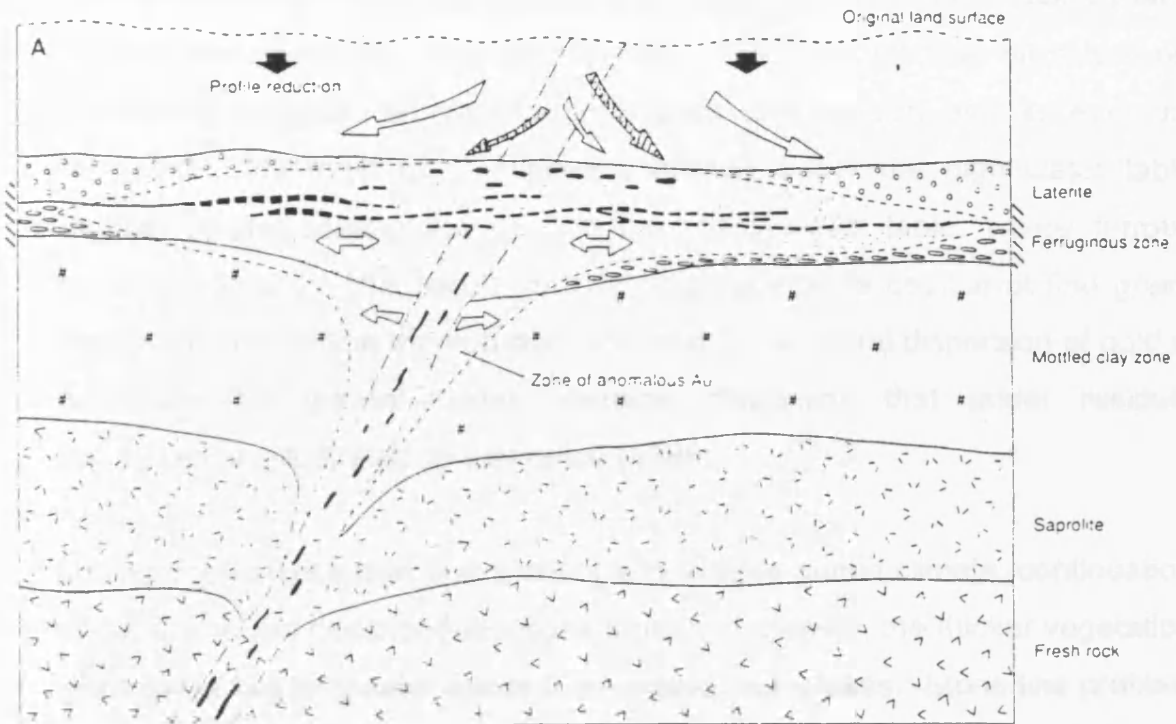
Firstly, lateritic supergene deposits. These are in essence flat lying enrichments located within the ferruginous and mottled zone. Au grains of this type are typically fine grained and of high fineness. However, coarser grains and secondary Ag-poor grains associated with iron oxide may also exist. Au dispersion can vary from several metres to hundreds of meters.

Secondly, saprolitic supergene deposits. These are enrichments either confined to, or laterally dispersed from, the vein. Enrichment is usually of one or more sub-horizontal zones that often reflect past redox or water table horizons.

Butt (1988a) and Lawrance (1988a) have produced similar models to help explain these Au distributions within the regolith (Fig 12 and Fig. 13).

During lateritisation (Fig. 12-I and Fig. 13a) the water table lies high in the profile at the zone of maximum ferruginisation. At the weathering bedrock interface Au may be released if suitable complexing ligands are present. Butt (1988a) and Mann (1984b) propose that at such an interface thio-complexes could be the most likely species; considering the lower oxygen fugacity and given alkaline to near acidic pH. However, the mobility of such species is limited and beneath the water table little dispersion is reported to occur within the surrounding weathered wall rocks (Zeegers, 1987; cited in Butt, 1988).

Fig. 13 Gold distribution within the profile.



 Physical remobilization of Au
  Chemical remobilization of Au
  Primary Au
  Secondary Au
  Watertable position

Taken from Lawrence (1988).

Enrichment occurs, however, within the mottled and ferruginous horizons, through a number of processes. These are: (i) residual concentration by land surface reduction, as illustrated in Fig. 13a and (ii) the chemical re-mobilisation of gold as organic complexes and colloids and its eventual illuviation. The gold of (ii) migrates laterally under the high water table regime, re-precipitating the gold at the redox water table, where ferrous oxidation occurs. This results in a lateritic supergene deposit of fine grain, high purity gold within the iron oxide horizon. The lateral dispersion of gold is potentially far greater under chemical dispersion than under residual processes, as illustrated by Lawrance (1988).

During post-lateritisation and a change to a more humid climate, continuation of the previously described reactions remain. However, the thicker vegetation often gives rise to greater action from organic complexes. Stone line profiles^c formed from the increased surface leaching accumulate at the lower limit of rainwater impregnation, often 0.5-2 m depth from the surface (Lecomte, 1988). Leached Au-complexes of the upper horizon are precipitated in and above the stone line with neo-formed Fe-oxides (Gray et al., 1992).

At Dondi Mobi in Gabon, gold dissolution by hydroxichloride and organic complexes is thought to have occurred along with the translocation of residual gold grains, both vertically and laterally. The result is a large "mushroom" shaped surface enrichment halo described at Dondo Mobi, and Ity, Côte d'Ivoire, to have a surface halo greater than 200m, considerably larger than that found in the saprolite (Lecomte and Colin 1989; Colin and Vieillard 1991; Lecomte and Zeegers 1992). However, at Kubi, Ghana (Bowell et al., 1995), and the Ghanaian Ashanti concession (Bowell et al., 1991) no reference is made to a well-developed stone line in these tropical rain forest environments. The surface haloes indicate very little lateral or vertical re-distribution of gold, compared to more mature profiles of Gabon (Bowell et al.,

^c Stone lines are a recent alteration formed under present humid climates (rainforests) or during an intermediate period of humidity. Stones may be quartz, lithorelics, degraded cuirasse or even sedimentary.

1991). Organic complexes, typically fulvic acid and cyanide, are considered principal ligands responsible for gold mobilisation. Thiosulphate complexing is postulated at depth, whilst chloride complexing is dismissed based upon inadequate Cl^- concentrations in the soil.

The spatial distribution of gold in lateritic profiles modified under humid equatorial conditions is generally not too dissimilar from that exhibited in regions where the climate has been relatively stable since formation (i.e. continuing savannah style climate). Although water table fluctuations exist between wet and dry seasons, the severity of which is determined by latitude, gold accumulation is essentially characterised by near surface lateritic supergene deposits, (Zeegers 1987 cited in Butt 1988b; Freyssinet et al., 1990a), as described. Unlike the rainforest situation stonelines are rarer and surface dispersion halos are generally smaller. Organic action though still a contributing factor to gold dispersion is perhaps not as prominent as in the rainforest regime, due to vegetation die-back in the dry season.

This situation can be contrasted with the spatial distribution of gold found in profiles modified under a later arid climate. Provided surface erosion has not removed the surface enrichment produced during the initial lateritisation, the gold will remain preserved due to the protection from the iron oxides and as a result of the reduced solubility of high fineness secondary gold (Mann, 1984b). A change to a more arid climate has two effects. Firstly, it reduces surface vegetation making organic or cyanide complexes less abundant, and secondly, it causes a lowering of the water table (Fig. 12-III). Lowering of the water table is, interrupted by standstills or periodic rises due to climatic fluctuations. A decrease in leaching allows the accumulation of particulates from rainfall, concentrating Cl^- , whilst an increase in rainfall leaches chloride salts. Cl^- ions aided by high oxygen fugacity, and acidity produced by the solution percolating through the zone of ferrolysis (Equation 4), can dissolve and transport gold present in the upper parts of the saprolite as a chloride complex (Webster and Mann, 1984; Lawrance, 1988a; Equation 5). In the

Yilgarn Block, Western Australia a lowering of the water table and the onshore westerly winds are presumed to have carried and deposited salts since possibly the Tertiary, promoting gold chloride complexing (Mann, 1984a). Gold re-precipitation, as explained by Webster and Mann (1984) and Gray et al. (1992) usually occurs when these percolating fluids reach the water table, or when contact is made with Fe^{2+} ions (Equation 5). If climate fluctuations persist in the lowering of the water table there can develop not only a number of enrichment horizons within the saprolite, as illustrated in Lawrance's model (Fig. 13b) and seen at Australia's Boddington gold deposit, but also zones of major Au depletion due to leaching. The most severely leached region would be the area of the upper saprolite, between the lateritic supergene gold horizon and the first saprolite supergene gold horizon (Fig. 12-III-IV). A region referred to as the depletion zone (Butt, 1988).

In conclusion, although there are a variety of complexing ligands capable of dissolving and transporting gold (Table 13) the complex is largely controlled by the surrounding Eh/pH environment, and the mode of gold occurrence (i.e. free gold particles or within the lattice of other minerals). However, as already pointed out, pH conditions can be influenced by the composition of the vein and host rock. Consequently, with regard to the oxidation of one of the most prolific iron sulphide minerals pyrite, both acid and alkaline pH can result depending upon the concentration of pyrite and carbonate present. The removal or leaching of Fe^{2+} by heavy rain prior to its oxidation could account, as discussed by Mann (1984a), for the development of thiosulphate complexes in areas of high rainfall, an example being Wau, Papua New Guinea (although this is a carbonate-quartz vein). However, in regions of lower rainfall and where there exists a complete profile formation, acidic oxidation of pyrite is favoured. As Mann (1984a) concludes, high rainfall alone does not preclude thio-complexation. However Butt (1988a,b), with reference to the spatial enrichment of gold within the regolith, believes the observable differences and the dominant ligand complexes can be related to weathering/climatic history. Consequently in rainforest and savannah

climates where there has been less dramatic fluctuations in the water table regime, gold forms near-surface lateritic supergene deposits, with little enrichment in the saprolite. A change to a more arid climate, which produces a successive lowering of the water table, results in supergene enrichment. Butt (1988a) suggests that a change in climatic regime from humid to arid also changes the dominant ligand complexes, from principally organic complexing in humid climates to chloride complexing in arid climates.

3.7 Laterite within the research area.

Since the Tertiary, Mali has experienced relatively stable climatic conditions Kusnir et al (1987). Prolonged and contrasting wet and dry seasons have resulted in the formation of a thick (>30 m) and regionally extensive weathered regolith, referred to as laterite. According to Kusnir et al., (1987) the process of lateritisation is believed to have begun around the Eocene period. Although the laterite is considered to have developed in-situ and is regarded as litho-dependent, personal communication with Drury (2000) suggests that one can not rule out the likelihood of fluvial process for its formation. Laterite within the region blankets both the bedrock and the mineralisation. Processes operating within the evolving laterite gradually alter the geochemical signatures of mineralisation and bedrock, producing a surface expression that is somewhat geochemically removed from its source, as described throughout this chapter.

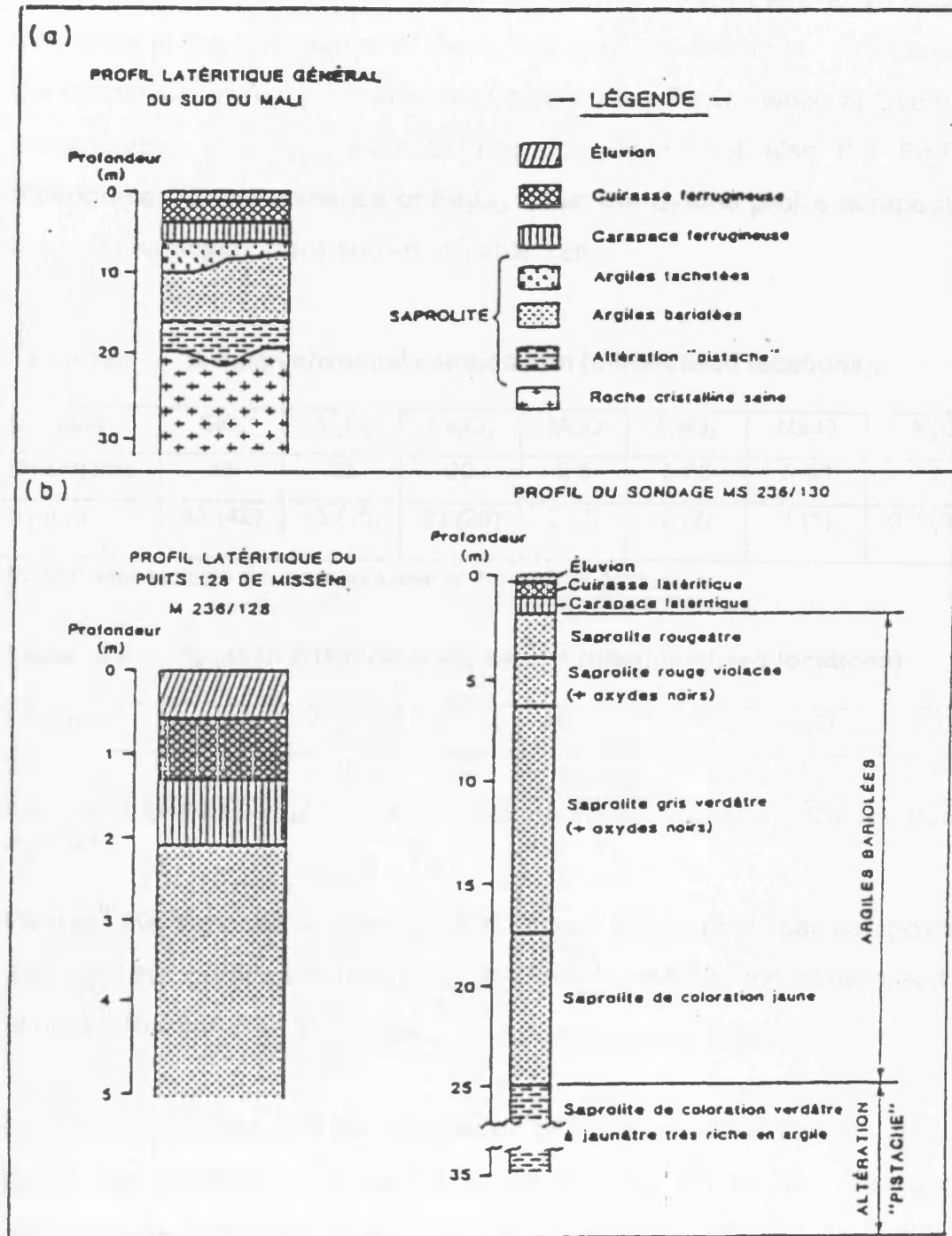
3.7.1 Description of the lateritic profile and its geochemistry.

Laterite in the research area has been detailed because of investigative work based upon soil gold anomalies (Section 3.7.3). The published works reviewed here report upon the findings from two localities, that of Syama (Bowell et al., 1995) and another anomaly located between the villages of

Pitangoma and Pifongoni in the far south of the region (Séa et al., 1990). Both anomalies lie within Birimian rock sequences (Chapter 2, Section 2.5). Although laterites in both these areas are thought to have developed in-situ there are noticeable differences between the profiles. The Syama profile is described as comprising the full complement of horizons (Section 3.3): parent rock; saprolite; mottled zone and variegated ferruginous zones. It can therefore be described as a typical southern Mali profile (Séa et al., 1990). The description of the Pitangoma laterite differs in that the mottled zone (or *Argiles tachetees*, as illustrated in Fig. 14), appears to be absent according to evidence from two pits. Consequently, the ferruginous carapace zone directly overlies the upper saprolite (Fig. 14). Explanations for the absence of the mottled zone at Pitangoma have suggested that the topographic position of the site is the most likely factor (Séa et al, 1990). Butt et al. (1989); Roquin et al. (1990), and Zeegers and Lecomte (1992), acknowledge that differential surface erosion can result in the removal of upper horizons, thereby allowing stratigraphically lower horizons (i.e. the saprolite) to be directly overlain by a younger and less evolved ferruginous horizon, such as the carapace. However, an alternative explanation utilises the concept of profile disequilibrium (Millot, 1983; cited in Lucas and Chauvel, 1992). This is reported to result when horizons do not advance equally throughout the profile. Disequilibrium is established resulting in the “take-over” and eventual disappearance of a horizon over time. However, on comparing the topographic positions of the Syama and Pitangoma sites, Pitangoma is seen to lie at a lower altitude than Syama. This gives some credence to the concept of Syama resembling an older, and more evolved profile which is consequently found at a higher altitude. Whereas Pitangoma could represent a profile that has been eroded or truncated through landscape evolution, as discussed by Zeegers and Lecomte, (1992), Section 3.8.1.

On examining the mean chemical compositions for the two mineralised profiles, little difference exists between individual zones. Table 12a illustrates

Fig. 14 Typical southern Mali lateritic profiles.



- (a) A lateritic profile from southern Mali
- (b) Lateritic profile Misseni (pit128)

Taken from Séa et al. (1990).

that in both sites SiO₂ is the major element, (representing up to 46%), followed by Al₂O₃ and Fe₂O₃. However, between sites there is a noticeable difference in the abundance of these two previous elements. At Pitiangoma the proportion of Al₂O₃ is fractionally higher than Fe₂O₃, while at Syama the concentration of Fe₂O₃ exceeds not only Al₂O₃, but also the Fe₂O₃ at Pitiangoma. The dominance of Fe₂O₃ within the Syama profile is repeated in the unmineralised profile shown in Table 12b.

Table 12a % mean chemical composition (mineralised locations).

Location	SiO ₂	Al ₂ O ₃	Fe ₂ O ₃	MgO	CaO ₂	Na ₂ O	K ₂ O
Pitiangoma	46	22	20	0.5	0.05	0.03	1
Syama	43 (42)	15 (15)	23 (26)	2 (2)	2 (2)	1 (1)	0.7 (0.7)

Parentheses indicate the mean inclusive of the surface gossan.

Table 12b % mean chemical composition (unmineralised locations).

Location	SiO ₂	Al ₂ O ₃	Fe ₂ O ₃	MgO	CaO ₂	Na ₂ O	K ₂ O
Syama	45	16	26	2	2	1	1

Information for Tables 12a and 12b adapted from sources Séa et al. 1990, and Howell et al., 1995.

Overall, the two site locations have similar mean chemical compositions, although the greatest similarity is still found between the mineralised and unmineralised profiles at Syama.

Further examination into the distribution of these constituents throughout the profile are revealed in Table 13 to 15 and Fig. 15 to 20. The general geochemical distribution at Syama and Pitiangoma indicates an increase in Fe₂O₃ towards the surface, a reduction in SiO₂ towards the surface, and an Al₂O₃ content which is higher in the saprolite and mottled zone, decreasing in the ferruginous horizons (Fig. 15, 16 and 17). These findings are similar to those reported by Zeeger and Lecomte (1992). However, in both the Syama profiles there appears to be an obvious geochemical difference between those horizons which lie below the ferruginous ferricrete (or carapace), and

Table 13 Geochemistry of the unmineralised profile - Syama.

	Protolith	Saprolite	Mottled-clay zone	Ferricrete	Cuirasse	Soil
SiO ₂	47.86	46.80	41.55	35.81	32.70	65.78
Al ₂ O ₃	14.87	16.00	17.92	13.91	11.90	18.64
Fe ₂ O ₃	14.95	20.50	19.28	41.95	43.50	16.11
MnO	0.22	0.33	0.15	0.28	0.31	0.19
MgO	7.18	3.50	2.18	0.29	0.03	0.01
CaO	7.09	5.20	1.72	0.31	0.11	0.01
Na ₂ O	3.19	2.19	1.09	0.81	0.31	0.42
K ₂ O	0.48	1.14	1.53	1.05	0.91	0.79
SiO ₂ /Fe ₂ O ₃	3.20	2.28	2.16	0.85	0.75	4.08
Al ₂ O ₃ /Fe ₂ O ₃	0.99	0.78	0.93	0.33	0.27	1.16

Table 14 Geochemistry of the mineralised profile - Syama.

	Protolith	Saprolite	Mottled-clay zone	Ferricrete	Cuirasse	Soil	Gossan
SiO ₂	43.86	47.65	43.32	28.42	31.63	62.95	33.25
Al ₂ O ₃	12.37	17.23	19.58	12.98	12.47	14.59	13.92
Fe ₂ O ₃	12.51	13.45	17.65	42.88	36.08	14.98	47.53
MnO	0.12	0.22	0.13	0.17	0.17	0.14	0.29
MgO	5.67	5.10	0.68	0.09	0.16	0.01	0.15
CaO	7.09	4.20	0.69	0.11	0.19	0.01	0.15
Na ₂ O	2.08	2.63	1.67	0.51	0.31	1.28	0.45
K ₂ O	0.61	0.34	0.41	0.85	0.91	1.08	0.85
SiO ₂ /Fe ₂ O ₃	3.15	3.54	2.45	0.66	0.88	4.20	0.70
Al ₂ O ₃ /Fe ₂ O ₃	0.99	1.28	1.11	0.30	0.35	0.97	0.29

Table 15 Geochemistry of the mineralised profile - Pitiangoma (Pit 128).

	Saprolite			Carapace	Cuirasse	Eluvion (soil)
	(1)	(2)	(3)			
SiO ₂	53.69	49.22	49.62	48.16	42.74	34.60
Al ₂ O ₃	20.80	23.36	23.83	23.35	21.57	18.51
Fe ₂ O ₃	13.22	13.94	13.94	15.87	23.16	35.46
MgO	0.78	0.69	0.19	0.49	0.40	0.18
CaO	0.05	0.04	0.03	0.04	0.05	0.06
Na ₂ O	0.05	0.03	0.01	0.03	0.04	0.02
K ₂ O	1.90	1.30	0.89	0.92	0.73	0.30
SiO ₂ /Fe ₂ O ₃ ^a		3.70		3.00	1.80	0.97
Al ₂ O ₃ /Fe ₂ O ₃ ^a		1.65		1.47	0.93	0.52

Note: ^a For the Saprolite only the better of the three is given
 Parentheses represent sample depth (1) approx. 14.20 m
 (2) approx. 13.00 m
 (3) approx. 12.25 m

Data source: adapted from Séa et al. (1990) and Bowel et al. (1995).

Fig. 15

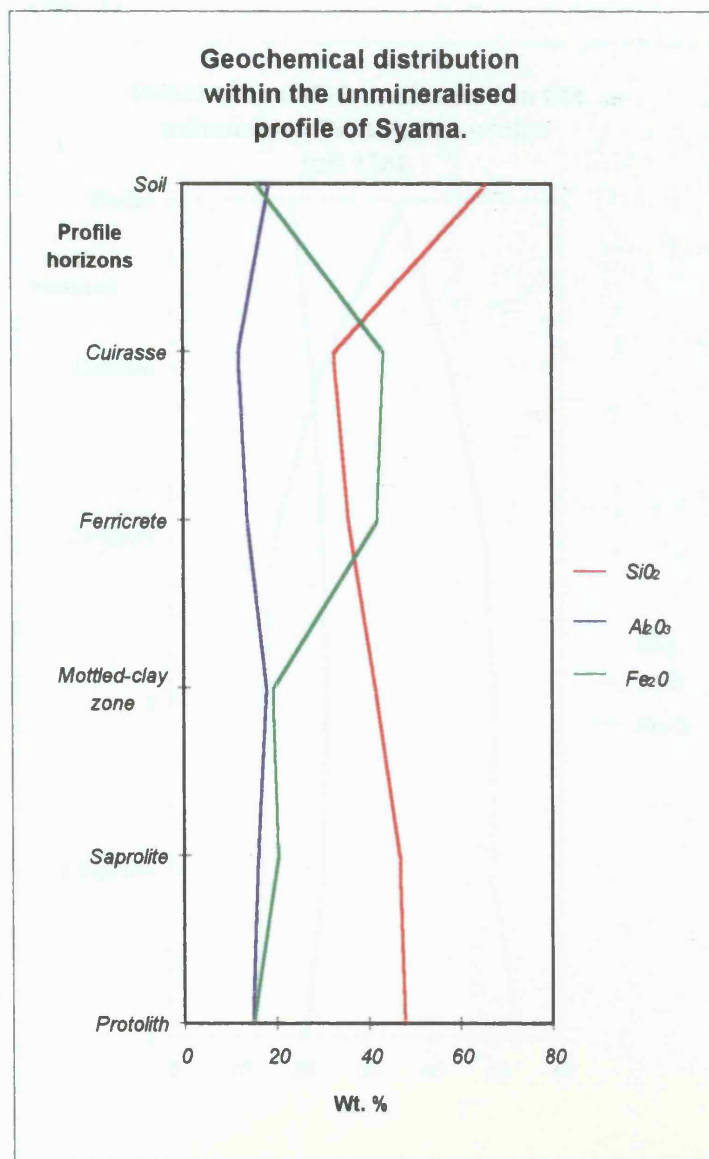


Fig. 16

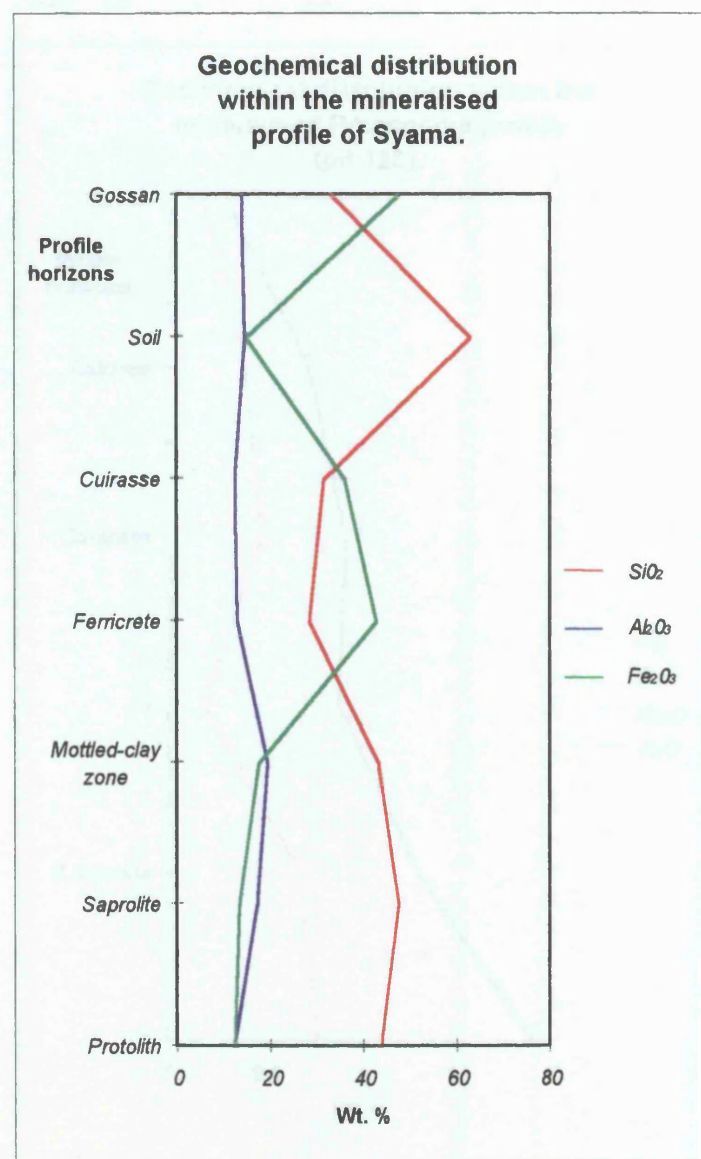


Fig. 17

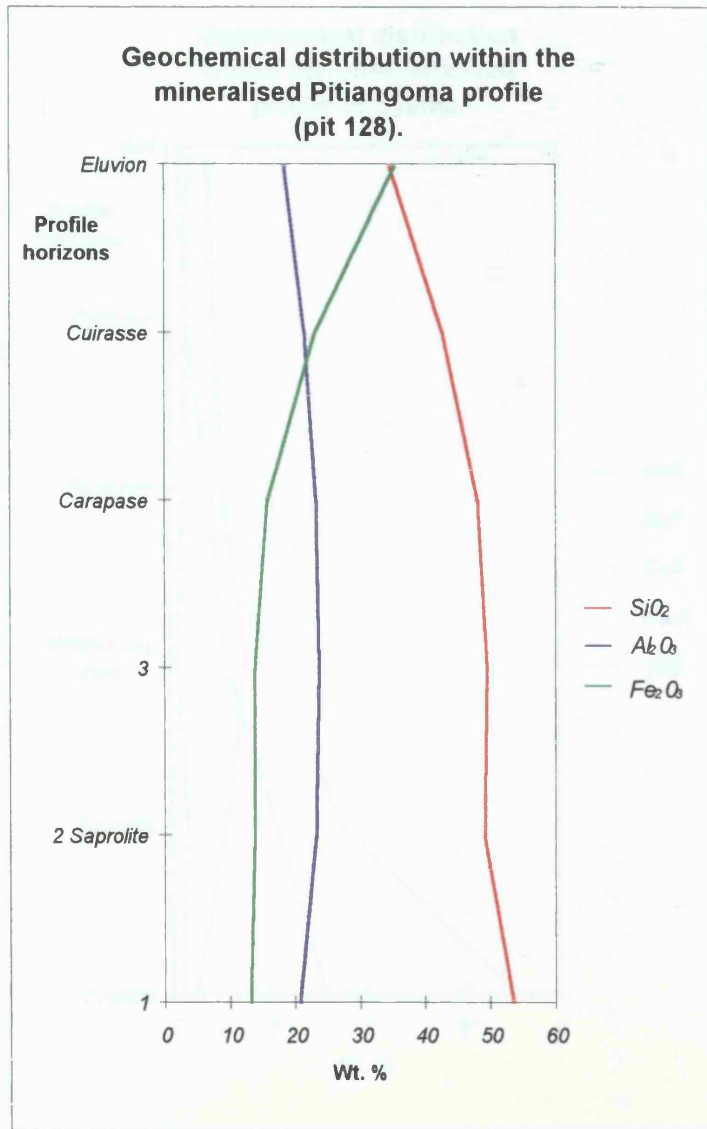


Fig. 18

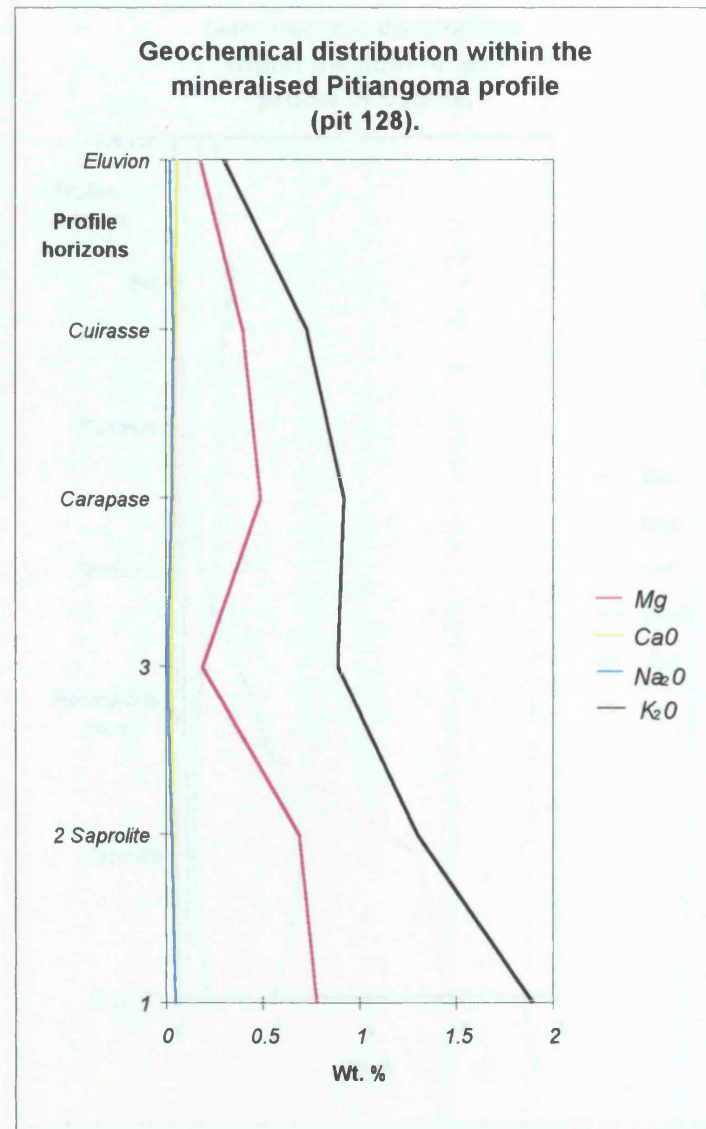


Fig. 19

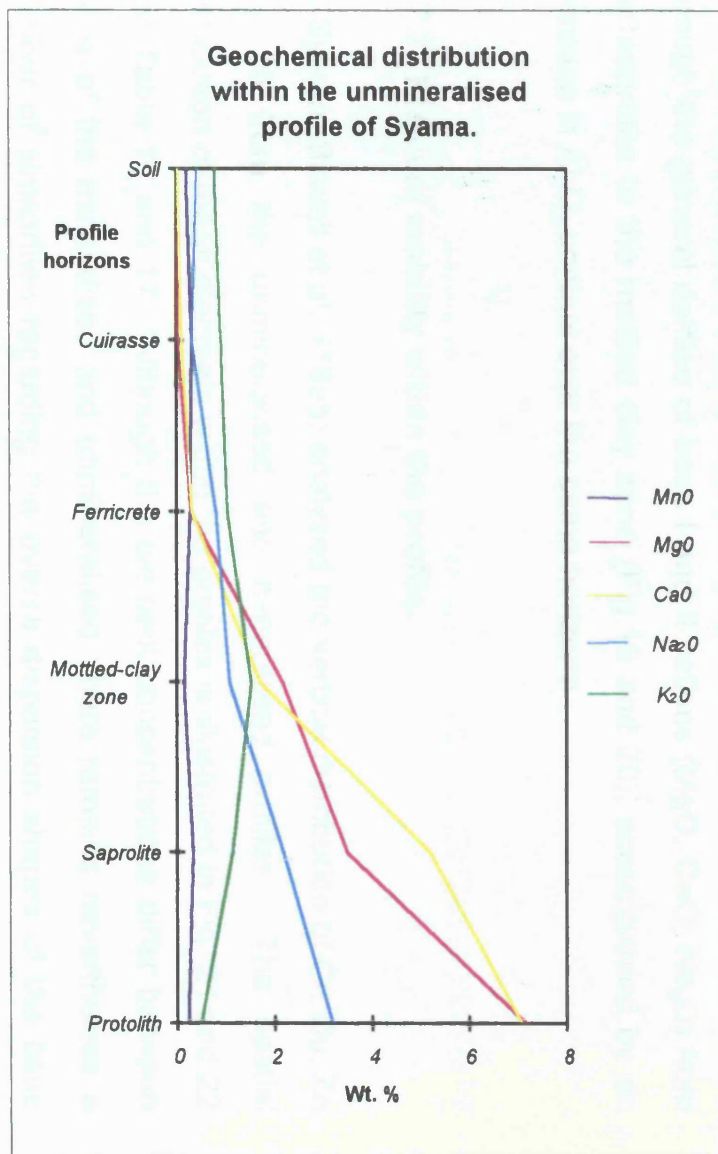
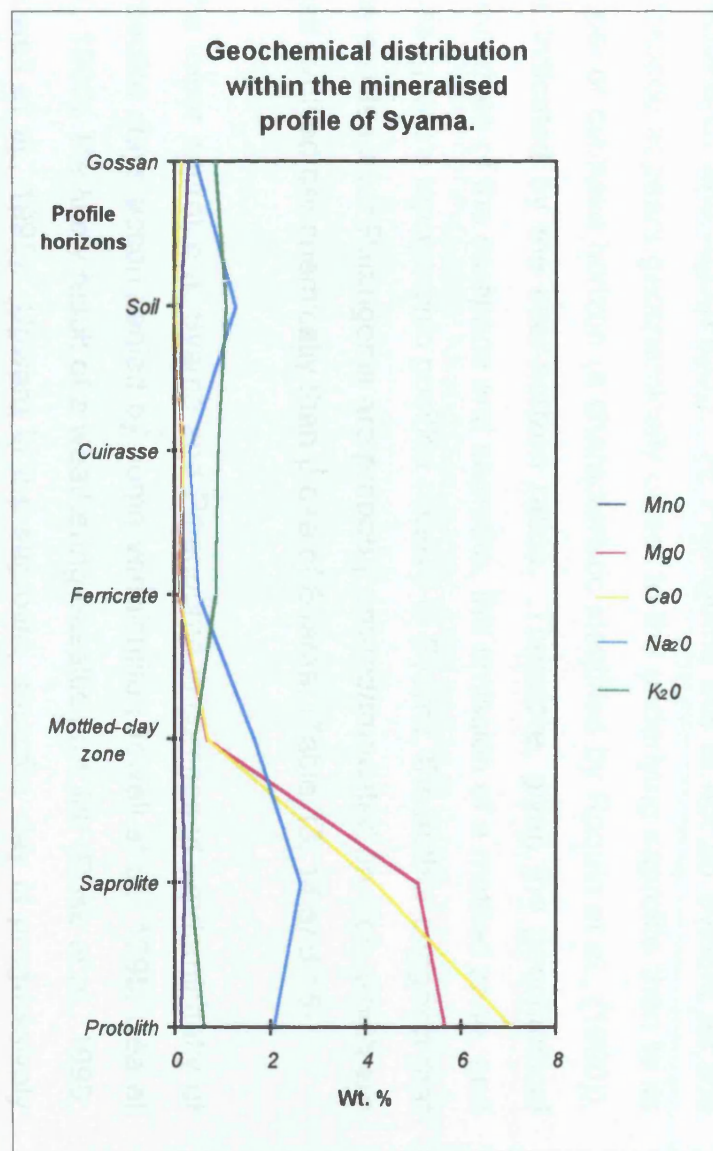


Fig. 20



those which lie above as clearly indicated by the inter-horizon ratios ($\text{SiO}_2/\text{Fe}_2\text{O}_3$ and $\text{Al}_2\text{O}_3/\text{Fe}_2\text{O}_3$). At Pitiangoma this is not so evident for the carapace appears geochemically closer to the underlying saprolite than to its superior cuirasse horizon (a characteristic identified by Roquin et al., (1990)), as indicated by the inter-horizon ratios. Therefore, given the geochemical similarities of the carapace and saprolite, the omission of a mottled zone, and Pitiangoma's topographic position relative to Syama, the author suggests that the profiles near Pitiangoma are probably eroded/truncated profiles, which are less evolved geochemically than those of Syama. (Table 13, 14 and 15).

The lower saprolite at Syama and Pitiangoma is composed predominantly of smectite clays accompanied by some vermiculite (Bowell et al., 1995; Séa et al., 1990), the likely result of a weathering basaltic protolith (Rose et al., 1990; Bowell et al., 1995). Upward in the saprolite, smectite clay is progressively altered to kaolinite. This transformation is depicted in the work of Séa et al., (1990) indicating a low kaolinite, high MgO content in the lower saprolite, changing to a high kaolinite, reduced MgO content in the upper saprolite, carapace and cuirasse (Fig. 18). A similar situation can be inferred at Syama, through the general demise of base I and II cations (MgO, CaO, Na_2O) from the saprolite to the mottled clay zone (Fig.19 and 20), accompanied by an increase in Al_2O_3 content over the same horizons.

3.7.2 Element mobility within the profile.

At Syama, Bowell et al., (1995) analysed the vertical distribution of Cr, Cu, Zn and Ni from the unmineralised and mineralised profiles. The spatial distribution of these elements within the profiles is illustrated in Fig. 21 and 22 and Table 16 and 17. Although the element concentrations differ between those of the mineralised and unmineralised, there remains nevertheless a number of similarities regarding the overall dispersion shapes of the base metals. Omitting the gossan from consideration, Cu, Ni and Zn all show their highest concentrations in the saprolite, with reductions occurring upwards in

Table 16 Elements of the unmineralised profile – Syama.

	Protolith	Saprolite	Mottled-clay zone	Ferricrete	Cuirasse	Soil
Cr	133	100	159	415	311	355
Cu	109	70	59	35	26.8	18.4
Zn	106	105	40	35	10.8	3.1
Ni	103	98	86	39	30.6	19.7

Table 17 Elements of the mineralised profile – Syama.

	Protolith	Saprolite	Mottled-clay zone	Ferricrete	Cuirasse	Soil	Gossan
Cr	181	158	259	400	279	198	388
Cu	188	168.9	149	84.5	43.8	12.9	167
Zn	176	133.5	69.5	47.6	44.6	43.7	86.7
Ni	84	81	65	62	29.3	19.8	80
Au	2.3	8.6	2.1	1.1	0.98	0.9	2.3

Table 18 Elements of the mineralised profile (ppm)- Pitangoma (Pit 128).

	Saprolite			Carapace	Cuirasse	Eluvion (soil)
	(1)	(2)	(3)			
Cr	475	523	476	567	668	1021
Cu	250	480	290	345	470	350
Zn	265	410	290	349	550	880
Ni	59	46	42	63	63	53
Mo	4.4	13.1	5.1	10	36	42
Li	32	17	17	18	14	6
Pb	1	1	3	3	9	12
Au	0.112	0.091	0.065	0.110	0.109	0.056

Table 19 Elements of the mineralised profile (ppm) - Pitangoma (Pit 130).

	Saprolite					Carapace	Cuirasse	Eluvion (soil)
	(1)	(2)	(3)	(4)	(5)			
Cr	167	263	206	208	288	317	550	782
Cu	614	564	711	416	397	372	499	333
Mn	725	827	1482	445	923	4170	1596	531
Zn	34	40	35	26	31	35	33	26
Ni	30	24	30	21	16	34	38	18
Pb	31	41	50	30	60	54	38	34
Mo	3.4	5	9.3	2.4	4.6	3.8	12.5	12.5
Li	6.2	6.5	4.3	4.6	5.7	9.1	8.3	3.7
Au	1.01	0.707	0.5	0.36	0.397	0.709	0.226	0.066

Parenthesis represent sample depth (1) approx. 16.75 m
 (2) approx. 15.50 m
 (3) approx. 14.60 m
 (4) approx. 13.60 m
 (5) approx. 12.50 m

Data sources: adapted from Séa et al. (1990) and Bowell et al. (1995).

Fig. 21

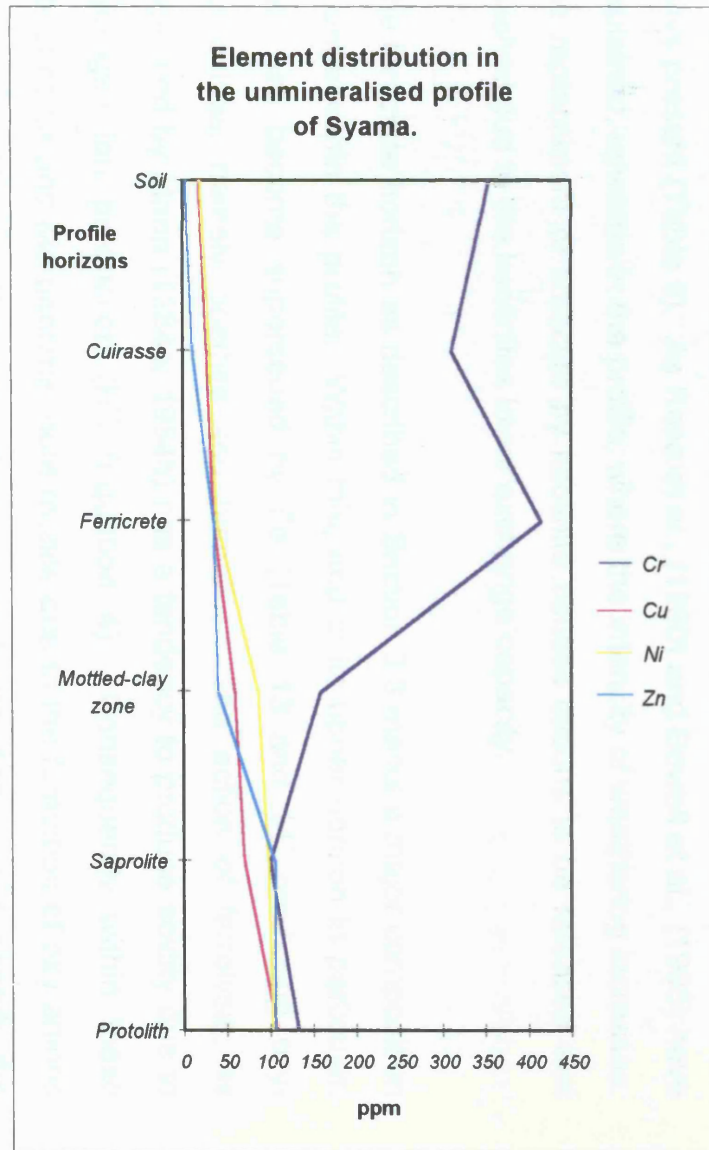
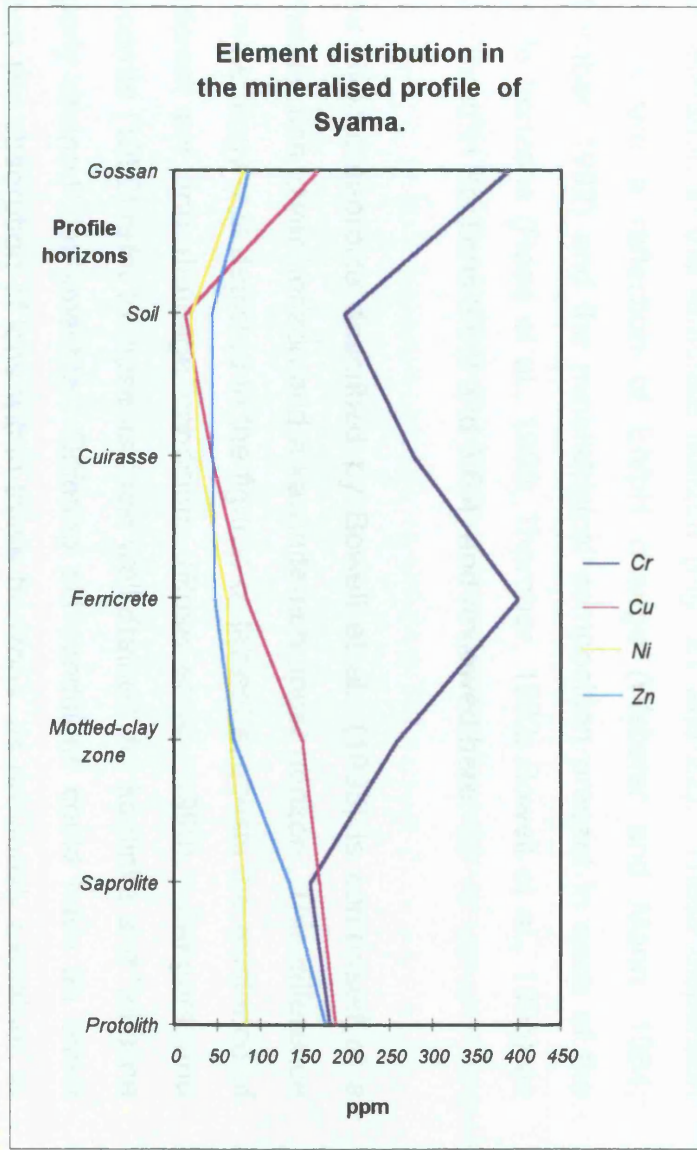


Fig. 22



the profile. In contrast, Cr increases upwards through the profile, peaking in concentration in the ferricrete horizon (Fig. 21 and 22). These dispersion shapes are a reflection of Eh/pH change (Webster and Mann, 1984; Thornber, 1992) and the mineralogical composition present in each of the profile horizons (Rose et al., 1990; Thornber, 1992; Bowell et al., 1995) as discussed in Sections 3.6.3 and 3.6.4, and reviewed here.

The Syama saprolite described by Bowell et al., (1995) is comprised of a smectite-rich lower horizon and a kaolinite-rich upper horizon. This difference in mineralogy (not depicted in the figures or tables) suggests the existence of different pH and drainage conditions (Rose et al., 1990). Zeegers and Lecomte (1992) refer to these as “acid well-drained” for kaolinite and “alkaline poorly drained” for smectite. Differing pH conditions could have an effect upon the absorption of ions within these horizons, as previously explained in Section 3.6.4 and illustrated in Table 8. Similarly the reduction in cation concentration (Cu, Ni and Zn) observed between the saprolite and kaolinite rich mottled zone (Fig. 21 and 22) could be a response to changing pH conditions or more likely a result of the different exchange capacities of the clays present (Table 9). As Rose et al., (1990) and Bowell et al., (1995) have explained, upwards in the profile, where the intensity of weathering increases, the replacement of smectite by kaolinite causes cations to be released and leached due to the kaolinites lower exchange capacity.

The ferricrete horizon as described in Section 3.3 marks a major composition change within the profile. Within this, and in its upper horizon in particular, clay has become superseded by Fe (Table 13 and 14) producing oxy-hydroxides: namely goethite and hematite. The action of ferrolysis, as explained by Mann (1984a, 1984b) has a tendency to produce acidity due to hydrogen ion production (H^+) (Equation 4). Consequently within these horizons Cr and Mo become more mobile due to the formation of oxy-anions (Thornber, 1992). Positively charged oxy-hydroxides, would absorb the mobile anions and oxy-anions whilst leaching cations of Cu, Ni and Zn. The

mobilisation and concentration of Fe-oxides and oxy-hydroxides initiated in the mottled zone and concentrated in the ferricrete are recognised in the Syama profiles though an increase in Cr and a reduction in Cu, Ni and Zn over these horizons (Fig. 21 and 22). Leaching in the cuirasse causes further loss of cations and a drop in Cr concentration. *Bowell et al.*, (1995) suggest that the partial replacement of goethite by hematite would explain this reduction in Cr due to the hematite's lower absorption capacity for oxy-anions. The soil horizon, composed essentially from the degradation of the cuirasse, illustrates a further reduction in the concentration of Cu, Ni, and Zn, a likely result of surface leaching. The concentration of elements in unmineralised and mineralised soils appear similar for Cu and Ni (Table 16 and 17). However, within the mineralised soils there does appear to be a much higher concentration of Zn and a lower concentration of Cr than the soils of the unmineralised profile.

At the surface of the mineralised profile is a silicified Fe-rich gossan (*Bowell et al.*, 1995), composed predominantly of Fe_2O_3 (47.53%), followed by SiO_2 and minor Al_2O_3 (Table 14). Within the gossan horizon an increase occurs in all elements compared to its underlying soil horizon (Table 17). Although leaching from downward percolating waters can cause the removal of elements, the scavenging nature of the oxy-hydroxides and the SiO_2 (*Kühnel*, 1987) results in the retention and enhancement of elements. In this acid pH horizon Cr would be adsorbed by oxy-hydroxides whilst dissolved base metal cations (Cu, Zn, Ni) bind through co-precipitation and adsorption to Fe-hydroxides and oxy-hydroxides. However, not only is cation adsorption pH dependant, as discussed in Section 3.6.4, but there is a sequence to their adsorption. Of all the bases Cu shows the greatest affinity to Fe-oxides and oxy-hydroxides, and is therefore the most likely cation to be retained, as discussed by *Thornber and Taylor* (1992). This sequence affinity appears to be demonstrated in the Syama gossan, with Cu highest in concentration followed by Zn and Ni (Fig. 21, Table 17). Also within the gossan the

negative surface charge of SiO_2 may adsorb base cations as discussed by Kühnel, (1987) and illustrated in Table 10.

Comparing the overall concentration change in elements from the protolith to the gossan it appears that, irrespective of a mineralised or unmineralised profile, there is a continual reduction in the concentration of base cations from the protolith upwards, indicative of progressive leaching. The base cation concentrations in the gossan (though still lower than those of the protolith) show a closer resemblance to the values found within the saprolite and mottled clay zones than to its underlying Fe-rich horizons. This is contrasted with the distribution of Cr which increases dramatically upwards in the profile, to levels in excess of those observed in the protolith.

The elemental analyses at pit 128 of Pitiangoma are illustrated by Séa et al., (1990) in Table 18 and Fig. 23. In brief, Cr and Mo increase in concentration upward in the profile. The alkali metal Li decreases in concentration in the cuirasse and eluvion compared to the lower carapace and saprolite horizons. Pb concentrations though low throughout the profile show a small increase towards the top of the profile. Base metals such as Cu, Zn and Ni (although indicating intra-saprolitic variation) show an overall increase in concentration towards the cuirasse horizon. Although this appears an opposing trend to that seen at Syama, without protolith samples no profile trend can be truly established for these elements.

Within the saprolite horizon, fluctuations in element concentrations are observed. Zone (2) indicates an increase in Cu, Zn, Cr and Mo whilst zone (3) shows a reduction in their concentration (Fig. 23). A possible explanation proposed by the author is that this could be related to a change in clay composition. Zone (2) may contain a smectite (or even vermiculite) clay characterised by a high exchange capacity, while zone (3) could contain kaolinite clay characterised by a lower exchange capacity (Table 10). Evidence in support of this theory comes from the reduction in mica and

Fig. 23

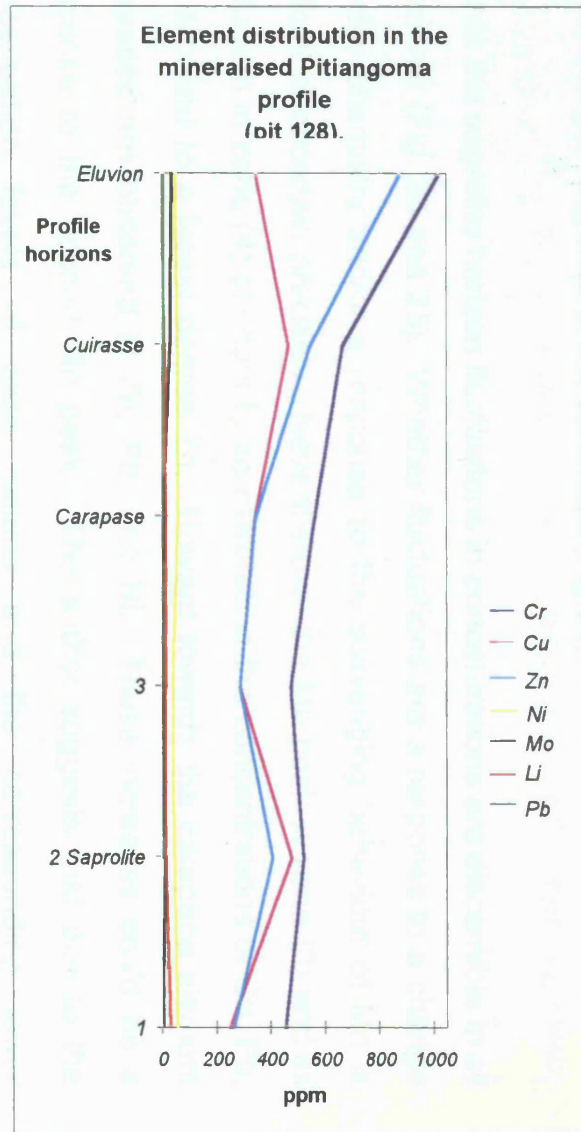


Fig. 24

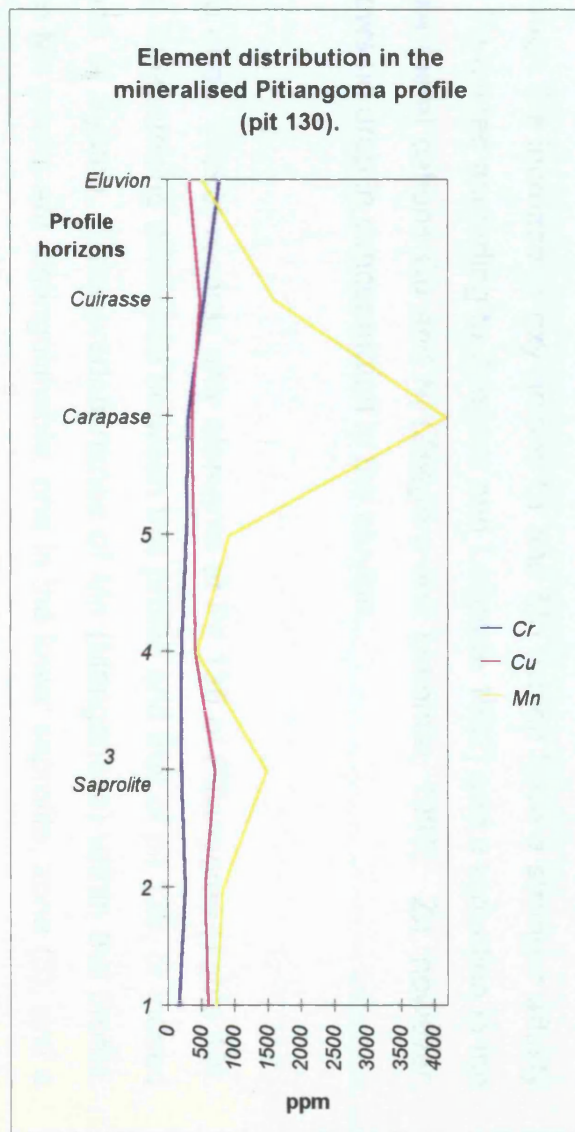
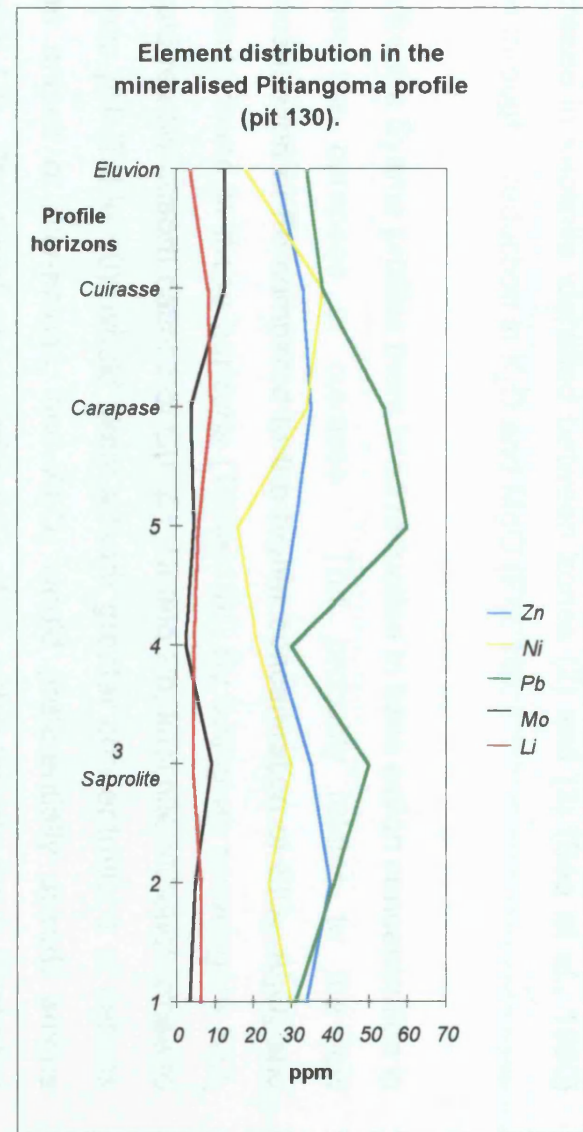


Fig. 25



increase in kaolinite identified between zones (2) and (3) (Séa et al., 1990) and through a reduction in K_2O and MgO (Fig. 18).

Unlike the Syama profiles there is no reduction in base cation concentration in either the carapace or cuirasse. This probably relates to the low concentration of Fe compared to the higher concentration of SiO_2 , Al_2O_3 and kaolinite found in these horizons (Table 15). By acting as scavengers SiO_2 would readily adsorb cations of Cu, Zn, Ni and Pb, kaolinite although close to its pzc pH (Table 10), would likely adsorb greater concentrations of cations than anions or oxy-anions, and Al_2O_3 would preferentially absorb anions (Table 10). The eventual predominance of Fe within the eluvion is illustrated through the increase in oxy-anions Cr and Mo (which have a stronger affinity for Fe-oxides according to Zeegers and Lecomte 1992) and a reduction in the base metal cations Cu and Ni (Zeegers and Lecomte, 1992). Zn, however, shows no drop in concentration in the eluvion.

Séa et al., (1990) records only elements at Pit 130 of Pitiangoma (Table 19). The most striking difference between this profile and that of pit 128, or indeed those at Syama, is the predominance of Mn (Manganese) within the profile. Two Mn peaks are distinguishable, one in the lower saprolite, zone (3), and a second larger response in the carapace (Fig.24).

Within the saprolite horizon fluctuations in concentrations are discernible in all elements (Fig. 24 and 25). Whether fluctuations are a response to a change in clay chemistry and/or a response to the scavenging behaviour of Mn is difficult to ascertain precisely. Nevertheless, the Mn peak in zone (3) and its reduction in zone (4) appears to be mirrored in the concentrations of Cu, Pb, Ni, Mo and to a lesser degree Zn. Upward towards the carapace element increases are observed in Zn, Pb, and Ni. These increases could be a response to the second Mn peak. The author suggests that due to the concentration levels of base cations and the corresponding lower

concentrations of Cr and Mo (which show affinity for Fe-oxides, Zeegers and Lecomte, 1992; Thornber and Taylor, 1992; Rose et al., 1990), the carapace is probably composed predominantly from SiO₂ and Al₂O₃ with subservient Fe₂O₃ as in profile 128. This, however, is contrasted with the cuirasse and eluvion horizons in which Fe is believed to increase in concentration, an assumption based upon the increase in Cr and Mo and the antipathetic reduction in Cu, Pb, Zn and Ni. The bonding of base metals to the oxy-hydroxides of the eluvion (though subordinate to oxy-anions) resemble the sequence reported in Fig. 11.

3.7.3 The distribution and mobility of gold within the profile.

The distribution of Au within the Syama and Pitiangoma profiles is illustrated in Fig. 26, 27 and 28.

Bowell et al., (1995) describe the distribution of Au within the weathered Syama profile as comprising of two zones of enrichment, with Au depletion above and below these horizons. The first enrichment occurs in the lower saprolite and the other is reported as lying beneath the cuirasse. However, the author, notes that the second enrichment described by Bowell et al., (1995) is not distinguishable within the figures provided (Table 18), and that only the gossan indicates an increase in concentration. The author therefore, with some caution, assumes that Bowell's data shown in Fig. 26 is the result of subsampling from an originally larger population sample, and as a consequence detail within the profile is lost.

As the effects of weathering increase upwards in the profile, the morphology, grain size, and fineness of the Au grains change (Bowell et al., 1995; Colin et al., 1988). These changes are reported as reducing grain size, increasing Au fineness, and increased particle rounding and etching. These characteristics have also been observed in profiles at Kangaba, south Mali (Freyssinet et al., 1989; 1990a).

Fig. 28

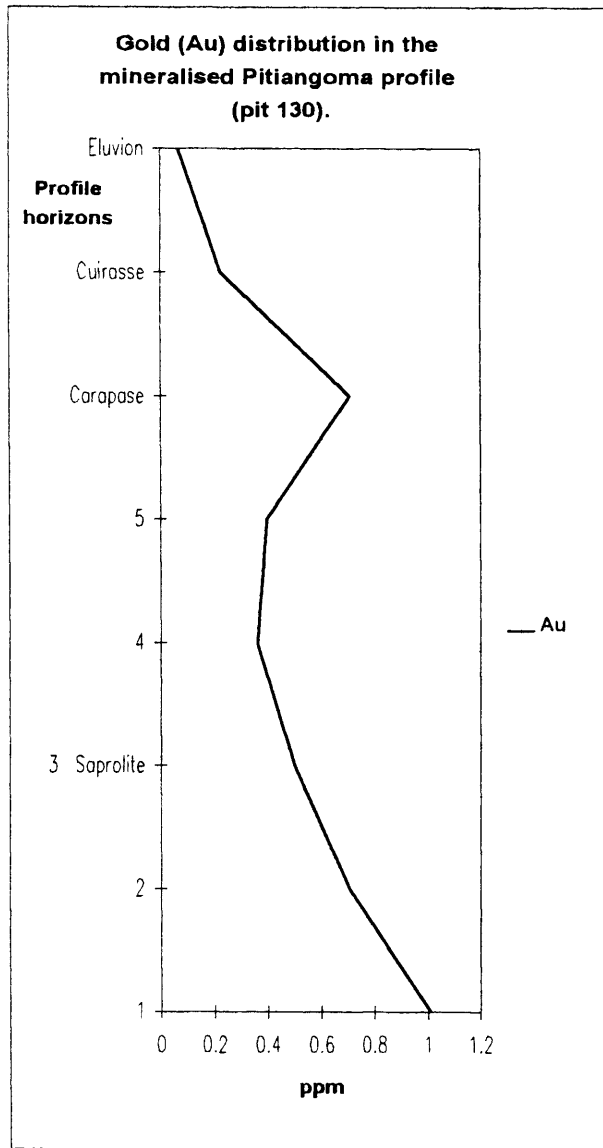


Fig. 27

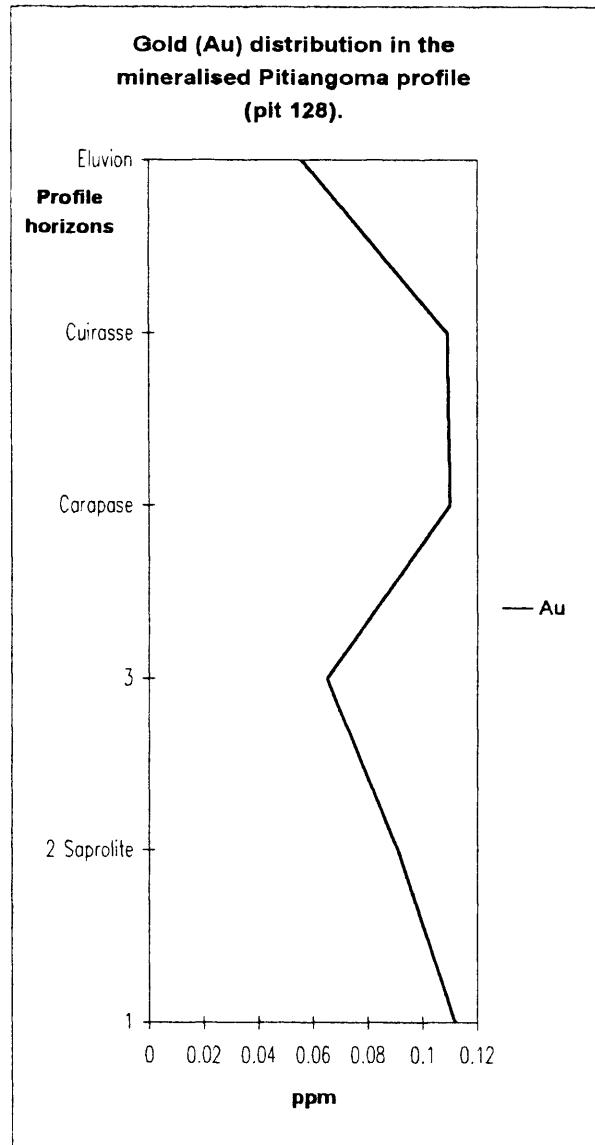
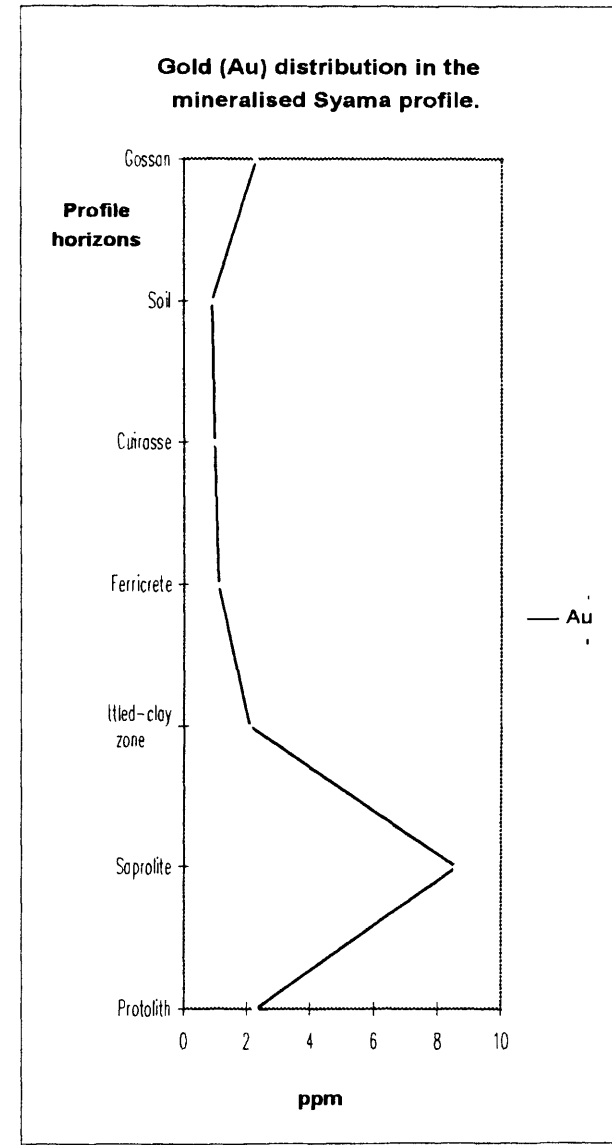


Fig. 26



Bowell et al., (1995) describe the Au grains of the protore as “well crystallised” with a grain size range of $<5 \mu\text{m} - 25 \mu\text{m}$. The Au/Ag composition varies between $\text{Au}_{85}\text{Ag}_{15}$ to $\text{Au}_{95}\text{Ag}_5$. The increase in Au concentration of the lower saprolite is accompanied by a small increase in Au fineness ($\text{Au}_{88-95}\text{Ag}_{5-12}$) and blunting of some crystal faces. In the mottled clay horizon Au fineness increases ($\text{Au}_{91-98}\text{Ag}_{2-9}$) and grain surface morphology indicates bluntness and pitting. Additionally, some grains indicate an Au-rich rim. The morphological and chemical observations have led Bowell et al. (1995) to conclude that the Au grains are residual and primary in origin. Bowell et al.’s description of Au within the cuirasse infers a further reduction in grain size ($<1 \mu\text{m} - 150 \mu\text{m}$) and a mix of chemical compositions; an Au-Ag alloy, and a high-fineness virtually pure gold ($\text{Au}_{94-99}\text{Ag}_{1-6}$). Gold grains in the surface soil are predominantly between $300-1500 \mu\text{m}$ in size although 10% of some crystalline grains indicate size ranges of $80-250 \mu\text{m}$. The grains of this horizon tend to show flattened and blunted morphologies with Au-rich rims.

The two Au profiles of Pitiangoma (Fig. 27 and 28) indicate a sigmoidal distribution similar to that reported by Bowell et al. (1995) at Syama. Two zones of enrichment occur, the first in the lower saprolite and the second within the carapace. Between these two horizons the Au grade reduces. Although the carapace is the horizon where Au concentrates, the cuirasse can also indicate a similar (or weaker) concentration of Au (Séa et al., 1990), as shown at Pit 128 (Fig. 27). Whether this increased Au concentration extends into the cuirasse or not, the overlying eluvion (soil) horizon is always inferior with only minimum Au reported (Séa et al., 1990), as shown in Table 18 and 19. Séa’s work (cited) makes no reference to the character of the Au (morphology or fineness) within the profile horizons.

These regolith enrichments, sited within the ferruginous and lower saprolite horizons, have also been reported by Butt (1988a) in his description of Au distribution within the Yilgarn block of Western Australia. These are described as lateritic and saprolitic supergene enrichments (as described in

Section 3.6.5). However, the saprolitic enrichment of the Yilgarn Block has developed following an arid period during post-lateritisation, in which the water table gradually lowered into the saprolitic horizon. Subsequent leaching resulted in a “barren” or highly leached horizon developing between the two zones of enrichment (Section 3.6.5). Although a depletion is similarly reported by *Bowell et al. (1995)*, a brief personal communication with *Butt (1997)* suggested that this as a reduction in concentration rather than a true barren zone. He infers that because southern Mali has not experienced the post-lateritic aridity exhibited in western Australia, where water tables reside considerably lower than when lateritisation occurred. Consequently the distribution of gold within the Syama regolith is most closely representative of a lateritic supergene enrichment deposit.

Gold at the top of the profile is likely related to the dissolution of gold during lateritisation. The presence of surface vegetation would allow the gold to be mobilised as organic complexes (*Freyssinet et al., 1990a; Séa et al., 1990*) which later re-precipitated on contact with oxidising Fe^{2+} , as shown in Equation 12, Section 3.6.5. The description of this process at Kangaba, SW Mali, by *Freyssinet et al. (1989)* refers to the dissolution of primary grains and colloidal gold within the cuirasse and its subsequent lateral re-precipitation within the same horizon, and also below in the mottled zone. This process would result in gold of high fineness, as is reported by *Bowell et al. (1995)*. The surface accumulation of gold would be further enhanced by natural residual concentration through land surface reduction, and also by physical eluviation as suggested by *Freyssinet et al. (1989)*. Consequently gold within the surface ferruginous horizons is likely to have been concentrated by both chemical and mechanical processes. This contrasts with the truncated regolith of Loulo, West Mali, in which the surface gold halo is primarily the result of mechanical dispersion (*Zeegers and Lecomte, 1992*).

The reported mobilisation of Au within the saprolite (*Bowell et al., 1995; Séa et al., 1990*) is probably a post-lateritisation event. Although Mali has not

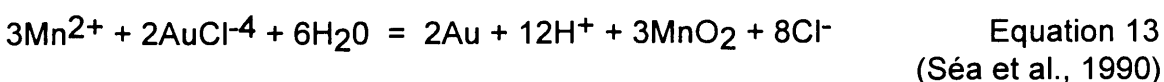
suffered dramatic climatic changes (Section 3.4), it has been subjected to climatic fluctuations in humidity (Kusnir et al., 1987) resulting in some rise-and-fall cycles of the water table. It is unlikely, given the depth of the saprolite, that organic complexes are responsible for this gold mobilisation (Webster and Mann, 1984; Séa et al., 1990). However, chloride or thiosulphate ligands are possible. Which of these two is responsible is difficult to ascertain as neither *Bowell et al. (1995)* nor *Séa et al. (1990)* record the groundwater or surface pH conditions, or give any indication regarding the sulphide/carbonate ratio of the mineralisation (Section 3.6.5).

However, it is known from the mineralogical description given in Chapter 2 that pyrite is the principal gold bearing sulphide. Pyrite oxidation, as discussed by *Mann (1984a)* and *Trescases (1992)*, produces acidification through the subsequent release of hydrogen ions (Equation 2 and 3). This acidification can be neutralised by carbonate which, according to Section 2.3 and Table 2, is present in the form of ankerite $(\text{CaMgFe})\text{CO}_3$, and, possibly, in the form of calcite and dolomite (*Colin et al., 1988*). It would appear from the observations of *Colin et al. (1988)* that the carbonates are only present at the base of the weathered profiles studied, whilst *Bowell et al. (1995)* reports the presence of “pyrite and other sulphides” in the lower saprolite showing alteration. Tentatively one could suggest that at the weathering interface of bedrock and lower-saprolite the potential acidity produced by pyrite oxidation, and from trace sulphides (Section 2.6.5), could be neutralised by the carbonates, especially if the disseminated nature of the pyrite is taken into account (*Thornber and Taylor, 1992*). Such an environment would, given the lower oxygen fugacity, favour Au dissolution by thio-complexes. Meanwhile in the lower saprolite the oxidation of pyrite probably results in a lowering of pH for groundwater solutions. Another potential source of low pH could be meteoric water percolating down through the iron-rich ferruginous horizons. Most importantly the climate, which is described as seasonal dry savannah by *Séa et al. (1990)* and *Bowell et al. (1995)*, will result in vertical water table fluctuation. In the wet season the profile is likely to be saturated, especially in

the topographically lower regions, but during the longer dry season when the water table is much lower, iron and manganese may oxidise (Equation 4), lowering the pH (Mann 1984a, 1984b).

Séa et al. (1990) have proposed that gold at Pitiangoma is mobilised by Cl⁻ ions. They regard the source of the ions as originating from the fact that the Birimian sediments were marine. This is a somewhat different proposition to that of Mann (1984a, 1984b) who believed the principal Cl⁻ source to be on-shore westerly winds. *Bowell et al.* (1995) also makes reference to a possible saline groundwater source for the mobilisation of gold at Syama. Morphological and chemical studies of gold particles report the presence of NaCl crystals (*Colin et al.*, 1988), therefore indicating possible Au dissolution by Cl⁻ ions. Unfortunately measurements of chloride concentrations within waters are not referred to within the works of *Bowell et al.* (1995) or *Séa et al.* (1990). Also, at Syama, the increased fineness of gold upwards in the profile could be a characteristic sign of chloride-complexing (Mann 1984a; *Webster* 1984, 1986; *Mackay* 1944, cited in *Webster* 1986). However, *Freyssinet et al.* (1989) reporting upon a similar increase in Au fineness between the saprolite, mottled, and ferruginous horizons of the Kangaba regolith of SW Mali, proposes that there exists a simple relationship between gold fineness and weathering intensity within the profile.

Gold dissolved in low pH solutions by Cl⁻ ions could be precipitated by reduction with Fe²⁺ (Equation 6), or through contact with Mn (Equation 13).



Séa et al. (1990) reports the presence of MnO₂ where gold precipitation has occurred in the saprolite. This could indicate Cl⁻ complexing for, as *Webster* (1986) reports, in the absence of Ag complex Au thiosulphate shows immunity to MnO₂ oxidation and would therefore not precipitate (Section 3.6.5). In fact both Syama and Pitiangoma indicate increased concentration of Mn within the saprolite and upper ferruginous horizons. However, such an

association, is not observed in the upper saprolite of Syama for an increase in the Mn concentration is not mirrored by an increase in Au, but instead a decrease is observed. This region of decrease is what *Bowell et al.*, (1995) refers to as the Au leached zone.

Both *Séa et al.*, (1990) and *Bowell et al.*, (1995) have suggested the presence of chloride complexes for gold mobilisation in the saprolite. However, it remains unclear whether this “enrichment” is a product of the dry savannah climate (as inferred by *Bowell et al.*, 1995) or if it reflects the presence of an ancient groundwater table (*Séa et al.*, 1990), where gold has been protected by the presence of iron oxides (*Butt*, 1988).

3.8 Regolith geochemical dispersion models.

Geochemical dispersion models were born in essence from an understanding that there exists an inherent link between geochemical dispersion, landscape evolution, and regolith formation. This is known collectively as the landscape geochemical approach (*Fortescue*, 1975), and has been the building block in predictive model building for geochemical dispersion, since the pioneering work of *Polynov* in the late 1930s (*Bradshaw*, 1975; *Fortescue*, 1975). Between 1930 and 1980 *Polynov* and co-Soviet workers *Perel'man* and *Glazovskaya* assisted greatly in building ideas and making links between the geographical landscape and geochemistry. Unfortunately their integrated and somewhat holistic landscape approach was little adhered to in the non-Soviet world of mineral exploration, as described by *Fortescue* (1992).

Exploration case histories were published by many companies (being informative and essential to further understanding). They were, however, very site-specific and have been described by *Vickers* (1965, cited in *Bradshaw*, 1975) as a “laborious approach to understanding”, with variability lending itself to potential misinterpretation. It was perhaps this dichotomy of trying to draw valid conclusions and generalisations from copious complete

and incomplete case histories (Fortescue, 1975; Bradshaw 1975) that drove Bradshaw (1975) to compile and edit '*Conceptual Models in Exploration Geochemistry*'. These comprehensive case history models were designed to describe the principles and mechanisms of anomaly formation in the secondary environment of the Canadian Cordillera and Shield, deriving information which could assist interpretation in other areas of similar landscape. Fortescue (1992) regarded this publication as "a significant step towards the linking of concepts of landscape geochemistry with the data from non-Soviet exploration geochemistry". In 1978 Lovering and McCarthy also contributed to model building in arid North America. The essential ingredient of a geochemical dispersion model is collaborative research, that is information derived from commercial case histories, field and laboratory experience taken together these help form what are generalised predictive models. Since the 1980s models developed for regolith exploration in Australia have installed these ingredients and have pushed the development of models forward, based upon type areas or type districts (Smith, 1996).

Butt and Smith (1980) brought an understanding to element dispersion in Australia by designing models corresponding to facet and landform (as described by Thomas 1974), and classified upon profile preservation which was subcategorised on the basis of relief and further again on the presence and type of overburden. Butt (1987) described, through the use of models, typical geochemical dispersion patterns in humid and arid regoliths. The models seek to emphasise the profile character and the dispersion mechanism with reference to the level of surface truncation and presence of overburden. The models also pay homage to Thomas, (1974) landform facet classification. Butt's (1988) description of gold dispersion within the regolith (Section 3.6.5) are in essence predictive models. He has modelled gold distribution based upon climatic situation and profile horizon. Butt and Zeegers (1992) have edited and contributed to a comprehensive study guide, presenting geochemical-landscape evolution models from tropical and subtropical terrains. These models help to explain dispersion within particular

climatic zones of low to moderate relief. The approach in essence is not that dissimilar from Butt and Smith (1980). A detailed description of this savannah model is presented in Section 3.8.1.

Smith (1996) reports upon Australia's continued efforts and advances in developing models which help to predict and describe dispersion within the regolith, and where concealment from a post-laterite cover exists. Robertson (1996) described a model on precisely this for geochemical exploration in Australia. Smith (1996) acknowledges the work of the Australian CSIRO and AMIRA research programs and the continued efforts to produce models, which allow the transferral of technology. On this very topic Zeegers and Butt (1992) believe that by developing models from type areas it is possible to then use that knowledge of geochemical behaviour and extrapolate it to areas of similar climatic-weathering history for which no a priori dispersion model exists. The technology/information transfer therefore allows comparisons between spatially differing but climatically similar regions, as illustrated below by Zeegers and Butt (1992).

semiarid	:	north-east Brazil, Western Australia
savannah	:	West Africa, northern Australia, Brazil,
rainforest	:	Brazilian Amazonian, Malaysia, Gabon, Indonesia, French Guyana

The regolith geochemical dispersion models have aided understanding and developed a framework of study for regolith research. Although they tend to be descriptive in nature they do however contain a predictive element. Consequently, depending upon the climatic situation and the level of landscape truncation, predictions can be made regarding a horizons element accumulation, depletion, relative size and concentration of dispersion, as discussed in Section 3.8.1. However, to assess whether Fortescue's (1975) objective has been achieved namely, "to obtain mathematical models of landscapes" in which "the behaviour of elements within them can be predicted

accurately”, one would have to query his usage of “mathematical” and “accurately”.

3.8.1 The savannah geochemical dispersion model.

The models reviewed in Butt and Zeegers (1992) attempt to explain geochemical dispersion in humid rainforests, savannah, and semiarid climatological terrains. The individual models are code classified according to the preservation of the regolith, recent accumulation or neoformation, and the presence and type of any overburden. As illustrated below in Table 20.

Table 20 Classification of geochemical dispersion models (tropically weathered)

Pre-existing profile	A Mostly preserved	B Partly preserved	C Fully truncated.
Recent alteration	(0) minor,	(1) low,	(2) moderate, (3) strong
Recent accumulation, cementation or neoformation	(0) none,	(Al) Al-oxides, (AS) Al-silicates,	(Ca) Ca & Mg carbonates (calcrete), (Gy) gypsum, (Fe) iron oxides, (Si) silica (silcrete), (Sm) smectites.
Overburden on pre-existing Profile	(0) none,	(1) residual soil,	(2) semi-transported (3) transported

Example: A00[01] lateritic cuirasse, outcropping or beneath residual soil.
An asterisk (*) can be used to generalise any model e.g. B**[3]

Table adapted from Butt and Zeegers (1992).

As the research area lies in a savannah climate, Zeegers and Lecomte’s (1992) savannah model was chosen as the method of understanding geochemical-landscape dispersion.

Geochemical dispersion is described through three possible model scenarios, which are based primarily around the degree of topographic dissection encountered within the landscape:

Model A:

The lateritic profile is preserved, with iron-rich cuirasse outcropping or sub-outcropping.

Model B:

The profile is truncated due to erosion and therefore there is likely no iron-rich cuirasse. Truncation maybe:

- (i) high in the profile (i.e. the mottled zone or upper saprolite), or
- (ii) low in the profile (i.e. the lower saprolite).

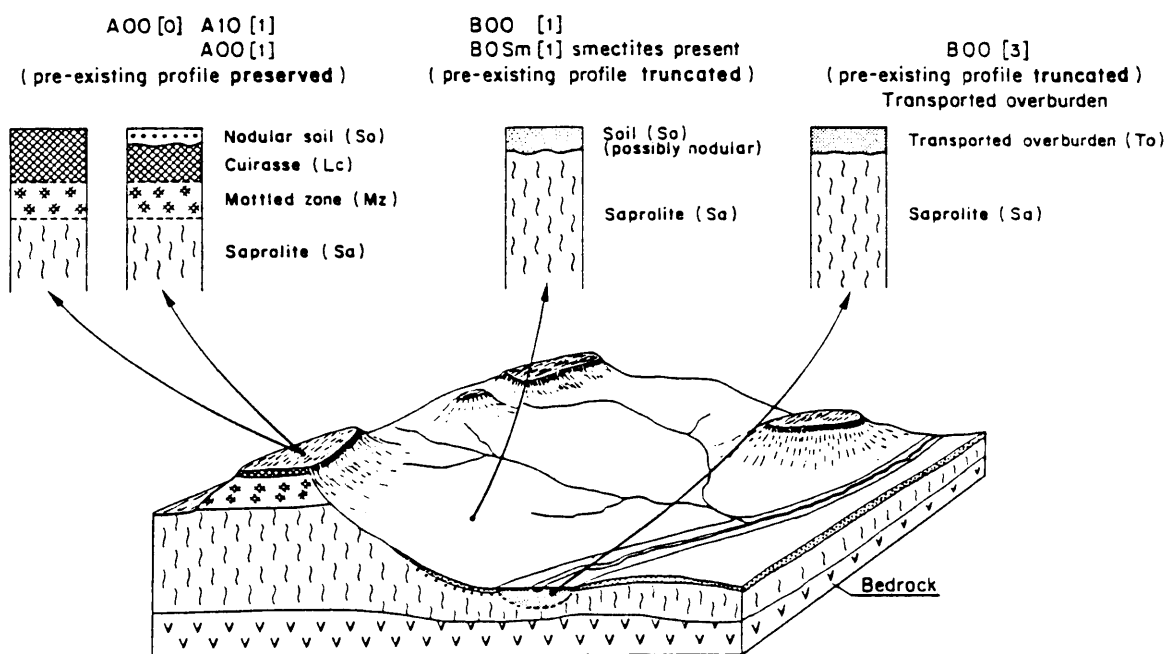
Model C:

The removal of the regolith by erosion has been completed and the soil surface is the result of current climatic conditions.

Although three models exist, Model C is not discussed within the savannah environment described by Zeegers and Lecomte, although Butt and Zeegers, (1992) suggests it is a scenario typical of very arid areas. Fig. 29 illustrates within a fictitious savannah landscape the likely relationships between landscape situation and profile. The interaction of climate and erosion on landscape invariably produces a complex topography, which on the surface results in a mixture of geochemical environments from one location to the next. The codes therefore attempt to reflect the likely character of the landscape geochemistry, which in turn effects the interpretation of element mobility.

As explained in some detail throughout the latter part of this Chapter, it is the chemical composition of the profile horizons that help to determine whether elements are retained or leached. One of the principal factors is the iron-to-clay ratio between horizons of the profiles, as discussed in Sections 3.7.1 and 3.7.2. The surface truncation level (either "A" or "B") is therefore interpreted as a fundamental control to the distribution and mobility of elements.

Fig. 29 A generalised landscape cross-section illustrating the codes relative to truncation level.



HORIZONS

To	Transported overburden
So	Soil
Lc	Lateritic cuirasse
No	Nodular horizon
Mz	Mottled zone
Sa	Saprolite
Br	Bedrock

SAMPLE TYPE

G	Gossan
G(S)	Gossan, surface
G(SS)	Gossan, subsurface
OM	Oxidized mineralization
OM(S)	Oxidized mineralization, surface
OM(SS)	Oxidized mineralization, subsurface
M	Mineralization
M(S)	Mineralization, surface
WB	Weathered bedrock
F	Fault ironstone
PG	Pseudogossan
SL	Residual soil
TO	Transported overburden
SS	Stream sediment

MECHANISMS AND ANOMALY TYPES

M	Mechanical (physical, clastic)
H	Hydromorphic (chemical)
R	Residual

Taken from Zeegers and Lecomte (1992).

Roquin et al. (1989, 1990) discovered precisely this by examining the spatial distribution of elements within the lateritic landscape. Although the principal contrast was observed between the outcropping ferricrete of the plateaux and the silty clay covers in the flats, element distribution could be divided based upon three topographic regions:

- (1) The ferruginous upper regions.
- (2) The kaolinite-rich, Fe-poor slopes, which are composed of gravely material from the dismantling of the upper ferruginous horizons and,
- (3) The silty-clay soils of the flats, regarded as allochthonous.

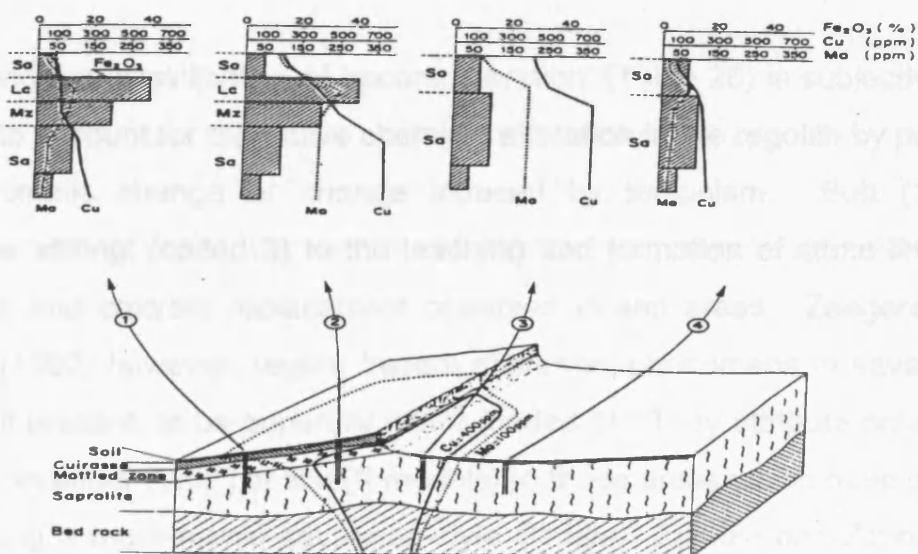
A further subdivision was also made which allowed the ferricrete to be chemically partitioned into an upper older Al-rich ferricrete, and a lower quartz-rich ferricrete. In essence the results produced by their differentiation index (Roquin et al., 1989; 1990) indicated that in the ferricrete horizons oxy-anions (P, V, Nb, As, Cr and Mo) showed the greatest affinity to the Fe oxy-hydroxides. Of the cations, Cu, and to a much lesser degree Ni, also showed an Fe affinity (as discussed in Sections 3.6.4 and 3.7.2), but their presence was also indicated within the gravely layer of the downslopes. The highly mobile element, Zn, on indexing indicated a stronger presence within the downslope gravely soils and flats than to the upper ferruginous horizons from which it is leached.

In the Dioga region of Burkina Faso, Ambrosi (1984) confirms the affinity oxy-anions have for the Fe oxy-hydroxide horizon. In this full profile (A00[1]) V, Cr and As are retained, enriched and bound to the irons. This is contrasted with elements of Cu and Ni, which being less stable in such Fe-rich environment become reduced in concentration by solubilisation and partial leaching.

In Burkina Faso at the Goren Cu-Mo mineralised area, Zeegers and Lecomte (1992) report similar geochemical dispersion characteristics. Mo showed an affinity for the iron-rich cuirasse horizon while Cu, although detectable at the surface, showed a distinct increase in concentration with profile depth,

reiterating the antipathetic nature of Cu to Fe and its affinity for clay (as discussed in Section 3.6.4). Zeegers and Lecomte (1992) therefore conclude that Cu and Mo indicated quite different dispersion characteristics depending on whether the profile was preserved (A00[1]) or truncated (B00[1]). This is illustrated in Fig. 30.

Fig. 30 The geochemical landscape of the Goren Cu-Mo prospect.



Taken from Zeegers and Lecomte (1992).

Although geochemical dispersion responds differently between preserved and truncated profiles, the actual level of truncation is also considered important with regard to the mineralogical composition of the horizon (Zeegers and Lecomte, 1992), (Sections 3.5, 3.6.1, and 3.7.1). High level truncation implies erosion at the mottled zone or upper saprolite. In the mottled zone Fe-oxides are predominant whereas in the upper saprolite although iron minerals are present the dominant mineral is kaolinite. In comparison, low level truncation, in areas of poor drainage or over basic rocks, are likely characterised by the presence of smectite clay and, possibly, primary rock forming minerals. Between these two differing truncation levels of a kaolinite dominated profile (B00[1]) or a smectite dominated profile (B0Sm[1]) the possibility exists for

differing pH conditions and physical differences in the clay's exchange capacity. These changes, which were discussed in Sections 3.7.2 and 3.6.4, can result in changes to the geochemical signature. Zeegers and Lecomte, (1992) use the Petite Suisse Cu prospect in Burkina Faso to illustrate the effect truncation has upon Cu concentration. Here, a distinct reduction in Cu content occurs between the lower smectite horizons (B0Sm[1]) with approximately 2500 ppm and the upper kaolinite horizon (B00[1]) with approximately 1000 ppm.

Determining the classification of 'recent alteration' (Table 20) is subjective. It attempts to account for distinctive chemical alteration in the regolith by past or current climatic change or change induced by tectonism. Butt (1992) associates 'strong' (coded 3) to the leaching and formation of stone lines in rainforests and calcrete replacement observed in arid areas. Zeegers and Lecomte (1992) however, regard 'recent alteration' phenomena in savannah climates, if present, to be generally minor (coded 1). They attribute only 'low' alteration (in either A10[*] or B10[*] models) to those areas which have or are experiencing a more humid savannah-style climate. Zambia and Zimbabwe of east Africa fall into this category. Their profiles tend to exhibit recent alteration through partial immature development of a stone line.

Recent accumulation, cementation or neoformation refer to changes in the degree of profile leaching (Butt, 1992). As illustrated in Table 4 the amount of available water helps to determine the hydrolysis reaction and the residue produced. Consequently, in wet savannahs where leaching is more prominent, kaolinite is the likely secondary residual produced by monosiallitization, while in dry savannah and arid areas smectites may dominate over kaolinite. With climatic change profile leaching alters, this can produce a variety of mineralogical accumulations or cementations, such as the presence of calcrete or silcrete cements in arid areas. However, with regard to the presence of smectite (coded Sm), as Zeegers and Lecomte (1992) and Rose et al. (1990) explain, its presence may not be directly linked

to climate. For smectites are also found in environments of impeded or poor drainage as well as the initial weathered phase overlying basic host lithologies; for example in the lower saprolite of the Syama and Pitiangoma profiles. The likely situations in which the presence of smectite within the landscape would be present are illustrated in Fig. 29. Consequently, as already explained by Zeegers and Lecomte's Petite Suisse Burkina Faso example, the truncation level can determine whether the coding is geared towards kaolinite (B00[*]) or smectite (B0Sm[*]) interpretation.

The thickness and type of overburden can also effect the surface geochemical response. Overburden can be classified as any of four types, as illustrated in Table 20. The presence of each is very much controlled by the position within the topographic landscape as discussed in Section 3.5. Consequently, on the most elevated regions and areas of steep slopes overburden is most likely non-existent, or in-situ residual soil. Therefore as these regions are topographically the highest, it would not be unreasonable to suspect that there would be no sediment contribution from any other source area. This is contrasted with low angle slopes and valley floors. In these environments overburden can progressively accumulate and mix transgressing from semi-residual to transported respectively (Roquin et al., 1990). Essentially the thicker the overburden and the more allochthonous in nature the less likely it is that underlying element signatures will be detected (Zeegers and Lecomte, 1992; Smith, 1996; Robertson, 1996). Zeegers and Lecomte (1992) report such a problem at the Gan prospect in Burkina Faso. Here transported overburden lies upon the saprolite (B0Sm[3]) obliterating evidence of any underlying anomaly. However, in certain lowland valley situations, if the transported overburden is thin and likely accompanied by the interaction of the water table, weak hydromorphic dispersions may prevail (Butt, 1987; Zeegers and Lecomte, 1992). At the Filon Bleu gold prospect in Guinea sampling in the 1 m thick residual soil overlying the cuirasse (A00[1]) produced the worst Au contrasts than any of the two other sampling sites (A00[0]) and (B00[1]), (Zeegers and Lecomte, 1992). Freyssinet et al. (1990)

and Roquin et al. (1990) reiterate the allochthonous nature observed in the soils of the valley flats (or lows).

The soil composition is complicated by the addition and mixing of material derived from upslope termite activity. Material extracted from the mottled zone by termites may be transported mechanically, but more likely by surface runoff, for hundreds of metres before depositing in the lower gradients of the valley flats. These silty clay deposits increase soil heterogeneity and, as reported by Freyssinet et al. (1990), have in the case of gold produced strong surface anomalies which bear little or no relationship to the grade in the underlying ferricrete. This highlights the need to be able to identify within the geochemical environment areas of erosion and areas of deposition.

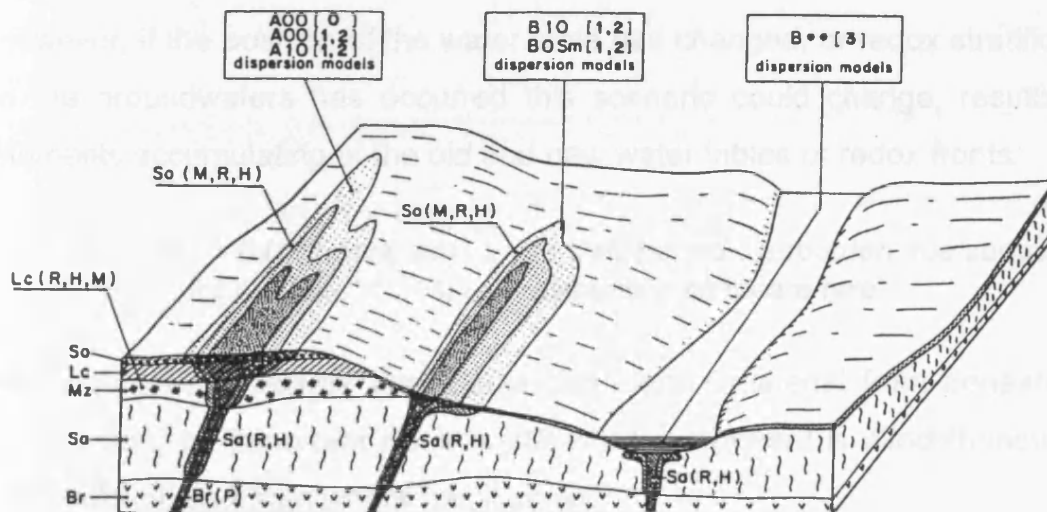
Accompanying the same landscape situation Fig. 31 illustrates within profiles the principal mechanism responsible for dispersion, the relative size of the dispersion halo between horizons and the influence topography has upon the shape and mechanism of dispersion.

In a full "A" type savannah profile the halo of geochemical dispersion increases upwards in the profile (resembling a mushroom shape) as illustrated by Freyssinet et al. (1989) in the Kangaba region of Mali. In the saprolite the halo is characteristically narrow, formed by residual and some hydromorphic processes. Whilst in the mottled zone dispersion widens reaching its maximum width in the cuirasse (and soil) horizon. Within this horizon mechanical as well as hydromorphic and residual processes become the mechanism of dispersion creating a wide laterally dispersed halo. Although dispersion is wide it is often developed at the expense of reduced trace element concentrations due to leaching (Sections 3.6.4 and 3.7.2).

In truncated profiles lateral dispersion within the saprolite is relatively low as exhibited in the north Karamoga region of NE Uganda (cited in Zeegers and Lecomte, 1992). Zeegers and Lecomte (1992) attribute a lot of this to the

incorporation of metals in stable minerals, which increases immobilisation. Also the clay produces an environment which favours trace element retention rather than the leaching associated with the Fe-rich horizons (Section 3.6.4 and 3.7.2). The mechanisms of dispersion within the saprolite are residual and hydromorphic. Any lateral dispersion is generally restricted to the soil horizon, where once again mechanical, hydromorphic and residual coexist.

Fig. 31 Idealised models of dispersion in preserved or truncate lateritic profiles.



Taken from Zeegers and Lecomte (1992).

Contrasting the size of surface dispersion haloes of "A" and "B" landscape situations, "B" are characteristically smaller and provided that there has been no significant surface leaching, the anomaly to background contrast within the truncated profile is often greater (Zeegers and Butt, 1992). The size of dispersion haloes can be enlarged through mechanical and hydromorphic processes if the topographic gradient allows downslope movement, creating an asymmetrical dispersion halo as illustrated in Fig. 31. In regions of low relief little mechanical dispersion exists. However, elements may show different dispersion characteristics depending upon their mobility and affinity for absorption by Fe and Mn oxides. Such a situation is described at the Pb-

Zn deposit of the Coastal Province of Kenya (Bugg, 1982). There more mobile Zn is hydromorphically dispersed further downslope than elements exhibiting lower mobilities and a greater readiness for absorption onto Fe and Mn oxides, such as Pb and Cu. Zeegers and Butt (1992) conclude the following;

Sum (R, H, M) = A > B > C

Generally the dispersion halo formed from residual, (R), hydromorphic (H) and mechanical (M) will be at its largest in "A" model situations, smaller in "B" model locations or completely eroded in "C" model situations.

However, if the position of the water table has changed, or redox stratification in the groundwaters has occurred this scenario could change, resulting in elements accumulating at the old and new water tables or redox fronts.

Sum (R, H, M) = 0 (or nearly so)
for models * * * (3)

In transported overburden true surface dispersion halos are rare.

Although termite activity and plants can extract material from beneath the overburden, an important issue is still what component is allochthonous, in-situ residual, and from where has it come.

Fig. 29 and 31 and Table 20 summarise through study a landscape-geochemical model developed for the savannah environment. The object of the model is to demonstrate how the landscape can be used advantageously in understanding and interpreting geochemical data.

3.9 Summary – The established problem.

Laterite developed under a savannah climate is characterised by horizons, which are distinct morphologically and geochemically from those above and below. The upper iron rich surface of the laterite is the region which has undergone the most severe and prolonged weathering attack, and as such is the most changed geochemically from its original underlying parent rock.

However it is the composition of these horizons accompanied by Eh/pH that influences the overall distribution of elements/minerals in the laterite. Consequently elements which show affinities to the chemistry of a horizon will often result in their retainment and possible concentration whilst elements indicating an antipathetic character, are depleted. The spatial distribution of gold within the profile though similarly influenced by Eh/pH, is also a product of the palaeoclimate. Environments where a prolonged savannah climate has operated often result in the formation of lateritic supergene deposits rather than the saprolitic supergene deposits of arid climates. The introduction of "landscape geochemistry" takes these findings a step forward, for it links geography and geochemistry by acknowledging that the geochemical patterns in the landscape are a product not just of geology but also climate and topographic relief. The acceptance that landscape geochemistry could aid exploration drove the development of conceptual models, based upon the summation of data from various prospected regions. The intention of the models was also to act as guides for the study of dispersion in those regions deemed to be equivalent to the model, but for which no a priori knowledge existed. One such model based around a savannah environment was discussed with examples in the latter part of this chapter. This model indicates a number of important restraints upon the geochemical surface expression caused by the terrain.

(i) The first point explores the consequences of profile preservation or truncation. Fully preserved profiles capped by a cuirasse, an iron-rich ferruginous horizon, characteristically retain and concentrate anions and oxy-anions (typical elements Cr and Mo), and to a lesser degree some cations; Cu, Pb, Zn and Ni. In a truncated profile the opposite is generally observed, cations are the elements retained and concentrated compared to anions.

(ii) The second point considers the importance of overburden and how its presence can reduce or obscure geochemical signals. Essentially the model necessitates an awareness of environments of deposition compared to its uncontroversial counterpart, areas of erosion.

(iii) The third and final point is concerned with the size and contrast of the dispersion halo. Exploration ideally requires a large sized halo and a strong anomaly / background ratio or contrast for detecting potential mineralisation. Field evidence indicates that halo size increases upward in the profile generally attaining its maximum dimension at the surface due to dispersion from both hydromorphic and mechanical processes. Whereas contrast reduces with height and distance from its source region.

Zeegers and Butt (1992), in summing up the practicalities of using such a model recommend that regolith landform maps be prepared of the area under study. The maps produced by field evaluation would serve to identify:

- (a) the degree of truncation of the lateritic regolith,
- (b) the nature and thickness of any overburden and
- (c) the location of erosional and depositional environments.

In the absence of such landform maps specific mineral mapping could help identify the level of regolith truncation. Such examples include: high Fe values, likely indicating the presence of a ferruginous cuirasse; high Al_2O_3 possibly representing the presence of a kaolinitic saprolite; and SiO_2 pointing towards a surficial soil horizon. Highlighted throughout the use of this model is the need for knowledge concerning the regolith landform. Unfortunately, as with much pre-1990 regional geochemical surveying, regolith landform mapping was not performed nor seen to be of value. As a consequence no map exists for this study region, nor is there any information regarding Fe, Al_2O_3 , or SiO_2 distributions across the region. In order to overcome this dilemma the author uses computer techniques in an attempt to create a regolith landform map of the research region. Its construction is explained in Chapter 5 (Section 5.2) and in Chapter 6 it is used to help understand the spatial location of 'known' gold occurrences and to assist in the prioritisation of gold areas.

CHAPTER 4

DATA ACQUISITION AND PRELIMINARY PROCESSING.

Contents.

- 4.1 Introduction.
- 4.2 Data acquisition.
- 4.3 Computer and software specification.
- 4.4 Field data.
 - 4.4.1 Fieldwork aims, objectives and logistics.
- 4.5 Data processing.
 - 4.5.1 Remote sensed data.
 - 4.5.1.1 Correcting line dropouts.
 - 4.5.1.2 Atmospheric correction.
 - 4.5.1.3 Atmospheric methodology.
 - 4.5.1.4 Geometric rectification.
 - 4.5.1.5 Image mosaicking.
 - 4.5.1.6 ERS-1 data.
 - 4.5.1.7 Speckle suppression methodology.
 - 4.5.2 Geochemical data.
 - 4.5.2.1 Data quality and verification.
 - 4.5.2.2 Data solutions.
 - 4.5.2.3 Geometric rectification.
 - 4.5.2.4 Data interpolation.
 - 4.5.2.5 Grid mosaicking.

- 4.5.3 Radiometric data.
 - 4.5.3.1 Data processing and error corrections.
- 4.5.4 Magnetic data.
 - 4.5.4.1 Data processing.
- 4.5.5 Digitising of published cartographic data.
 - 4.5.5.1 Geological data input.
 - 4.5.5.2 Published mineral localities.
 - 4.5.5.3 Topographic data.
 - 4.5.5.4 Lateritic escarpment data.
 - 4.5.5.5 Hydrological data.
 - 4.5.5.6 Attribute linkages.
- 4.5.6 The digitising of unpublished cartographic data.
- 4.5.7 Coverage rectification and warping.
- 4.5.8 Cartographic data quality assessment.
- 4.6 Geochemical statistical analysis.
 - 4.6.1 Global geochemical data.
 - 4.6.2 Statistics related to lithology: a GIS approach.
 - 4.6.3 Data thresholding and anomaly recognition.
- 4.7 Global radiometric statistical analysis.
- 4.8 Summary.

4.1 Introduction.

This chapter is concerned with preliminary data processing and the construction of a GIS database. It begins in Section 4.2 by describing briefly the type and form of data received, and the software specifications used to process these data. When building a geodatabase it is rare to find source data in a format that are compatible for direct entry to the GIS. Instead considerable time and effort is normally required to reformat data prior to input into the system. At the same time it is necessary to check for errors and to ensure that all datasets conform to a common geographical projection; as discussed in Section 4.5. This chapter explains the steps undertaken to make each major source of input data used in this work accessible to the GIS. It also identifies how various errors and initial inadequacies were addressed. It begins with a discussion of remotely sensed imagery (Section 4.5.1), then proceeds to geochemical data (Section 4.5.2), radiometric data (Section 4.5.3), magnetic data (Section 4.5.4), published cartographic map data (Section 4.5.5), and finally, unpublished map sources (Section 4.5.6). Acquiring good spatial accuracy and registration between these dataset is important for minimizing error in future analyses, as is explained throughout these sections and reiterated by the necessity for a warping procedure as discussed in Section 4.5.7. However, it is recognized in Section 4.5.8 that a truly error-free geodatabase is an impossibility, and a point must be reached at which the database is accepted as adequate on pragmatic grounds.

The following two Sections (4.6 and 4.7) discuss the nature of the geochemical and radiometric data and analyse their information content within a statistical framework. The data are looked at as a whole, and the geochemical datasets are also subdivided based upon lithology and threshold values to highlight possible anomalous regions.

The chapter concludes with a summary in Section 4.8.

4.2 Data Acquisition.

Most data used in this research project were supplied by BHP (Mali Inc.). All were supplied 'raw' (i.e. largely unprocessed) and its general nature reflected a regional reconnaissance purpose, comprising of various dates, formats and forms as is illustrated in Table 21. Although numerous 'in-house' maps were also supplied by BHP, many were rejected because of their incompatibility to the 'regional' theme, or dismissed due to poor cartographic quality. Consequently, the information shown Table 21 is a product of some degree of data screening. The imagery and geochemical data were one-off commissioned events so the author was denied any quality selection.

4.3 Computer and Software Specification.

The majority of the work reported here was undertaken on a SUN workstation. A typical system comprised of a SPARC Station running the Solaris 5.4 operating system, providing a UNIX working environment. Use was also made of the University's central computing facilities, consisting of Silicon Graphics hardware running a proprietary UNIX operating system called IRIX. Some work has also been performed on IBM PC compatible computers, with various specifications ranging from 60MHz 486 processors to 300MHz Pentium II systems.

4.4 Field Data.

Although fieldwork is not always an essential component of a GIS based project it can be a great benefit. In particular it offers an opportunity to perform various error checking tasks, allows collection of field data to aid georeferencing of input data sets, and provides greater familiarity with the terrain being analysed.

Table 21 Data specifications.

Data	Description	Scale / Resolution	Area coverage/swath	Format
REMOTELY-SENSED DATA.	1 Full scene SPOT. (3/3/87) 2 Full scene TM. (7/1/86) 1 Full scene ERS-1. (1/6/93)	SPOT-XS 20 m. Landsat TM 30 m. ERS-1 SAR 25 m.	60 km 185 km 100 km	C.C.T. BIL & BSQ (8mm data tape). BIL (8mm data tape).
GEOCHEMICAL DATA.	32 regional sample location maps.	1:50,000 @ 400 x 1000 m 200 x 1000 m	Approx. 6,000 km ²	Dye-line paper source, representing four provinces of: Lobougoula, Fourou, Dioumantene and Misseni. (8 element maps per region)
	ASCII digital data. Four disks, one per province.			ASCII data. 4, double sided high-density floppy disks.
AIRBORNE RADIOMETRICS	Regional data, Thorium (Th), Potassium (K), Uranium (U) and Total count (sampled in cps)	Resampled @ 80 x 80 m	Approx. 1,000 km ²	ASCII data. 4, double sided high-density floppy disks. One disk per element
AIRBORNE MAGNETICS.	Regional data	Resampled @ 80 x 80 m	Approx. 1,000 km ²	ASCII data, on 1 double sided high-density floppy disk.
CARTOGRAPHIC MAP DATA (published).	Topographical map data Geological map data.	1:200,000	Approx. 12,000 km ²	Paper maps, 3 regions: Massigui NC-29-XXIV Kadiana NC-29-XVIII Kadiolo NC-30-XIII
CARTOGRAPHIC MAP DATA (unpublished).	BHP "IN-HOUSE" map, concession area.	1:25,000 (1:100,000)	Approx. 250 km ²	One paper map covering the BHP Syama concession area.

BHP supported and planned a field visit for the beginning of November 1994. This lasted three weeks, with the first week spent at BHP Headquarters in Bamako, and the remaining two weeks spent in the field at the Syama mine site.

4.4.1 Fieldwork aims, objectives, and logistics.

The principal aim for the fieldwork was to collect data to facilitate the georeferencing of both remotely-sensed images and soil geochemical datasets. The objective was to collect ground control points (GCPs) using hand-held global positioning system (GPS) receivers (specifically Magellan and Trimble devices). These field-based GCPs were considered to be the most accurate source of geographical coordinates available to this project. The task was undertaken across as much of the 65 km x 120 km study area as possible, within the time available. This apparently simple task was considerably more difficult to implement in the field than had been anticipated. Collecting GCP data proved an arduous and lengthy process. The major cause of difficulties was the coincidence of the fieldwork with the end of the rainy season. As a consequence, all river levels were high making many crossing points impassable. This in turn made journeys between key GPS sampling points long and somewhat tortuous, if possible at all. These problems were exacerbated by the fact that many of the roads shown on paper maps turned out to be only narrow footpaths, and when approaching a village tracks often fractionated into a web of alternative routes that made accurate identification of the GPS site difficult. The end result was a poor distribution of GCPs in the north and in the extreme east and west of the study area.

4.5 Data Processing.

The principal aim of the preliminary processing stages was to transform the acquired datasets into a workable quality. This involved correcting data errors,

ensuring file formats were compatible with the GIS, and transforming all data sets to a common geographic registration. The choice of map projection was dictated by the published 1:200,000 geological and topological maps, and by BHP's desires to employ a UTM projection. Consequently, all available data sources were transformed to a common coordinate base of UTM Zone 29 North. In order to achieve the aims outlined above a series of logical, if somewhat lengthy, procedures were undertaken, as described below.

4.5.1 Remotely Sensed Data.

This data consisted of two full-scene Thematic Mapper (TM) images, a full-scene SPOT High Resolution Visible (XS) image, and a full-scene ERS-1 SAR image. The generic characteristics of each of these images are listed in Table 22. The SPOT XS and Landsat TM images are collected by so-called "passive" scanners which collect ambient electromagnetic radiation reflected or emitted by the Earth's surface. In contrast, ERS-1 SAR images are collected by an "active" (radar) scanning system operating in the microwave portion of the electromagnetic spectrum. It utilizes a radar beam to actively "illuminate" the ground passing beneath the satellite platform.

Table 22 Imagery specifications.

Sensor	Landsat-5 TM	Spot-2 XS	ERS-1 SAR
Band designation	Wavelengths sensed		
1	0.45 - 0.52 μ m	0.50 - 0.59 μ m	-
2	0.52 - 0.60 μ m	0.61 - 0.68 μ m	-
3	0.63 - 0.69 μ m	0.79 - 0.89 μ m	-
4	0.76 - 0.90 μ m	-	-
5	1.55 - 1.74 μ m	-	-
6	10.40 - 12.50 μ m	-	-
7	2.08 - 2.35 μ m	-	-
'C'	-	-	3.8 -7.6 cm
Spatial resolution	30 m	20 m	30 m
Image area	185x185 km	60x60 km	100 km ²

Source :ERDAS (1997)

4.5.1.1 Correcting line drop-outs.

Both of the TM images (p198r53 and p198r52) showed clearly visible sporadic line drop-outs occupying the full sensor swath. These are common errors arising either from a total malfunction or a temporary swamping of a detector. The usual correction for these errors is to replace each pixel in the drop-out line with either: (i) the pixel value or digital number (DN) found in the line immediately above or below, or (ii) by the average of these two values (Drury, 1987; Mather, 1989). The latter method was selected as the replacement technique in this work.

4.5.1.2 Atmospheric Correction.

The atmosphere interacts with solar and terrestrial emittance by processes of reflection, absorption, and scattering of electromagnetic energies. Due to these processes the signal received at the sensor, and thus recorded in the image's DN values, is not 'true' with respect to the ground leaving radiance in a non-atmospheric situation (Curran, 1985; Tanré et al., 1986; Mather, 1989; Drury, 1987; ERDAS, 1994). Effects due to absorption and scattering are further complicated by the spatial and temporal variability in humidity, terrain elevation and orientation, and aerosol concentrations (Tanré et al., 1986; ERDAS, 1994; Teillet et al., 1995). In general the effects of atmospheric interference increase inversely with wavelength. Thus images collected in the visible part of the spectrum (for example, TM bands 1, 2, and 3) are the most affected. The purpose of atmospheric correction is to suppress the effects of the atmosphere, and in particular to remove the additive brightness caused by atmospheric luminance. Unless this is corrected it will introduce an atmospheric brightness bias into any subsequent band ratio operations, which are to be used in this research. Atmospheric correction is also desirable whenever there is an intention to make comparisons between multi-temporal imagery, or when DN radiances are to be input into finite physically-based models. Research into

atmospheric correction has resulted in a number of estimation methods (Tranre et al., 1986, Mather, 1989, ERDAS, 1994 and Teillet et al., 1995):

- a) Dark-pixel subtraction.
- b) Radiance-to-reflection conversion.
- c) Linear regression estimators.
- d) Atmospheric modeling.

Each approach requires varying levels of mathematical and procedural complexity in order to determine the atmospheric effect in each recorded spectral band. Method (c) was selected for use in this work because: (d) requires extensive mathematical modeling and additional data in order to be implemented effectively (Tanré et al., 1986); (b) is principally field-based and (a) although operating under broadly similar principles to method (c) (Mather, 1989), is generally considered to be less robust. Furthermore, method (a) requires the presence of a deep clear water body or large cloud shadow (Teillet et al., 1995), both of which were absent in the images used in this work.

4.5.1.3 Atmospheric Methodology.

Regression analysis was performed on 32 of the darkest pixels distributed throughout the TM and XS scenes. At each location DNs were extracted for band numbers 1, 2, 3, 4 and 5 of the TM image, and 1, 2, and 3 of the XS image. Using the EXCEL spreadsheet a linear regression was performed on these data, with the independent variable represented by the (presumed non-scattered) NIR band. A standard least-squares regression produced a "best-fit" line through the data and an estimate of the atmospheric luminance term is given by the point of interception on the x-axis. Table 23 and 24 illustrate the results.

Table 23 TM atmospheric correction terms.

Landsat T.M.	Band 1	Band 2	Band 3
Band 5	67	18	16
Band 4	52	9	5
Average	60	14	11

Table 24 TM atmospheric correction terms.

SPOT XS	Band 1	Band 2
Band 3	15	3

With the TM imagery a decision was made to regress against both the near infrared bands (i.e. 4 and 5). Results show the inherent variability of the method, with Band 5 clearly leading to higher atmospheric luminance estimates than Band 4. The average of the two estimates was used as the best atmospheric correction estimate. The final stage was to subtract these correction terms from each pixel in the respective visible wavelength images. In the rare situation where the original pixel value was less than the correction factor the pixel DN was set to zero.

4.5.1.4 Geometric rectification.

A “map” is a graphical representation of spatial data, possessing a scale and a specific projection. A remotely sensed image in its unprocessed state is not inherently a map since it lacks a consistent scale and a recognized projection. Geometric rectification is the technique used to transform the distorted geometry of original imagery into a true geographical space.

Prior to geometric rectification the full-scene TM and ERS-1 images were subscened to avoid unnecessary data processing and to reduce file storage requirements. All images (TM, XS, and ERS-1) required geometric rectification but the purpose was not simply to ensure they were correctly projected into a

common geographic space, but also to ensure that pixel locations matched between images. This pixel-to-pixel matching is vital to reduce spatial errors in subsequent processing, especially if imagery from different sources are combined in some way. To achieve this aim one image is first geo-rectified and it then acts as a base map to which other images are co-registered, or matched, using points visible in both images. The TM image was selected as the “master image” due to its superior clarity and greater area coverage. The SPOT XS and ERS-1 images were subsequently co-registered to the geo-rectified TM image. The methodology and procedures used for geo-rectification are now presented.

Field-based GPS recordings provided GCPs for rectifying the TM image. Poor quality GPS readings were rejected, as discussed in Gilbert (1997). Obtaining an even distribution of GCPs across the image is desirable since a more dispersed and non-linearly distributed GCP pattern provides a more reliable transformation (ERDAS, 1994). Locating GCPs on the image was often difficult, and sometimes impossible, due to constraints imposed by the 30m spatial resolution of the TM. and the nature of the landscape imaged. Despite this, at least 35 GCPs were located on the p198r52 image, and 15 on the smaller p198r53 image. The GCPs were located principally by river and road intersections. A transformation coefficient matrix was computed and used in polynomial transformation equations. A first-order polynomial was considered to be adequate as images collected by narrow swath scanners like the TM and HRV are normally free from complex distortions caused by platform yaw, roll and pitch ERDAS 1994. Scale, rotation, and location are correctable with a simple 6 coefficient linear transformation:

$$\begin{matrix} X' = & a_c a_y a_x \\ Y' = & b_c b_y b_x \end{matrix}$$

Transformation coefficient matrix.
Where: c = constant.

$$\begin{matrix} X' = & b_c + b_y x_1 + b_x y_1 \\ Y' = & a_c + a_y x_1 + a_x y_1 \end{matrix}$$

1st order polynomial equation.
Where: x_1 and y_1 = input source coordinates,
 X' and Y' = output rectified coordinates

The minimum number of GCPs required, N, is given by the following formula:

$$N = [(t+1)*(t+2)]/2$$

Where: t = transformation order

The accuracy of the transformation is reported by the RMS (root-mean-square) error, which indicates the average discrepancy between each GCP and its predicted location using a transformation based on all other GCPs. A number of standard methods exist to reduce RMS error (personal communication Langford 1996):

- (i) Remove GCPs that contribute the greatest error to the total RMS (provided the minimum number needed is not violated).
- (ii) Select a higher-order polynomial to allow a more complex geometric correction.
- (iii) Tolerate a higher RMS error than was originally specified.

Method (i) was adopted since method (ii) often only results in an apparently better transformation due to the more complex geometric distortions introduced. This may create a better fit with GCP data, but if these data are inherently erroneous the overall quality of the correction may actually suffer. Table 25 lists the final RMS errors associated with the image rectification stage.

Table 25 Image RMS errors.

Image	RMS distance (pixels)	Map Distance (m)
TM (p198r53)	1.33	40
TM (p198r52)	1.24	37
XS	1.11	22
ERS-1	1.68	49

There are three possible reasons why RMS error could not be further reduced:

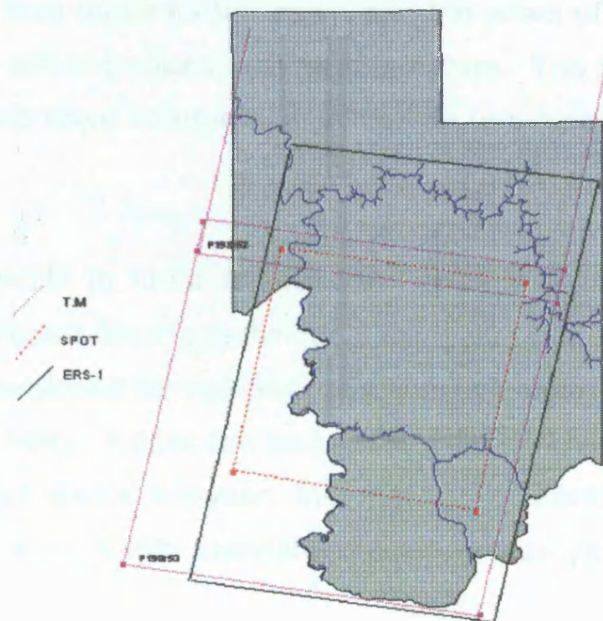
- (i) Differential GPS was not used in the field (due to resources) so the inherent variability in GCP locations prevented any better accuracy.
- (ii) Due to field logistics GCPs were not ideally spatially distributed throughout the study region.

- (iii) The study area straddles two UTM zones (29 and 30) so inevitable inaccuracies occur when data is transformed to a single zone. The result is to cause greater distortion of data in the unconforming zone.

With the geometric correction established, source images were interpolated into geo-rectified grids. The cubic convolution interpolator was adopted which uses the 16 nearest pixels to the interpolated position to derive an estimated DN value, via a polynomial surface-fitting function. This approach was preferred to the main alternative, a bilinear interpolator, as it is widely reported as the most accurate both spatially and spectrally (Park et al., 1983; Atkinson, 1985; Roy et al., 1994).

On completion of geo-rectification the TM and SPOT images displayed good pixel-to-pixel matching, as estimated visually throughout the scene. Results for the ERS-1 image were not so good, due to its blurred and speckled nature, but were considered acceptable. The spatial coverage of these images are illustrated in Fig. 32.

Fig. 32 Sketch map of areal extent for remote-sensed imagery.



4.5.1.5 Image Mosaicking.

To produce one continuous image of the research area the two TM images required mosaicking. Initially a mosaic using “featheredge matching” was applied. This produced poor pixel-to-pixel matching within the overlap zone, probably due to combining images with differing RMS errors. The practical solution adopted was to insert many common registration points within the overlap zones of both images. Although time consuming, this produced an excellent edge map, and since both images were the same date, no discernible spectral differences could then be observed.

4.5.1.6 ERS-1 Data.

Preliminary processing of the radar data was aimed at reducing the presence of image speckle, an inherent feature of such images (ERDAS, 1994). Radiation waves emitted by the sensor travel through space in-phase, but return out-of-phase after impact and reflection from the Earth's surface. This is a result of the distance impact phenomenon where objects closer to the sensor have a faster return signal than those further away, and the effect of signal scatter on impact which can be either fractional or simple in nature. The end result is constructive and destructive wave interference giving rise to a ‘speckly’ mixture of dark and light pixels.

Reducing speckle in radar images can result in improved visual quality. A number of different filtering techniques, using variable window sizes, have been specifically developed for speckle reduction / elimination (see ERDAS Imagine Field guide, 1994). A filter can be passed over an image any number of times, but a trade-off exists between the number of iterations and the resultant resolution. As no single standard procedure has yet been established, the

process is largely controlled by visual analysis of results on a pass-by-pass implementation.

4.5.1.7 Speckle suppression methodology.

A sub-scene of unprocessed ERS-1 SAR image is illustrated in Fig. 33. The only features clearly identified through the speckle are the principal east-west and north-south flowing rivers. The identification of these features is made easier by the low reflective response of the surrounding bare sandy/muddy riverbanks. On enlargement in certain regions of the image vegetated and non-vegetated lands are distinguishable, to a degree, by corresponding light and dark pixels, whilst those areas typified by steep topographic gradients can, in some instances, be identified by very high reflective responses.

Nevertheless, feature identification in the Mali image is extremely difficult. In light of this a decision was made to perform a quick comparative assessment of its quality especially as the image histogram displayed distinctive and unexplained 'gaps' (Fig. 34).

Fig. 34 ERS-1 SAR histogram.

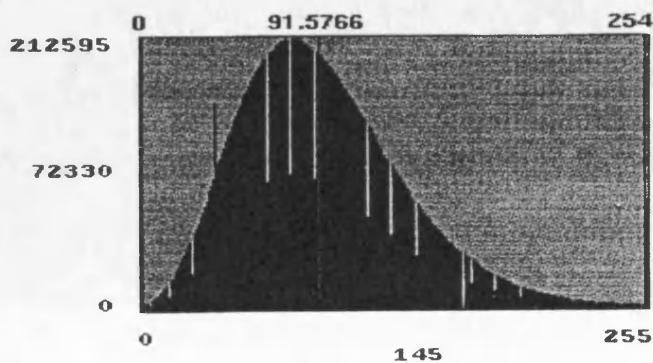
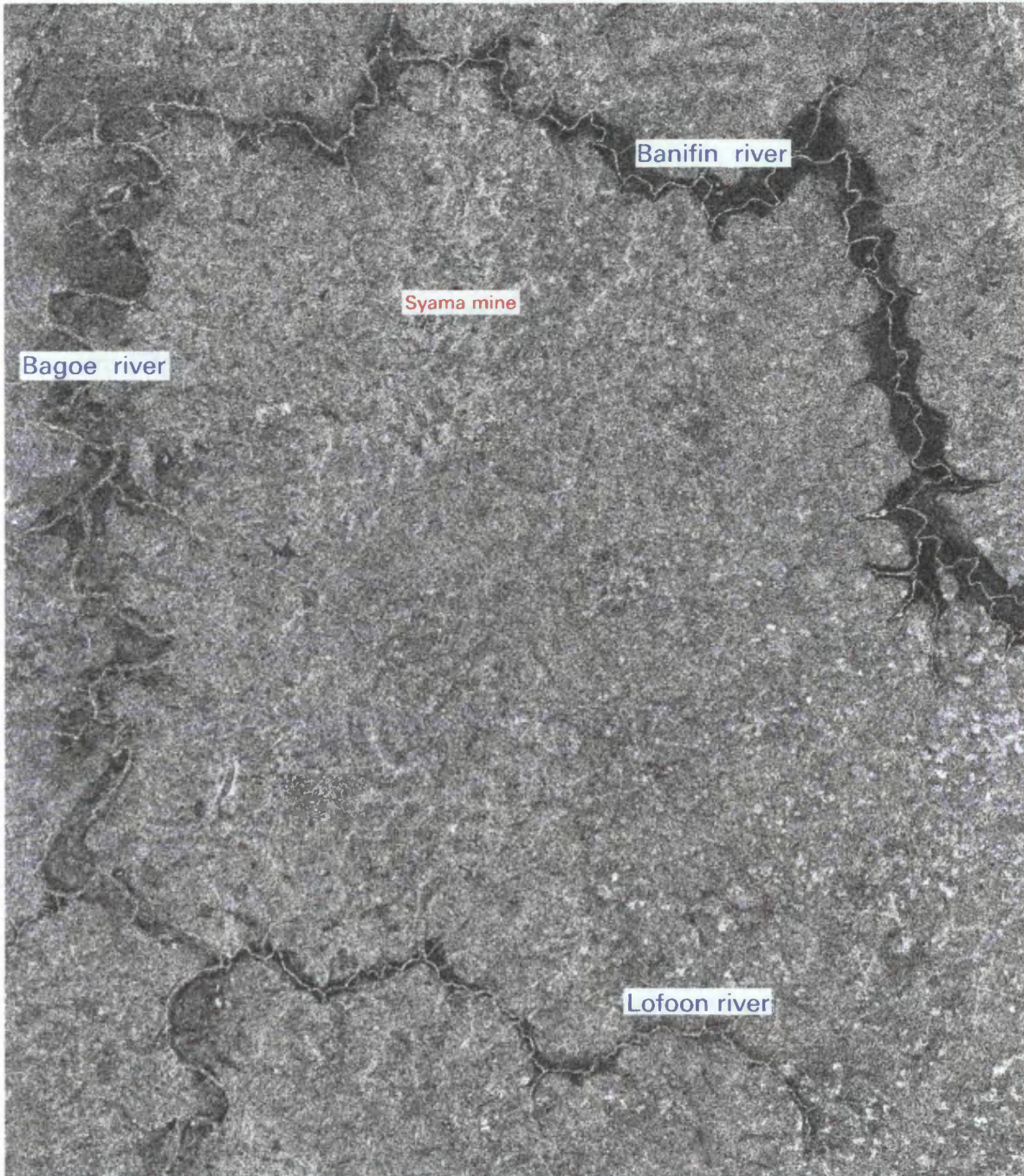


Fig. 33 ERS-1 SAR image.

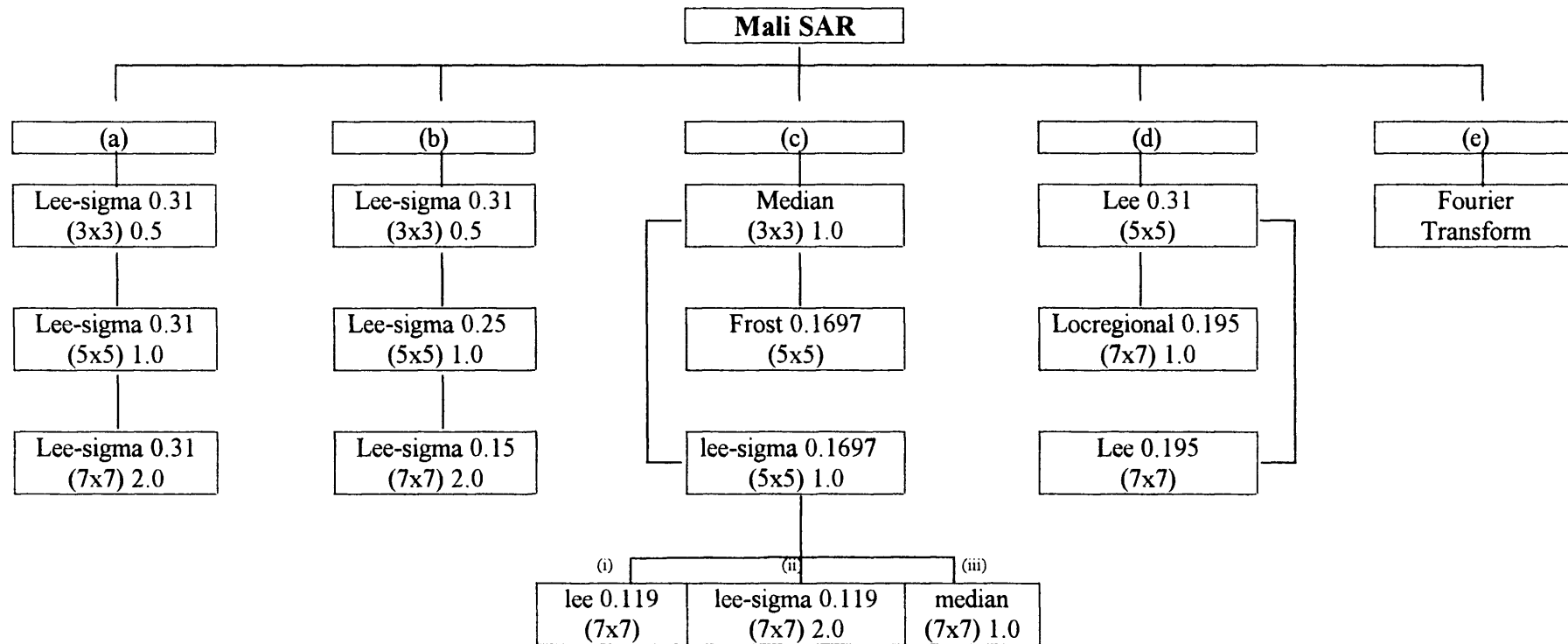


The image was compared visually with raw SAR imagery from Jordan (courtesy of K. Tansey), Colombia (courtesy of C.I.A.T., Cali, Colombia) and with test data sets provided by ERDAS Imagine. All these images showed significantly less speckle and clearer feature definition than the Mali image. This suggested that an exceptionally high level of image speckle plagued the Mali image, as later communications with BHP confirmed. However, it was not rejected as a viable information source at this stage since it may have had considerable value in illustrating geological structure (Drury, 1987; ERDAS, 1994).

A variety of speckle suppression filters were applied to the image. The flow diagram (Fig. 35) illustrates a selection of the methods applied. Method (a) and (b) are procedures recommended by ERDAS, whilst methods (c) and (d) represent attempts to further improve upon these results. In all tests applying a one-pass filter of any specified window size did not significantly improve the image quality. Better results were achieved with three passes of increasing window size. Overall, methods (a) and (c-iii) produced the best visual output. However, close inspection showed image quality remained poor with blurring of detail and the presence of a spurious black speckle. The inability to significantly improve image quality by spatial filtering led to investigations into the use of the Fourier Transform technique.

The Fourier Transform operates in what is known as the frequency domain, rather than the spatial domain associated with the previous filtering operations. The Fourier Transform converts an image into a form of diffraction pattern in which its information content is represented as a series of sine waves of varying frequency, magnitude, and direction. These frequency components, when combined, reproduce the original image. High frequency components appear towards the edge of the Fourier pattern, and low frequency components towards the center. Simple masking techniques allow selective frequency and directional components to be suppressed or removed from the transformed image, before an inverse transformation returns an enhanced spatial image. This approach is

Fig. 35 Speckle suppression flow-diagram.



Value next to filter type represents the calculated coefficient of variation for the processed filter.
 Value in parenthesis represents filter window size.
 Value right of parenthesis represent coefficient of variation multiplier.

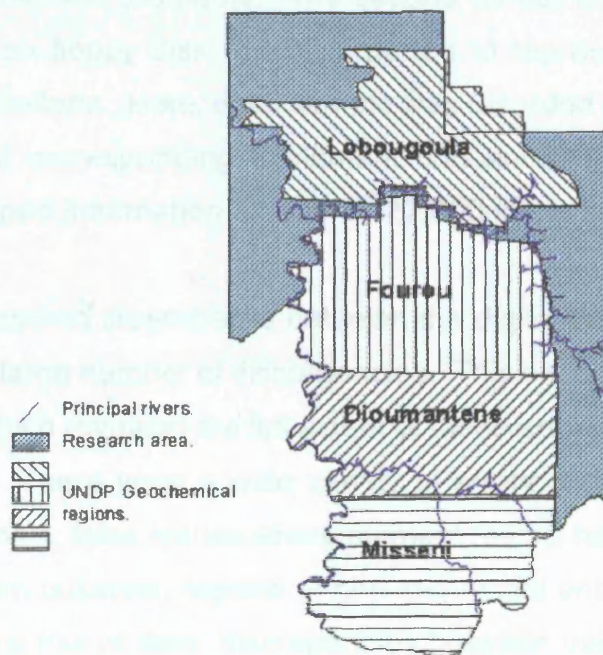
particularly appropriate if the 'interference' present in the original image is of a cyclical or periodic nature. Several attempts were made to use frequency domain filtering to reduce speckle in the Mali image. Unfortunately it was found to be impossible to improve upon the results obtained from method (c-iii).

The results of de-speckling were far from satisfactory, after exhausting various techniques resultant image quality remained poor. It was therefore decided to reject this data, something which BHP had also loosely advised.

4.5.2 Geochemical Data.

The UNDP (1983-1985) regional geochemical soil-sample program covered approximately 65 km x 120 km representing four regions; Lobougoula, Fourou, Dioumantene, and Misseni (Fig. 36).

Fig. 36 Sketch map of geochemical sample regions.



Sampling was principally on a 400 m x 1000 m grid, with 200 m x 1000 m spacing in areas of particular interest. BHP estimated the depth of soil samples, taken by local workers, to lie between 20 cm and 30 cm. Samples were dried and sieved to 80 mesh before analysis in an AAS (Atomic Absorption Spectrometer) for eight elements (Au, Cu, Zn, Pb, Ni, Mo, Li, and Cr). Results were reported at the ppm (parts-per-million) level with the exception of Au. This was extracted by MIBK, analysed by AAS, and reported as ppb (parts-per-billion). Further details were unavailable from BHP.

4.5.2.1 Data quality and verification.

The geochemical data was received in two formats. First as thirty-two dye-line paper maps at an approximate scale of 1:50,000. These comprised of eight element maps for each of the four provinces, showing the location and concentration value of each sampling point with row and column indicators. These data were superimposed on a distorted map showing hydrology, laterite caps/escarpments, and footpaths. The second format was a number of ASCII files presented on floppy disk which purported to represent the same data in machine-readable form. Here, each sample was recorded with a row and column number and the corresponding 8 element concentration levels. In total the database contained information for some 127,000 samples.

Unfortunately, random crosschecks between the digital database and the paper maps showed a large number of discrepancies. This encouraged further detailed investigations which revealed the full extent of these errors to amount to ~55% of all data entries. There were a wide variety of errors, such as multiple entries; inconsistent formats; false entries where element results had been copied across into other element columns; regions of non-sequential entries resulting in areas of mixing within a row of data; discrepancies between values in the ASCII files

and those printed on the paper maps; and extensive areas of missing data. The last two error types were the most serious and common.

4.5.2.2 Data solutions.

Discussions with BHP highlighted and confirmed the inadequacies of the ASCII files (due to poor input data management) and they suggested the dye-line maps were the most reliable source of information. Procedures were therefore implemented to remove the errors observed within the ASCII files. To a large extent format inconsistencies and multiple entries were tackled through various techniques available within software packages such as EXCEL, WordPerfect, and the Sed/Awk commands available under Unix. Nevertheless, missing and misrepresented data still gave error rates of between 35-40%. This left two choices: (i) ignore the remaining errors and assume they would not adversely affect subsequent analyses, or (ii) perform manual editing, making corrections based upon the dye-line maps. Since the geochemical data set was considered to be an important and integral part of the GIS database, providing a mechanism for assessing relationships and assumptions between other data layers, the first option was rejected. Consequently, manual checking and editing was undertaken, despite its laborious and soul-destroying nature, in order to obtain the best possible geochemical inputs, as explained in Garrett et al., (1980).

4.5.2.3 Geometric rectification.

The geochemical database possessed no georeferencing system although sample column and row numbers linked reported element values to sites on the dye-line maps. These maps had a backdrop giving some indication of the positioning of sample points, but they remained effectively unregistered. Consequently a rectification process was needed to spatially integrate these data with other information in the GIS. This section outlines the methodology adopted.

GCPs obtained during fieldwork were located on each of the four province maps, and a grid superimposed on top corresponding to the rows and columns on each map. At each GCP the UTM coordinate (X,Y) representing the destination grid, and a manually interpolated (row, column) coordinate, representing the source grid were collected and entered into an ASCII file. Using the IDRISI GIS a 1st order polynomial equation was calculated for each province in turn, providing a transformation coefficient matrix and RMS error. GCPs with the highest reported contribution to RMS error were excluded until an acceptable error level was achieved (Table 26).

Table 26 Geochemical RMS errors.

Province	No. GCPs used	RMS error (metres)
Lobougoula	10	44
Fourou	18	41
Dioumantene	11	42
Misseni	13	41

With the help of an EXCEL spreadsheet the transformation coefficients were used to construct predictive quadratic equations for true X and Y, which then allowed row and column coordinates to be transform to equivalent UTM locations.

The spatial positioning of these transformed data relative to the dye-line maps was compared. Arc/Info's GENERATE command facilitated this by converting the ASCII files to vector point coverages. Once projected, to UTM Zone 29, the points were overlain on the rectified SPOT XS and Landsat TM imagery. There appeared to be a good overall spatial correlation between these projected points and their positions as shown on the dye-line maps. However, the relationship was not consistent across the study area, but was clearly more accurate in the west and center of the region and notably poorer in the extreme east. This discrepancy appeared to be present in the X-plane only and at its greatest extent involved a positional mismatch of around 100 m. Although BHP personnel

appeared unconcerned by this, attempts were made to reduce the error using a warping function in Arc/Info, but this failed to improve overall correspondence between the dye-line maps and the digital spatial database. It was concluded that the distortion in the eastern region was most likely a result of using a single UTM zone when projecting these data.

4.5.2.4 Data interpolation.

Geochemical samples, although regularly distributed across the region, represent information only at a specific point in space. A more spatially continuous data set would be an aid when trying to infer and assess causal relationships between these data, other continuous-field data and spatially aggregated data sets. This problem can largely be overcome by using spatial interpolation methods to yield a discrete or gridded representation of a continuous surface or field from the original sample points. Spatial interpolation can be thought of as providing a “best-guess” for points lying between actual sampling locations using sound geographical principles (e.g. spatial autocorrelation).

The UNIRAS software suite was used to perform spatial interpolation due to its sophisticated functionality. Arc/Info point vector coverages were exported and manipulated into a format suitable for input to UNIMAP. After some testing the procedure adopted used a search radius of 1300 m to account for the row separation of the samples, the bilinear interpolator, and a smoothing factor for the output grid set to -1 . The spatial resolution of the output grid was set as 200m square. This appeared to give the best compromise given the spacing of the input samples and the desire to maintain as high a spatial resolution as possible, without unnecessary disk storage overheads.

UNIMAP reversed the original row order of the data when saving to an ASCII file so the TRANSPOS command in the IDRISI GIS was used to correct this

problem. The final stage was to employ a bespoke 'C' program to modify the file format from single-line TAB-delimited to a space-delimited structure (see Appendix, geochemistry). With the addition of a header information file, the data could then be read to an Arc/Info grid. Each grid needed its projection updated, at which point these data were fully compatible with other information stored in the GIS.

4.5.2.5 Grid mosaicking.

The four provinces of interpolated geochemical data required mosaicking to produce a continuous regional coverage in the GIS. This is possible in Arc/Info but was undertaken in ERDAS Imagine, which is easier to use and offers better functionality. All thirty-two Arc/Info grids were imported to ERDAS Imagine using Arc/Info's GRIDIMAGE command. Each province was mosaicked with adjacent regions using the "feather stitching" technique in areas of data overlap. As the provinces had been interpolated separately there were some inevitable mismatches along some of the join lines, but these were accepted due to the relatively low quality of the database as a whole.

4.5.3 Radiometric data.

BHP flew an airborne radiometric survey in the western area of the research region in 1993. The survey covered approximately 14 km x 70 km, forming a sinuous, elongate north-south trace, centered over the Syama volcano-sedimentary sequence. The gamma ray source elements identified were Uranium (U), Thorium (Th), Potassium (K) and total count (τ). Unfortunately, little further information detailing the survey has been made available, other than the 300 m flight line spacing and a possible terrain clearance of 90 m.

4.5.3.1 Data processing and error corrections.

Each radiometric element was supplied as self-extracting compressed files. On extraction the ASCII data consisted of X and Y UTM coordinates and a count reading. Data had been gridded, probably through an interpolation procedure, to an 80 m x 80 m mesh with over 133,000 sampling points per element. Embedded in the ASCII files were text lines indicating the start of each grid line. There were no accompanying header or metadata files so it was decided to import this information to Arc/Info as point vector coverages using its EXPORT format, with the intention of converting them later to a raster grid. This method would circumvent any possible problems relating to the unknown boundary shape of the sampling mesh. A bespoke FORTRAN program was used to modify the files to EXPORT format (see Appendix, radiometric). Data were then imported as vector point coverages, and BUILD used to create topological information. Once read by Arc/Info a vector-to-raster process allowed the creation a raster grids with an 80 m x 80 m spacing.

When displayed, the raster grids revealed errors in the U, Th and τ datasets. This took the form of a translocation or lateral shift of the upper half of each grid, with displacements of as much as 320 m in the east-west plane. This irregular error was clearly identified by the edges of the sampling grid, and when overlaid with the K grid. The absence of any problem in the K grid suggested the source was in prior data handling or interpolation carried out by BHP, rather than the import procedures outlined above. The solution adopted to solve this problem to use "grid warp" in ERDAS Imagine. Using 24 GCPs on each of the erroneous grids, and with the K grid acting as the reference coordinate system, a 2nd order polynomial transformation fitted the distorted data sets to match the correctly spaced K grid.

4.5.4 Magnetic Data.

A magnetic survey had been run concurrently with the airborne radiometric data, with identical aerial extent and flight plan.

4.5.4.1 Data processing.

The airborne magnetic data was supplied in a self-extracting compressed format. These data had been diurnally corrected, leveled, and the first-order trend removed (pers. comm. D. West, 1995). After extraction the data format was found to be identical to the radiometric data. Thus the same FORTRAN program was used to import those data into Arc/Info as point vector coverages, and a vector-to-raster function used to create the raster grids. Fortunately, none of the problems noted above for the radiometric datasets were encountered here.

4.5.5 Digitising of published cartographic data.

BHP supplied cartographic maps of geology and topography. No digital sources were available so information contained on these maps had to be manually digitised. The aim was to capture selected geographical information that would help to explain the interactions between landscape geomorphology and element dispersion, thus two data themes were required: geology and topography.

Digitising used an A0 Calcomp 9100 table linked to a PC running Arc/Info's ADS software, with data captured by both keyboard and electronic puck.

4.5.5.1 Geological data input.

Prior to digitising, the three adjoining geological maps of Massigui, Kadiana and Kadiolo were taped together and eight TIC points (i.e. GCPs) selected to aid future registration. Two separate coverages were to be derived from these

geology maps, capturing lithology and structure. Once digitized, coverages were transferred to Arc/Info running on a Sun Workstation.

Manual digitising always produces errors, many of which were corrected using manual and semi-automatic processes. Any remaining errors were identified once the coverages had been 'cleaned', displaying the original digitised coverage as a backdrop to the new cleaned coverage to ensure that no distortion had been introduced by 'node snapping' and other operations performed during topology creation.

The resultant outputs were: (i) faults and structure stored as line objects and (ii) lithology stored as polygons. Each lithology polygon required its own unique ID code to aid identification. This can be entered during digitising but prior experience has shown it is often more reliable if added later. Finally, the Arc/Info command BUILD was used to construct topology for both vector coverages. This is essential in order to be able to analyse spatial relationships between recorded features and to attach further attribute information to the arcs and polygons.

4.5.5.2 Published mineral localities.

As discussed in Section 1.4.3, Mali has a long history of gold exploration, characterised by small-scale artisan methods of extraction and river panning. Within the research area it is believed that many of these small extraction sites still lay undiscovered (pers.com. E. Hanssen, 1994). This claim is partly substantiated by recent small artisanal findings within the BHP concession area, which were previously unmentioned in the work of Kusnir et al. 1989. It is therefore probable that mineral extraction sites located on the 1:200,000 scale geological maps represent the larger of these artisanal sites.

Within the geological map sheets of Massigui, Kadiana and Kadiolo, thirteen Au mineral localities are shown, plus one Cr/Ni occurrence (Fig. 5). Each of these

mineral occurrences was digitised and given a unique ID. The result was cleaned and built as a point vector coverage.

4.5.5.3 Topographic data.

Topographic information was captured by digitising contour lines and spot heights from 1:200,000 scale topographic maps. Unfortunately, only partial information existed, with only two of the three map regions available. The situation was further complicated by the fact that one of the two sheets was a monochrome photocopy in which following and tracing contours proved to be a tortuous task. Furthermore, geometric distortions caused by photocopying resulted in very poor matching of lines across the map sheet boundaries.

An alternative source for topographic information was found in the 1:200,000 scale geological maps. The key advantage of using these maps was that contours and spot height information, although partially obscured by geological symbolism, was available for the full study region and thus caused no edge-matching errors.

Contours and spot heights were digitised as separate coverages. Contour lines were carefully traced in stream-mode and each contour line given an ID-code equal to its elevation. Spot heights were digitised in point-mode again with ID-codes representing elevation. Digitised coverages were checked for errors, and topology constructed using the CLEAN and BUILD commands.

4.5.5.4 Lateritic escarpment data.

Laterite escarpments were denoted as lines of irregular encasement, or unconnected irregular lines, on both the topological and geological maps. These features were captured from the geological maps, error checked, and cleaned. Additional information on laterite sites was added from the UNDP geochemical

dye-line maps to ensure that all possible occurrences were captured. These locations were added using on-screen digitising, with locational precision achieved by using both the TM image and the geochemical data as backdrops to the laterite coverage.

4.5.5.5 Hydrological data.

Hydrological data was initially obtained from the geological maps. Rivers were digitised in accordance to their 1:200,000 symbolism that identified whether they were perennial or ephemeral in nature. A detailed error correction and cleaning procedure was needed to ensure all rivers connected correctly prior to construction of topology. After rectification (Section 4.5.7) a small amount of supplementary hydrological information was added using information obtained from the rectified TM image. This was entered using on-screen digitising using the TM image as a backdrop to the hydrological coverage.

4.5.5.6 Attribute linkages.

A GIS does not only capture spatial data but also manages the descriptive non-geographic information (attribute data) that are linked to the spatial features held within any coverage. Attribute data improves understanding in the display of complex spatial data and allows greater flexibility in developing querying and selection criteria. Relevant attribute data were encoded and added for the lithology, mineral occurrence, and hydrology coverages.

4.5.6 Digitising unpublished cartographic data.

As discussed earlier in Section 4.2, BHP produced a number of “in-house” maps for their concession area. Those deemed to be a useful contribution to the GIS database were manually digitised.

The 1:25,000 scale Syama district geology map was captured for it represented a synopsis of some of the investigative work performed by BHP. This map covers an elongate area centered through the Birimian volcano-sedimentary unit, and extending approximately 28 km north-south and 18 km east-west (Fig. 5, insert). This was a complex map displaying a lot of diverse information and a number of coverages were derived from it. Structural and lithological information, airborne potassium anomalies, chert outcrops, the location of current pit operations and old workings, hydrological and road information were individually digitised.

Data capture began with the entry of twenty identical TIC points scattered across the map surface, all located with respect to clearly identifiable features such as road and river intersections. As usual, coverage topology was constructed and relevant attribute information added once digitizing errors had been eliminated

4.5.7 Coverage rectification and warping.

Coverages produced by manual digitising of published and unpublished maps needed to be rectified to the same UTM projection that was used by other datasets. This process was undertaken in Arc/Info using the TICS digitised with each coverage.

The first to be rectified were those obtained from the published map sources since these were the first to arrive from BHP. As fieldwork had yet to be undertaken at this time, geo-coordinates for TIC locations were obtained from the geological maps and expressed as UTM values. Each coverage used the same set of TIC marks so the same RMS error was associated with each transformation. This was a relatively poor 102 m, due in part to the small scale of the source maps, but also because captured data spanned two UTM zones. Several attempts were made to reduce this error, firstly by making small adjustments and re-calibrations of the UTM coordinates. Secondly, coverages were split into two separate UTM zones, each transformed individually and then

joined using a mosaicking operation. The latter approach produced a small reduction in RMS error, however, any advantage was counteracted by problems with edge matching along the join between the two projected maps. These practical difficulties mirror similar situations reported by Tobler (1988); Rhind and Clark, (1988) and Fisher (1991).

A decision was made to accept the original rectification and later a warp function was used to realign all projected coverages to the rectified TM image. Hydrological information was warped first, as this was the only coverage to possess a full spatial extent of features easily identified on the TM image. Approximately 60 river intersections were identified, and used to generate the warp function, reducing RMS error to an acceptable 38 m. This same warp was then applied to all other map-derived coverages to achieve the same level of spatial accuracy.

Finally a spatial accuracy check was performed to assess the compatibility between the (X,Y) coordinates of the map and those derived from projected coverages. Ten random points and ten selected points were established, the latter being chosen as tripoint or bipoint river intersections. The (X,Y) coordinates of these locations were located on the paper maps and were found to possess very respectable degree of correspondence.

4.5.8 Cartographic data quality assessment.

The assessment of data quality within a GIS is concerned with the concept of error, which is documented in many forms, from source data generalisations, through analogue-to-digital conversions, to data processing errors (Blakemore 1984; Burrough 1986; Chrisman 1982, 1987, 1989; 1991; Chrisman and Yandell 1988; Goodchild 1988; Openshaw, 1989; Veregin, H 1989; Fisher 1991). The multiple sources of potential error and their propagation during processing relinquish any concept of an error-free database. The acknowledgement of error

highlighted in this section is concerned with that derived from source data and its digital conversion.

Commonly, much of the information stored in a GIS is sourced from paper maps. In this research maps (both published and unpublished) have made significant contributions to the diversity of the database. However, maps are not perfect representations but reflect generalisation of a complex reality, where the geodetic base, projection basis, map scale/resolution and human error may take the form of data omission or commission errors (for further discussion see Burrough, 1986; Goodchild 1988; Rhind and Clark, 1988; Fisher, 1989; 1991).

Boundary demarcations are subject to conjecture on geological maps (Burrough, 1986; Goodchild, 1988) unless there is clear uninterrupted exposure. The placing of a boundary line is a subjective process, especially when covered by a thick weathered lateritic material. For example the Birimian volcano-sedimentary sequence, so well described by Olson et. al. (1992), and the source for the majority of gold, is not truly delineated on the published geological maps but inferred through the presence of jasperoids and as such represents an integral part of source data error. Marker symbols used to denote mineral sites are often misplaced with respect to their true location. For example, the location of the Syama Au symbol does not coincide when overlaid with BHP's pit location.

As it is not an objective of this research to re-map the geology of the region many of these source errors, whether detected or not, must be accepted as intrinsic to the nature of the data being used. Thus it is acknowledged that a geodatabase and its derived sources are rarely, if ever, error free.

A second confinable form of error incorporated into a GIS is that associated with manual digitizing. Quite simply a boundary line on a map is often a misconstructured error in terms of its width and what it represents with regard to the map scale, as discussed by Tobler (1988) and Burrough (1986). Therefore

there is a great need for accurate, careful digitising which has characteristically implied digitising the middle and not the edges of a line. Digitising a straight line is simpler and relatively error-free as opposed to complex curves typical of hydrological and contour data. Too few points on curved lines will, even after applying line smoothing techniques, result in errors of omission or commission either side of the line feature. These types of errors are reduced by careful digitising, which has been rigorously adhered to during the generation of coverages for this research.

4.6 Geochemical statistical analysis.

A purpose of using geochemical data in this research was to identify and segregate samples relating to possible mineralisation from those of a lower or background level. This is common practice in mineral exploration but there is no single nor preferred method. Consequently the literature reviews a number of techniques used in delineate anomalies. These techniques range from the use of probability graphs, histograms, the mean plus a selected standard deviation and percentiles, to principal component analysis and factorial kriging, fractal/multifractal modelling, and a moving average windowing technique (Sinclair 1974; Garrett et al., 1980; Stanley and Sinclair 1987; Rose et al., 1990, Jimenez-Espinosa et al., 1993; Cheng et al., 1994; Cheng et al., 1996).

4.6.1 Global geochemical data.

A combination of univariate and multivariate analyses have been performed on the UNDP geochemical data set to help establish:

- 1) The distribution of each element
- 2) The relationship between elements

The purpose of these analyses is to act as a tool in the identification of background and anomalous data points, the results of which are discussed in

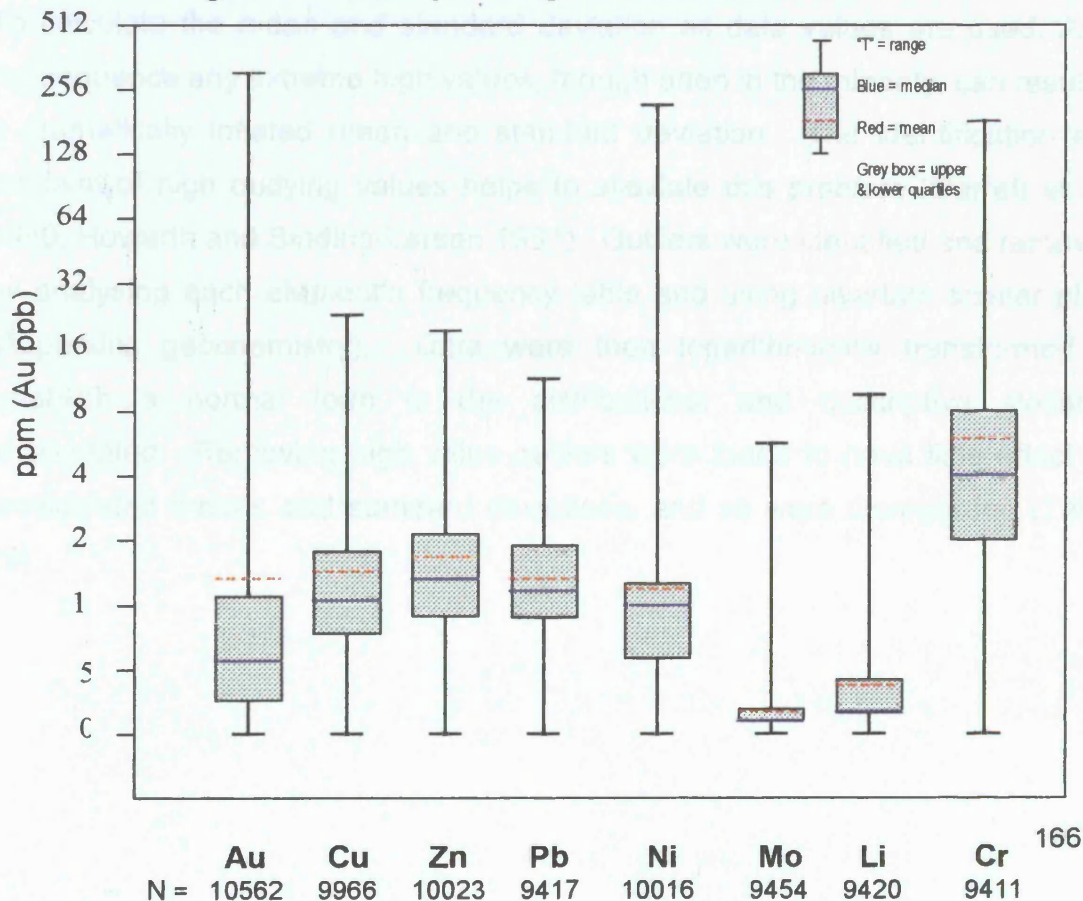
Section 4.6.3. The initial analysis phase consisted of computing central tendency and dispersion characteristics for each element (See Table 27 and Fig. 37).

Table 27 Elements statistical characteristics.

	Mean	Median	Mode	Min.	Max.	Inter-Quartile range LQ	UQ	S.D	N.
Au	14	6	2	0	3100	3	11	73	10562
Cu	15	11	8	0	238	8	18	14	9966
Zn	17	14	8	0	181	9	21	13	10023
Pb	15	13	10	0	130	9	19	9	9417
Ni	14	10	8	0	2260	6	14	44	10016
Mo	2	1	1	0	60	1	2	2	9454
Li	4	2	2	0	102	2	4	4	9420
Cr	66	40	20	0	1830	20	80	84	9411

(Values rounded to whole number. All values expressed as ppm except Au, which represents ppb).

Fig. 37 Box-plot diagram for all elements.



This information plus the histogram frequency plots (Appendix, geochemistry), show all elements have a positive skew, a distribution characteristic of minor elements (Shaw, 1961 cited in Sinclair, 1992), and observed through the modal values and the inter-quartile range. However, a skewed distribution is of limited value if the mean plus a standard deviation or Pearson correlation are used to obtain results, for both are based upon normal theory (Garrett et al. 1980). Therefore, to normalise the data, each element was logarithmically transformed.

An important change to the data was necessary prior to transformation. Value zero, which according to BHP personnel represents the lowest analytical level detectable by the machine, will produce an error if log-transformed. To avoid this whilst still retaining all samples in the analysis zero values were changed to 0.5 (i.e. half the detection limit). The results of the log transformation are illustrated in Table 28 and Fig. 38. Near normal distributions are obtained for virtually all elements, with the exception of the highly skewed Mo and, to a lesser degree, Li and Au (see log histogram frequency graphs, Appendix, geochemistry).

To calculate the mean and standard deviation all data values are used. As a consequence any extreme high values, though often in the minority, can result in a dramatically inflated mean and standard deviation. The identification and removal of high outlying values helps to alleviate this problem (Garrett et al., 1980; Howarth and Sinding-Larsen 1983). Outliers were identified and removed by analysing each element's frequency table and using bivariate scatter plots (Appendix, geochemistry). Data were then logarithmically transformed to establish a normal form to the distributions, and descriptive statistics recalculated. Removing high value outliers were found to have little effect on recalculated means and standard deviations, and so were disregarded (Table 29).

Table 28 Element statistical characteristics log-normal transformed.

	Mean	Median	Mode	Min.	Max.	Inter-Quartile range		S.D	N.
						LQ	UQ		
Au log	1.70	1.79	0.69	-0.69	8.04	1.10	2.40	1.17	10562
Cu log	2.46	2.40	2.08	-0.69	5.47	2.08	2.89	0.72	9966
Zn log	2.62	2.64	2.08	-0.69	5.20	2.20	3.04	0.64	10023
Pb log	2.50	2.56	2.30	-0.69	4.87	2.20	2.94	0.65	9417
Ni log	2.24	2.30	2.08	-0.69	7.72	1.79	2.64	0.76	10016
Mo log	0.33	0.00	0.00	-0.69	4.09	0.00	0.69	0.75	9454
Li log	0.92	0.69	0.69	-0.69	4.63	0.69	1.39	0.80	9420
Cr log	3.74	3.69	3.00	-0.69	7.51	3.00	4.38	0.94	9411

Fig. 38 Box-plot diagram for all logged elements.

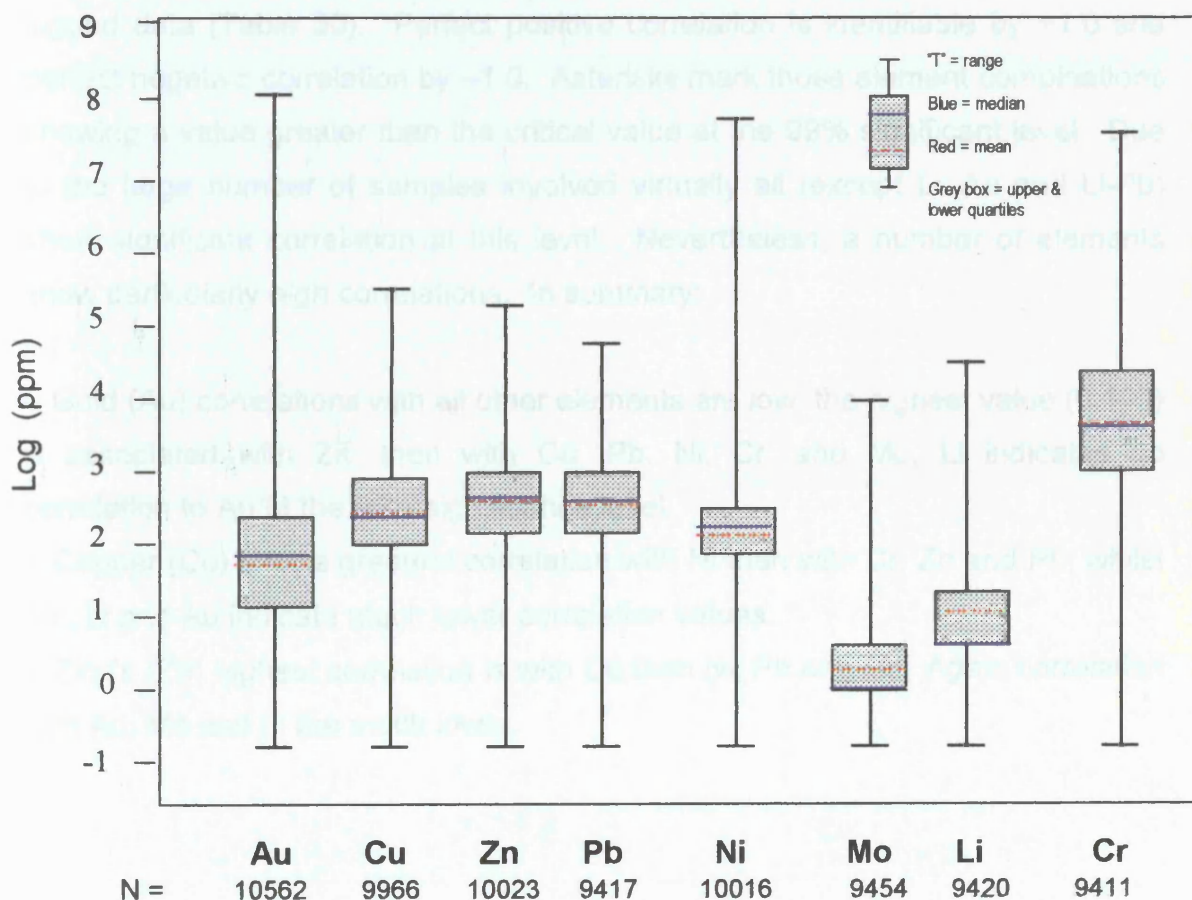


Table 29 Mean and standard deviation comparisons – outliers removed.

	Au	Cu	Zn	Pb	Ni	Mo	Li	Cr
Mean All values	1.69	2.46	2.62	2.50	2.24	0.33	0.92	3.74
SD All values	1.17	0.72	0.64	0.65	0.76	0.75	0.80	0.94
(N) Number	10562	9966	10023	9417	10016	9454	9420	9411
Mean Outliers removed	1.69	2.46	2.62	2.50	2.23	0.33	0.92	3.74
SD Outliers removed	1.17	0.72	0.64	0.65	0.75	0.75	0.80	0.94
(N) Number	10556	9959	10020	9413	10009	9452	9418	9407

(Logarithmic data. All values reported in ppm, except Au, which is ppb).

Although information has been gained on the character of each element, little is understood regarding the interaction between the elements. Therefore a number of techniques were used to help identify possible inter-element relationships.

Firstly a Pearson's product-moment correlation matrix was computed on the logged data (Table 30). Perfect positive correlation is identifiable by +1.0 and perfect negative correlation by -1.0. Asterisks mark those element combinations showing a value greater than the critical value at the 99% significant level. Due to the large number of samples involved virtually all (except Li:-Au and Li-Pb) show significant correlation at this level. Nevertheless, a number of elements show particularly high correlations. In summary:

- Gold (Au) correlations with all other elements are low, the highest value (0.192) is associated with Zn, then with Cu, Pb, Ni, Cr, and Mo, Li indicates no correlation to Au at the 99% significance level.
- Copper (Cu) shows greatest correlation with Ni then with Cr, Zn and Pb, whilst Mo, Li and Au indicate much lower correlation values.
- Zinc's (Zn) highest correlation is with Cu then Ni, Pb and Cr. Again correlation with Au, Mo and Li are much lower.

Table 30

Element correlations.

		Au_LOG (ppb)	Cu_LOG (ppm)	Zn_LOG (ppm)	Pb_LOG (ppm)	Ni_LOG (ppm)	Mo_LOG (ppm)	Li_LOG (ppm)	Cr_LOG (ppm)
Au_LOG (ppb)	Pearson Correlation Sig. (2-tailed) N	1.000 . 10562							
Cu_LOG (ppm)	Pearson Correlation Sig. (2-tailed) N	.145** .000 9854	1.000 . 9966						
Zn_LOG (ppm)	Pearson Correlation Sig. (2-tailed) N	.192** .000 9883	.474** .000 9957	1.000 . 10023					
Pb_LOG (ppm)	Pearson Correlation Sig. (2-tailed) N	.122** .000 9363	.452** .000 9374	.394** .000 9406	1.000 . 9417				
Ni_LOG (ppm)	Pearson Correlation Sig. (2-tailed) N	.088** .000 9882	.683** .000 9954	.404** .000 10005	.494** .000 9411	1.000 . 10016			
Mo_LOG (ppm)	Pearson Correlation Sig. (2-tailed) N	.028** .007 9402	.206** .000 9411	.102** .000 9444	.315** .000 9404	.241** .000 9447	1.000 . 9454		
Li_LOG (ppm)	Pearson Correlation Sig. (2-tailed) N	-.013 .207 9362	.205** .000 9372	.096** .000 9405	-.015 .157 9401	.318** .000 9409	-.076** .000 9404	1.000 . 9420	
Cr_LOG (ppm)	Pearson Correlation Sig. (2-tailed) N	.059** .000 9359	.472** .000 9369	.306** .000 9403	.559** .000 9397	.492** .000 9406	.357** .000 9401	-.139** .000 9396	1.000 . 9411

** . Correlation is significant at the 0.01 level (2-tailed).

- Lead (Pb), the highest correlations are observed between Cr, Ni, Cu, Zn and Mo respectively. Au is lower, whilst Li although negative in value shows no significant correlation to lead.
- Nickel (Ni) shows its strongest correlation with Cu then with Pb, Cr and Zn. Much lower values are observed in Li, Mo and finally Au.
- Molybdenum (Mo) has a lower value of correlation with all its elements, the highest value is observed with Cr, followed by Pb, Ni and Cu. The primary relationship with Cr could be a response to their co-existence in the upper Fe-rich horizons of the laterite. A low value is observed with Au, whilst Li indicates a negative correlation.
- Lithium (Li) shows low values of correlation with all elements. Of these Ni is the highest then Cu and Zn. All other elements show varying degrees of negative correlation, with Cr the highest. Pb and Au however appear not to be correlated at this level of significance.
- Chromium (Cr) shows its highest correlation with Pb followed by Ni, Cu, and then Mo and Zn. A much lower value is observed with Au, whilst Li shows a negative correlation.

From this, and through comparing the values reported in Table 30, it is possible to rank and form generalised groups from the element correlations. The most obvious is the base metal association (Cu, Ni, Zn, Pb and Cr) all showing high inter-correlations. Due to the low overall correlations of Li and Mo a second group forms. This mixed group is a likely reflection of alkali metal association (Li), and Mo weak association to base metals. The final group is that of Au mineralisation. Although the association with all paired elements is low there is still a relationship to the base metals, seen mostly with Zn, Cu, and Pb.

Before investigating these findings further a check was made to ensure that correlations recorded in Table 30 were not a response to spurious data points, as explained by Howarth and Sinding-Larsen (1983). Scatter plots of the logged data (Appendix, geochemistry) and a new Pearson's correlation matrix was

computed with the omission of high outlying values, as explained previously. The logged scatter plots showed no obvious outliers, unlike previously, and the recalculated Pearson values remained virtually identical with only Au:Mo changing from a correlation significant at the 0.01 level to a reduced 0.05 significance. Consequently the data recorded in Table 30 were accepted.

Two final points of caution regarding the data recorded in Table 30 are;

- 1) Low Au correlations could potentially be higher. The author is aware that especially around the Syama mine where gold values are extremely high there are surprisingly no other element concentrations recorded in the UNDP data. Consequently on computing the Pearson matrix these high gold values will be omitted from the calculation due to there being no other paired data available.
- 2) The Chromium data appears to have been affected by a systematic laboratory sampling error. This feature is not discernible on the original cartographic map, only when the data has been put into a frequency table (Appendix, geochemistry). The true effect of this on the paired correlations is unknown.

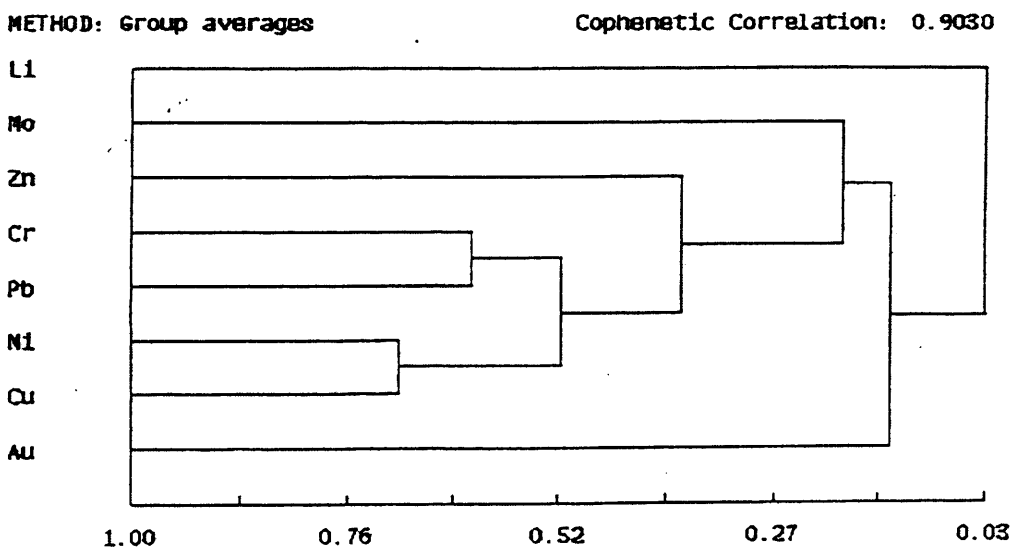
A further attempt was made to investigate the validity of the previously described groupings by performing an R-mode cluster analysis. The chosen classification scheme was hierarchical, since this the most widely used in Earth science, (Davis, 1986). The hierarchical classification operates by connecting first the most similar observations and then the following successively similar observations to these. Finally the dendrogram is built from the similarity levels at which connection occurs. Unfortunately the whole UNDP data set was computationally too large for the computer software. Consequently a subset representing one of the four geochemical regions was selected from the data, thus allowing an assessment as to the relationship between the elements.

A common issue of cluster analysis is that the chosen linkage or clustering method controls the construction of the dendrogram and as there are many

methods, the results and interpretations can vary. A method to eliminate this subjectivity, and adopted by this research, is to use the linkage method with the highest cophenetic correlation coefficient (Davis, 1986). By choosing the highest value distortion within the dendrogram is kept to a minimum. The linkage method used was group averages, which had a cophenetic correlation of 0.9030 (Appendix: geochemistry).

The cluster analysis results are shown in the dendrogram in Fig. 39. These reveal a similar underlying structure to that seen in the Pearson product moment correlation. The greatest group similarities are between Cu / Ni (0.6980) and Cr / Pb (0.6130) which are linked together and then influenced as a whole by Zn at a lower (0.3772) similarity level. This observed structure confirms the base metal grouping previously described. Mo is also shown to have an influence upon this base metal group, but its effects are low, as indicated by the 0.1932 similarity level. Au follows closely behind Mo, with a similarity level of 0.1393, linking eventually through to the base metal group. However, Au according to this data shows no association to Li, for Li is the lowest and therefore most statistically dissimilar cluster to all others.

Fig. 39 Dendrogram for R-mode cluster analysis.



4.6.2 Statistics related to lithology: a GIS approach.

An issue of large geochemical data sets is that they rarely sample a single lithology. In reality the geochemical results obtained are not of one but a combination of differing lithological signals. Therefore the global mean and standard deviation are not truly representative of individual lithologies, (as explained in the working example of Levinson et al.1987). This is a somewhat pivotal point if a threshold for future work is calculated on the bases of these values. For one of the characteristics of large data sets are the presence of multiple populations. This problem is often eliminated if statistics are drawn from individual lithologies, and in doing so reduces the likelihood of omission and commission errors i.e. data misclassification, when estimating thresholds.

Using Arc/Info the geochemical statistics of every lithology were extracted for each element, although this seemingly straightforward procedure turned out to be relatively arduous. Separate coverages were created for each individual lithology using the ARC command RESLECT. These coverages were then overlaid with each geochemical point coverage using the ARC command INTERSECT. Where points and polygons intersect a new point coverage is formed. However, this procedure was complicated by Arc/Info's inability to recognise and eliminate polygons (or islands) within the polygons being reselected. To tackle this the command ERASE was needed. For example, to obtain the unique geological polygon (Bs) Fig. 4, lithologies Bj, BB, Tcg, Btb and Bx were individually erased, a process that had to be repeated eight times for each element sampled. In total seven different geological polygons needed this procedure. Unfortunately the ARC command STATISTICS was unable to produce the statistical information desired, so each point coverage was converted to a grid to allow access to central tendency and dispersion characteristics.

Of a possible 33 unique geological polygons only 20 intersected with the geochemical data, the remainder either lay outside of the UNDP sampled region

or the lithology was too small an area to intersect with a sample (e.g. polygon g18 known as (Ep) on Fig. 4). Alluvium was omitted due to its non-geological nature. Statistical results are presented in Tables 31–38 and reviewed briefly here.

None of the lithological elements are normally distributed, virtually all are positively skewed and some show a distinguishing flat form i.e. platykurtic. Those lithologies without form are not necessarily the same for each element sampled. The lack of symmetry within the distributions could point towards complex geochemical situations as explained in Garrett et al. (1980). An attempt was therefore made to establish if a normal distribution could be achieved by changing the area of a lithology. This was made possible through BHP's structural mapping of the volcano-sedimentary sequence, referred to here as g41 (Bj). At the 1:200,000 scale this lithology is narrower than that interpreted by VLF studies (Fig. 5). This extended area was converted to a polygon and used in conjunction with the other 'Bj' regions. Although the number of sample points more than doubled the positive skew remained, with little overall change statistically, as illustrated in these gold values:

MIN 0, MAX 920, \bar{x} 47.035, SD 110.756, MODE 15, MEDIAN 15, NO. 202.

This suggests that in the case of lithology 'Bj' the skew was not necessarily controlled by the lithology alone, and that an increase in area appears to have little effect on the element character.

Finally, as with all statistics where sample points are few, results and conclusions should be viewed with caution. This is especially important for the five lithologies (Bq, Btb, Gki, Ep, Ev) featured in Table 31-38. Also the analytical error observed in Cr (Section 4.6.1) reveals itself where the sample size increases i.e. g6 (Y/Yb), g35 (Tgr); g26 (Bs); g40 (Ba) and g37 (Tg). The effect it has on lithologies of smaller sample size remains difficult to ascertain. Above all, outliers are present within some of the lithologies signifying possible mineral potential.

Table 31 Lithology based statistical information for Gold.

Lithology	Minimum value	Maximum value	Mean	Standard Deviation	Mode	Median	No. of sample points (f)
g44 (Bq)	9	18	13.5	4.5	9, 18	13.5	2
g41 (Bj)	0	920	43.7	129.1	11, 15	10	85
g40 (Ba)	0	2420	11.3	98.7	3	4	611
g37 (Tg)	0	920	19.2	73.0	3	9	365
g35 (Tgr)	0	1860	14.8	67.5	2	8	1160
g34 (Tcg)	0	76	11.3	11.4	10	9	144
g33 (Btb)	5	8	6.3	1.2	5, 6, 8	6	3
g30 (Bx)	1	27	6.5	4.9	6	6	33
g28 (BB)	2	118	30.6	29.2	10, 13, 15	17	19
g26 (Bs)	0	3100	21.4	111.2	3	8	3072
g25 (Bv)	3	72	25.5	23.8	5, 18	18	16
G24(Gr1)	0	25	2.4	3.8	0	1	68
g23 (Gr2)	0	47	3.4	7.0	0	1	56
g20 (Gki)	0	2	1.2	0.7	1, 2	1	5
g19 (Ep)	5	10	7.5	2.5	5, 10	7.5	2
g16 (Ev)	3	14	7.3	4.8	3, 5, 14	5	3
g15 (Eo)	0	170	13.6	29.3	2	5	39
g10 (Ez)	0	500	15.1	58.1	1	3	85
g8 (Eza)	3	51	8.9	7.9	5	8	34
g6 (Y/Yb)	0	1130	10.1	36.2	2	6	4186

Table 32 Lithology based statistical information for Copper.

Lithology	Minimum value	Maximum value	Mean	Standard Deviation	Mode	Median	No. of sample points (f)
g44 (Bq)	16	18	17.0	1.0	16, 18	17	2
g41 (Bj)	6	140	36.2	25.8	9	30	76
g40 (Ba)	1	73	11.5	6.3	9	10	602
g37 (Tg)	2	58	12.9	8.1	10	10	298
g35 (Tgr)	1	120	20.2	15.9	9	22	1305
g34 (Tcg)	4	80	20.7	13.5	10	16	137
g33 (Btb)	13	47	30.3	14.3	13, 37, 47	37	3
g30 (Bx)	9	115	29.9	20.5	13	23.5	32
g28 (BB)	5	130	26.2	33.6	8, 17	17	11
g26 (Bs)	1	200	18.3	14.5	10	16	3124
g25 (Bv)	14	62	37.3	13.3	All samples	39.5	16
g24 (Gr1)	2	119	12.5	17.2	7, 8	8	69
g23 (Gr2)	3	42	14.1	10.2	8	10	56
g20 (Gki)	2	12	5.0	4.4	0,2,3,8,12	3	5
g19 (Ep)	10	45	27.5	17.5	10, 45	27.5	2
g16 (Ev)	4	11	8.7	3.3	11	11	3
g15 (Eo)	5	210	57.8	58.1	10, 19	36	51
g10 (Ez)	7	56	24.6	10.6	17, 26	24	82
g8 (Eza)	8	78	27.5	19.0	9, 16, 18	20	34
g6 (Y/Yb)	0	238	10.7	10.5	6, 8	9	4127

Table 33 Lithology based statistical information for Zinc.

Lithology	Minimum value	Maximum value	Mean	Standard Deviation	Mode	Median	No. of sample points (f)
g44 (Bq)	20	55	37.5	17.5	20, 55	37.5	2
g41 (Bj)	5	90	26.6	18.0	9,13,15,16,21	21	78
g40 (Ba)	1	34	10.3	4.7	8	10	602
g37 (Tg)	6	105	18.6	11.8	16	16	298
g35 (Tgr)	2	181	20.9	17.6	8	16	987
g34 (Tcg)	5	73	24.0	12.9	20	22	137
g33 (Btb)	2	16	9.3	5.7	2, 10, 16	10	3
g30 (Bx)	6	44	18.3	9.2	9, 14, 20	17	32
g28 (BB)	6	92	29.1	24.1	13, 14	16	11
g26 (Bs)	2	138	16.9	12.9	10	14	2720
g25 (Bv)	13	54	30.4	12.8	14, 19	27	16
g24 (Gr1)	0	22	8.8	4.1	6, 7, 11	8	65
g23 (Gr2)	2	27	11.9	5.0	9	11	56
g20 (Gki)	0	12	5.2	4.5	0, 2, 3, 9, 12	3	5
g19 (Ep)	14	31	22.5	8.5	14, 31	22.5	2
g16 (Ev)	15	34	23.3	10.5	9, 27, 34	27	3
g15 (Eo)	2	70	26.3	15.2	20	24	51
g10 (Ez)	5	80	12.9	8.8	10, 12	11	82
g8 (Eza)	10	41	20.9	7.7	15	19	34
g6 (Y/Yb)	0	160	16.3	11.6	10	13	4006

Table 34 Lithology based statistical information for Lead.

Lithology	Minimum value	Maximum value	Mean	Standard Deviation	Mode	Median	No. of sample points (f)
g44 (Bq)	4	21	12.5	8.5	4, 21	12.5	2
g41 (Bj)	2	72	19.4	13.5	20	16	60
g40 (Ba)	0	37	12.8	6.8	10	12	602
g37 (Tg)	1	112	19.0	12.5	13	16	297
g35 (Tgr)	0	130	15.3	9.8	10	13	862
g34 (Tcg)	4	61	20.5	11.3	9, 10, 18	18	105
g33 (Btb)	8	31	17.7	9.7	8, 14, 31	14	3
g30 (Bx)	3	36	15.1	9.4	6	15	21
g28 (BB)	7	19	15.0	5.8	16	15	11
g26 (Bs)	0	120	14.9	9.2	10	13	2444
g25 (Bv)	13	37	22.8	6.5	25	22.5	16
g24 (Gr1)	0	35	13.2	8.7	7	11	69
g23 (Gr2)	1	32	15.4	6.9	15	14	52
g20 (Gki)	2	24	8.0	8.1	2, 3, 5, 6, 24	5	5
g19 (Ep)	11	15	13.0	2.0	11, 15	13	2
g16 (Ev)	7	27	15.7	8.4	7, 13, 27	15	4
g15 (Eo)	3	54	17.1	11.8	8, 9	12	39
g10 (Ez)	0	64	18.1	13.6	5, 7, 20	17	82
g8 (Eza)	7	40	21.2	8.8	21, 24	21	27
g6 (Y/Yb)	0	109	13.9	8.7	10	12	3904

Table 35 Lithology based statistical information for Nickel.

Lithology	Minimum value	Maximum value	Mean	Standard Deviation	Mode	Median	No. of sample points (f)
g44 (Bq)	12	17	14.5	2.5	12, 17	14.5	2
g41 (Bj)	2	51	18.8	9.9	13, 16	16	78
g40 (Ba)	0	52	9.6	5.1	8	9	602
g37 (Tg)	0	44	9.4	5.2	8	9	297
g35 (Tgr)	0	64	13.6	9.0	9	11	989
g34 (Tcg)	2	57	14.9	8.9	13	13	137
g33 (Btb)	4	28	14.0	10.2	4, 10, 28	10	3
g30 (Bx)	2	55	19.6	11.7	20	20	32
g28 (BB)	4	81	17.8	20.8	4, 12, 14	12	11
g26 (Bs)	0	103	12.5	9.2	8	10	2705
g25 (Bv)	8	36	21.1	7.8	14,17,19,20,27	19.5	16
g24 (Gr1)	0	48	10.7	8.0	11	10	69
g23 (Gr2)	4	29	13.8	5.9	9, 10	12	56
g20 (Gki)	0	10	4.6	3.3	5	5	5
g19 (Ep)	10	63	36.5	26.5	10, 63	36.5	2
g16 (Ev)	12	41	24.0	12.4	12, 19, 41	19	3
g15 (Eo)	9	2260	270.8	499.3	16	35	51
g10 (Ez)	2	50	15.8	8.9	8, 14	14	82
g8 (Eza)	5	57	17.8	11.7	12	14	34
g6 (Y/Yb)	0	1040	10.5	26.8	7, 8	9	4000

Table 36 Lithology based statistical information for Molybdenum.

Lithology	Minimum value	Maximum value	Mean	Standard Deviation	Mode	Median	No. of sample points (f)
g44 (Bq)	2	3	2.5	0.5	2, 3	2.5	2
g41 (Bj)	0	10	1.9	1.9	1	2	61
g40 (Ba)	0	8	1.6	1.2	1	1	602
g37 (Tg)	0	60	2.7	4.8	1	2	297
g35 (Tgr)	0	22	1.8	2.2	1	1	870
g34 (Tcg)	0	4	1.2	1.0	1	1	110
g33 (Btb)	1	2	1.3	0.5	1	1	3
g30 (Bx)	0	14	4.2	3.8	3	3	21
g28 (BB)	0	5	2.2	1.3	2	2	11
g26 (Bs)	0	40	1.7	1.7	1	1	2464
g25 (Bv)	0	27	8.9	7.7	3	5	16
g24 (Gr1)	0	2	1.0	0.7	1	1	69
g23 (Gr2)	0	3	1.3	0.9	1	1	56
g20 (Gki)	0	3	1.0	1.1	0, 1	1	5
g19 (Ep)	0	2	1.0	1.0	0, 2	1	2
g16 (Ev)	0	3	1.3	1.2	0, 1, 3	1	3
g15 (Eo)	0	3	1.2	1.0	1	1	39
g10 (Ez)	0	16	3.2	2.7	2	2	67
g8 (Eza)	0	4	1.8	1.4	1	2	27
g6 (Y/Yb)	0	43	1.8	2.0	1	1	3904

Table 37 Lithology based statistical information for Lithium.

Lithology	Minimum value	Maximum value	Mean	Standard Deviation	Mode	Median	No. of sample points (f)
g44 (Bq)	0	3	1.5	1.5	0, 3	1.5	2
g41 (Bj)	0	11	2.5	2.0	2	2	60
g40 (Ba)	0	28	3.4	3.4	2	2	602
g37 (Tg)	0	16	2.4	1.9	2	2	297
g35 (Tgr)	0	26	2.5	1.9	1	2	861
g34 (Tcg)	0	8	2.7	1.6	2	2	105
g33 (Btb)	1	2	1.7	0.5	2	2	3
g30 (Bx)	0	8	3.3	2.3	3	3	21
g28 (BB)	0	4	1.8	1.3	1, 3	2	11
g26 (Bs)	0	34	3.5	3.8	2	2	2445
g25 (Bv)	1	12	3.0	2.6	1	2.5	16
g24 (Gr1)	0	6	2.2	1.4	2, 3	2	73
g23 (Gr2)	0	5	2.7	1.1	3	3	56
g20 (Gki)	0	3	1.4	1.0	1	1	5
g19 (Ep)	2	3	2.5	0.5	2, 3	2.5	2
g16 (Ev)	2	9	4.7	3.1	2, 3, 9	3	3
g15 (Eo)	1	14	3.6	2.4	2	3	42
g10 (Ez)	1	30	4.6	4.5	2	3	82
g8 (Eza)	1	6	2.7	1.3	2	2	27
g6 (Y/Yb)	0	70	2.9	2.9	2	2	3899

Table 38 Lithology based statistical information for Chromium.

Lithology	Minimum value	Maximum value	Mean	Standard Deviation	Mode	Median	No. of sample points (f)
g44 (Bq)	30	130	80.0	50.0	30, 130	80	2
g41 (Bj)	10	300	66.2	54.6	50	50	60
g40 (Ba)	10	310	53.3	48.0	20	40	602
g37 (Tg)	0	650	82.5	77.8	20	60	297
g35 (Tgr)	0	1530	96.9	107.3	20	64	862
g34 (Tcg)	10	445	95.9	88.9	30	67	106
g33 (Btb)	10	80	36.7	30.9	10, 20, 80	20	3
g30 (Bx)	19	470	166.7	117.9	19	182	21
g28 (BB)	10	240	83.5	63.2	60, 130	70	11
g26 (Bs)	0	540	58.1	54.8	20	40	2428
g25 (Bv)	50	750	247.5	190.7	90, 110, 210	210	16
g24 (Gr1)	10	470	79.3	84.8	30, 40	50	69
g23 (Gr2)	10	300	96.6	65.2	30	90	56
g20 (Gki)	0	30	16.0	10.2	20	20	5
g19 (Ep)	40	1000	520.0	480.0	40, 1000	520	2
g16 (Ev)	40	140	96.7	41.9	40, 110, 140	110	3
g15 (Eo)	21	1830	364.8	450.3	110, 380	167	39
g10 (Ez)	8	520	128.3	97.9	108, 150	104	82
g8 (Eza)	12	431	155.4	102.0	All samples	154	27
g6 (Y/Yb)	0	1450	58.7	80.3	10	38	3899

4.6.3 Data thresholding and anomaly recognition.

The fundamental objective in exploration geochemistry is to identify regions of potential mineralisation by separating data values into background and anomalous. This process is referred to as thresholding.

Siegel et al. (1993) working on suspensates in the USA produced thresholds based upon the mean (\bar{x}) plus multiples of the standard deviation (σ). Background was therefore represented by ($\bar{x} + 1.1\sigma$), moderately anomalous – just above regional background ($>\bar{x} + 1.1\sigma$), and strongly anomalous by ($>\bar{x} + 2\sigma$). Whilst Rose et al. (1990) also make reference to the mean plus two standard deviations. However there is concern as to the validity of thresholds derived in this manner, especially when datasets are large and not normally distributed. The choice of multiplier is, as explained by Sinclair (1974) and Stanley and Sinclair (1987) somewhat arbitrary, as there is no geochemical reasoning why the upper 2½ % of a data set represent anomalous data. Sinclair (1974) also points out that this method fails to adequately address the common problem of multiple populations and their separation and in doing so samples are misclassified. These commission and omission misclassification errors are explored and evaluated further in the work of Cheng et al. (1996).

Therefore the procedure adopted here was another traditional method of thresholding based on distinctive breaks observed in histogram frequency distribution. Prior investigations, with the use of the interactive P-PLOT program and involving subsets of the regional data, indicated that the cumulative probability plots were composed of multi-populations and that in essence four and five divisions could be distinguished within the log-transformed data. The fifth division often associated with extreme outlying values.

Although the process for thresholding the data had been established, there remained two possible options as to the method. The first was to use all data for each element (Section 4.6.1), the second to use data derived from individual

lithologies (Section 4.6.2). The later option would be more advantageous for results are based upon individual lithologies. However, on examining these histograms a number of statistical problems existed;

- 1) Normal distributions were not evident, virtually all data showed a positive skew, a result which could be a response to further heterogeneity within the lithologies or an indication of a complex secondary environment. This therefore pointed away from the implementation of a simple threshold, i.e. background and anomalous, but instead signified multi-population data.
- 2) The number of sample points varied both between and within elements. Consequently, results obtained from lithologies which had few sample points (typically g44-Bq; g33-Btb; g20-Gki; g19-Ep and g16-Ev) require some caution if used to infer a threshold level.
- 3) Thresholding based on breaks in the histogram were not always possible, especially in the platykurtic data, using count/frequency alone. In some cases thresholds could be inferred based on noticeable breaks in the values of the elements. An example is illustrated:

(Zn) lithology g28(BB).

Value	Count (f)
6	1
→ 13	2
14	2
16	1
→ 22	1
36	1
45	1
→ 49	1
92	1

Class intervals can be inferred through jumps in the flow of the 'value'. The arrows indicate where a significant change in value occurs. The highlighted value at the end signals a potential outlier point.

- 4) A further point of consideration is where the median value lies close to the maximum value the likelihood of finding mineralisation is low. Therefore on reviewing Table 31-38 there are a number of lithologies complying with this. For example, lead concentrations in lithology g28 (BB), Table 34 or Lithium in g23 (Gr2), Table 37.

With these points in mind the author decided to use element information derived from the whole dataset to determine thresholds. Each data set was split into four classes on the basis of the frequency distribution. However, wishing not to dismiss totally the information obtained from the lithology analysis, cross-checking was performed to try and ensure that the chosen threshold values, especially class 3 and 4, encompassed the breaks, jumps and/or outliers observed within the lithologies. These classes/thresholds were named as;

Class 1	Regional background.	(map colour green)
Class 2	Local background.	(map colour yellow)
Class 3	Of interest.	(map colour pink)
Class 4	Of significance.	(map colour red)

The author is aware that geochemical data can be expressed as a percentile, as demonstrated in Simpson et al., (1993). By way of a comparison the 90th percentile in all elements (except Au) coincides with the lower values of class 3 whilst for Au, class 3 represents the 95th percentile.

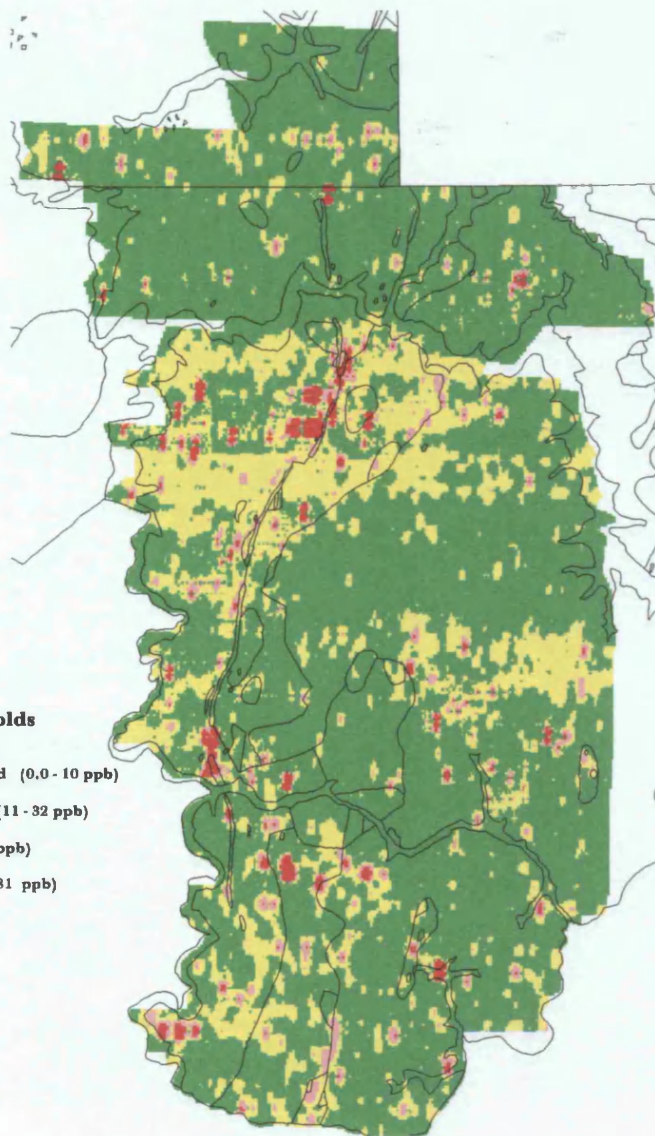
Figs. 40-43 illustrate the spatial distribution of the four class thresholds with relation to the local geology. In brief:

- Au: shows many class (3) and (4) sites distributed throughout most of the lithologies. However visually there appears to be a greater spatial frequency associated with the Birimian lithologies and its volcano-sedimentary unit than with the granite or diorite intrusions.
- Cu: reasonably large areas of class (3) and (4) sites appear spatially associated with the Birimian volcano-sedimentary unit, the undifferentiated volcano-sediments in the south, the diorite intrusion, the Birimian sediments and the ultra-mafic intrusions to the East and South-east. The granite indicates a strong spatial relationship to class (1).
- Zn: class (3) and (4) appear distributed throughout all lithologies. However there does seem to be some evidence of analytical error associated with this

Fig. 40

Geochemical thresholds.

Gold (Au) thresholds.



Copper (Cu) thresholds.

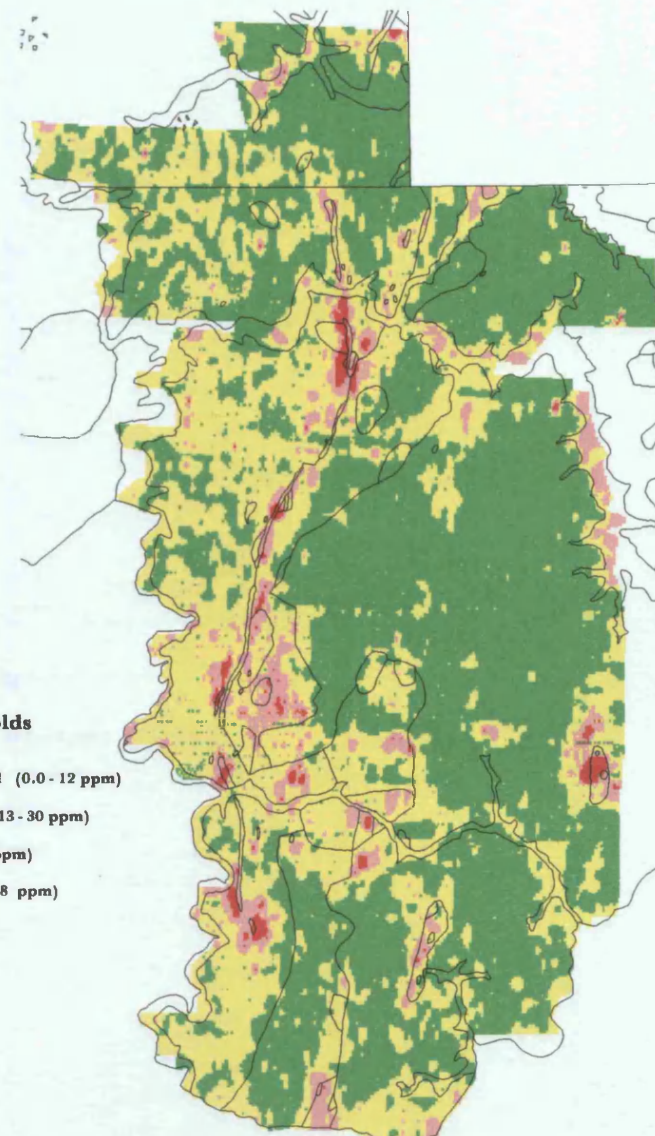


Fig. 41 Geochemical thresholds.

Zinc (Zn) thresholds.

Lead (Pb) thresholds.

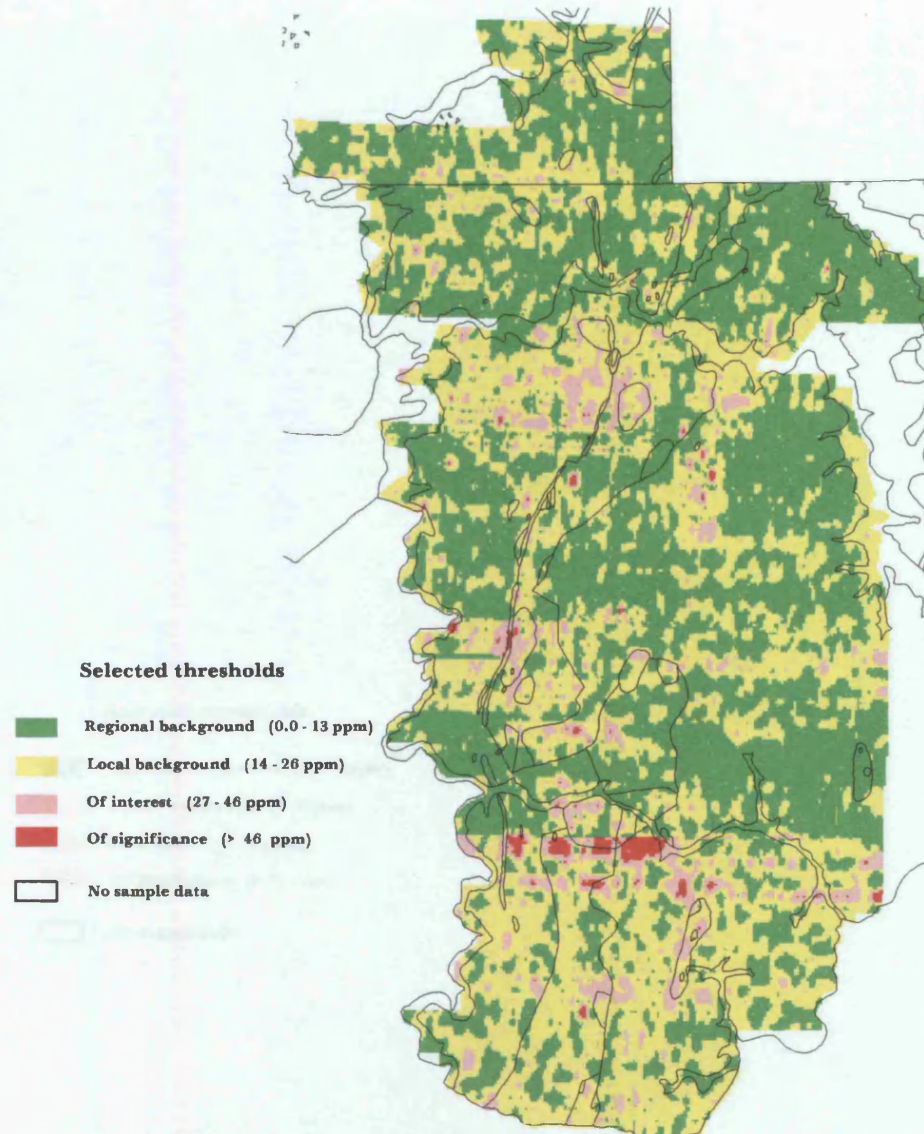
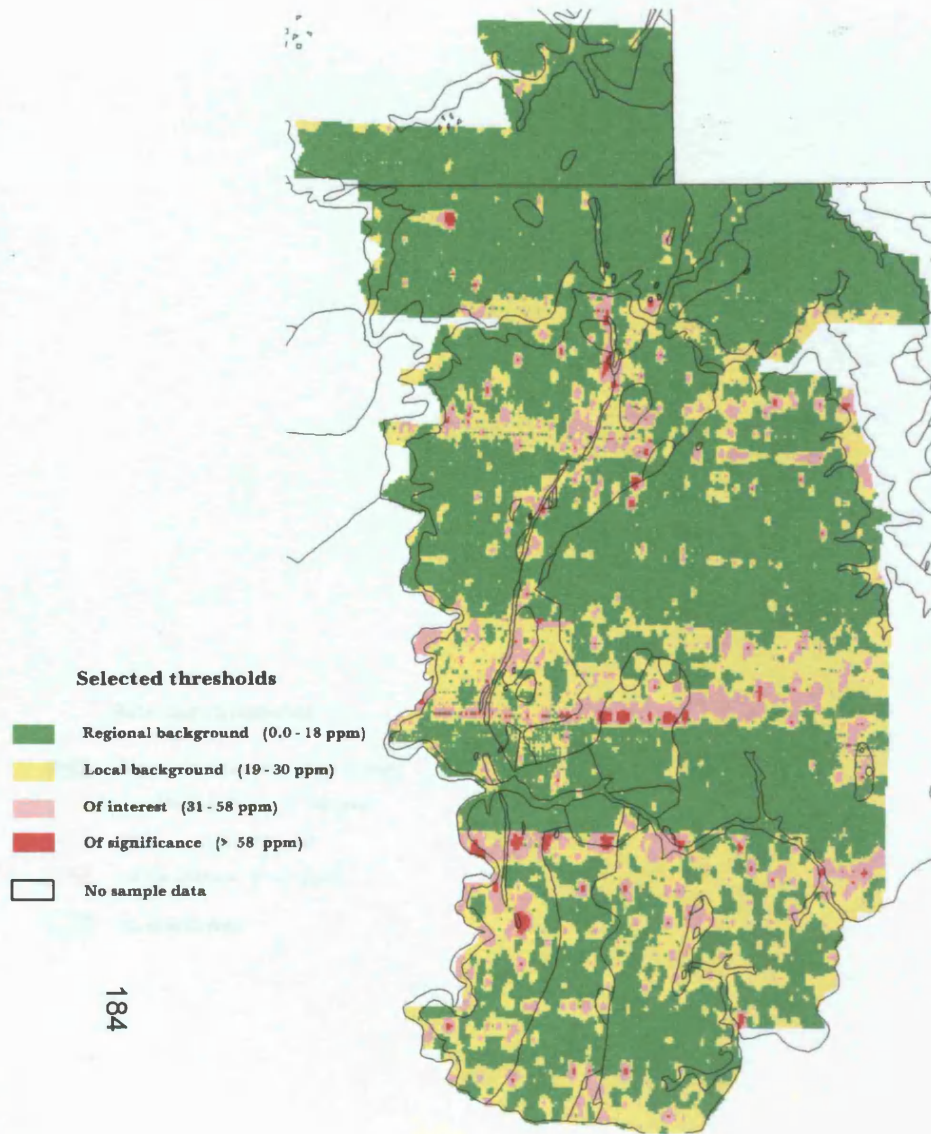
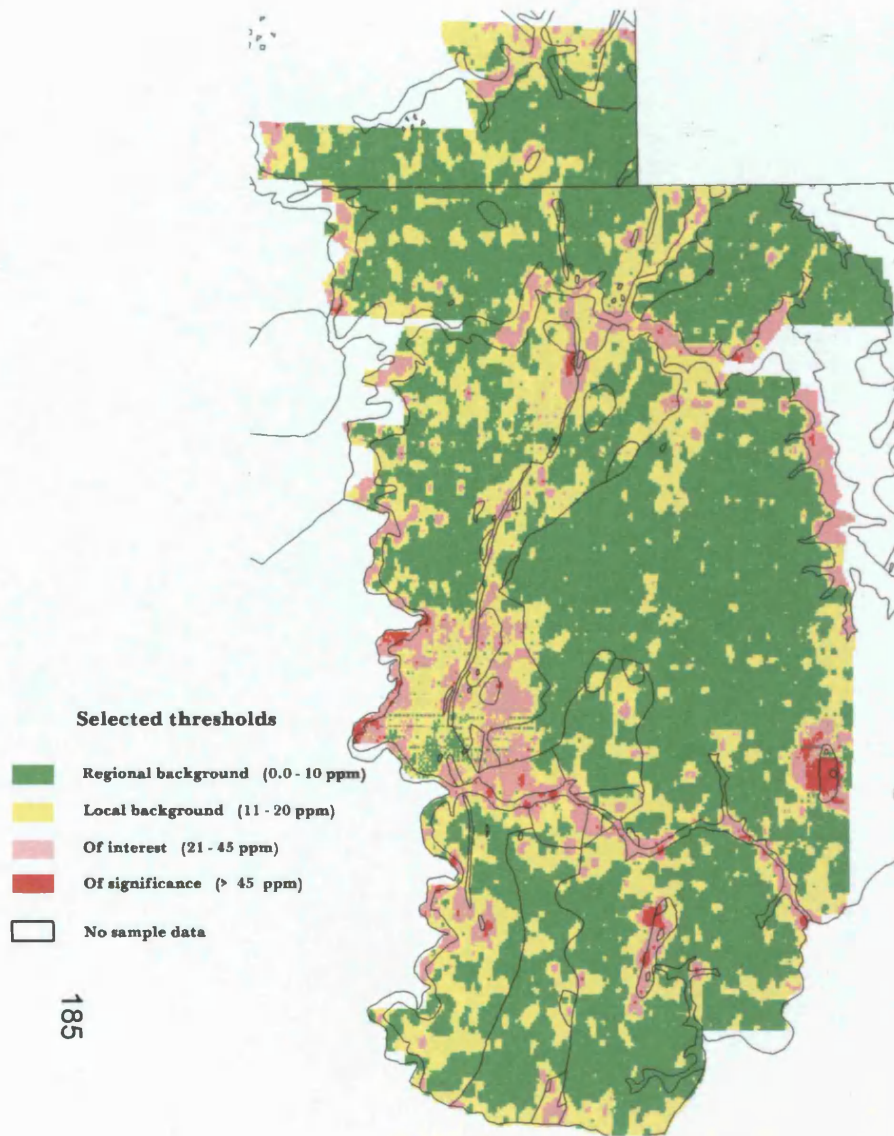


Fig. 42 Geochemical thresholds.

Nickel (Ni) thresholds.



Molybdenum (Mo) thresholds.

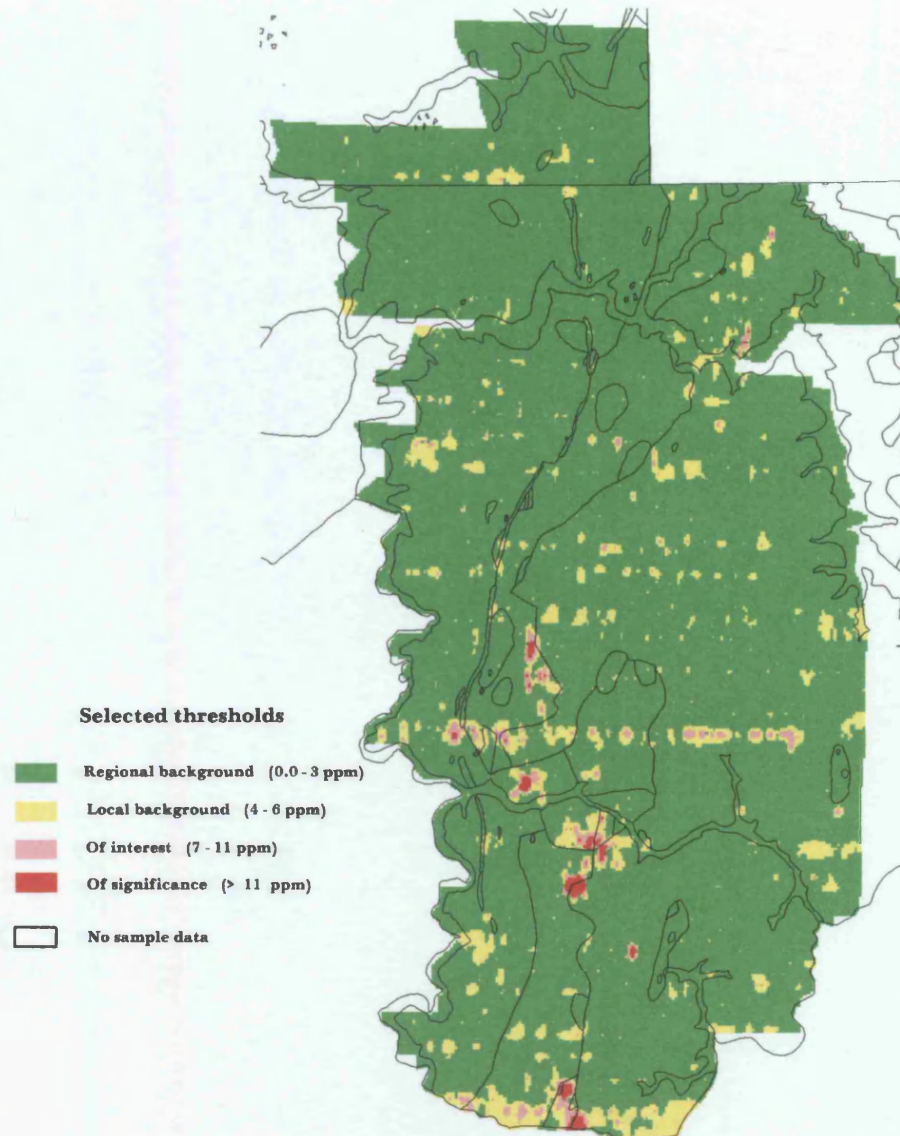
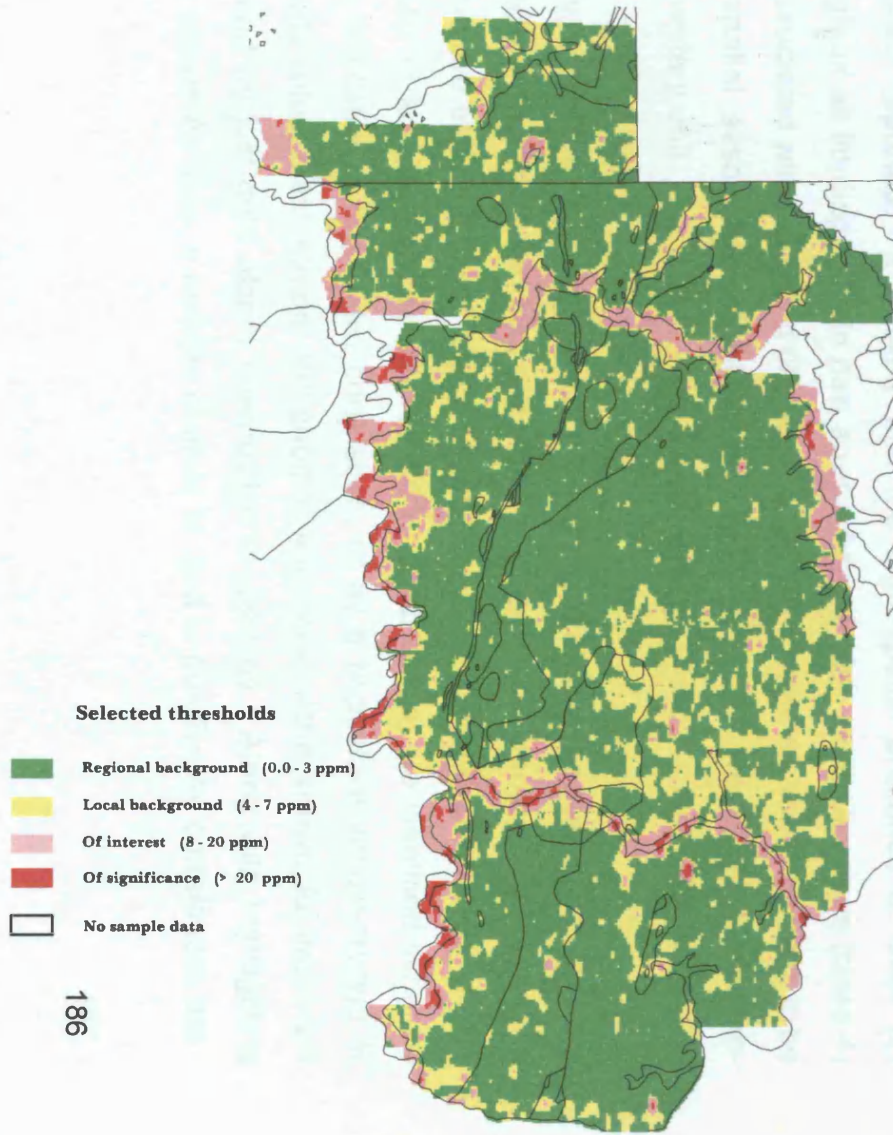
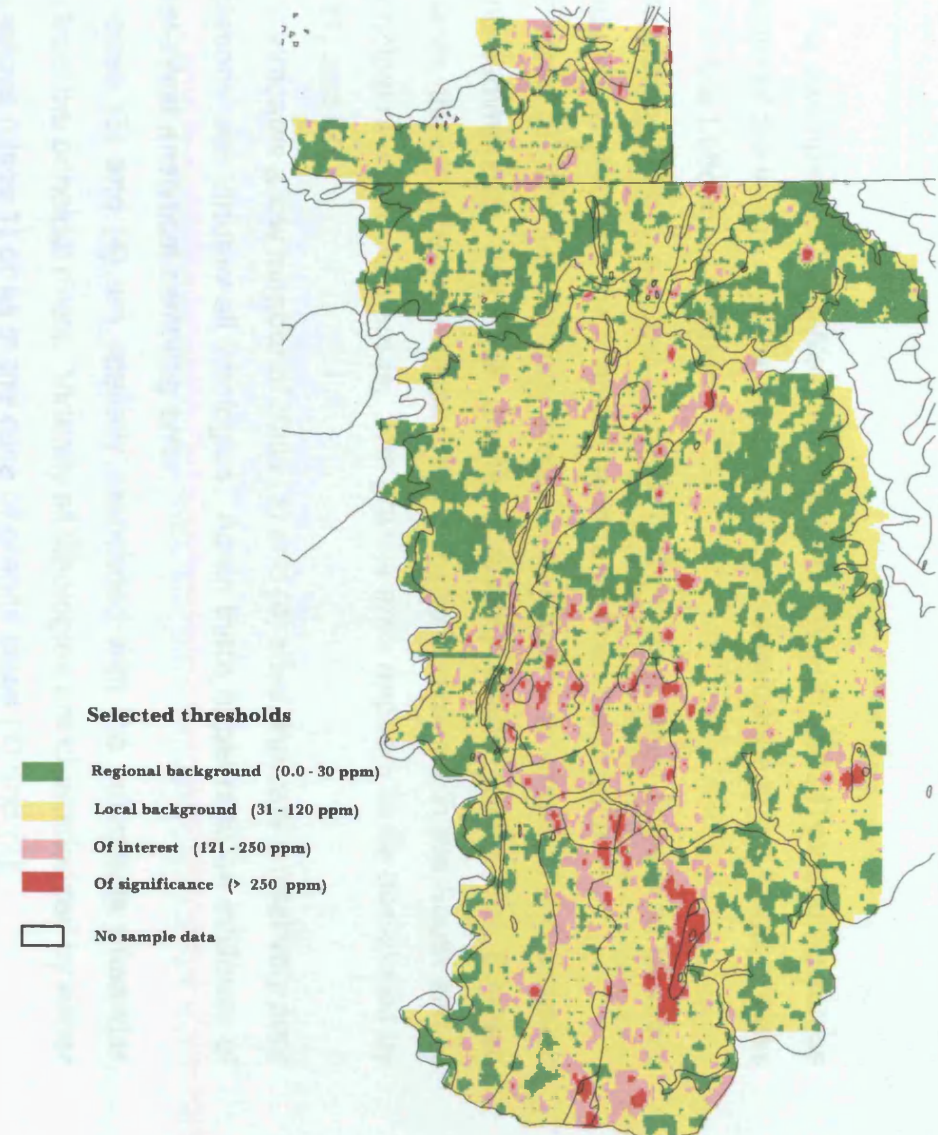


Fig. 43 Geochemical thresholds.

Lithium (Li) thresholds.



Chromium (Cr) thresholds.



data. For example, an East-West lineament of class (3) and (4) extending across the center of the image and the unexplained predominance in the North of class (1) within the Lobougoula region.

- Pb: although there are few class (3) and (4) sites, they appear to be more spatially associated with the Birimian sediments than the granite.

- Ni: class (3) and (4) indicate spatial associations to areas of the Birimian volcano-sedimentary unit, the diorite intrusion, areas within the Birimian sediments, the ultra-basic intrusions, the volcano-sediments in the South and to the principal river/alluvium areas. The granite area appears to be dominated by class (1) and (2).

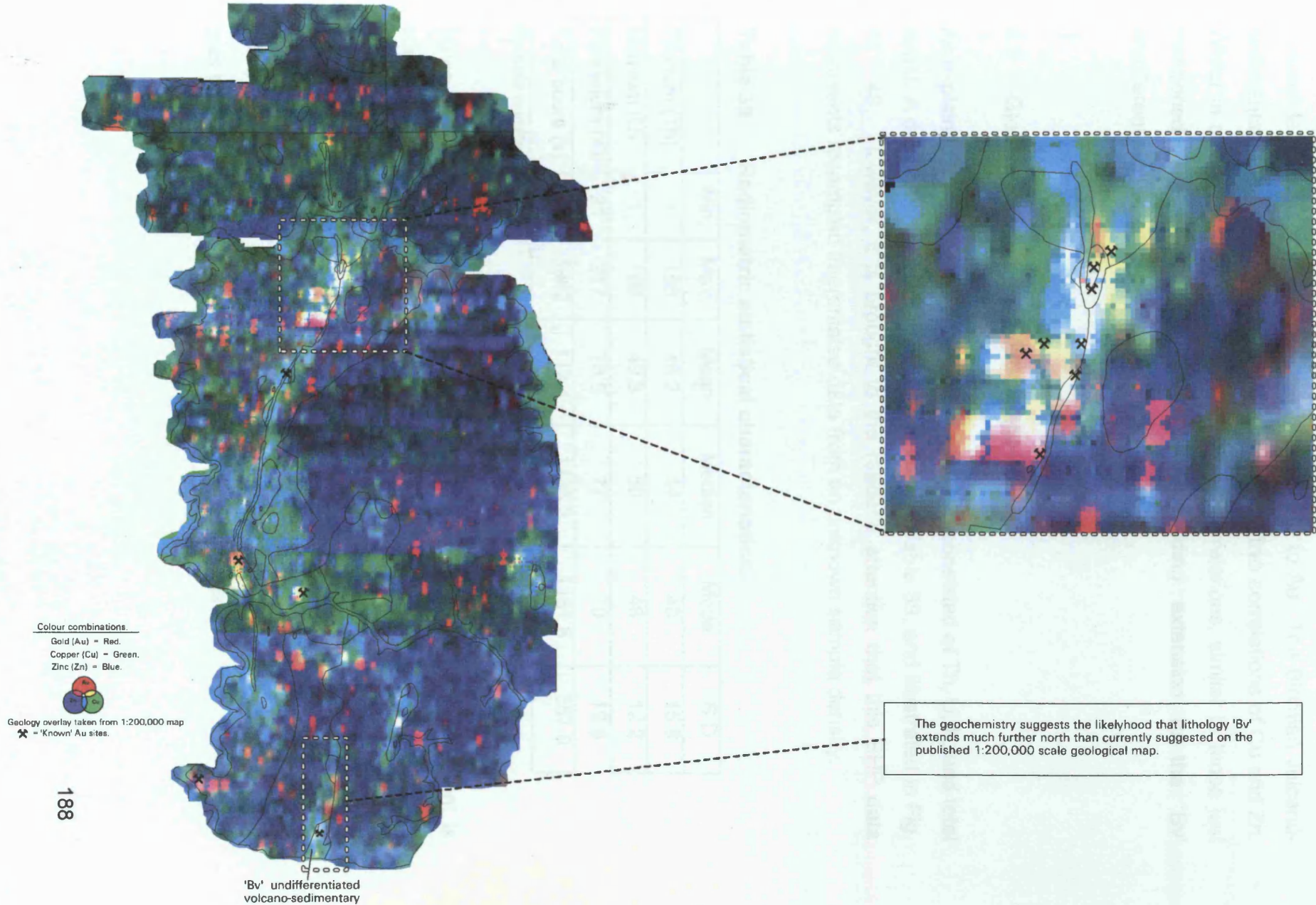
- Mo: indicates a low number of class (3) and (4) sites, indicating relatively poor associations with virtually all lithologies. Again there appears to be evidence of an East-West analytical sampling error.

- Li: class (3) and (4) are spatially associated with the sediments (meander traps) from the principal rivers. Virtually all lithologies are characterized by either low Li values (class 1) or as in the case of granite class (1) and (2).

- Cr: caution is required when interpreting this data due to the serious errors previously reported. It is likely that the high spatial presence of class (2) throughout all lithologies is in part a reflection of this. High Cr values (class 4) are associated with basic and ultra-basic intrusions however, there appears to be little spatial association of either class (3) or (4) to the Birimian volcano-sedimentary unit.

Finally, combining the geochemical images into colour composites can also help visualize any spatial relationships between elements and geology. In Fig. 44, Au and the two elements most highly correlated with it (Cu and Zn) are combined. Virtually all 'known' Au sites (alluvial not included in this) are identified either by white, indicating a tri-positive correlation, or by a bi-positive yellow-orange or magenta colour combination. Put another way, none of the 'known' Au areas are indicated by just gold alone, irrespective of geology. Along with highlighting these known Au sites, a number of other tri- and bi-positive Au correlations are

Fig. 44 Geochemical composite Au - Cu - Zn (R,G,B).



noticeable, as well as some responding principally to Au. The Birimian volcano-sedimentary unit is also clearly defined by the positive correlations of Cu and Zn. Whilst in the south positive Cu and Zn (\pm Au) correlations, similar to those just mentioned, suggest a likely linear NNE trending extension to the 'Bv' undifferentiated volcano-sediments.

4.7 Global radiometric statistical analysis.

As explained in Section 4.5.3 the radiometric data consisted of Th, U, K, and total count. A description of their statistics is shown in Table 39, and illustrated in Fig. 45 - 48. However, it is brought to the reader's attention that this BHP data represents resampled interpolated data from an unknown sample density.

Table 39 Radiometric statistical characteristics.

	Min.	Max.	Mean	Median	Mode	S.D
Thorium (Th)	1	168	46.2	44	40	15.8
Uranium (U)	1	168	49.8	50	48	12.2
Potassium (K)	21	217	78.5	77	70	19.6
Total count (τ)	1	3982	112.4	1136.2	1151.8	387.0

Sample number = 133,873

Using the same procedure as reported in Section 4.6.3 each radioelement is classified into 7 classes based upon breaks in the histogram distribution, leading to the displays illustrated in Fig. 49-52. By displaying the data in this manner and as grey-scale images random pixel errors, a likely result of pixel-overload at the sensor level were evident. This random error was at its worst in the total count data, as illustrated by the severe speckle throughout Fig. 52. The total count data was therefore rejected and excluded from further analysis.

Fig. 45 Thorium histogram plot.

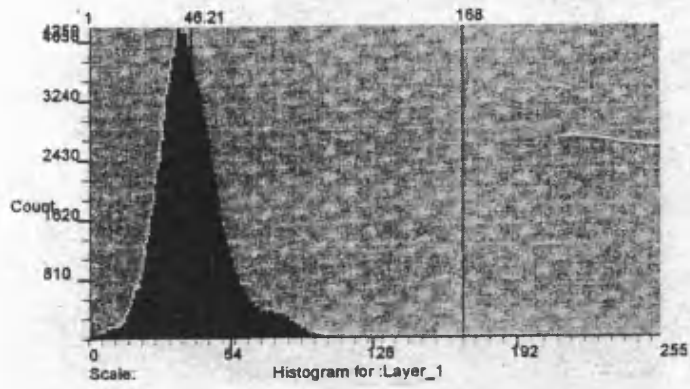


Fig. 46 Uranium histogram plot.

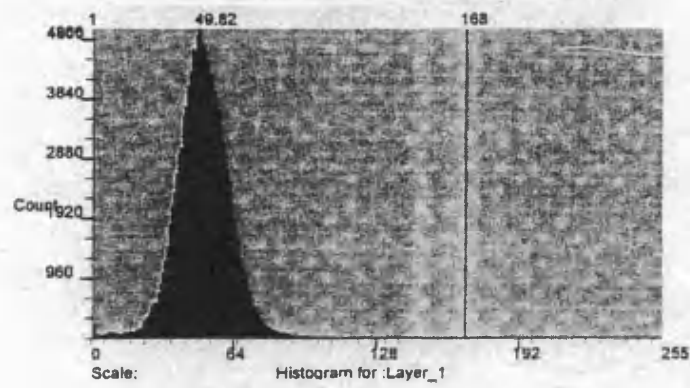


Fig. 47 Potassium histogram plot.

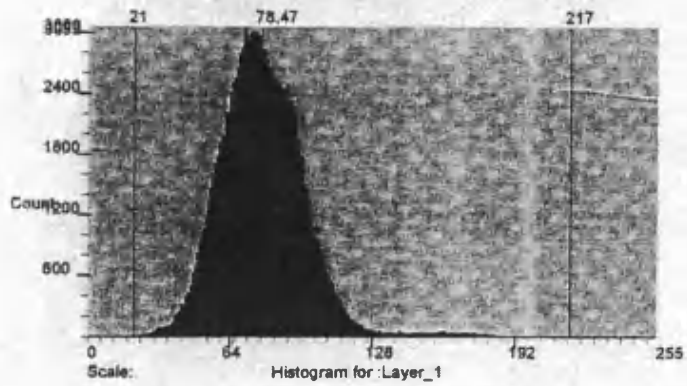


Fig. 48 Total count histogram plot.

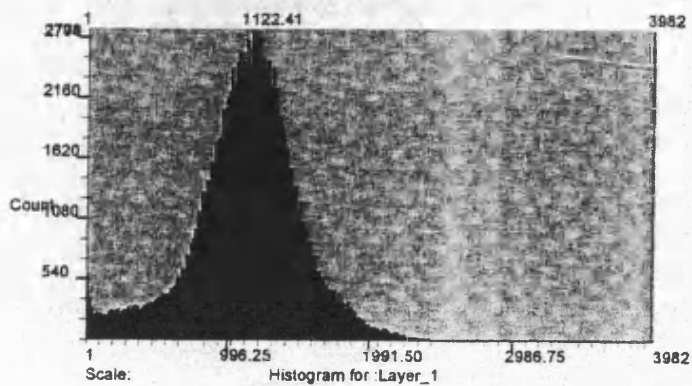
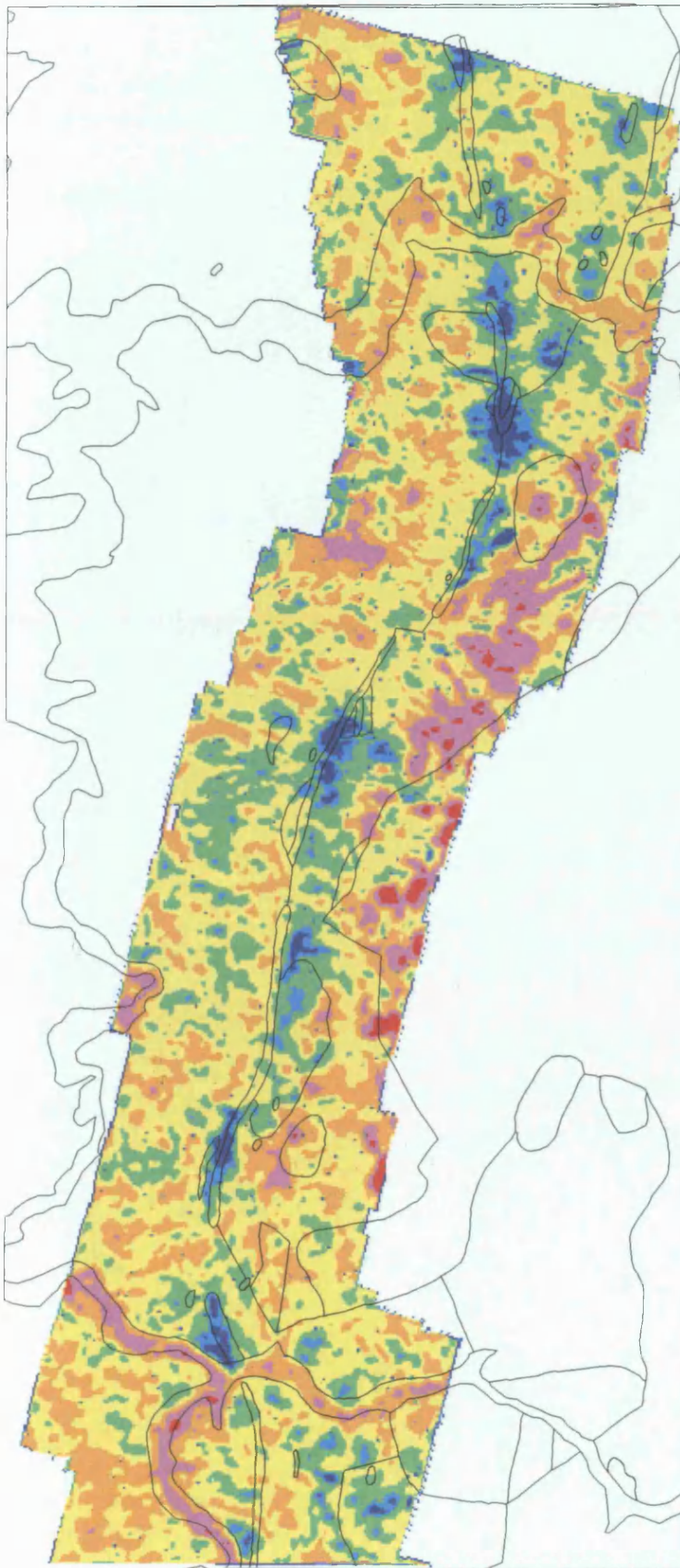


Fig. 49 Airborne radiometric data -Thorium.



Thorium (Th) cps

0 - 19
20 - 25
26 - 36
37 - 52
53 - 71
72 - 96
> 96

(Class intervals based upon histogram breaks.)

Fig. 50 Airborne radiometric data -Uranium.

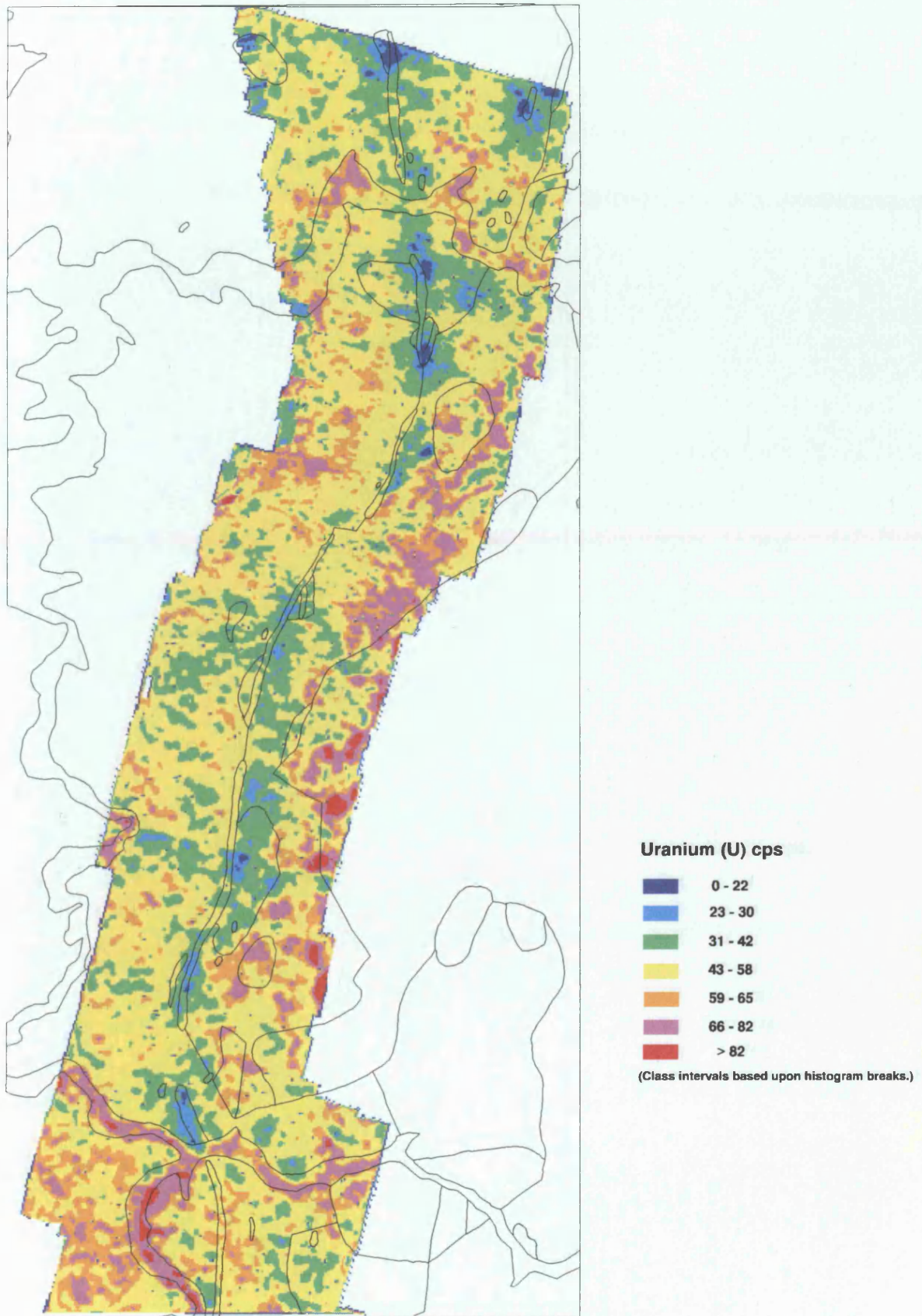


Fig. 51 Airborne radiometric data - Potassium.

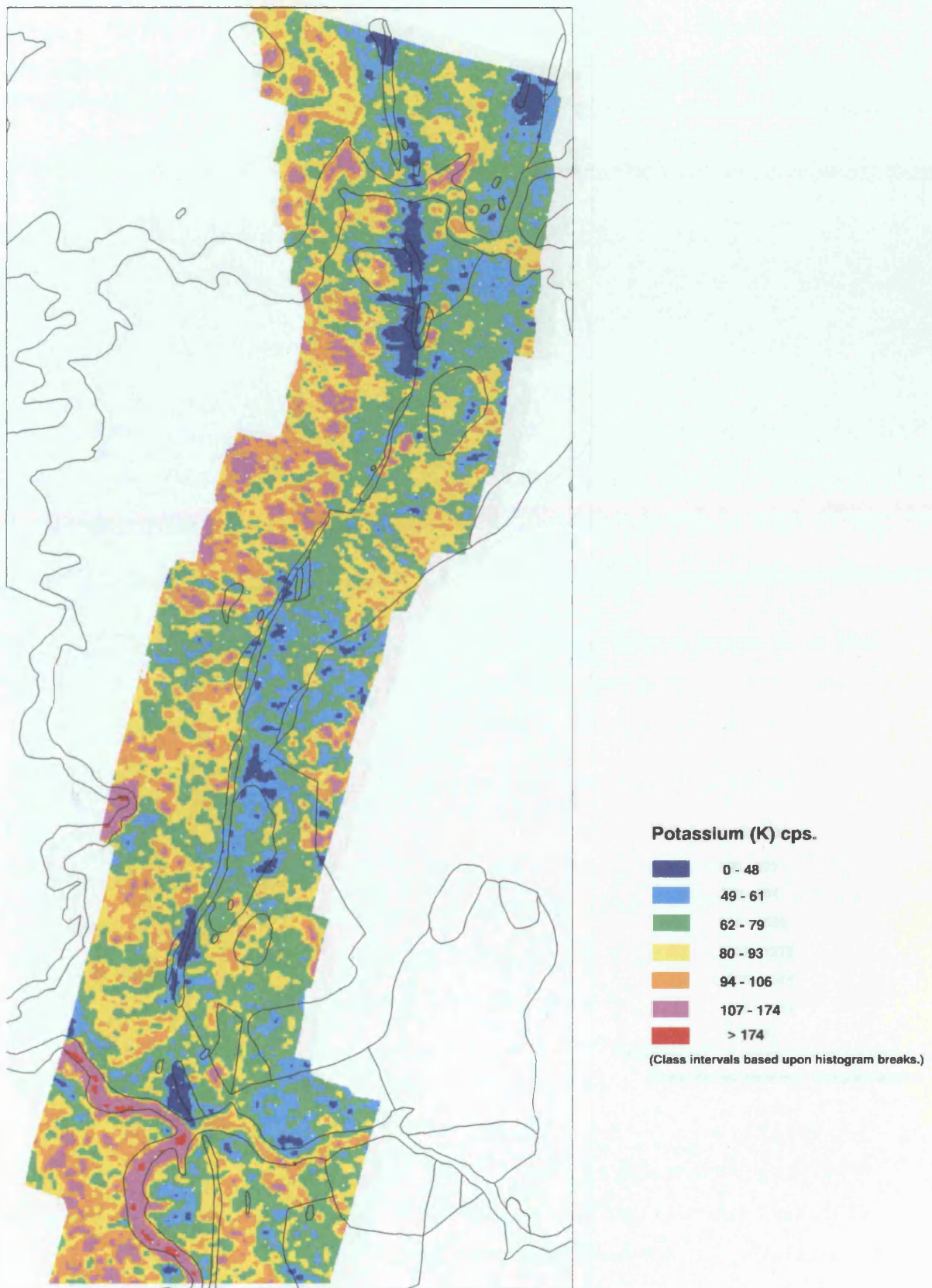
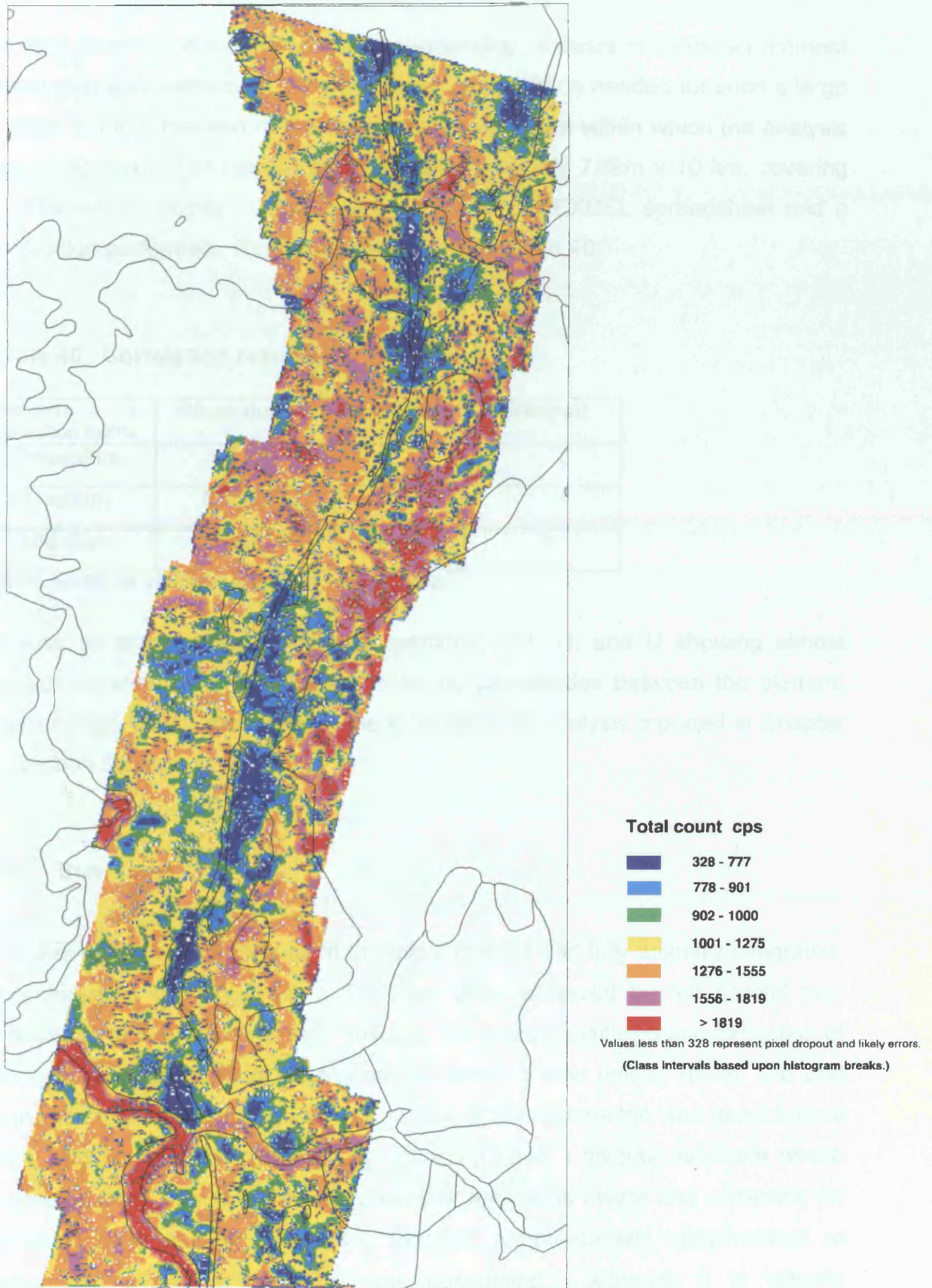


Fig. 52 Airborne radiometric data -Total count.



To help understand the inter-element relationship, a Pearson's Product moment correlation was performed. The excessive computation needed for such a large sample number resulted in the selection of a sub-area within which the analysis was performed. The sample area was approximately 7.5km x 10 km, covering 17,374 sample points. Data were exported to the EXCEL spreadsheet and a correlation performed. Results are presented in Table 40.

Table 40 Correlation results.

Pearson's correlation matrix	Potassium	Thorium	Uranium
Potassium	1		
Thorium	0.497	1	
Uranium	0.563	0.946	1

NB All results are significant at the 0.01 level (2-tailed).

Results all show strong positive correlations, with Th and U showing almost perfect correlation. There appear to be no peculiarities between the element relationships, which gives way to the more detailed analysis reported in Chapter 5 (Section 5.6).

4.8 Summary.

The aim of this chapter has been to build a diverse and fully spatially integrated, georeferenced GIS database. This has been achieved by the careful pre-processing of the remote-sensed imagery; the manual digitising and extraction of topographical and geological information, creating new unique (point, line and polygon) coverages; the input and correction of the radiometric, and geochemical data; and finally the magnetic data. Building such a diverse database where formats change from one dataset to another and being aware and correcting for errors in each dataset, (be it the reported remote-sensed, geochemical or radiometric errors) is incredibly time consuming. Although it is virtually

impossible to obtain a completely error free database, every effort has been made in this pre-processing stage to curtail the transmission of human error through into the processed derived coverages of Chapter 5.

Statistical analysis of the geochemical data has helped to highlight relationships between elements and enabled element thresholds, which when mapped allow spatial comparisons between elements and the geology. Although gold is the target (indicator) element its natural low level of abundance, problematic analytical properties and its characteristic low mobility make detection difficult. The solution has been to identify suitable pathfinder elements, i.e. elements which are more easily detected and show association to the target, the mineralisation or the host lithology. Under differing circumstances the chalcophile suite would be most appropriate, however these elements were not available. The Pearson correlation coefficient has therefore been used to assess inter-element relationships and pathfinder associations. This revealed weak but positive relationships between gold and base metals Zinc, Copper, Lead and Nickel respectively. However, the correlation takes no account for spatial variability, it is only a measure of the global strength and linearity of the two elements. The spatial context is more easily observed once elements have been thresholded and mapped. As revealed from Figs. 40-43 Lead is far less helpful as a spatial pathfinder of Gold than suggested by Pearson correlation. In comparison Copper, Nickel and Zinc are more favorable as both lithological pathfinders due to their association to ferromagnesian minerals and as Gold pathfinders because of their known association to mineralisation, as reported in Chapter 2, Section 2.6.5. As a final point, as far as the author is aware BHP have not performed continuous spatial mapping of the UNDP elements as illustrated here. Yet the results as suggested have highlighted not just an improvement with respect to viewing data spatially but are also able to pinpoint areas where analytical sampling errors appear to have occurred.

Although the SPOT image has the highest spatial resolution of the processed satellite data, its use as an aid to mineral exploration is limited by its poor spectral properties and with particular reference to this image, its small area coverage. As a consequence the SPOT data has been used principally to locate, identify and reference features between the different satellite images.

In conclusion, Table 41 helps to summarise the outcome of the data resulting from the analysis of this chapter and its destination.

Table 41 Data summary as derived from Chapter 4.

Source data type	Next destination	Destination info
TM image	Chapter 5	Further analysis.
SPOT image	Chapter 5	Geographic reference only due to poor spectral properties and small area coverage.
SAR ERS-1 image	N/A	Rejected. Poor data quality.
Geochemical data		
Au	Chapter 6	Criteria layer.
Cu	Chapter 6	Criteria layer
Zn	Chapter 6	Criteria layer
Ni	Chapter 6	Criteria layer
Pb	Chapter 6	Criteria layer
Mo	N/A	Rejected. Poor Au spatial and inter-correlations.
Li	N/A	Rejected. Poor Au spatial and inter-correlations.
Cr	N/A	Rejected. Poor data quality.
Radiometric data		
Thorium	Chapter 5	Further analysis.
Uranium	Chapter 5	Further analysis.
Potassium	Chapter 5	Further analysis.
Total count	N/A	Rejected. Poor data quality.
Magnetic data	Chapter 5	Further analysis.
Cartographic map coverages		
Lithology	Chapter 6	Referenced also in Chapter 5
Structural	Chapter 6	Referenced also in Chapter 5
Mineral occurrences	Chapter 6	Referenced also in Chapter 5
Hydrological data	Chapter 6	Discussion application.
Spot heights	Chapter 5	Terrain surface construction.
Contour data	Chapter 5	Terrain surface construction.
BHP own in-house maps		
Structural	Chapter 6	Referenced also in Chapter 5
Potassic areas	Chapter 5	Comparison analysis.
Lithology/chert	Chapter 6	Layer association criteria.

CHAPTER 5

THE GIS DATABASE AND PROCESS DERIVED COVERAGES.

Contents.

- 5.1 Introduction.**
- 5.2 Terrain models.**
 - 5.2.1 Triangular irregular network surface (TIN).**
 - 5.2.2 TIN construction.**
 - 5.2.3 Quality assessment.**
- 5.3 TIN derivations.**
- 5.4 Vegetation mapping using remotely sensed data.**
 - 5.4.1 Methodology.**
 - 5.4.2 Results.**
 - 5.4.3 Problems of classification accuracy.**
- 5.5 Mineral prospecting using remotely sensed TM data.**
 - 5.5.1 Aims and objectives for TM analysis.**
 - 5.5.2 Iron oxide and hydroxyl-bearing mapping.**
 - 5.5.3 Principal component analysis (PCA).**
 - 5.5.4 Combining and mapping coincidences.**
 - 5.5.5 Lineament mapping.**
- 5.6 The use of airborne radiometric data to aid Lithology and alteration mapping.**
 - 5.6.1 Selecting the appropriate methodology.**
 - 5.6.2 The application of feature space mapping.**
- 5.7 The use of airborne magnetic data.**
 - 5.7.1 Airborne magnetic interpretation.**
- 5.8 Summary.**

5.1 Introduction.

As detailed in Chapter 4, the GIS database consists of a diverse and spatially integrated set of coverages and images. However, through further analyses it is possible to extract additional information from the landscape which can also be used within the GIS model. This information can be derived from many sources. In Section 5.2 a terrain model is developed for the region yielding additional landscape information on elevation and slope characteristics in the modelled environment. This is followed in Section 5.4 and 5.5 by the analysis of TM satellite data. Here procedures are adopted that first attempt to isolate and remove any possible interference from vegetation. Following this various techniques are experimented with aimed at best identifying hydroxyl-bearing clays and iron oxides, since both are considered to be important indicators of mineral alteration. Section 5.6 discusses how the radiometric data was processed in order to identify signatures potentially relating to 'Birimian-type' basic lithologies and signatures that are most likely to be responding to alteration due to high potassic values. Finally, a magnetic dataset is investigated in Section 5.7, using differences in the magnetic gradient to map underlying geology. The chapter is brought to a close by concluding remarks in Section 5.8.

Throughout this chapter the author acknowledges the existence of numerous alternative techniques for each of the tasks identified above. Many of these were tested and some are discussed more fully than others, but in general only the technique found to be most informative is illustrated with a figure.

5.2 Terrain models.

A digital terrain model is at its simplest an image that, through a process of interpolation, represents a topographic surface of height (or elevation) data. They have many varied uses, ranging from simple visual enhancement (e.g. the “draping” of overlays onto perspective plots) through to more analytical processes that extract or interpolate further information from the surface parameters, as described in Hutchinson and Gallant (1999). Information derived from analytical processes can be of considerable value in aiding the understanding of, and explaining the interactions between, co-registered datasets.

There are two principal data models used to create and represent terrain surfaces; namely triangulated irregular networks (TINs), and lattices (or digital elevation models - DEMs). The type of source data used to create the surface is often a controlling factor in determining which of these two surface models is most appropriate although there are other considerations too, such as data volume and the accuracy of resultant surface representations. Lattices use a regularly spaced set of elevation values and are most appropriate if the source data display a similar tendency towards regular spacing. They can, however, be derived from irregularly spaced elevation data too by spatial interpolation methods. TINs on the other hand are often more appropriate if source data is very irregularly spaced. Typically, they yield a more compact data structure than a DEM and have the powerful advantage that the spatial density of elevation points can be matched to the local complexity of the surface being represented.

5.2.1. Triangular irregular network surface (TIN).

In this research a TIN surface was constructed, primarily due to the derivative data sources of contour lines and randomly spaced spot-heights. In Arc/Info's TIN module a surface is constructed by a process of triangulation known as Delaunay triangulation. Tsai (1993) writes in detail about this methodology, but in brief a triangle is formed by connecting a sample point to its nearest two

neighbours such that, when all three vertices are encompassed by a circle this does not include any other sample point within its circumference. If this criterion is not fulfilled, the segmentation resorts in further triangulation. The resultant faceted surface can also use additional information known as breaklines to place constraints on the triangulation process. Breaklines control the behaviour or flow of the surface (ArcInfo: surface modelling with TIN, 1993) and can be used to force conformance with known topographic ridge and trough lines, or to preserve the hydrological integrity of the surface.

5.2.2 TIN construction.

Contour lines and spot heights were digitised from 1:200,000 scale geological maps since only these maps gave full regional coverage with a contour interval of 40 m. Some data inconsistencies were found to exist between the two adjacent maps of Kadiana and Kadiolo, principally in the introduction of an additional contour interval when crossing the boundary. This additional contour interval was only incorporated if its full trace could be observed on the map, (e.g. the Kadiolo map). A non-convex 'hull' was also created in Arc/Info's TIN module, this being a polygon that defines the outer perimeter of the surface to be generated.

Contour data and spot-heights were input to the TIN generator in accordance with Arc/Info formats together with breaklines taken from the hydrology coverage. Various tolerances were experimented with in an attempt to influence the triangulation procedure and so minimise the occurrence of long thin triangles within the TIN.

5.2.3 Quality assessment.

Visually, the resultant TIN appeared to model the input data reasonably well. However, as discussed by Hutchinson and Gallant (1999) and Chrisman (1997), a combination of a 1:200,000 source scale and a somewhat widely spaced contour interval will impose limitations on the level of detail obtainable. It will

also limit the validity of any subsequent analysis of slope profiles. For this reason complex slope information pertaining to concavity and convexity has not been included in this study. To a lesser extent information on slope gradient should also be treated cautiously, simply because of the nature of the source data and the interpolation procedures used in their computation.

5.3 TIN derivations.

By overlaying coverages onto the TIN, 3-D visualisations can be achieved and, with some further processing, it is possible to derive information about the slope characteristics of the landscape.

In a lateritic landscape the topographical location of a sampling point can be of importance in determining how much weight or reliability should be given to that information, as explained earlier in Chapter 3. Thus slope information allied to elevation can provide a very simple classification of the landscape into:

- Sloping regions
- Flat lying regions occupying low elevations
- Flat lying regions occupying high elevations

Placing these within context of the research landscape and using knowledge of landscape evolution enables the codes described previously by Zeegers and Lecomte (1992), in Fig. 29 to be implemented. This process is described in Chapter 6, Section 6.4.

5.4 Vegetation mapping using remotely sensed data.

Geological remote sensing is often considered to be most effective in arid or semi-arid climates since under these climatic regimes vegetation cover is not expected to create a barrier to the detection of soil and rock properties. Increasing vegetation density will reduce and interfere with the effectiveness of the geological signal, confusing any interpretation (Green and Huntington, 1987). Consequently, it is important in this savannah environment to establish

not only where vegetation is present, but also its density or degree of surface coverage. This establishes the degree to which the spectral signal of a pixel is considered “pure”, or whether in fact it must be treated as “mixed” in nature.

5.4.1 Methodology.

There are many remote sensing techniques that can be applied to the study and mapping of vegetation properties and characteristics (ERDAS, 1997). These include:

- a) Unsupervised classification
- b) Supervised classification
- c) Normalised Difference Vegetation Index (NDVI).

$$\text{NDVI} = (\text{NIR} - \text{RED}) / (\text{NIR} + \text{RED})$$

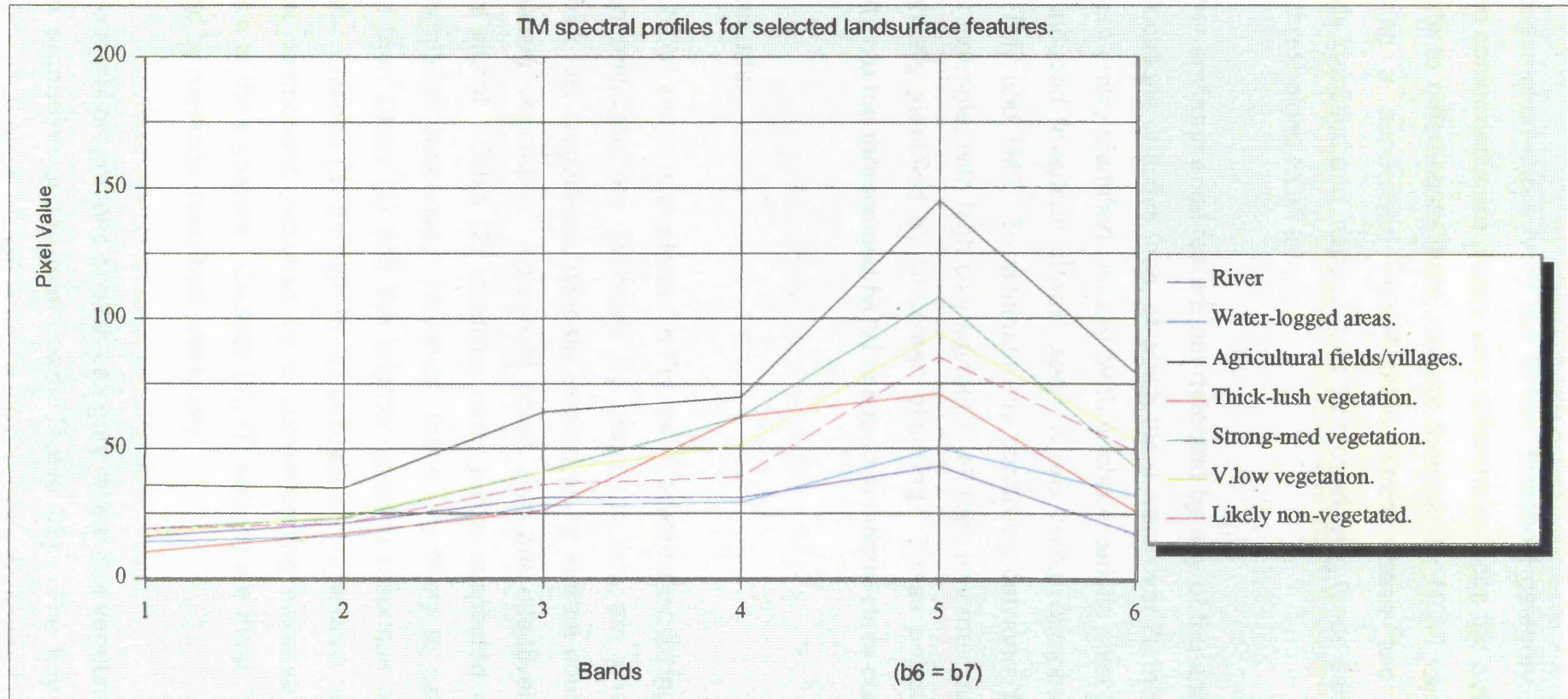
- d) Other spectral-slope and spectral-distance based vegetation indices

Of these, method (c) was selected, having previously investigated the potential of (a) and (b). This decision was primarily based on the analysis of individual pixels with known vegetated and non-vegetated spectral profiles, which indicated simple thresholding of NDVI values would work adequately (Fig. 53).

However, there were two environmental conditions that could not readily be differentiated by this method. First were high reflectance values observed in agricultural fields (identified as such by comparison with the higher resolution SPOT imagery and by their characteristic angular shapes and appropriate sizes) and within villages. Second were areas of low reflectance values, believed to coincide with water-logging and likely to be lacking in vegetation. Further confirmation of a water-logged status came from comparisons with the “brightness”, “greenness” and, most importantly in this situation, “wetness” images produced by a Tasseled Cap transformation (Crist and Cicone, 1984; Lillesand and Kiefer, 1994).

Although the mean reflectance of these features were very different, they had similar gradients between TM3 (red) and TM4 (near infrared) which resulted in

Fig. 53



their amalgamation into a 'very low to low' threshold category. As these two landscape components are clearly very different surfaces the author felt it more appropriate to differentiate them, despite their similar NDVI values. This was done using a supervised classification where these two classes were specifically identified and mapped, and then overlaying these particular features onto the thresholded NDVI image.

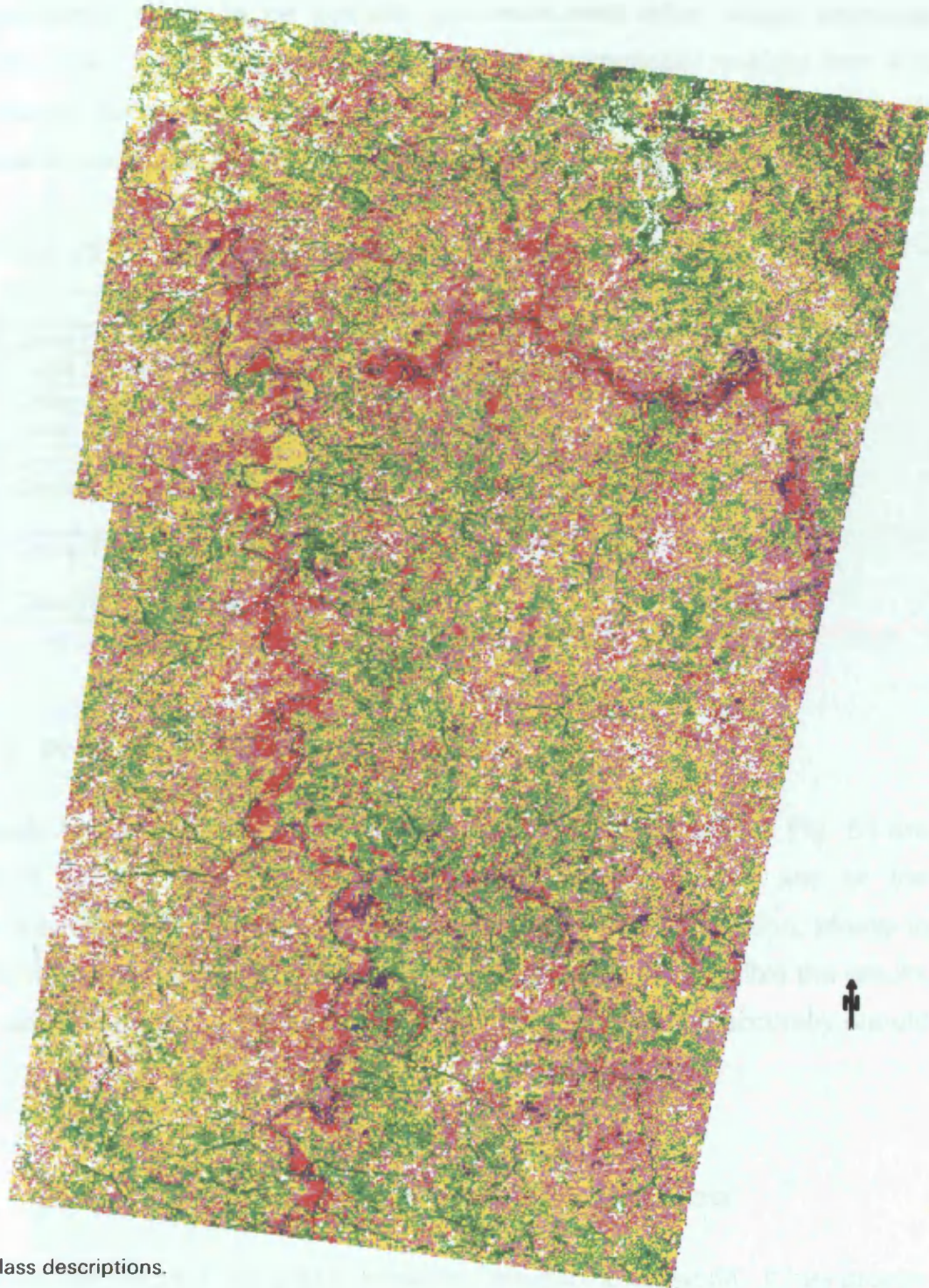
One further environmental feature not detected by any of the above techniques was the locations of active fires, of which there were over 70 in the study area. These were easily identified visually by their characteristic pixel overload and a scanner induced "overload streak" seen in any colour composite image that included TM7 and TM5. To eliminate any confusion between "fire pixels" and those, for example, with high clay signature, all fires and their overload streaks were manually identified by on-screen digitising. These polygons were then rasterised onto the thresholded NDVI image as a unique class code (8).

5.4.2 Results.

The final NDVI image is illustrated in Fig. 54. Locations exhibiting the strongest vegetation response are indicated by class (1) and are characterised by intense/thick lush vegetation, typically located along stream courses. This so-called "gallery vegetation" represents pixels that are effectively void of any geological signal. Class (2) identifies other pixels suspected of exhibiting a strong vegetation response. However, these are likely to be less densely vegetated than Class (1) and the brighter spectral response suggests dryer vegetation. Classes (3) through to (5) indicate a progressive reduction in the vegetation component, replaced by a corresponding increase in geological contribution to the signature. Classes (6), (7) and (8) are those that have been substituted by methods described previously.

Overall the aerial proportions of each category reveal that vegetation occupies a significant proportion of the total image (Table 42). The key advantage of developing this vegetation map is that it allows pixels dominated by vegetation,

Fig. 54 NDVI Classification of TM image.



Class descriptions.

-
-  Class 1 Vegetation intensity very strong (lush/thick veg)
 -  Class 2 Vegetation intensity high-medium
 -  Class 3 Vegetation intensity medium-low
 -  Class 4 Vegetation intensity low-very low
 -  Class 5 Vegetation intensity very low-unvegetated
 -  Class 6 Vegetation intensity likely very low, water logged/fire scars
 -  Class 7 Vegetation intensity likely very low agricultural fields/villages
 -  Class 8 Active fires

or any other class, to be spatially compared with other image processing results. Then, highly vegetated pixels can be automatically masked from these results to eliminate potential confusion on interpretation, especially when analysing band ratio results (for example using the TM5 /TM7.ratio).

Table 42. Percentage class contribution in TM image.

Class description	% contribution
Class (1) Vegetation intensity very strong (lush/thick).	4
Class (2) Vegetation intensity strong - medium.	17
Class (3) Vegetation intensity medium - low.	41
Class (4) Vegetation intensity low - very low.	23
Class (5) Vegetation intensity very low or non-vegetated	6
Class (6) Vegetation intensity likely to be very low; water logged with possibly some fires scars.	1
Class (7) Vegetation intensity likely to be very low; agricultural fields / villages.	8
Class (8) Active fires.	0.04

5.4.3 Problems of classification accuracy.

It would be naive of the author to state that results presented in Fig. 54 are without error. However, to acquire higher accuracy with any of the aforementioned techniques would need extensive field verification, ideally in the same month as image acquisition. Since this was not possible the results are viewed as a best overall estimate, and any remaining inaccuracy should not discredit their further use.

5.5 Mineral prospecting using remotely sensed TM data.

Landsat TM imagery has greatly benefited the geological world. It has proven a reliable and affordable option, especially in preliminary stages of a reconnaissance program where screening for mineral targets or aiding geological interpretation is required (Drury, 1987; Green and Huntington, 1987). Its synoptic view, repeated coverage, and unhindered access of remote and inaccessible regions otherwise too expensive to access, have undoubtedly encouraged its widespread use. Although there are reported uses of TM

imagery in most climatic environments, its greatest contribution for geological applications is within arid and semi-arid climates (e.g. Rothery, 1987; Crosta et al., 1989; Loughlin, 1991; Davidson et al., 1993). These environments exhibit higher rock exposure than more humid regions where vegetation cover limits effective remote sensing of mineralised zones.

Another potential barrier, equally problematic but less widely reported, is the occurrence of deep weathering, as discussed by Green and Huntington (1987). In deep weathering environments natural mineral breakdown produces the same clay and iron minerals that mineral exploration seeks. This makes discrimination very difficult unless the landscape has subsequently undergone deep dissection, or alternatively image analysis is aided by field evaluation. Reports of working in such an environment are given by Gabell et al., (1984) and Drury and Hunt, (1989) based in the Yilgarn Block of Western Australia.

5.5.1 Aims and objectives for TM analysis.

The principal aim in analysing TM data in this research was to identify evidence of mineralisation processes. This involves the detection of any hydrothermal alteration and gossan material in the form of iron oxides.

A number of techniques such as image differencing, band ratioing, and principal component analysis were explored in an attempt to establish whether any surface expression of mineralisation could be readily identified in an environment that exhibits both deep weathering and variable levels of vegetation cover.

It is appropriate at this stage to discuss the known limitations of TM data in such a task. Although TM can detect the presence of iron oxides and clay alteration products, its low spectral resolution makes it incapable of identifying individual minerals in each of these two groups. In a non-peritropical climate this does not create a major problem, as clay and iron species are rare enough to warrant further investigation whenever identified. When deep lateritic weathering has

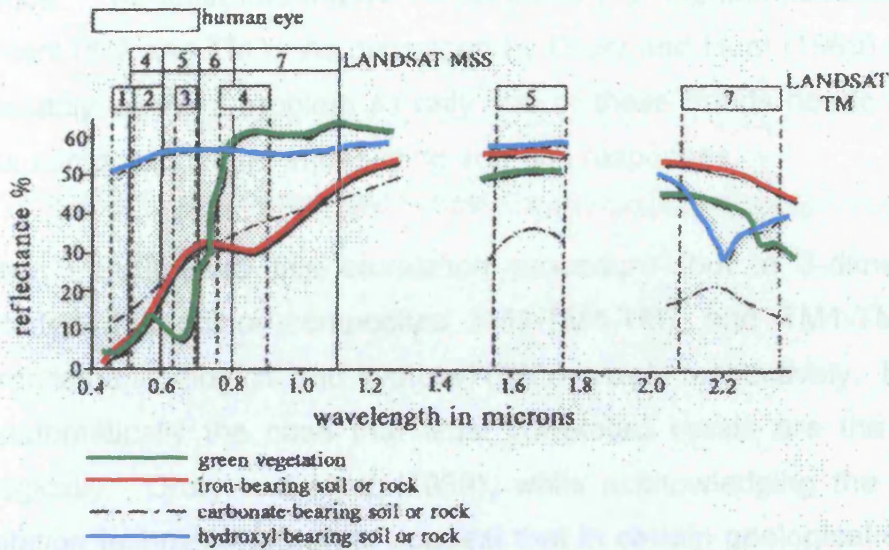
taken place these clays and iron oxides are likely to be widespread at the surface, as was discussed in Chapter 3. Consequently, it becomes highly desirable to discriminate between kaolinite and its high temperature form, dickite, alunite and the iron species jarosite (and limonite), since this would distinguish between simple weathering and potential alteration. Unfortunately, this is not possible with TM data.

5.5.2 Iron oxide and hydroxyl-bearing mapping.

Early field and laboratory analyses provide an understanding of the physical spectral properties of minerals, as reviewed by Buckingham and Sommer (1983). It is not the intention here to engage in detailed scientific explanations for spectral properties of particular minerals (the reader is directed to an appropriate text such as Drury, 1987 if this is required). However, a brief explanation is appropriate, and is presented next.

Fig. 55 shows characteristic spectral signatures associated with iron and clay minerals. Features important for the identification of iron-rich rocks occur within the visible to near-infrared (VNIR) region of the spectrum (i.e. TM bands 1 through to 4). Iron generally absorbs strongly in both TM1 and TM4, but displays a rising reflectance ramp between bands TM2 and TM3. In contrast, clay-rich rocks can be discriminated primarily on the basis of strong shortwave-infrared (SWIR) reflectance in TM5 and absorption in TM7. Important discriminatory features are therefore the spectral location of absorption and reflection properties, and ramps between the two.

Fig. 55 Diagnostic spectra of iron, clay, carbonate and chlorophyll adsorption.



Source Kaufman, (1987).

In the initial stages of investigation the data were displayed as false colour composites. In creating any such display a key objective is to select bands that possess the greatest discriminatory properties. A simple way to ensure this objective is achieved is to undertake a correlation analysis on a subset of the TM data (Table 43). Bands exhibiting the least correlation should, by definition, provide the most informative colour composites.

Table 43 TM band correlation analysis.

Tm	B1	B2	B3	B4	B5	B7
B1	1					
B2	0.8232	1				
B3	0.8231	0.9112	1			
B4	0.1969	0.4383	0.4524	1		
B5	0.6745	0.8172	0.8781	0.6817	1	
B7	0.8359	0.8049	0.8235	0.0485	0.6814	1

(Sample No. 24393)

From this table it is established that TM4 is the least correlated of all bands, suggesting it should be a good discriminator. Drury and Hunt (1989) describe this situation as a probable reflection of the fact that the Fe^{3+} absorption field is contained in this band. Although equally true here, it is also more likely that

vegetation differences in the area provide the greatest contribution to TM4 variance. The least informative combination (i.e. highest correlation) is found between TM2 and TM3. As discussed by Drury and Hunt (1989) this does not necessarily create a problem as only one of these bands needs be used in a colour composite aimed at depicting iron-rich responses.

Crippen (1989) used this correlation procedure (but in 3-dimensions) and concluded that colour composites TM1-TM4-TM7 and TM1-TM5-TM7 best differentiated lithological and hydroxyl-rich minerals respectively. However, it is not automatically the case that least correlated bands are the most useful geologically. Drury and Hunt (1989), while acknowledging the value of the correlation technique, go on to suggest that in certain geological environments known spectral responses for rock identification are equally important in determining good band selections. To a large extent Gillespie et al. (1986) overcame this dilemma by adopting a method known as the "decorrelation stretch". This allows even highly correlated bands to be displayed effectively. Fig. 56(a) and (b) illustrate the advantage of this technique which allows effective visual display of band combinations that are important mineralogically but have high inter-band correlations and thus are potentially least informative when visualised. The greatly improved vibrancy and discrimination of colours created by decorrelation stretching allows effective visual interpretation to take place. However, the presence of vegetation is not addressed by this technique and it remains a problem regardless of which band combination is used.

Band differencing is not widely used for mineral discrimination, but successes reported by Crosta and Moore (1989) and Moore et al., (1993) prompted its investigation in this research. This work showed that, due to the reflectance and absorption characteristics of clay minerals and iron oxides, their presence in an image can be enhanced by simple band subtraction. Therefore the following difference images were tested, both individually and as 3-band colour composites:

TM3-TM1 and TM4-TM1, for the enhancement of ferruginous soils

TM4-TM3, for vegetation detection

TM5-TM7 for the enhancement of hydrated minerals

Fig. 56 The use of Decorrelation Stretch with TM data.

(a) Colour composite using bands 5-7-3 (R-G-B)

811050, 1199666



825457, 1199666

811050, 1184108

825457, 1184108

(b) Decorrelation stretch colour composite, bands 5-7-3 (R-G-B).

811050, 1199666



825457, 1199666

811050, 1184108

825457, 1184108



However, it was found that, even after considerable efforts at display enhancement, this approach proved no more informative than that obtained from the original TM bands. One of the main problems encountered was the failure of this technique to deal adequately with the influence of vegetation.

In a final experiment a further 'compound difference' technique was tested which the author has adapted from Moore et al., (1993) to enhance iron and clay, whilst subduing vegetation. The methodology adopted was as follows:

- 1A: (TM3-TM1) stretch + TM3 To emphasise the expression of iron oxides.
- 1B: (TM5-TM7) stretch + TM5 To emphasise the expression of clay minerals.
- 1C: (TM4-TM3) stretch + TM4 To emphasise the expression of vegetation.

These are then subtracted from one another to suppress spectral information due to vegetation:

- 2A: (1A - 1C)
- 2B: (1B - 1C)

In both of these final images there was a tendency for the brightest pixels in the original bands to manifest themselves as brightest pixels again. Consequently, agricultural fields and paths (classified as Class 7 in Fig. 54) were emphasised. Furthermore, the iron image was seen in retrospect to be somewhat restrictive since comparisons with the NDVI classified map (Fig. 54) showed that the only pixels highlighted were those that were devoid of vegetation. Although this final method did appear to be more effective at enhancing iron and clay whilst suppressing vegetation response, overall the results were deemed to be poor and generally unsatisfactory.

Band ratios have proven a successful and widely used technique for geological applications (Goetz et al., (1975); Abrams et al., (1977); Podwyssocki et al., (1983); Elvidge and Lyon (1985); Drury (1987); Drury and Hunt (1989); Tanaka and Segal (1990); Davidson et al., (1993); O'Connor (1993). Ratios were thus investigated in order to establish whether they could provide an improvement on the results of the differencing technique described above.

Many different ratio combinations have been reported in the research literature but, as previously stated, the majority of this work was performed in arid

environments where vegetation is not a major concern. Consequently, TM4 is often utilised in many ratios. To some extent the choice of ratio combinations has been driven by the method producing the best result for any given environment, often supported by field evaluation. However the three most commonly used and empirically tested are:

- i TM3 / TM1 for iron oxide mapping.
- ii TM4 / TM3 for vegetation mapping.
- iii TM5 / TM7 for clay mapping.

These ratios were also selected for use here, having previously tested a number of alternatives. Amongst these alternatives the TM5/TM4 ratio had been reported to highlight iron and was used successfully in the semi-arid environment of Cyprus by Davidson et al., (1993). When applied to the Mali environment it appeared to respond strongly to high altitude regions, probably reflecting low soil moisture levels and corresponding low vegetation cover. It was thus rejected on the grounds of uncertainty.

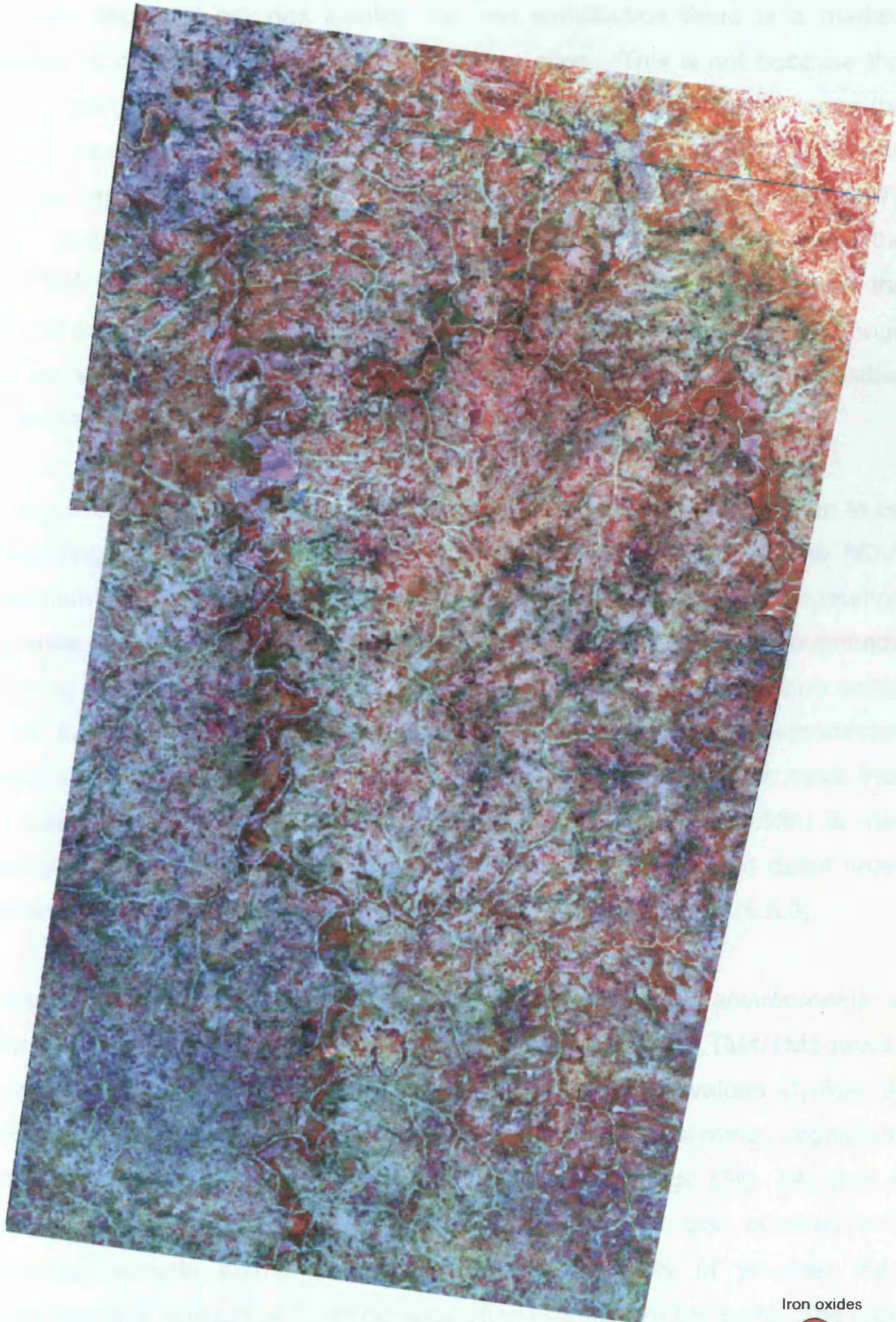
The results of combining the three ratios as a colour composite (shown in Fig. 57) are explained with the help of Table 44. This table illustrates some of the ratio contributions that are associated with particular composite image colours.

Table 44 Ratio contributions associated with composite colours.

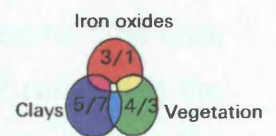
Image Colour	TM3/TM1 (red)	TM4/TM3 (green)	TM5/TM7 (blue)
Bright red - orange	VH – H	VL	VL - L
Purple	H – M	VL – L	H
Magenta	VH	H – M	VH
Light pink	VH	H	VH
Grey/pink	H	M - L	H
Cyan	H	VH	VH
White	VH	VH	VH
Yellow	VH	VH	H
Dull green / dark cyan	M	H	M

Where: VH = very high contribution; H = high; M = medium; L = low and VL = very low contribution.

Fig. 57 TM ratio image 3/1, 4/3, 5/7 (R, G, B).



This ratio image highlights the spectral similarity between clays and vegetation, and the problem of differentiating between the two.



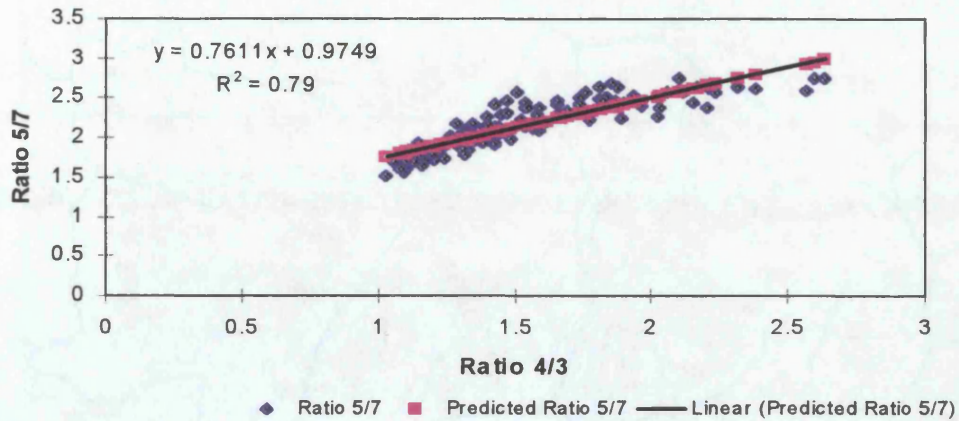
Although reds and oranges identify the iron contribution there is a marked absence of any clear strong blue representing clays. This is not because this signal does not exist, but rather because there is an intrinsic link between the spectral properties of clay and vegetation. This is especially so in TM5 and TM7, as reported by Elvidge and Lyon (1985), and Fraser and Green (1987). These spectral similarities are also evident, albeit to a lesser degree, in the TM3/TM1 ratio, as explained by Fraser (1991). The similarities between the spectral characteristics of clay, vegetation and iron can be emphasised through ratio correlations. When tested on a sample size in excess of 33,000, positive correlations of 0.7 for (5/7:4/3) and 0.3 for (3/1:4/3) were obtained.

Irrespective of the ratio combination, interference from vegetation is seen to be a recurring problem. A possible solution to this could be to use the NDVI vegetation map as a “mask” to eliminate all pixels with a strong vegetation response, along with pixels associated with fires and saturation overloads (implying class codes (1), (2) and (8)). However, an alternative solution exists in the form of a number of specially developed “de-vegetating” algorithms. These are perhaps a less crude approach than using a vegetation mask that has been unverified in the field. One such de-vegetating algorithm is that developed by Elvidge and Lyon (1985) and is discussed in some detail here. Another, based on a PCA transformation, is discussed in Section (5.5.3).

Elvidge and Lyon (1985) demonstrated that in semi-arid environments a common linear relationship exists between the TM5/TM7 and TM4/TM3 ratios. Provided the TM5/TM7 ratio contains no unusually high values (typical of alteration) the TM4/TM3 ratio can then be used to estimate vegetation contribution in the TM5/TM7 ratio. Using the NDVI image (Fig. 54) and a ‘feature-space’ crossplot of TM4/TM3 against TM5/TM7, one hundred and thirty-eight sample points were selected on the basis of whether they intersected with one of the (1) to (6) vegetation classes. At the same time care was taken not to sample in areas likely to show a high TM5/TM7 ratio, thus the geology overlay (Fig. 4) was used to ensure no samples were taken within the ‘Bj’ lithology. The two ratio values of each of the 138 samples were input to EXCEL and a linear regression was performed (Fig. 58).

Fig. 58

Vegetation contribution estimate.



This demonstrated an adequate 'goodness of fit' statistic ($R^2=0.79$), so the intercept and gradient terms were used to create the following equation:

$$\text{CVEG} = A + B(\text{TM4/TM3})$$

Where: CVEG = the TM5/TM7 background value; A = point of axial intercept. B = gradient

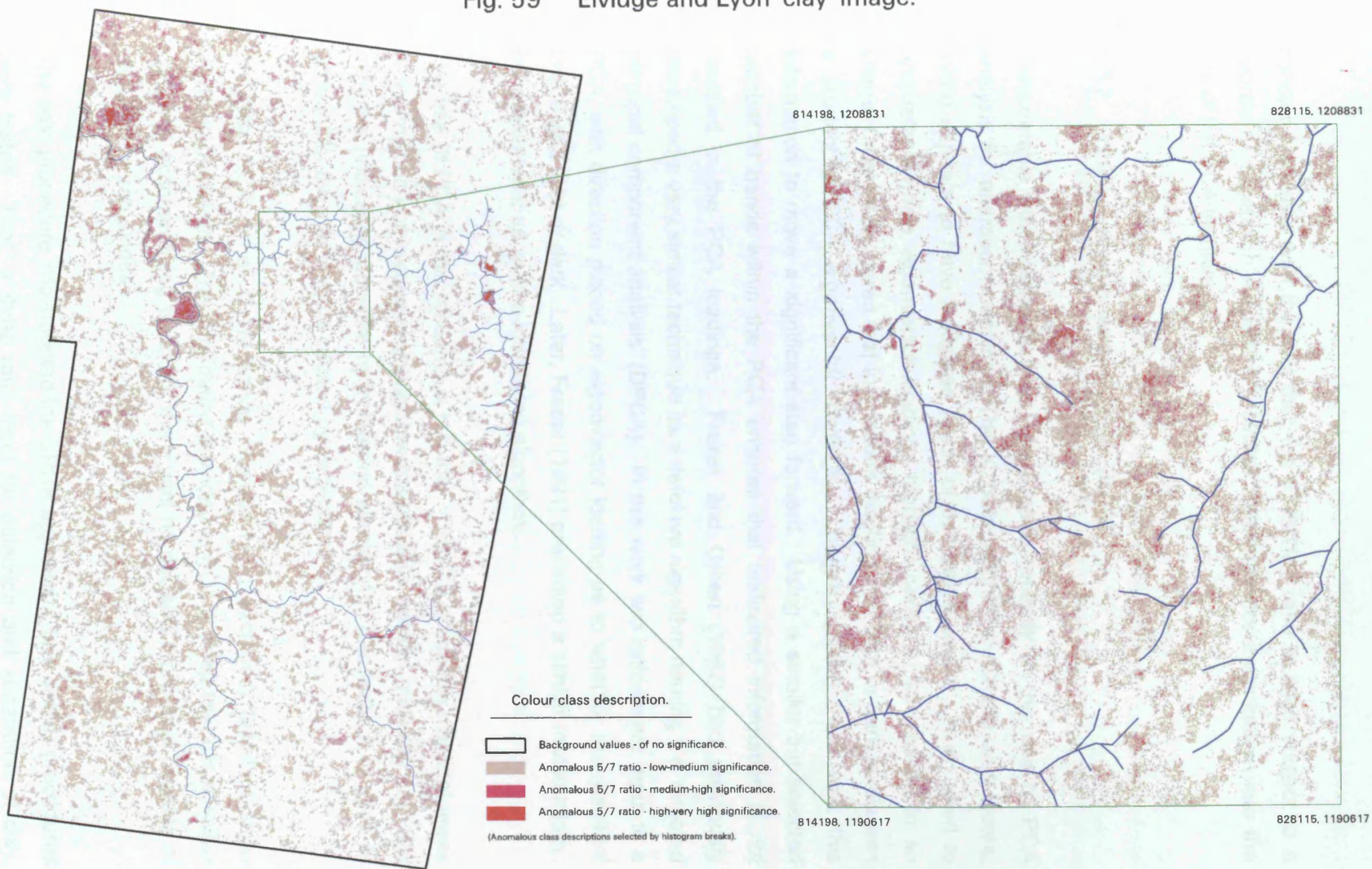
Using this it is possible to estimate anomalies in the TM5/TM7 ratio (CSUB) by subtracting the background image (CVEG) from the original raw TM5/TM7 image as follows:

$$\text{CSUB} = \text{CRAW} - \text{CVEG}$$

Image values of zero and less imply that neither rock nor soil is exposed, or that exposed rock and soil are of a background nature. To ensure the results did not include any superfluous information, such as active fires, line-pixel overloads, or very the lush vegetation of class (1), an overlay masking procedure was applied producing the result shown in Fig. 59.

As expected in a lateritic environment, this procedure highlighted many regions of interest. However the technique relies heavily on the intercept and gradient, which, without field verification, could create under or over estimations. This

Fig. 59 Elvidge and Lyon 'clay' image.



concern, together with the fact that the TM3/TM1 ratio is itself subject to a degree of vegetation response, provided motivation for investigation into the use of the PCA technique.

5.5.3 Principal components analysis (PCA).

Considerable advancements have been made recently in the use of PCA analysis for alteration mapping. The 'Crosta technique' (Crosta and Moore, 1989) appears to have instigated much of this development. In an effort to understand which eigenvector loadings highlight particular information in an image, Crosta deciphered that information displayed by light or dark pixels was a product of PCA eigenvector loadings. Loughlin (1991) then used this information to move a significant step forward. Using a smaller but selected number of bands within the PCA ensures that undesired information is not mapped in the PCA loadings. Fraser and Green (1987) had previously developed a very similar technique as a defoliant algorithm naming it a 'directed principal component analysis' (DPCA). In this work two ratios were input to a PCA, with direction placed on eigenvector loading as to whether the resultant image was light or dark. Later, Fraser (1991) presented a similar methodology, but presented it as an iron-identifying algorithm.

The use of PCA in this research is two fold. Firstly it is used to highlight areas of anomalous iron oxides (pointing towards possible gossan material) and clay minerals (indicating possible hydrothermal alteration). Secondly, it is used to account for the interference caused by vegetation.

An initial PCA on all 6 TM bands (thermal band excluded) failed to show anything decisively. The information provided in PC3 pointed towards possible clay with accompanying fires, but there was no decisive PC output capable of highlighting iron oxides.

The next procedure implemented the DPCA approach. Two similar procedures were tested: First, a three ratio input for detection and separation of clay,

vegetation and iron (TM5/TM7, TM4/TM3, TM3/TM1), and secondly, the Fraser “defoliant” approach with separate ratios for vegetation and clay (TM4/TM3, TM5/TM7), and vegetation and iron (TM4/TM3, TM3/TM1). Results (Table 45 and 46) indicated little difference between these two methods, except the Fraser approach does not require image negation due to the positioning of the positive loading within the DPC2. Also, by using only two input ratios rather than three, the eigenvalues, indicative of total variance, are slightly higher and image quality is therefore likely to be better.

**Table 45 Directed Principal Component Analysis
Three ratio input.**

DPCA	Eigen matrix			
	TM5/TM7	TM4/TM3	TM3/TM1	
DPC1	0.4526	0.8228	0.3438	-Albedo and vegetation.
DPC2	0.0909	0.3410	-0.9357	-Iron displayed as dark pixels.
DPC3	-0.8871	0.4547	0.0795	-Clay displayed as dark pixels

Eigenvalues

DPC1	160.72	(73%)
DPC2	43.50	(20%)
DPC3	15.56	(7%)

Table 46 Directed Principal Component Analysis-(Fraser).

DPCA	Eigen matrixes.			Eigen matrixes.		
	TM4/TM3	TM3/TM		TM4/TM3	TM5/TM7	
DPC1	0.9170	0.3990	-Albedo	0.8753	0.4837	-Albedo
DPC2	-0.3990	0.9170	-Vegetation dark iron ligh	-0.4837	0.8753	-Vegetation dark clay light

Eigenvalues

DPC1	131.07	(75%)
DPC2	43.19	(25%)

Eigenvalues

DPC1	147.50	(89%)
DPC2	18.04	(11%)

The Fraser results are shown as greyscale images in Fig’s. 60.and 61.

Finally the Loughlin (1991) ‘Crosta technique’ was tested. In this method iron and clays are mapped through the use of four selected bands. Iron is more likely to be mapped if only one SWIR band is included in the PCA, thereby

Fig. 60 Fraser's DPCA 'iron' image.

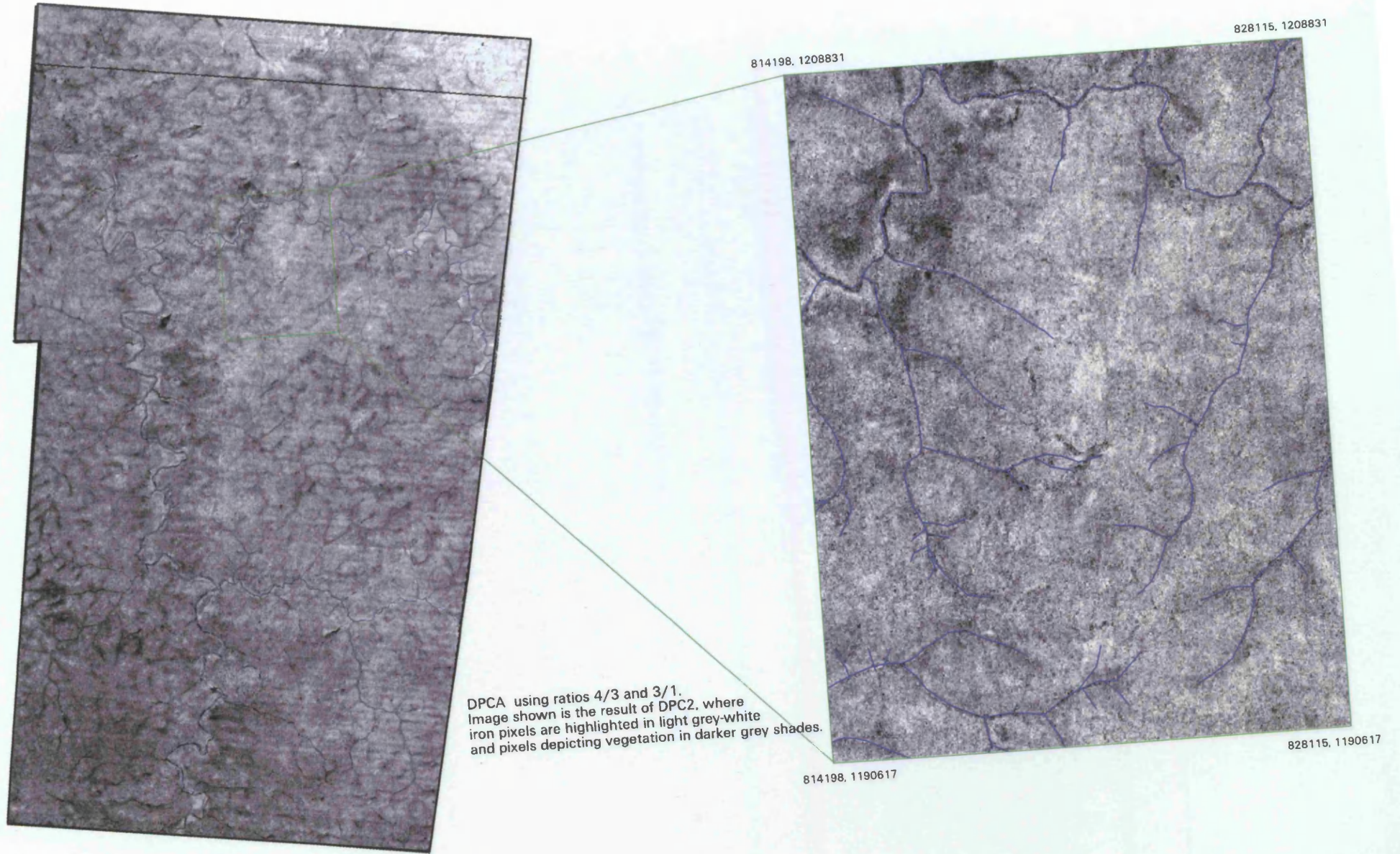
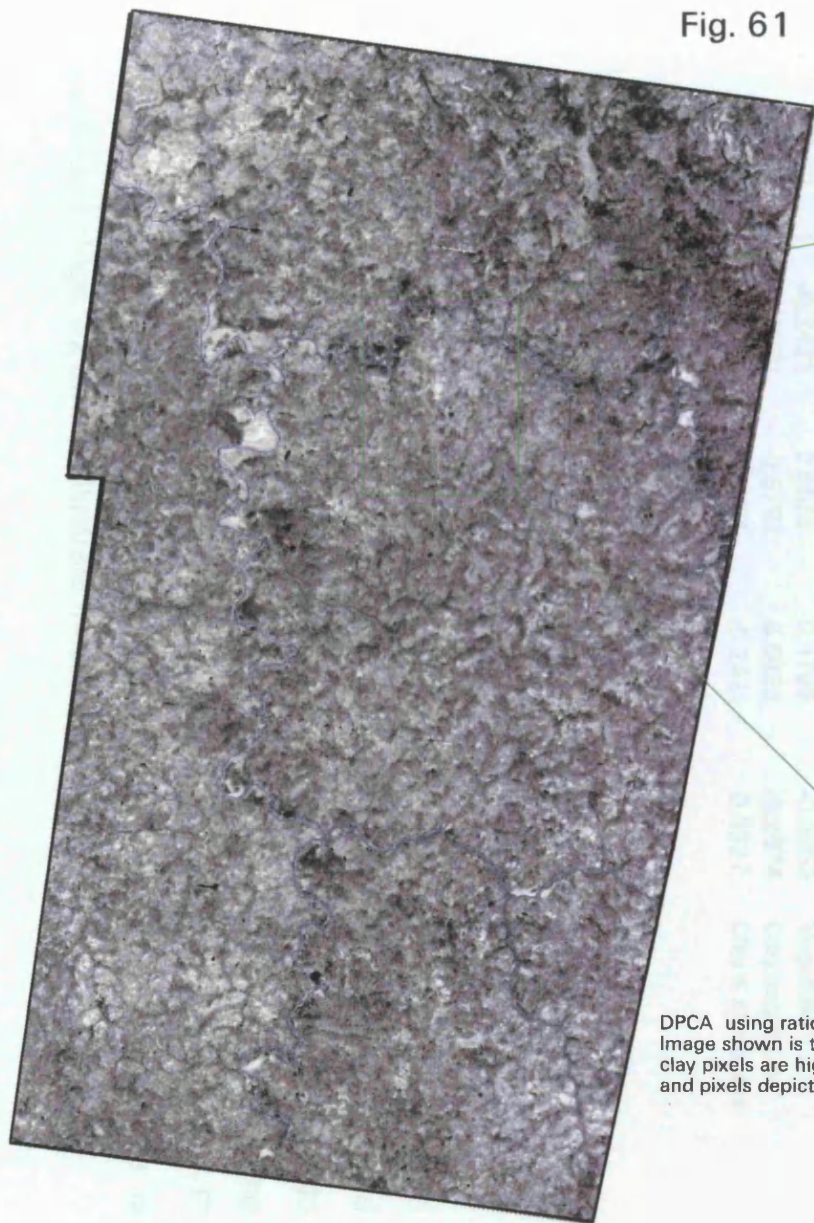


Fig. 61 Fraser's DPCA 'clay' image.



814198, 1208831

828115, 1208831



DPCA using ratios 4/3 and 5/7.
Image shown is the result of DPC2, where
clay pixels are highlighted in light grey-white
and pixels depicting vegetation in darker grey shades.

814198, 1190617

828115, 1190617

omitting the detection of hydroxyl-bearing minerals. Whereas including only one visible band in the mapping of clays precludes the mapping of iron oxides. Consequently TM bands 1, 3, 4 and 5 were used to map iron, and bands 1, 4, 5 and 7 were used to map clay. Tables 47 and 48 show the results.

Table 47 Iron-oxide mapping 'F- image'.

PCA – iron	B1	B3	B4	B5	
PC1	0.2145	0.3371	0.3575	0.8441	Albedo
PC2	-0.4639	-0.3814	0.7967	-0.0672	Vegetation
PC3	0.5473	0.4403	0.4855	-0.5205	Composite
PC4	0.6627	-0.7396	0.0411	0.1096	Iron dark

Eigenvalues

PC1	345.97	(90.7%)
PC2	21.85	(5.7%)
PC3	10.82	(2.8%)
PC4	2.71	(0.7%)

Table 48 Hydroxyl mapping 'H - image'.

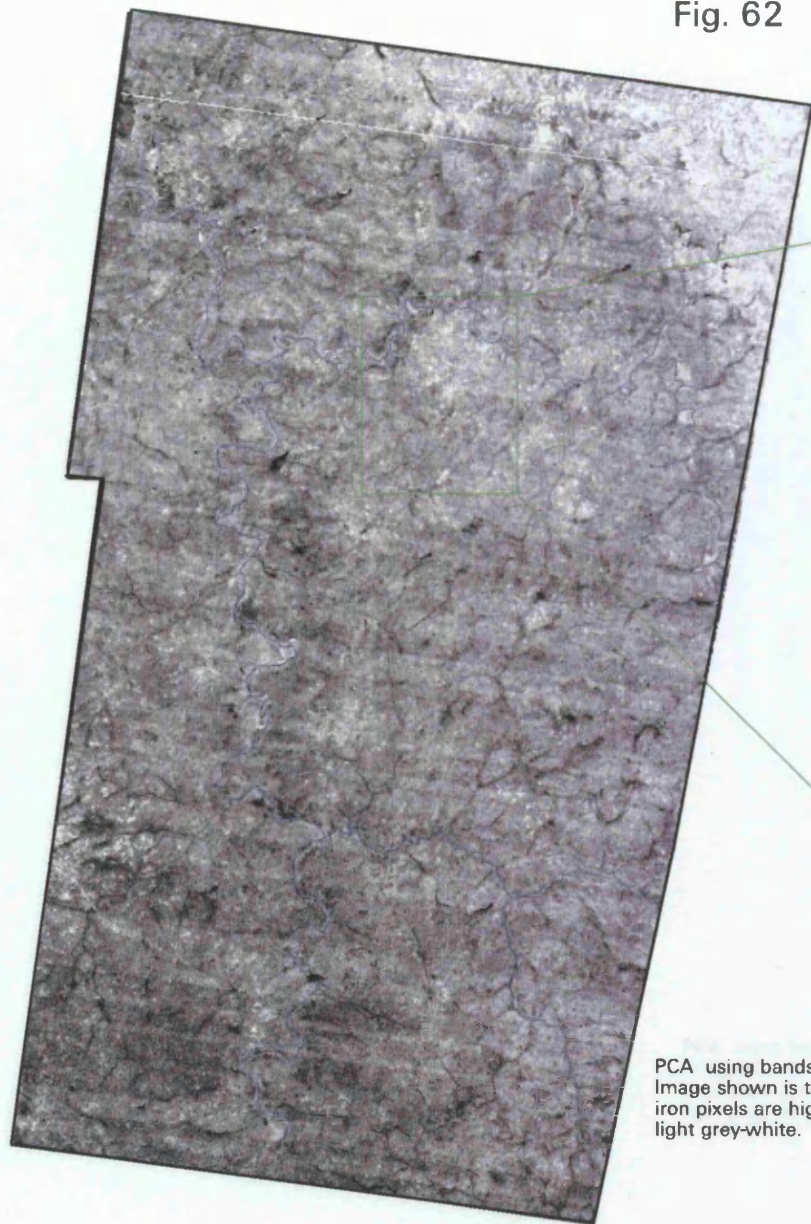
PCA - clay	B1	B4	B5	B7	
PC1	0.2113	0.3273	0.8115	0.4356	Albedo
PC2	-0.2431	0.6538	0.1729	-0.6953	Vegetation
PC3	-0.6070	-0.5792	0.5030	-0.2074	Clay bright
PC4	-0.7265	0.3604	-0.2421	0.5327	Clay & composite

Eigenvalues

PC1	373.28	(87%)
PC2	39.59	(9.3%)
PC3	9.13	(2.1%)
PC4	5.08	(1.2%)

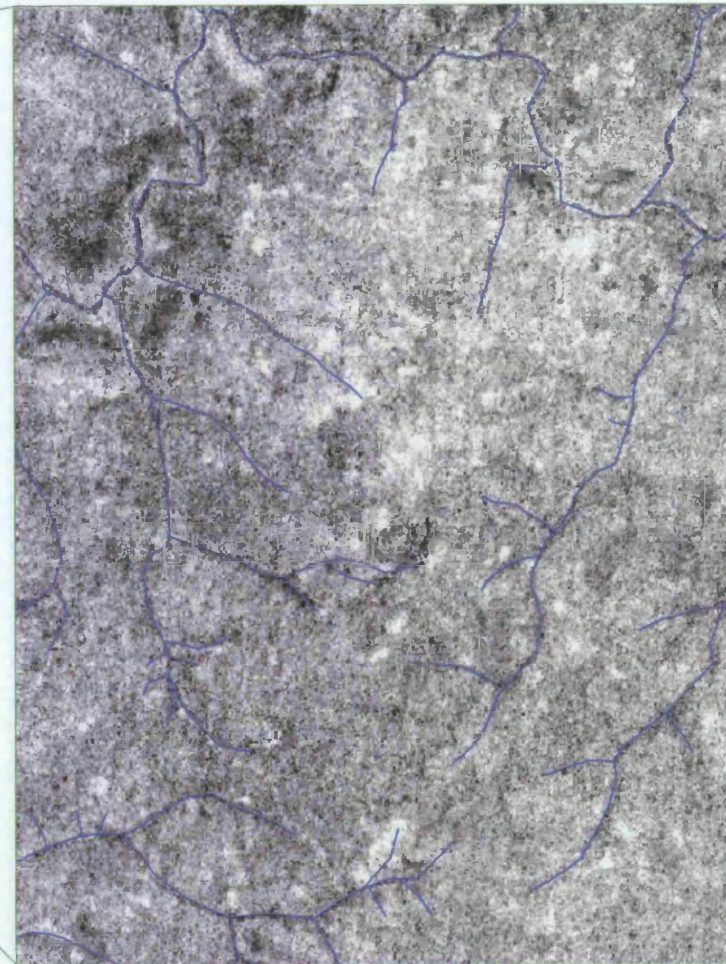
The PC most likely to map iron is PC4, since this has the strongest loading with opposite sign, though negatation is required, whereas the strongest loading and opposite sign of PC3 suggests it is mapping clay. In the latter case, PC4 could also map clays if negated, but this was not selected due to its very low scene variance (eigenvalue) and poor signal to noise ratio. Fortunately, in both the 'F' and 'H' images vegetation is mapped as dark pixels so its interference is minimised. Figs. 62 and 63 illustrate these results.

Fig. 62 Costa 'F' image (iron).



814198, 1208831

828115, 1208831

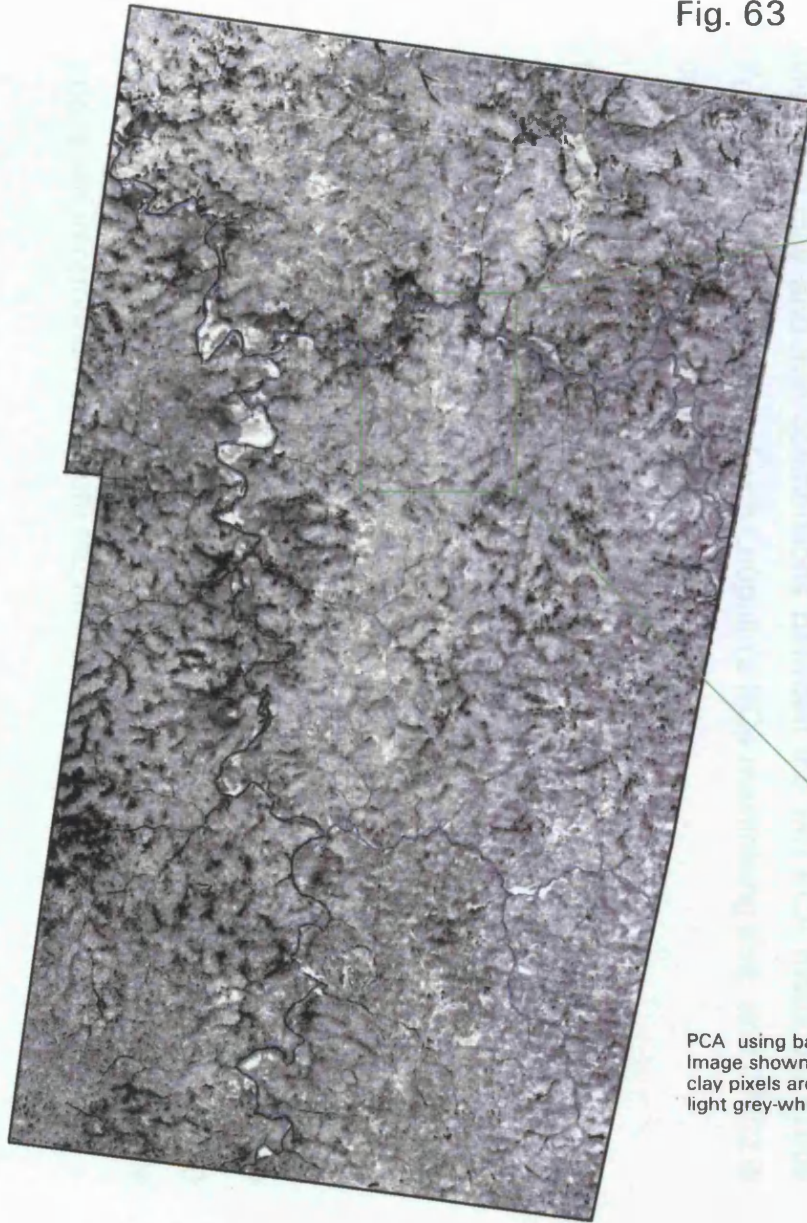


814198, 1190617

828115, 1190617

PCA using bands 1, 3, 4 and 5.
Image shown is the result of PC4 negated, where
iron pixels are highlighted in shades of
light grey-white.

Fig. 63 Costa 'H' image (clay).



814198, 1208831

828115, 1208831



814198, 1190617

828115, 1190617

PCA using bands 1, 4, 5 and 7.
Image shown is the result of PC3, where
clay pixels are highlighted in shades of
light grey-white.

In conclusion, comparisons between Elvidge's method and, for example, that of Fraser's (Fig.59 and 61) indicate a very high level of coincidence between the brightest image pixels, although the interference from vegetation in the TM5/TM7 ratio is dealt with by different approaches. However, the issue of concern with the former approach lies in the absence of field verified vegetation training sets and the requirement and difficulty of not including any altered rock/soil within the regression samples. Consequently, PCA methods were selected as the most appropriate technique for suppressing vegetation response whilst simultaneously highlighting pixels most likely to possess strong iron and clay.

5.5.4 Combining and mapping coincidences.

In both the previously tested Fraser and Loughlin techniques, it is presumed that areas of interest are represented by bright pixels. For the purpose of interpretation Loughlin (1991) adds the 'F' and 'H' images to produce a 3-band colour composite with F, F+H, H displayed on the red, green and blue guns respectively. Here a similar process is performed so as to maximise the individual clay and iron contributions between the two PCA methods. Thus Fraser's DPC2 is combined with Loughlin's PC4 maximising iron, and DPC2 is combined with PC3 to maximise clay.

For these data to be input as layers into the GIS the brightest pixels from the images must be categorised and coded. Four classes were chosen representing: "very high", "high", "medium" and "moderate-to-low" iron (or clay) content. Pixels falling outside of these classes were deemed insignificant and coded to zero. As a final measure the two images were then corrected for any additional spurious effects caused by 'active fires' and their pixel overloads, for line dropouts, and for the remote possibility of any inclusion from the lush vegetation of class (1). This was achieved by using two image masks ('active-fires' and NDVI vegetation) to eliminate this undesired information from both the iron and clay images.

The results shown in Fig. 64 and 65, indicate likely areas of significant iron and clay concentrations. In the iron image there is an overall finer dispersion to the pixels than seen in the clay image. However as shown in the enlargement section, areas of “medium” and above significance display a high level of spatial correlation to the Birimian volcano-sedimentary zone, where mineralisation is known to occur. In fact the bifurcation (i.e. the point at which the volcano-sedimentary sequence divides into two branches) is clearly distinguishable, especially within the iron image. There is also spatial correlation of iron to many areas of high ground, reflecting laterite surfaces. Overall these images show many areas that have significant iron and clay, which perhaps is not surprising considering the weathering of a laterite environment. Therefore their true importance will be better understood once they are assessed for coincidences with the other data sets held in the GIS and when their position within the landscape is considered (Chapter 6).

It is possible to apply a form of filtering to these two results to look for areas of coincidence. The reasoning for this is that a mineralised location could well be identified by both iron (the gossan) and clay (sericite alteration) as described at Syama. Therefore, mapping the spatial coincidence of the two could be of further importance and a GIS procedure was undertaken to map the coincidence level between these two images.

This could have been achieved with either an addition or multiplication operator; all that is required are unique non-duplicating codes for each of the five categories. In this particular case the largest code value is given to class (5), where the level of significance is at its highest. The example below illustrates the multiplier method used.

Iron map		clay map		combined coincidences			
10	10	6	8	100	80	36	64
2	8	6	6	4	48	12	36
0	2	0	2	0	4	0	0
0	0	8	2	0	0	16	16

Thus on either map:
 Very high = 10; High = 8; Medium = 6; Moderate/low = 2 and no significance = 0

Fig. 64 Combined 'iron' images.

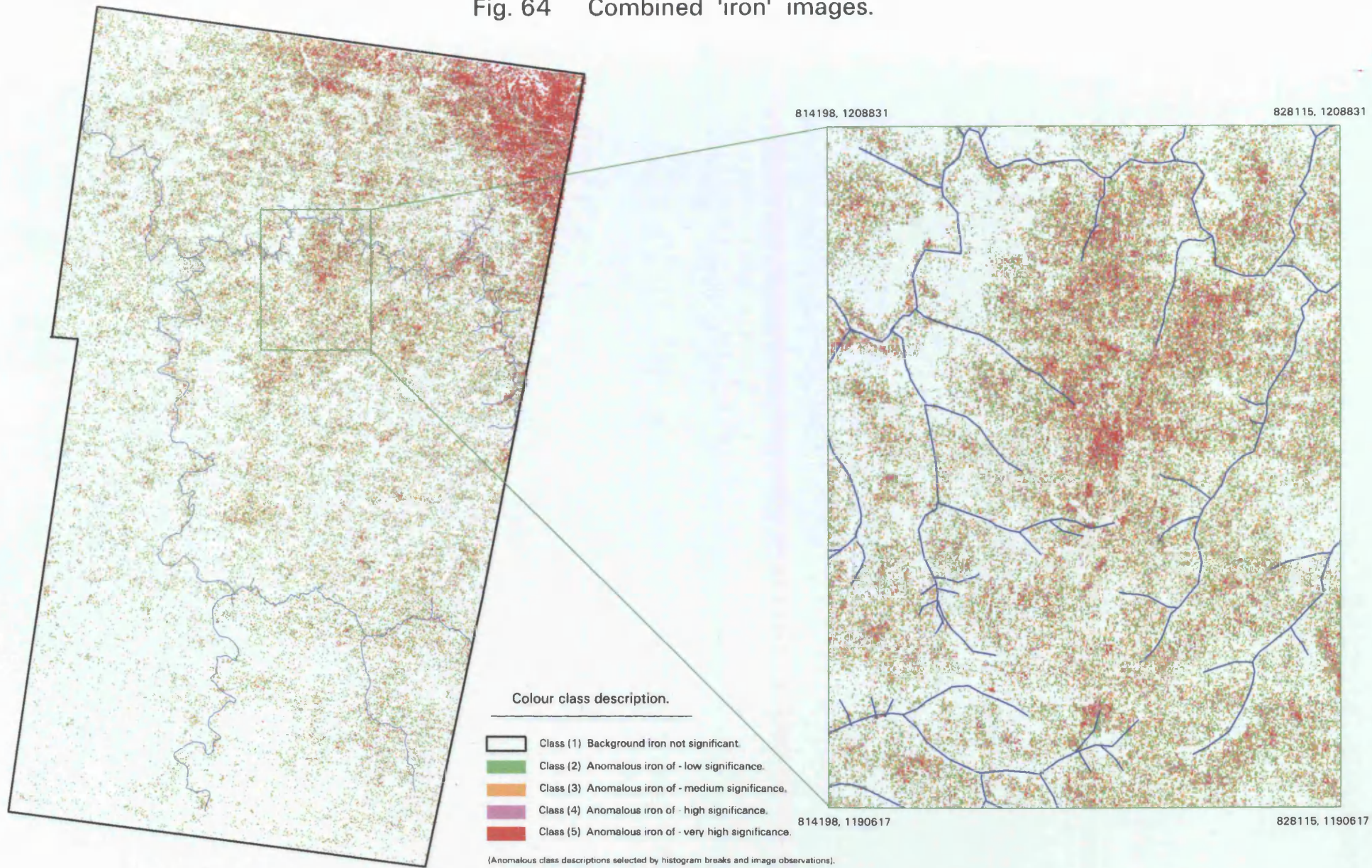
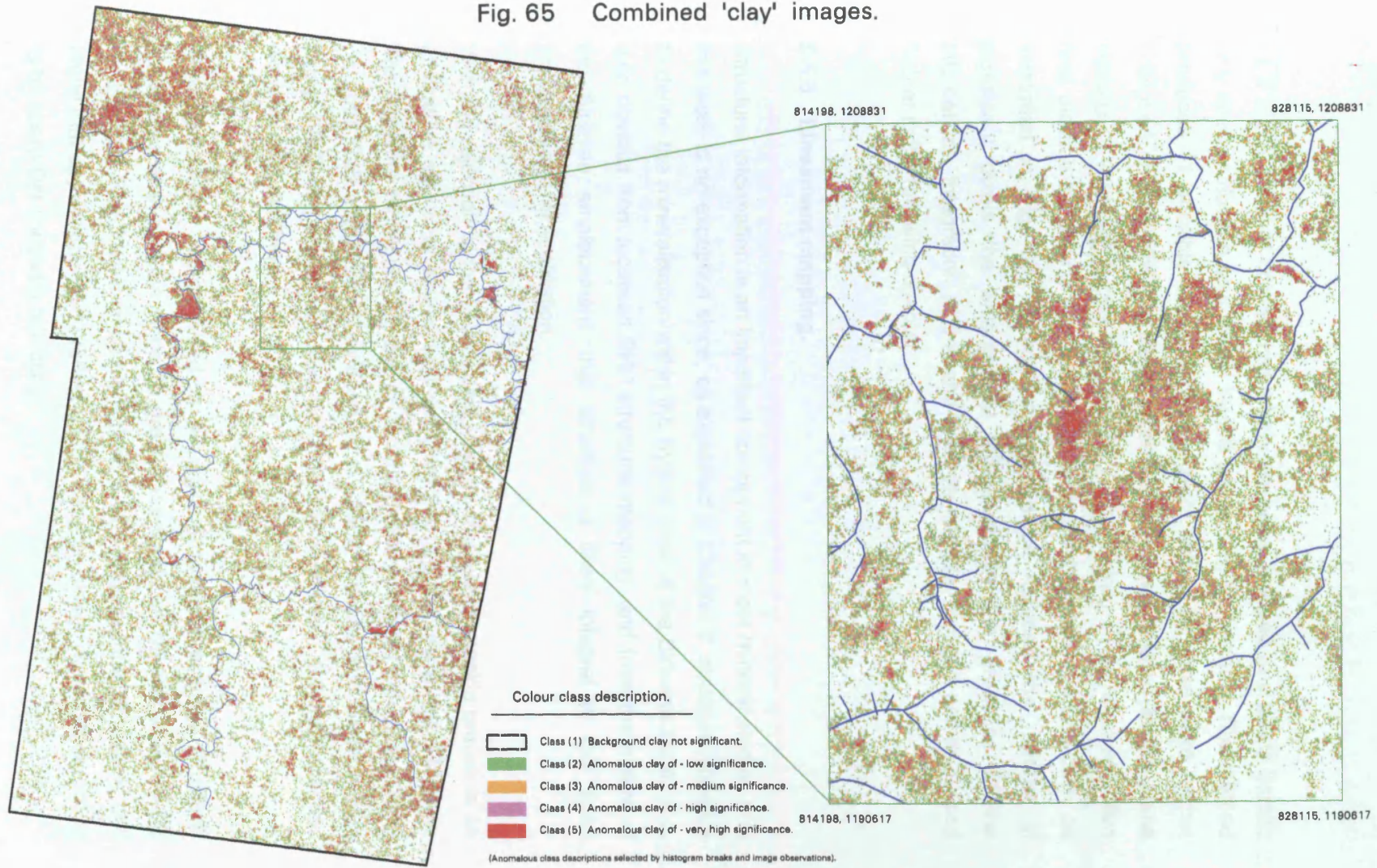


Fig. 65 Combined 'clay' images.



As it is the levels of coincidence which are being mapped any pixels having only one contribution source are, by this procedure, set to zero. This method produces 11 possible codes (including zero), which for ease were further collapsed so that similarly derived codes were amalgamated to the same class (e.g. very high x very high and very high x high). This resulted in five final classes describing the level of coincidence between iron and clay, as illustrated in Fig. 66. Although this technique reduced the number of significant pixels the enlargement still illustrates the presence of the bifurcation. Integration of this and the iron and clay images are discussed further in the following chapter.

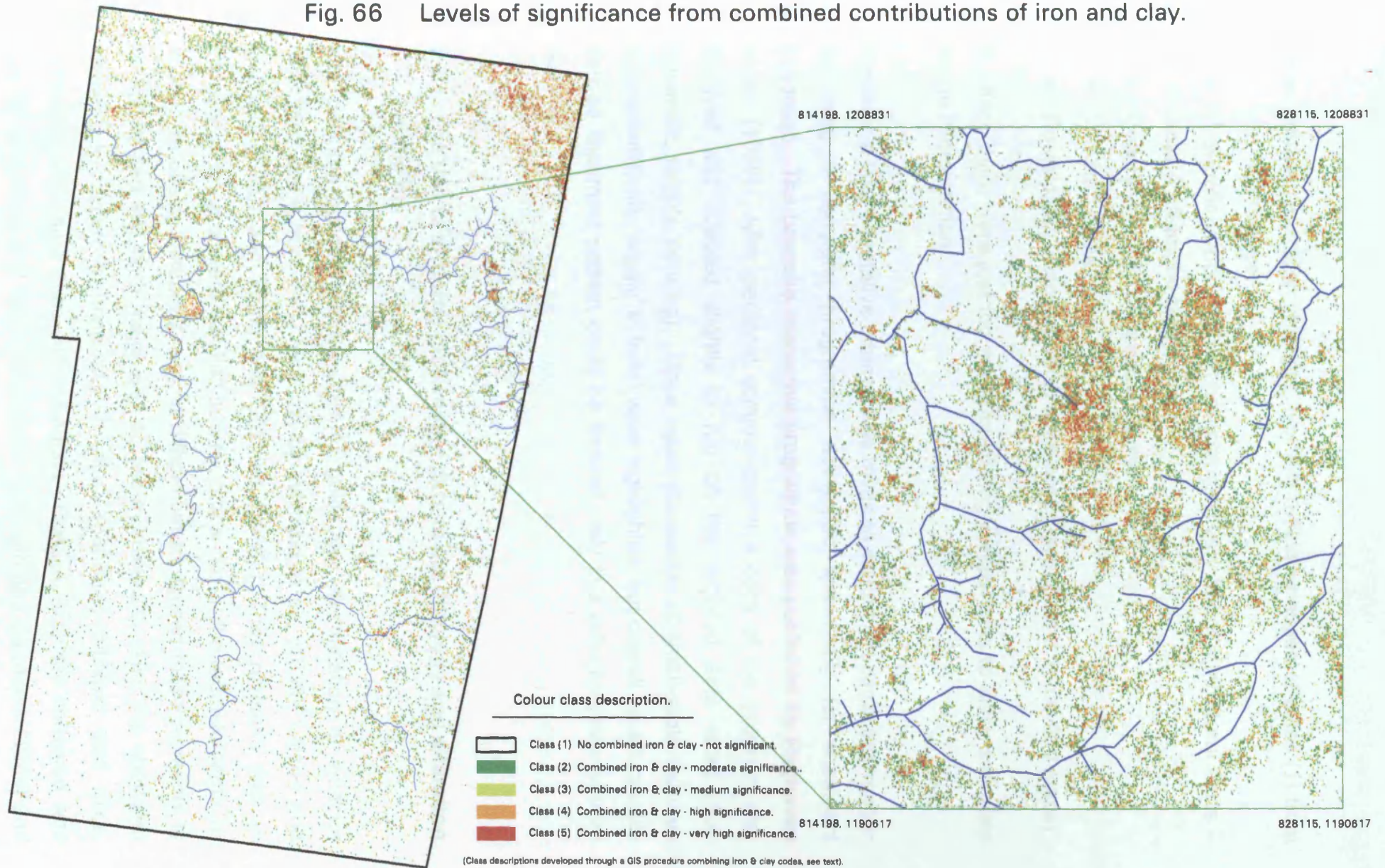
5.5.5 Lineament mapping.

Structural information is an important component in most mineral studies and this work is no exception since, as explained in Chapter 2, structure appears to define the mineralisation within the Syama area of the Birimian zone. It is also obvious from localised BHP structural mapping, and from the nature of the Birimian emplacement, that structure is likely integral to this zone irrespective of mineralisation.

With the rejection of the ERS-1 data, due to unsolvable speckle problems an alternative structural source was explored through the use of the TM data. The literature highlights the use of various directional edge-enhancing filters on both TM5 and PCA1 (Davidson et al., 1993; Tanaka and Segal, 1990; Drury 1987) as potential sources for structural extraction. Both approaches were investigated here.

Although images were filtered in all eight principal directions, structural knowledge of the region placed a greater emphasis on NE-SW and NW-SE lineaments. Resultant images highlighted a very large number of 'edges' and many that appeared likely to reflect a fault were, on closer interrogation, found to be sharp DN contrasts reflecting:

Fig. 66 Levels of significance from combined contributions of iron and clay.



- Abrupt vegetation changes, typically reflecting edges of class (1) from the NDVI image.
- Well-defined boundaries characterising very bright agricultural fields – class (7) from the NDVI image.
- Gallery vegetation of stream courses.
- The path of rivers
- Route/paths (many of which were not present on the 1:200,000 maps).

In effect, there were just too many interfering components to allow adequate image interpretation.

However a final alternative attempt was made to extract structural information by using a computer programme developed specifically for lineament extraction. The bespoke interactive programme was published by Raghavan et al., (1995). After personal communication a copy of the program was received and adapted slightly to run on the required data sizes (See Appendix, remote sensing). Once again thousands of small-scale features (characteristically 'wiggly' in form) were highlighted, but overall no structurally derived lineament pattern could be derived, only that reflecting river-stream courses.

5.6 The use of airborne radiometric data to aid lithology and alteration mapping.

The principal building blocks used to guide the identification of igneous lithologies came from early research by Whitfield et al., (1959); Larsen and Gottfried (1960) and Tilling and Gottfried (1969). They revealed that an increase in silica content resulted in a reciprocal rise in the radioelements Th and U. In effect, increased magma differentiation caused these elements to be substituted into both major and accessory minerals. Also the abundant element K, occurring principally in alkali (potassic) feldspar and mica, increased with rising silica concentrations. Consequently the converse was true for ultra-basic and basic lithologies. Galbraith and Saunders (1983) and

Ford and Carson (1986) confirmed and explored these findings further studying the relationship between average radioelement content of igneous and sedimentary rocks and the use of ratios. Unfortunately no clear distinction could be made with sedimentary rocks, other than the radioelements were more likely to represent the lithology from which they were originally derived.

Often a characteristic accompaniment of base metal and gold mineralisation is K enrichment / alteration. Darnley and Ford (1989) recite a number of interesting case histories where high K (and low Th) readings were associated with mineralisation. As a consequence potassium emissions have a dual purpose in identifying lithology and localities of alteration attributed to potential mineralisation.

However, airborne gamma-ray spectrometry is a remote surficial mapping technique and as such its effectiveness can be limited by transported soil, alluvium and even thick vegetation. Nevertheless, in areas of thick residual soil the gamma-ray response is able to provide information about the sub-surface geo-chemistry due to the in-situ nature of the weathering. In fact Darnley and Ford (1989) report its use within virtually all climatic regimes.

5.6.1 Selecting the appropriate methodology.

Techniques used to illustrate and explore radiometric data have ranged from:

- i) Single channel plots (with values coloured or contoured).
- ii) Three channel plots (ternary image).
- iii) Ratio plots.
- iv) Unsupervised classification (statistical analysis using a migrating means cluster).

(Duncan and Crabb, 1981; Darnley and Ford, 1989; Graham and Bonham-Carter, 1993).

As there appears to be no clear recommended method, these differing techniques are probably a reflection of end user requirements allied with advances in technology.

There were three principal aims for using radiometric data in this research;

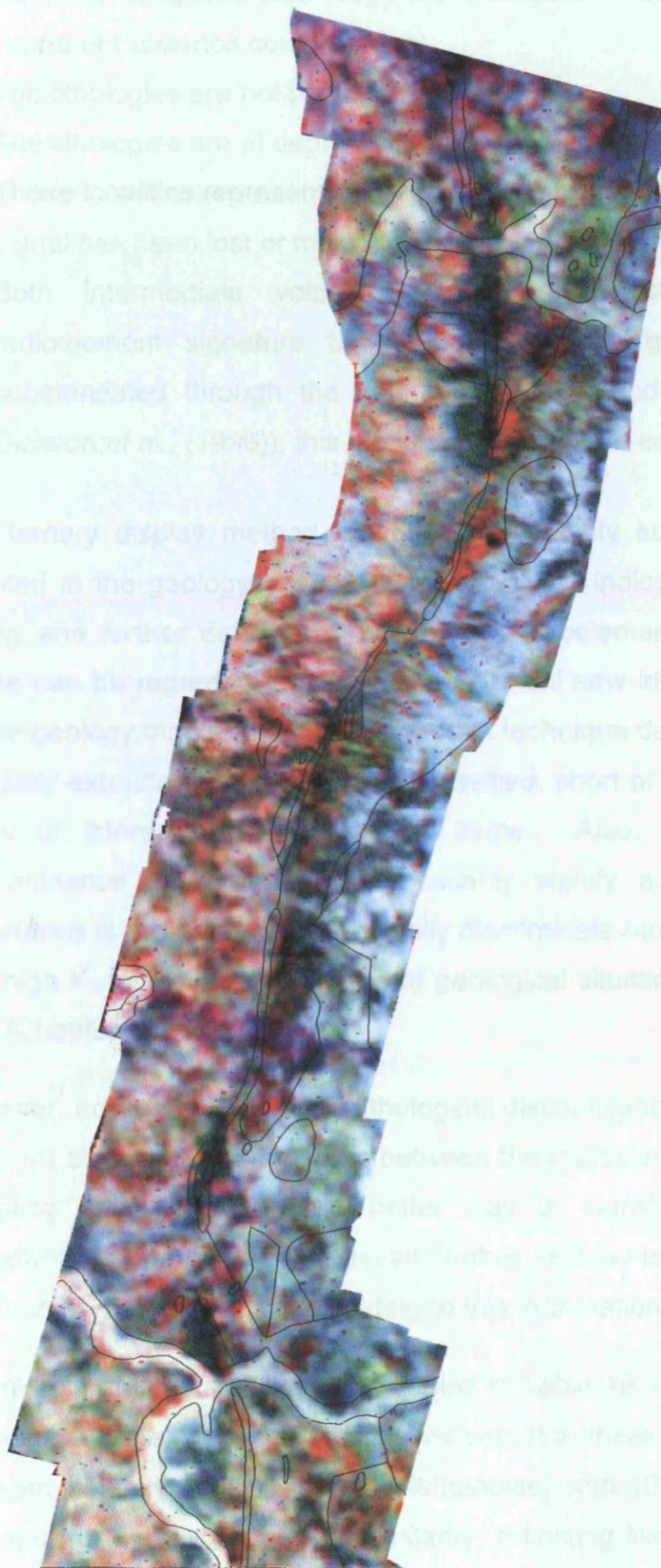
- 1) To establish if it is possible to identify different lithologies by their radioelement response (i.e. Basic – acid igneous, sedimentary).
- 2) Identify any further characteristic signatures, which could relate to possible undiscovered geology (especially basic igneous).
- 3) To try and identify any areas pertaining to K-alteration (especially within basic lithologies).

Techniques (ii) – (iv) from the list above were investigated to establish if each of the specific aims could be achieved.

Upon histogram normalisation a ternary image was produced to illustrate the distribution of the three radioelements within the survey region (Fig. 67). Observations indicate that the Birimian volcano-sedimentary unit (Bj) is identifiable by its low response in all three radioelements, representing a dark elongate trace. The lithology to the west of the Birimian volcano-sedimentary unit (identified on Fig. 4 as 'Bs') indicates a higher contribution from K than Th and U. This tends to confirm its sedimentary nature with possibly the arkose component superior to the greywacke. The region to the east identified predominantly as greywacke (Tgr), is distinguished from (Bs) by elevated Th and U and lower K. The two regions on the image indicating high responses from all three radioelements are; transported and deposited material from within the Bagoé River (Al), a likely response from a catchment draining predominantly sedimentary and granitic lithologies, and the edge of the granite mass (Y/Yb) in the east. In conclusion, the statistical character of each lithology is not dissimilar to those reported in previously cited works, i.e. generally low radiometric values for basic igneous contrasted with consistently high values for granite regions.

Unfortunately it is not possible to distinguish all the geology by the radioelements, as there appear to be a number of lithologies that show no

Fig. 67 Ternary radiometric image (K, U, Th).



Colour combinations.

Potassium (K) = Red.
Uranium (U) = Green.
Thorium (Th) = Blue.

Geology overlay taken from 1:200,000 map

characteristic signature. The small intrusions of diorite and andesite (Eza), (Bx) and the conglomerates (Tcg) are examples. Possible explanations for their apparent absence could involve;

- (a) The lithologies are not present.
- (b) The lithologies are at depth and therefore original signals are too weak.
- (c) These localities represent depositional environments, where the original signal has been lost or mixed up.
- (d) Both intermediate volcanics and conglomerates have a similar radioelement signature to the surrounding (Tgr) lithology (a claim substantiated through the work of Galbraith and Saunder (1983) and Dickson et al., (1996)), this alone would not allow easy differentiation.

The ternary display method does help to identify some of the lithologies denoted in the geology overlay (Fig. 4). It also indicates areas where K is strong and further dark areas where the radioelement responses are low. These can be regarded tentatively as potential new information, unidentified on the geology map (Fig.4). However, this technique does not allow results to be easily extracted and categorised/classified, short of drawing polygons (i.e. areas of interest) around selected items. Also, areas with a strong predominance of K may not necessarily signify alteration. Of greater importance is the ability to lithologically discriminate basic-type volcanic rocks with high K, for it is that very type of geological situation reported as hosting gold (Chapter 2, Section 2.6.2).

However, achieving success in lithological discrimination requires there to be sufficient statistical differentiation between the radioelements. Therefore sub-sampling each lithology is a better way to statistically understand the radioelement character, and as all further techniques are mathematically based their results will be responding to this information.

The results of sub-sampling are revealed in Table 49, whilst Figs 68 – 70 are a graphical representation. Results indicate that there is a degree of overlap between virtually all the sampled lithologies, with (Bs) and (Tgr) showing perhaps the greatest statistical similarity, reflecting likeness of geology, and (Bj) the least. The level of commonality between the sub-samples also varies

Fig. 68 Statistical spatial plot (K /Th)
for sub-sampled lithologies of Table 49.

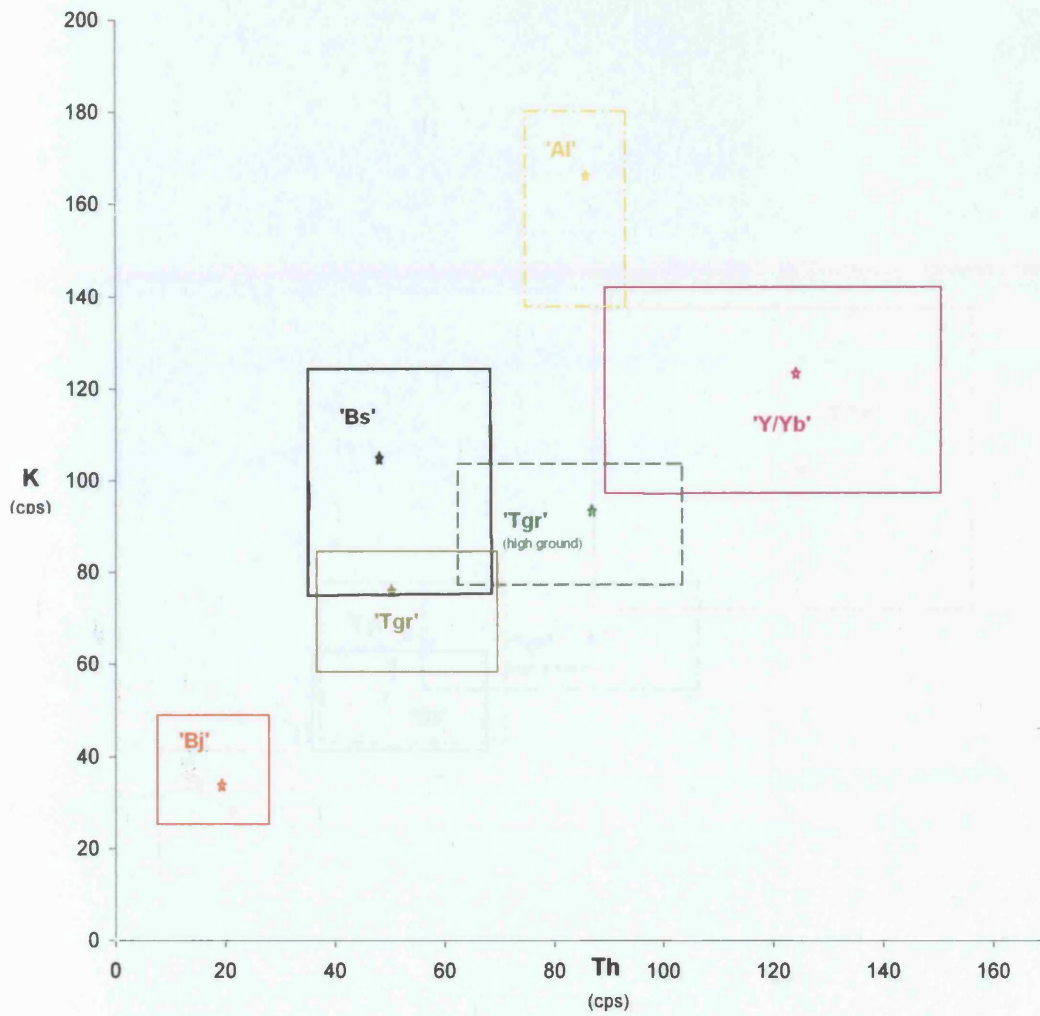
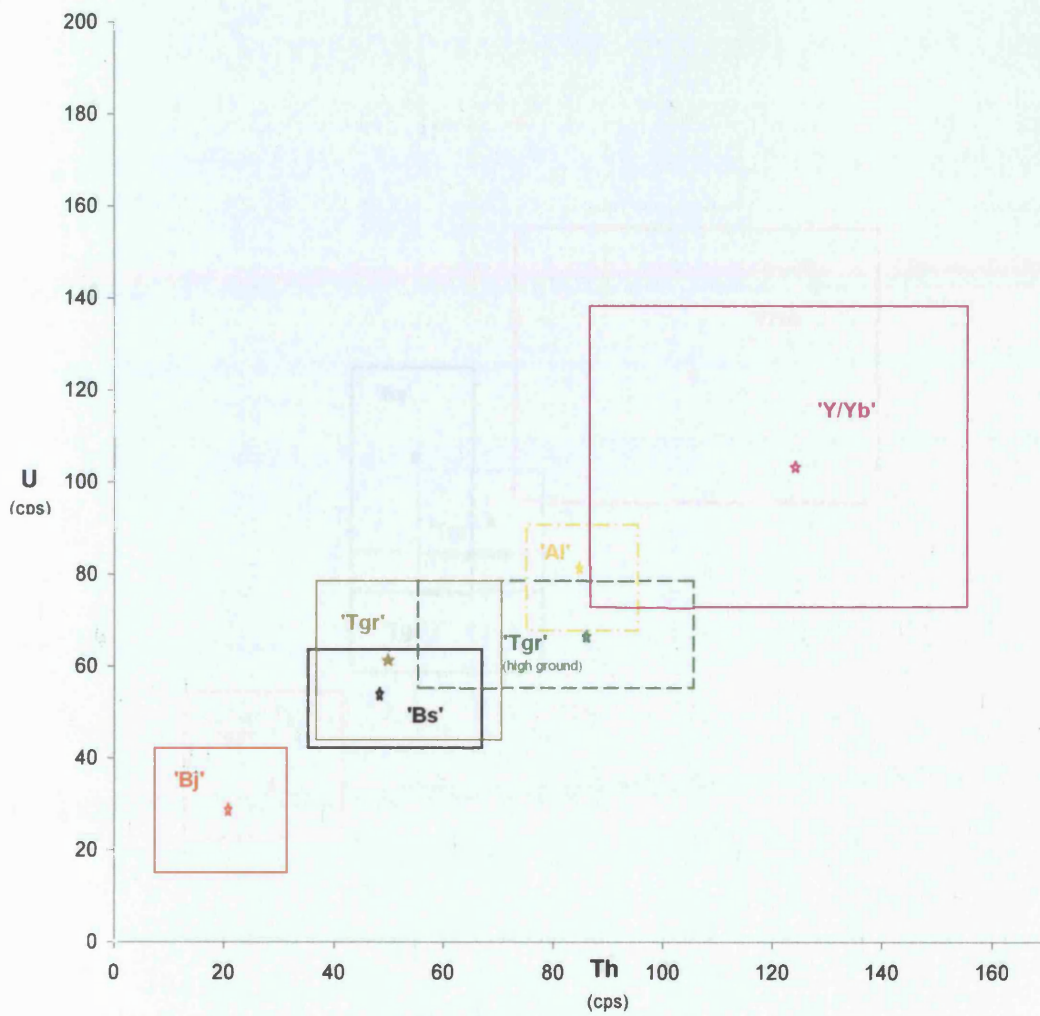
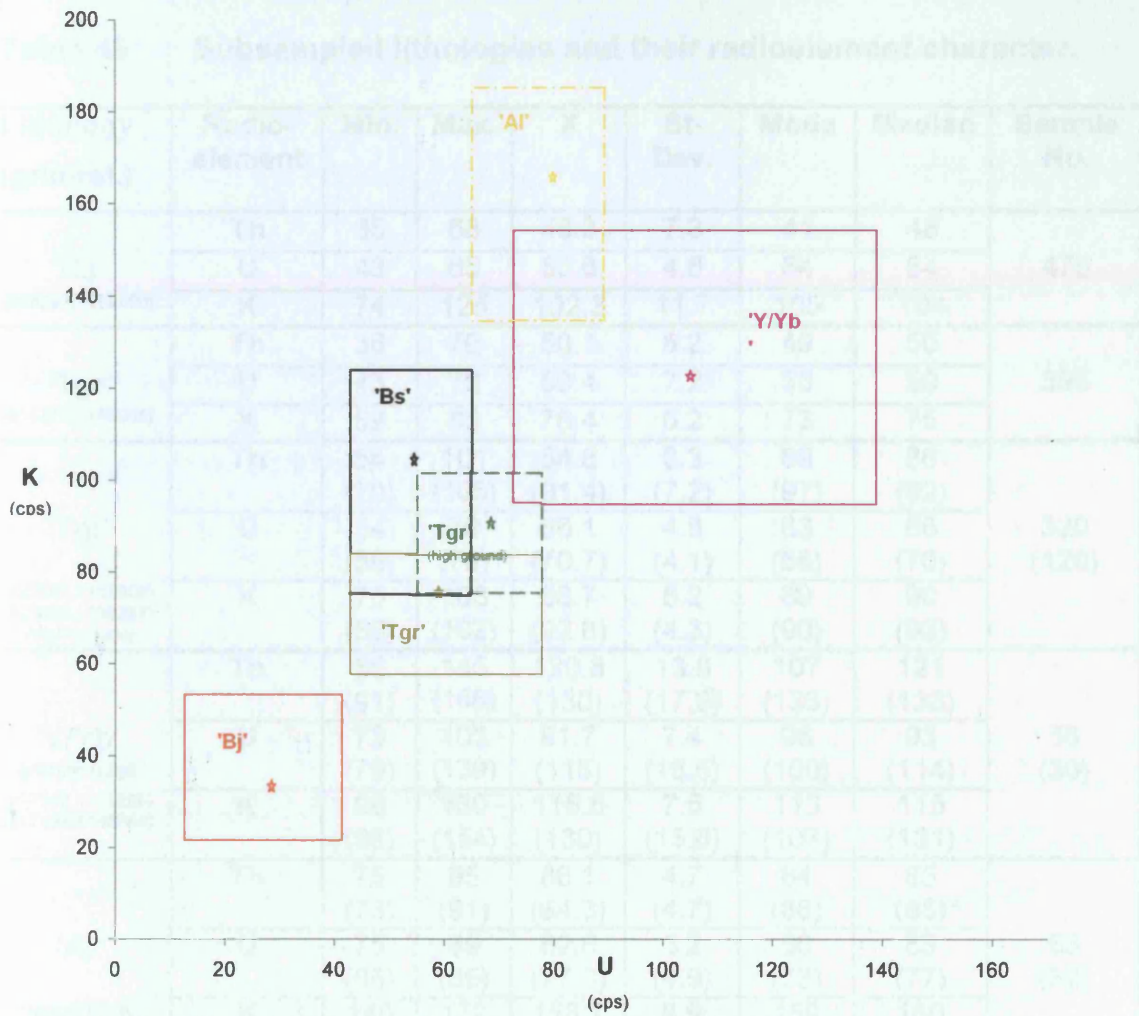


Fig. 69 **Statistical spatial plot (U/Th)**
for sub-sampled lithologies of Table 49.



Stars indicate sample mean. Where there are two samples the lowest & highest values are plotted..

Fig. 70 Statistical spatial plot (K/U) for sub-sampled lithologies of Table 49.



depending upon the radioelement combination. The highest overlap is seen with Th and U, the least is observed with Th and K. These findings run parallel with those of the element global correlation coefficients (Section 4.7, Chapter 4), which reports Th and K as the lowest correlation. This suggests this combination is the most dissimilar statistically and therefore in this case the most informative geologically. The implications of such findings are that the data (or environment) does not lend itself to precise lithological discrimination, though this should not discourage its use.

Table 49 Subsampled lithologies and their radioelement character.

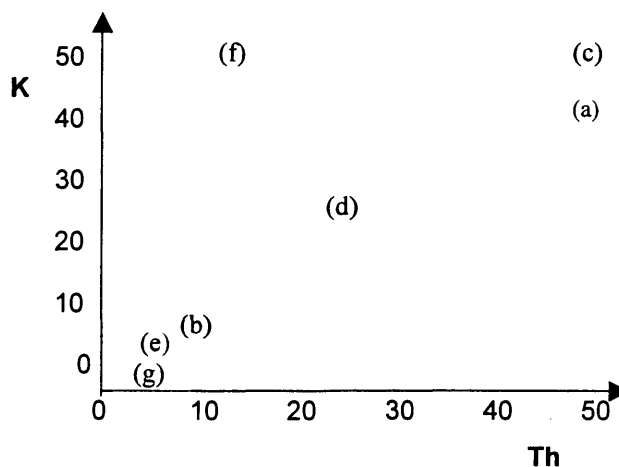
Lithology (grid-ref.)	Radio- element	Min.	Max.	X	St- Dev.	Mode	Median	Sample No.
'Bs' (818292,1199490)	Th	35	68	48.3	7.3	41	48	475
	U	43	65	53.6	4.8	54	54	
	K	74	125	102.3	11.7	105	104	
'Tgr' (815875,1168045)	Th	36	70	50.1	8.2	49	50	396
	U	43	79	59.4	7.2	55	59	
	K	59	83	76.4	6.2	73	75	
'Tgr' (822661,1190656) (825896,1196261) (high ground)	Th	54 (70)	101 (105)	84.8 (91.4)	8.3 (7.2)	89 (97)	86 (92)	320 (120)
	U	54 (59)	79 (78)	66.1 (70.7)	4.8 (4.1)	63 (68)	66 (70)	
	K	75 (80)	103 (102)	88.7 (92.8)	5.2 (4.3)	89 (90)	90 (93)	
'Y/Yb' granite edge (817310,1175200) (817199,1168780)	Th	86 (91)	145 (156)	120.8 (130)	13.8 (17.9)	107 (133)	121 (133)	56 (30)
	U	73 (79)	103 (139)	91.7 (115)	7.4 (16.6)	96 (100)	93 (114)	
	K	98 (96)	130 (154)	115.6 (130)	7.5 (15.6)	113 (107)	115 (131)	
'Al' Bagoé River (808428,1157284) (807762,1177167)	Th	75 (73)	95 (91)	86.1 (84.3)	4.7 (4.7)	84 (86)	85 (85)	63 (32)
	U	75 (66)	89 (85)	82.8 (77.3)	3.2 (4.9)	80 (73)	83 (77)	
	K	140 (137)	172 (187)	158.7 (170)	8.9 (13.1)	169 (160)	160 (174)	
'Bj' Syama volcanics (810417,1162592) (821937,1199752)	Th	8 (10)	25 (30)	20.3 (19.6)	2.4 (4.9)	20 (23)	20 (20)	100 (204)
	U	22 (13)	33 (40)	26 (31.9)	1.8 (5.0)	26 (35)	26 (33)	
	K	21 (27)	42 (54)	28.5 (37.9)	5.9 (5.3)	30 (40)	29 (39)	

(NB. Where sample number is low, parenthesis represent statistics for a second sample location).

The ratio method has been used for illustrating differences between radioelements and for characterising particular types of mineralisation (as reported in Peters, 1978; Rose and Wright, 1980; Galbraith and Saunders, 1983; Darnley and Ford, 1989; Cowan and Crabb, 1981). In the hope of achieving optimum discrimination, for lithology and potential alteration, the ratio technique was applied in the following combinations: Th/U; K/U and Th/K. Results are illustrated in Figs. 71 - 73 with the colours in Fig. 74 representing selected histogram breaks within the ratio image (Th/K). At first glance it appears that geology can be differentiated by ratios. However, care is required for there are many ways to obtain the same ratio value, sometimes irrespective of the geology, as discussed below.

For example, some hypothetical values of Th and K are listed along with the Th/K ratio.

Th	K	TH/K	
50	40	1.25	(a)
10	8	1.25	(b)
50	50	1	(c)
25	25	1	(d)
5	5	1	(e)
15	50	0.3	(f)
1	3	0.3	(g)



An acid igneous signature, characterised by high Th and K would plot in the top right-hand proportion of the graph, whilst the low values expected from ultra-basic to basic would plot in a bottom left position on the graph, as illustrated from examples (a) and (b). However, although these two lithologies have very different radioelement responses, when ratioed the same value is produced. The examples (c; d and e) representing different lithologies also result in the same ratio. The two final examples (f) and (g) are also relevant in this research, as (g) denotes a basic signature, whilst (f) represents a possible basic-intermediate lithology with high K (alteration?), yet the ratio does not allow differentiation.

Fig. 71 Ratio Thorium/Uranium (Th/U).

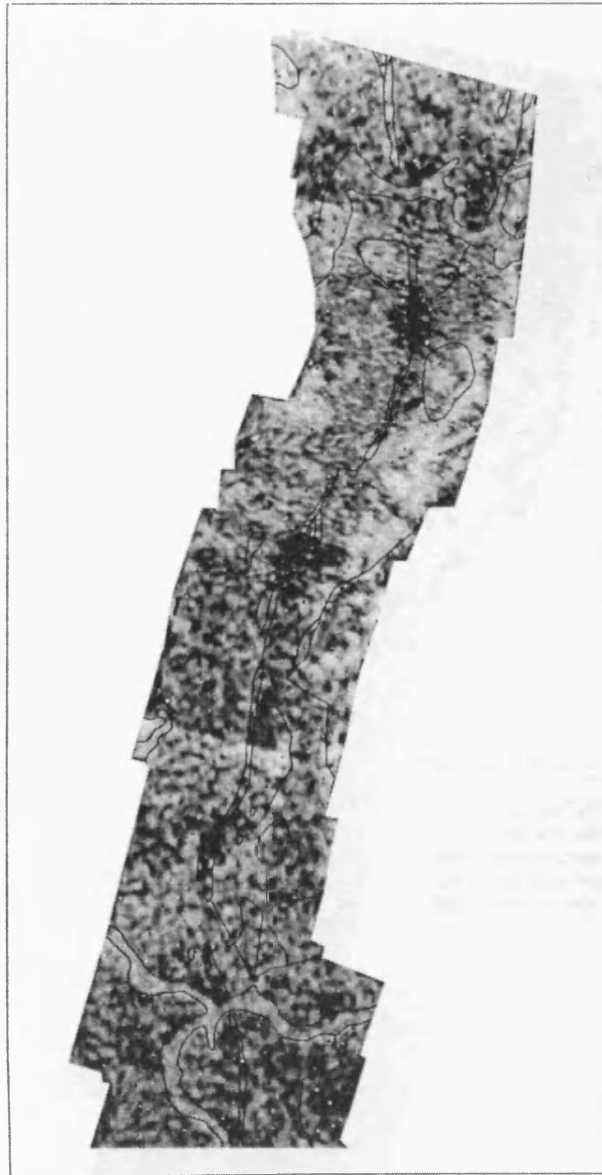


Fig. 72 Ratio Potassium/Uranium (K/U).



Ratio colour grade representation.

-  Very high ratio value
-  High ratio value
-  Medium / equivalent ratio values
-  Low ratio value
-  Very low ratio value

Fig. 73 Ratio Thorium/Potassium (Th/K).

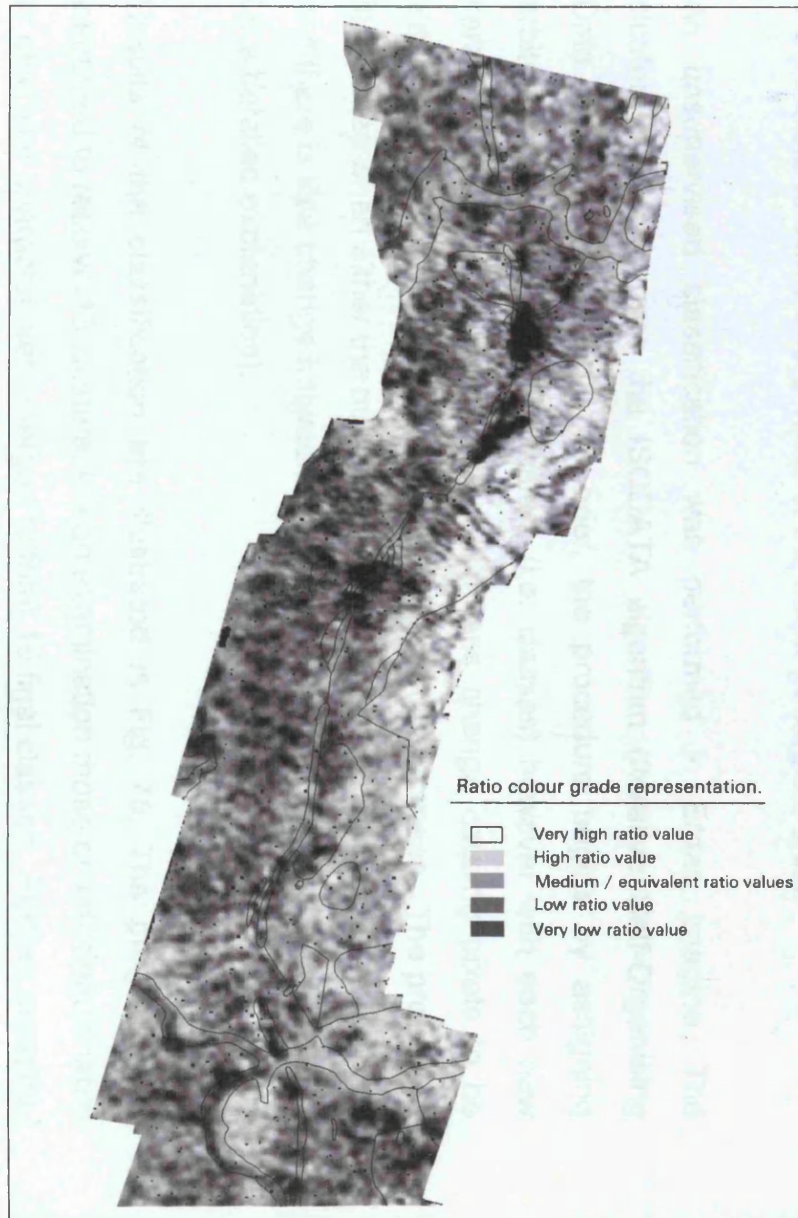
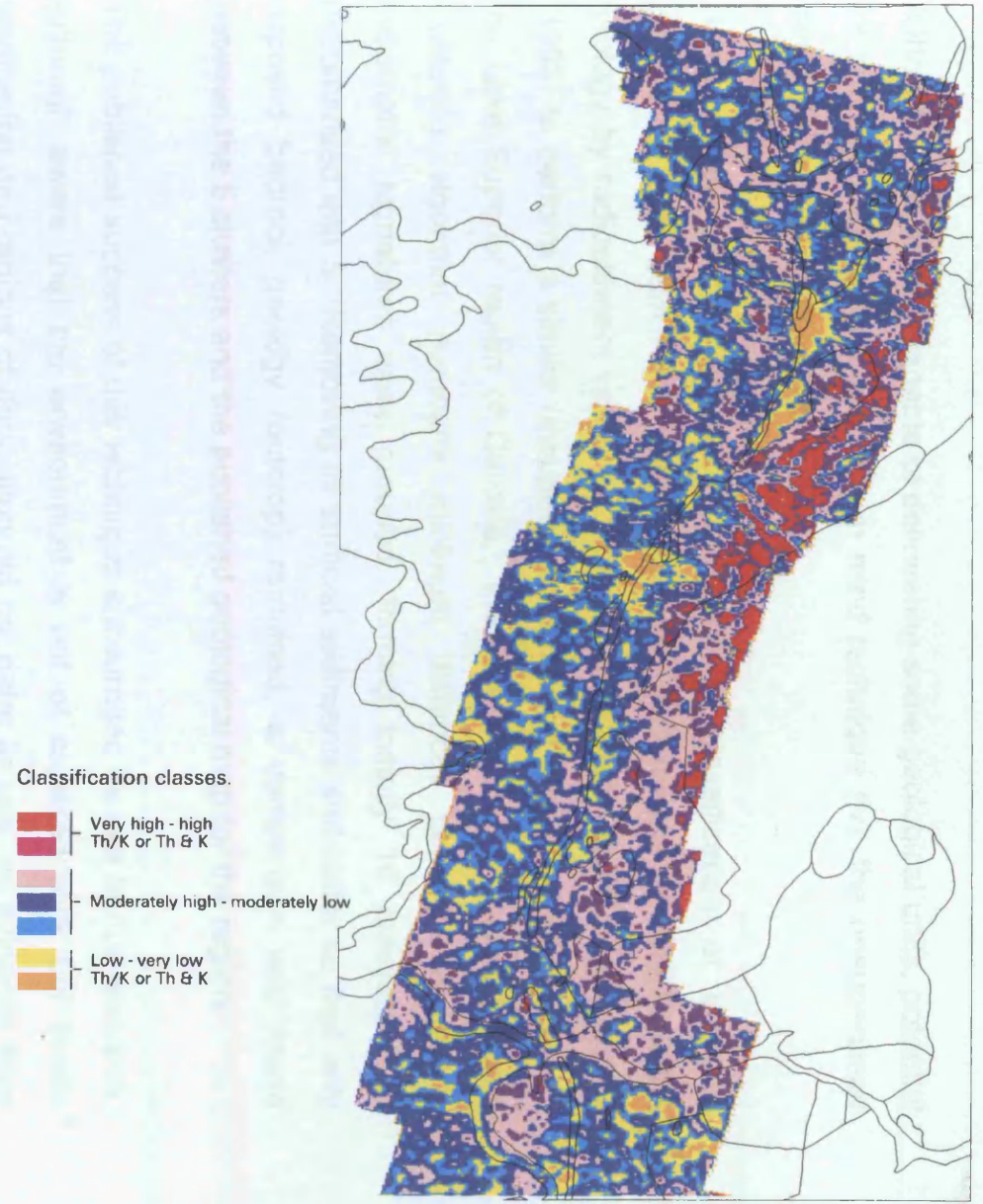


Fig. 74 Classification of ratio Th/K.



Although ratios appear capable of delineating some geological units, potential for confusion exists, and with this in mind technique (iv), the unsupervised classification was investigated.

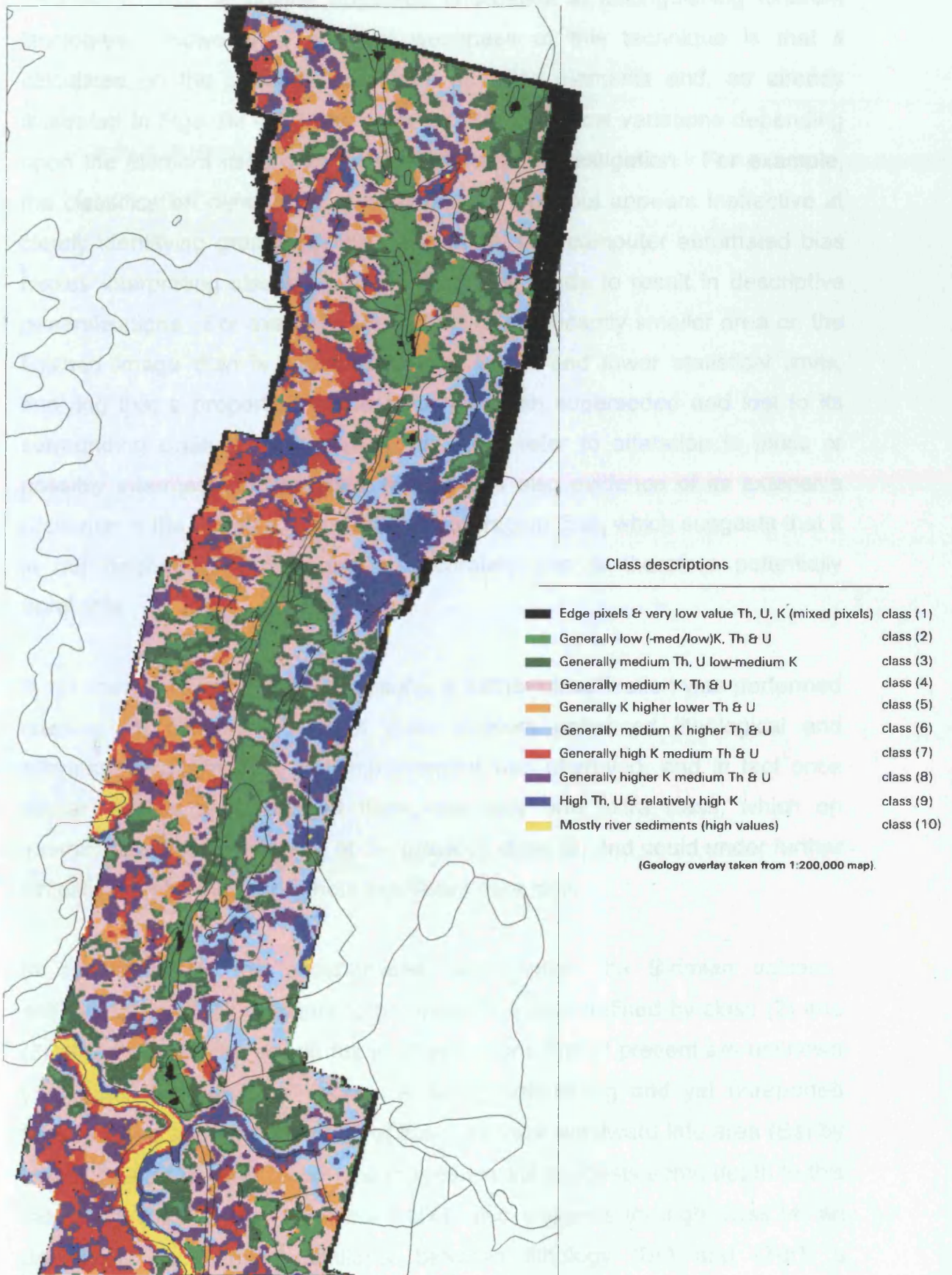
Harris, (1989) first investigated unsupervised classification of airborne gamma-ray data from Nova Scotia, Canada. Its success at differentiating geology by radioelement response later drove Graham and Bonham-Carter (1993) to perform a similar unsupervised clustering procedure on data from the Lake Superior region of Canada. With the use of a migrating means clustering algorithm (k-means minimum distance) pixels with similar radiometric signatures were grouped, forming initially 16 classes, later decomposed into 5. Removing all surficial sediments and water so that only exposed bedrock geology (outcrop) remained, a comparison was made between the 5 clusters and the published geological map for the region.

The published success of this technique encouraged its use in this research. Although aware that the environment is not of exposed rock but in-situ weathering and regions of deposition did not deter its use, as evidence from the ternary image Fig. 67 and the statistics of Table 49 already indicated that it is possible to discriminate some of the major geological units.

An unsupervised classification was performed in Erdas Imagine. The clustering method uses the ISODATA algorithm (Iterative Self-Organising Data Analysis Technique). In brief, the procedure begins by assigning arbitrarily means for the '*N*' clusters (i.e. classes) however with each new iteration and recalculation the cluster means change causing pixels to be either kept or reassigned to a statistically closer cluster mean. The procedure terminates when either the number of iterations defined by the user is reached or if there is little change between iterations (see Erdas field guide V.8.3, 1997 for a detailed explanation).

Results of the classification are illustrated in Fig. 75. The program was instructed to resolve 13 clusters, but on examination those of indistinguishable or of similar character were merged to form 10 final classes. Further merging,

Fig. 75 Radiometric unsupervised classification (Th, U, K).



although possible, would only resort in data dilution and was not deemed necessary. The technique appeared successful at distinguishing different lithologies. However a potential weakness of this technique is that it calculates on the basis of data from all three elements and, as already illustrated in Figs. 68 – 70, there are notable statistical variations depending upon the element used and the lithology under investigation. For example, the classification detects the river sediments well, but appears ineffective at clearly identifying granite (Y/Yb). Also the strong computer automated bias makes interpreting classes a little difficult and tends to result in descriptive generalisations. For example, class (1) is of significantly smaller area on the finished image than is suggested by its upper and lower statistical limits, implying that a proportion of the data has been superseded and lost to its surrounding class (2). Also class (5) could refer to alteration in basic or possibly intermediate lithologies, but there is also evidence of its extensive presence in the Birimian greywacke-arkose region (Bs), which suggests that it is not discriminating this feature accurately and is therefore potentially unreliable.

In an attempt to improve these results, a further classification was performed creating 20 clusters to see if more clusters enhanced lithological and alteration discrimination. No improvement was observed, and in fact once similar classes were merged there was only one extra class, which on examination was a derivative of the previous class (6) and could under further simplification be merged without significant data loss.

In conclusion, in the unsupervised classification the Birimian volcano-sedimentary unit (Bj) appears to be reasonably well defined by class (2) and (3), allied with similar signatures in other regions that at present are unknown to contain 'Birimian type' rocks. A further interesting and yet unreported feature is the apparent mirroring of the dyke trace westward into area (Bs) by class (2) and (3), even though the magnetic data suggests some depth to this feature (Section 5.7). This classification also suggests through class (4) an underlying geochemical similarity between lithology (Bs) and (Tgr), a characteristic also observed in Figs. 68 - 70, with only the (Tgr) sample taken

from higher ground showing obvious chemical differentiation. This result is therefore judged to be the most geological informative so far.

However as a technique its discriminatory power failed in a number of ways;

- (1) In the identification of the granite, which statistically should have been identified (Table 49).
- (2) In the lack of confidence in identifying alteration in basic lithologies, the signatures of which may be too subtle for a computer-automated technique.
- (3) A repeat of an inability to detect some of the smaller andesite, diorite intrusions and the conglomerate lithologies as previously discussed.

To reduce the element of generalisation, which to a large degree is inherent with an unsupervised classification, and home-in more specifically on areas that could host potential mineralisation requires a different hands-on approach: supervised classification. A frequently used method is to 'train' the classifier using field information, but unfortunately this was not possible. An alternative approach is to use 'known' mineralised sites as a training set. However this technique requires accurate spatial positions for each mine regardless of whether they are active or ancient. As there is confusion of mine locations between maps together with the common problem of symbol placing with respect to scale (as discussed in Section 4.5.8), this source of information cannot be relied upon with any great certainty. A completely different approach is to use *a priori* knowledge to guide the classification, and this technique is now described (Section 5.6.2).

5.6.2 The application of feature space mapping.

Supervised classifications require the user to have knowledge about the data. Knowledge can be in the form of field information, or be derived from other sources. In this study the knowledge base was constructed from previously published radiometric studies and from statistical information taken from known geological areas which have been sub-sampled (Table 49).

As this *a priori* knowledge was principally statistical in nature, the signatures used in the classifications were derived from feature space images. Feature space images are in effect scatter plots where values in one band are plotted against another. This interactive method has an advantage in that it allows clearer identification of image features through a 'mask' facility, whereby a signature's area of interest (AOI) can be compared to the original image and the parallelepiped limits to the sub-sampled plots (Fig. 68 - 70).

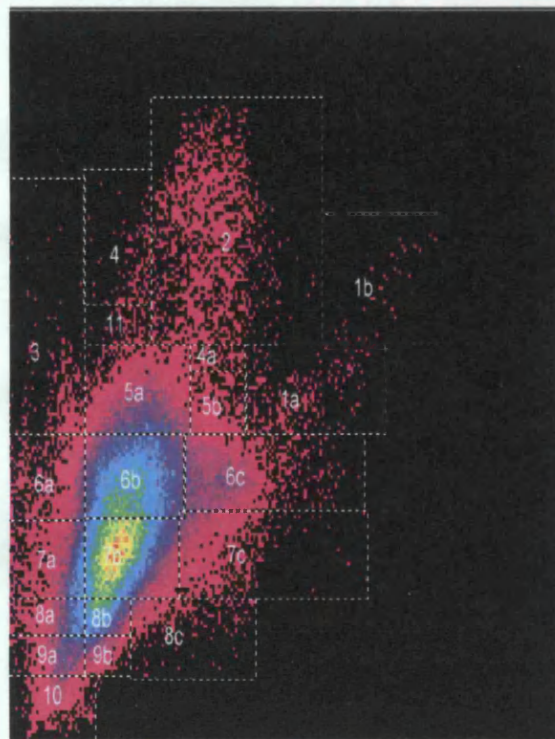
Although the aims had not changed it was hoped that a supervised technique performed in this manner would;

- (a) Differentiate the geology more clearly.
- (b) Indicate potential sites of alteration with greater clarity and
- (c) Enable a ranking system to be implemented, prioritising the most significant alteration within the Birimian / basic type signatures.

With the help of the sub-sampled statistical data and the image mask facility the feature space images were interrogated, dissected and signatures formed for each selected AOI (Fig. 76, 77 and 78). The method which established the upper Th, U and K level for determining likely Birimian / basic-type signatures in the feature space images came from establishing the statistical character of a number of sub-samples in suspected (Bj) i.e. Birimian regions. Once identified, any rise in K was deemed to reflect potential alteration. All signature files were then used to perform a non-parametric classification.

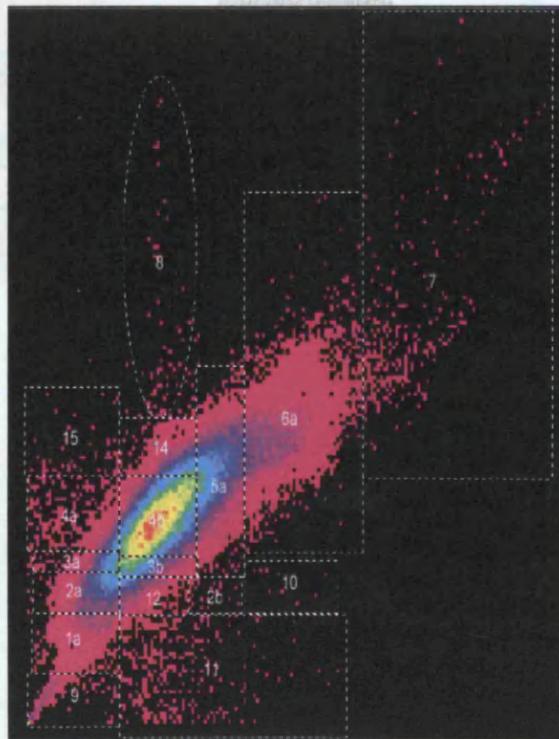
However each classification was plagued by randomly distributed pixel error, previously discussed in Chapter 4, Section 4.7. As these pixels were low in value their effect was to over and miss-represent basic-type signatures and basic-type signatures with alteration. The only way to overcome this problem was to create new coverages by identifying and drawing polygons around each error pixel. These coverages were then used as masks which, when overlaid with the classification images, forced all coincidence pixels to be reclassified to unclassified. Final classification results are shown in Fig. 79-81.

Fig. 76 Th and K feature space image showing supervised classes (A.O.I).



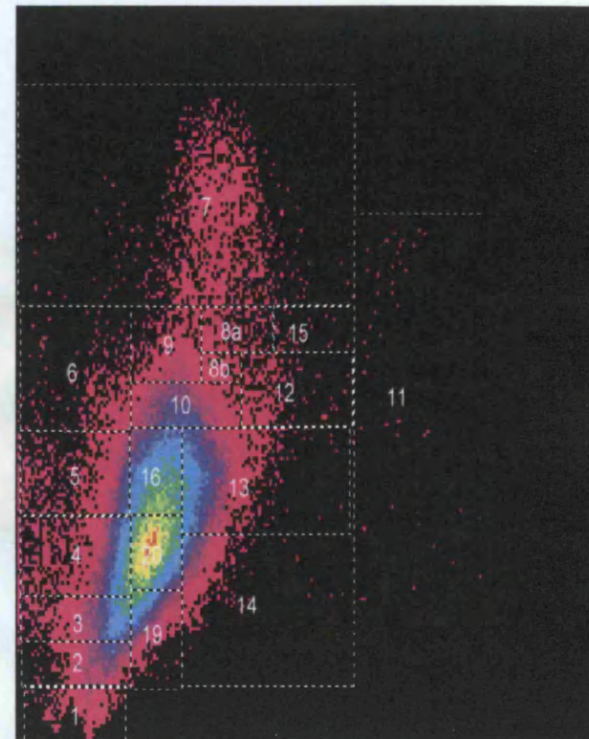
K
↑
Th →

Fig. 77 Th and U feature space image showing supervised classes (A.O.I).



U
↑
Th →

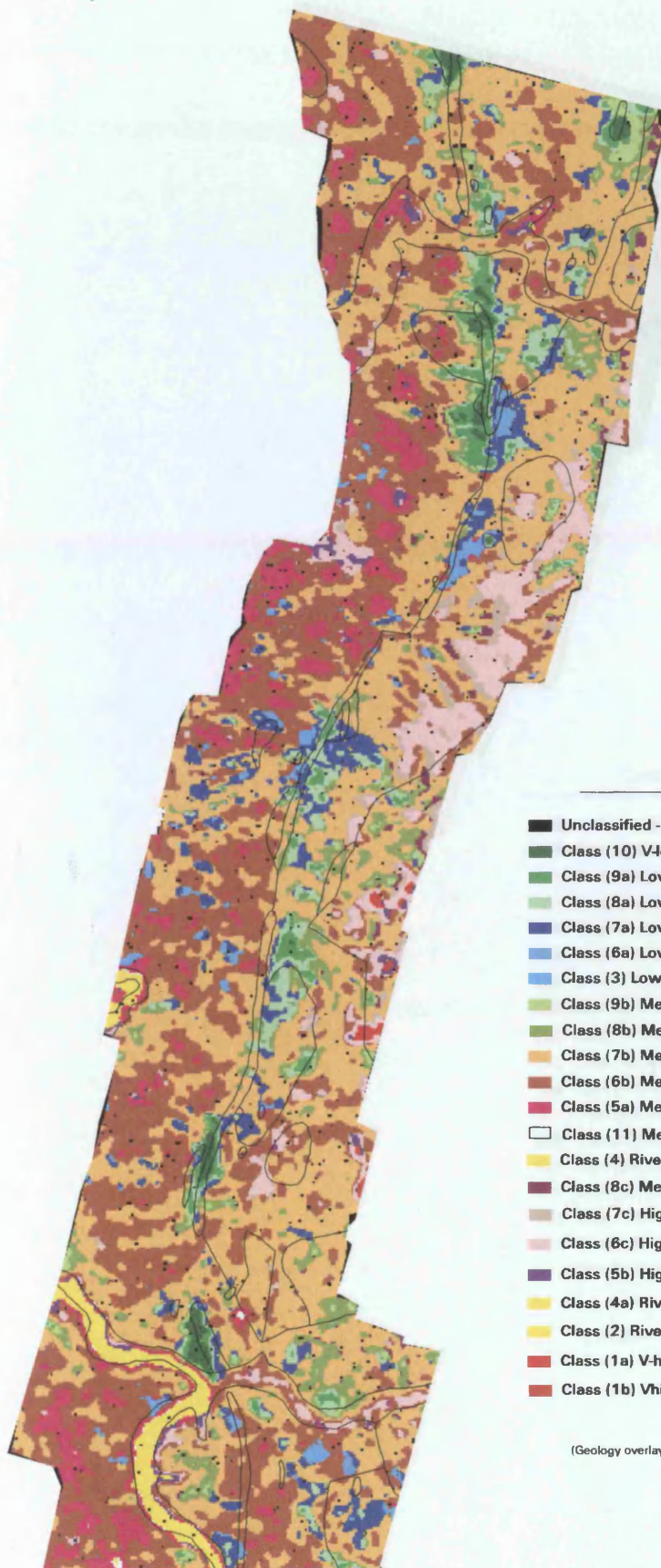
Fig. 78 U and K feature space image showing supervised classes (A.O.I).



K
↑
U →

See appropriate image classification for description of classes / AOI.

Fig. 79 Radiometric supervised classification (Th vs K).



Class descriptions.

- Unclassified - spurious random drop-out pixels.
- Class (10) V-low Th & K - basic-type Bj.
- Class (9a) Low Th & K - basic-type Bj.
- Class (8a) Low Th majority-low K - basic-type Bj.
- Class (7a) Low Th majority-medium K - basic-type & mild alteration.
- Class (6a) Low Th majority-high K - basic-type & medium alteration.
- Class (3) Low Th high K - basic-type & high alteration.
- Class (9b) Medium Th low K - association (8b) Tgr-(7b).
- Class (8b) Medium Th majority.low K - association Tgr-(7b), or (8a) (8c).
- Class (7b) Medium Th medium K - essentially Tgr & possible mix lower Bs.
- Class (6b) Medium Th majority high K - middle Bs & mix Tgr-high ground.
- Class (5a) Medium Th high K - top of Bs (possible alteration).
- Class (11) Medium Th v-high K - top of Bs (possible alteration).
- Class (4) River sediments.
- Class (8c) Medium-high Th low K - association Tgr (7b), (7c) & (8b).
- Class (7c) High Th med K - lower end of Tgr-high ground.
- Class (6c) High Th majority.high K - Tgr-high ground possible.mix Y/Yb.
- Class (5b) High Th high K - likely association Y/Yb.
- Class (4a) River sediments.
- Class (2) River sediments.
- Class (1a) V-high Th high K - Y/Yb association.
- Class (1b) Vhigh Th & K - Y/Yb.

(Geology overlay taken from 1:200,000 scale maps).

Fig. 80 Radiometric supervised classification (Th vs U).



Class descriptions.

- Unclassified - spurious random drop-out pixels.
- Class (9) Sporadic edge pixel errors.
- Class (6a) High Th & U - mix pixels Tgr / highground & river sediments.
- Class (3b) Majority-low U Majority-medium Th.
- Class (2b) Sporadic edge pixel errors.
- Class (10) Sporadic edge pixel errors.
- Class (11) Sporadic edge pixel errors.
- Class (8) V-high U medium Th.
- Class (7) Vhigh Th & U - Y/Yb granite association.
- Class (4a) Majority-medium U Majority-v-low Th.
- Class (5a) Upper majority (medium-high U & Th) pixel mix Tgr, Bs & river.
- Class (4b) Medium majority (medium-medium) pixel mix Bs & Tgr.
- Class (1a) Vlow Th & U - basic type Bj.
- Class (2a) Low Th & U - basic type Bj.
- Class (3a) Majority-low U, Majority-v-low basic relationship.
- Class (12) Medium Th low U.
- Class (14) High U medium Th.
- Class (15) High U low Th (some mixed pixel drop-outs).

(Geology overlay taken from 1:200,000 scale maps).

Fig. 81 Radiometric supervised classification (U vs K).

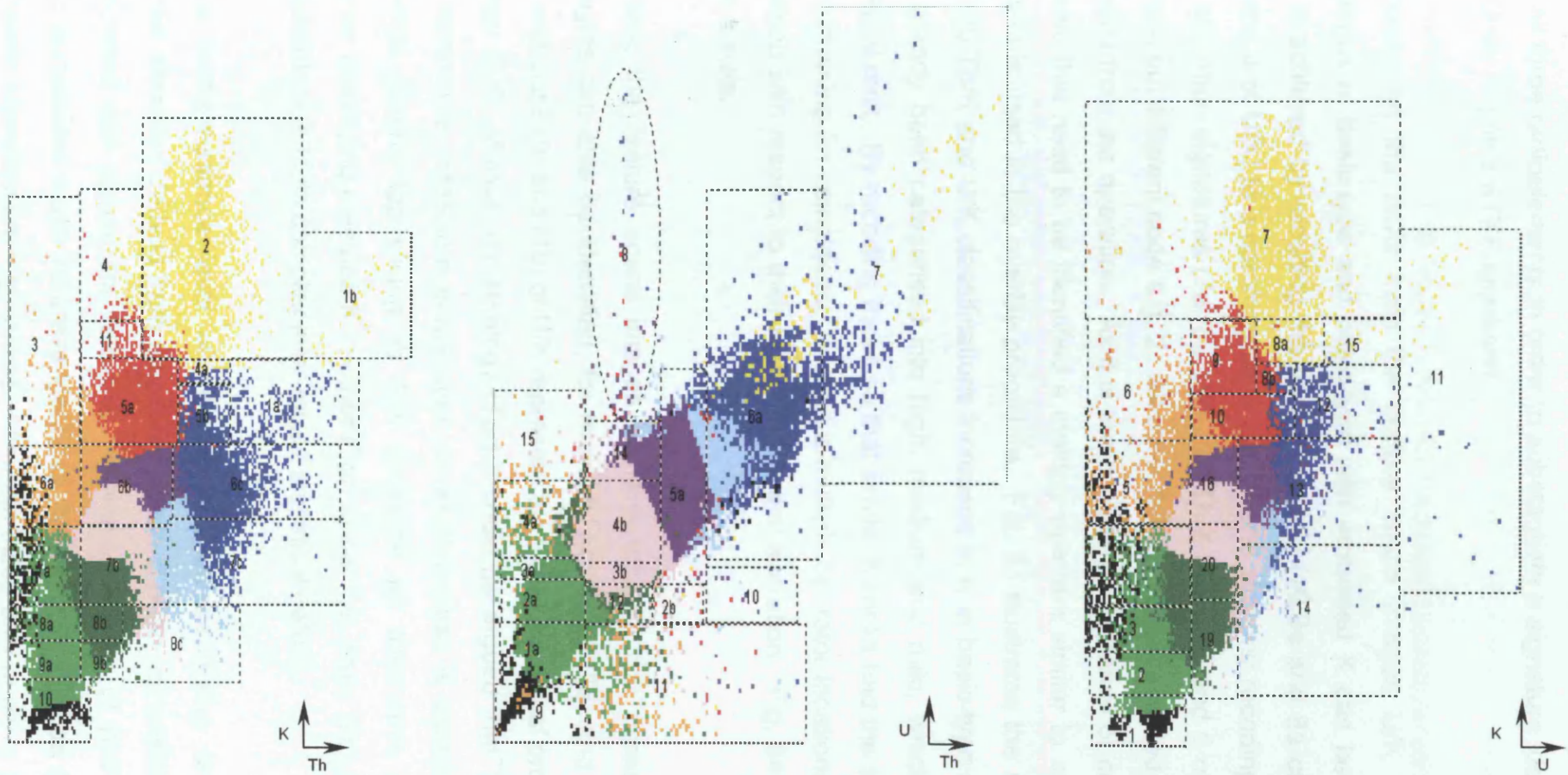


The indications from these findings are that the Th/K combination provides the best overall lithological discrimination, followed closely by U/K whilst Th/U proved to be the worst workable combination. The ease at which pixels can be identified and grouped in each feature space image is controlled by the integral nature of the global coefficient of correlation and the degree of statistical separability or overlap between individual lithologies, as illustrated previously in Fig. 68-70. Consequently, the almost perfect positive correlation of Th and U (0.946) makes for poor identification in many of the lithologies, regardless of the amount of AOI boundary manipulation. This is highlighted in the inability to separate river sediments from high ground in class (6a) and the difficulty at distinguishing between (Tgr) and (Bs) represented by classes (4b, 14 and 5a). This is contrasted with the Th/K and U/K where similar global coefficients of correlation result not only in clearer geological differentiation but also a strong spatial association between the classes.

Although (Bj) remains statistically the most unique of all lithologies, none of the combinations are capable of providing 'pure' unequivocal lithological identification, and as such AOI boundaries remain somewhat subjective. However, as a technique its discriminatory powers are greater than those of the unsupervised method. This can be illustrated by converting the unsupervised classification into feature space, then overlaying with the AOI classes from the supervised classification (Fig. 82). These plots illustrate where pixels from the unsupervised method have been misclassified and how the additive nature of using all three bands allows some classes to be over represented, the most noticeable and important are class (3) and (4) thought to signify basic type signatures and potential alteration.

If one combination were to be selected to best differentiate the geological environment, identifying basic type signatures that could house potential alteration, then Th/K would be the first choice. Galbraith and Saunders (1983) also found K followed by Th to be the two most useful radioelements for igneous rock identification, due in part to their more restricted mobility. However, according to the literature the identification of a basic type signature and those suggesting alteration should also indicate a low U concentration,

Fig. 82 Unsupervised Vs supervised class delimitations.



The black dashed lines and numbers correspond to the supervised AOI classes. The colours represent the classes from the unsupervised classification. See appropriate Fig's for class description.

therefore the requirement is to seek coincidence by combining information from all three radioelements in order to substantiate a signature identity. This effectively requires a GIS approach.

By combining the AOIs from the feature space images U/K and Th/K, signatures of basic-type and basic-type with increased K can be identified. This is achieved by recoding the basic-type AOI (10,9a and 8a of Th/K and 1,2, and 3 of U/K) to a common code e.g. 1, and similarly recoding all basic-type alteration signatures (7a, 6a and 3 of Th/K and 4, 5 and 6 of U/K) to a common but different code e.g. 2. All other AOI classes are coded 0, and are excluded from the operation. As it is the common occurrence or coincidence of pixels that need to be identified a multiply operator similar to an 'AND' or intersect is used in the overlay procedure. Fig. 83 illustrates the results. In both the Th/K and U/K classifications increases in K in basic-type signatures had already been categorised into high, medium and mild, which gave an individual rank. By recoding these so that similar K-ranks had the same code and combining for coincidence through a multiply operator locations could be prioritised with respect to their level of potential alteration. Fig. 84 illustrates these results.

By using the feature space images some potassium rich areas in other lithologies can also be identified, for example AOI/class (5a) and (11) from Th/K and class (9) and (10) of U/K represent the upper statistical proportion of lithology (Bs). Whilst with lithology (Tgr) it could be argued that Th/K class (6c) represents potassium enrichment, or as this class is associated with (Tgr)-high ground top slicing its AOI could be an alternative approach. However identifying elevated K in other (Tgr) areas (i.e. class (7b) of Th/K) is not possible due to its complex inter-mixed statistical nature.

At the reconnaissance level of investigation, substantiating an area of potential alteration derived from a new technique is often not possible unless collaborated with concurrent fieldwork. However on one of BHP own 'in-house' concession maps 19 areas identified (but not known to be confirmed) as potassic alteration are highlighted. Although these only apply to part of the

Fig. 83

Combining feature space classes (Th vs K & U vs K) to identify basic-type signatures and with alteration.

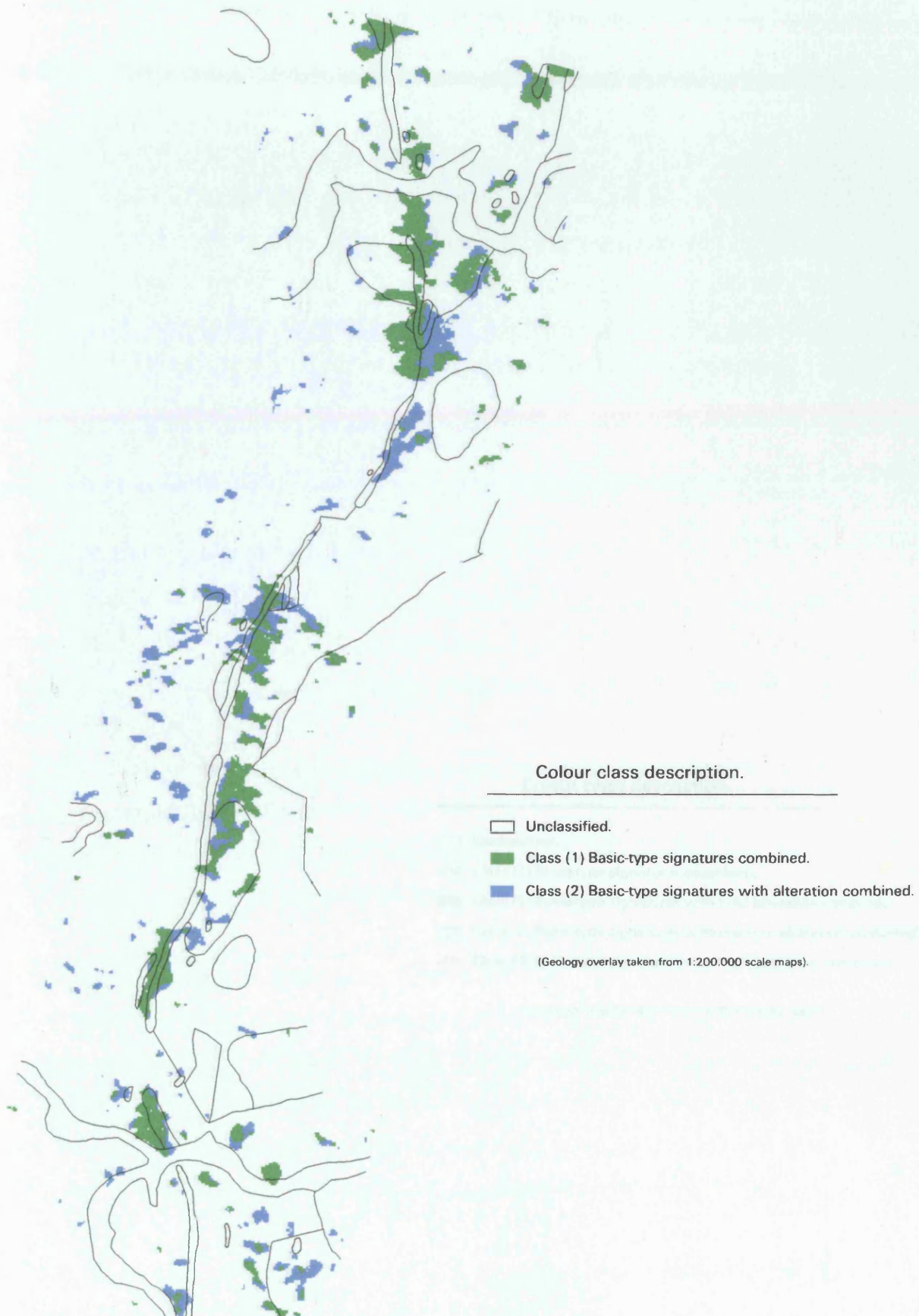
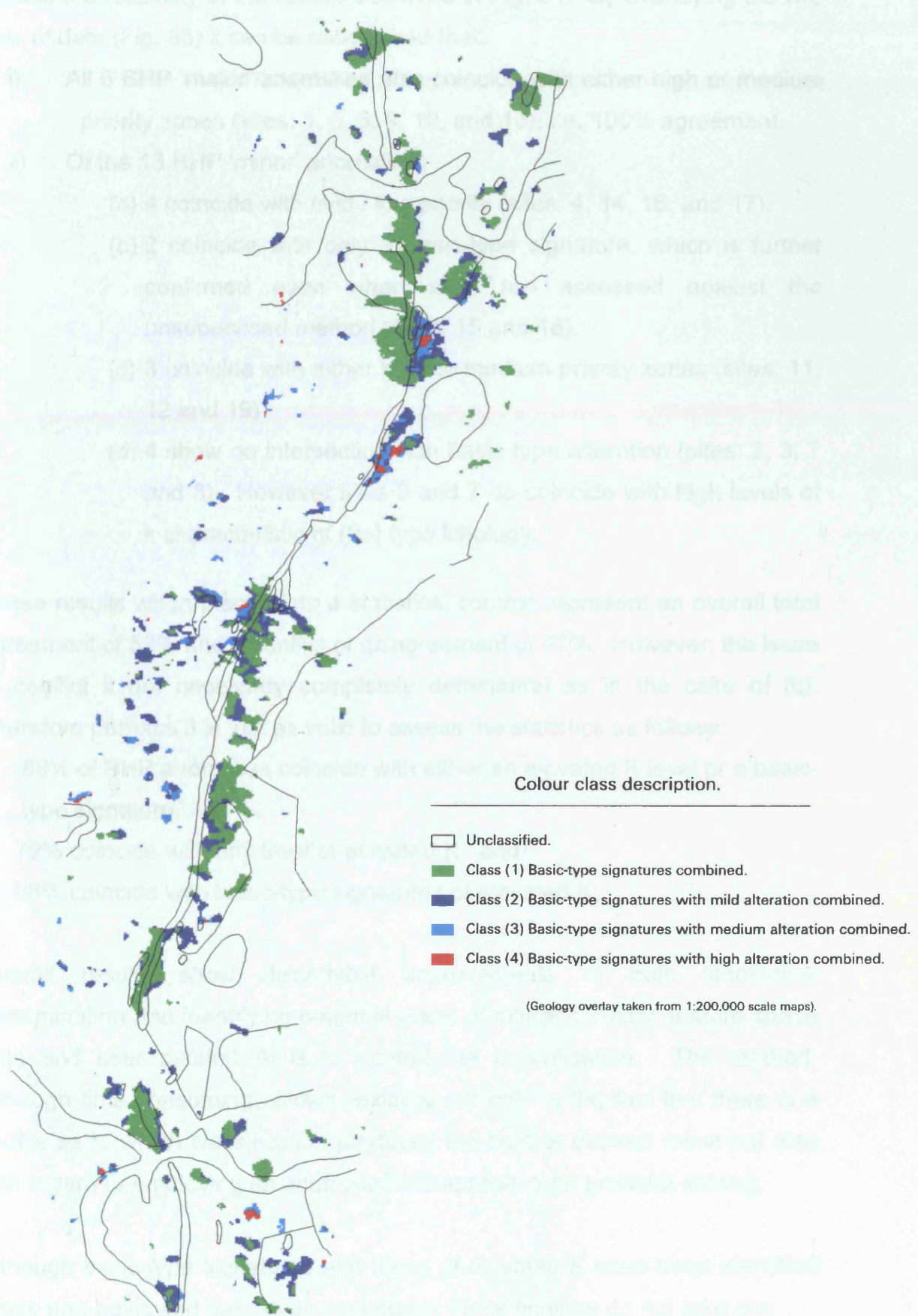


Fig. 84 Combining feature space classes (Th vs K & U vs K) to prioritise levels of potential alteration within basic-type signatures.



Birimian (volcano-sedimentary) zone a basic comparison can be made to help assess the reliability of the results observed in Fig. 84. By overlaying the two sets of data (Fig. 85) it can be established that;

- i) All 6 BHP 'major' anomalies also coincide with either high or medium priority zones (sites: 1, 5, 6, 9, 10, and 13), i.e. 100% agreement.
- ii) Of the 13 BHP 'minor' anomalies,
 - (a) 4 coincide with mild / low priority (sites: 4, 14, 16, and 17).
 - (b) 2 coincide with only a basic-type signature, which is further confirmed even when sites are assessed against the unsupervised method (sites: 15 and 18).
 - (c) 3 coincide with either high or medium priority zones (sites: 11, 12 and 19)
 - (d) 4 show no intersection with basic-type alteration (sites: 2, 3, 7 and 8). However sites 3 and 7 do coincide with high levels of k characteristic of (Bs) type lithology.

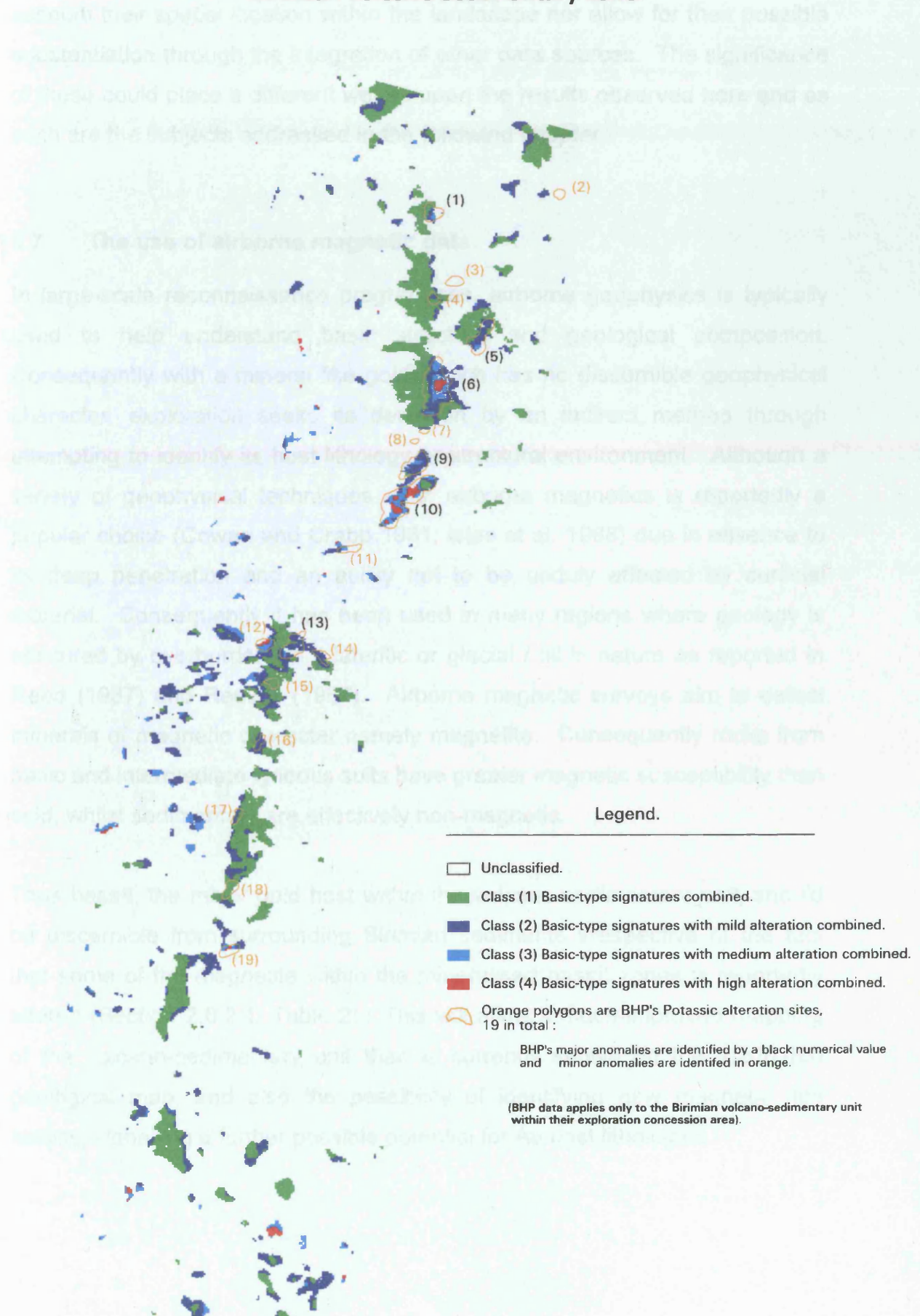
These results when placed into a statistical context represent an overall total agreement of 53% and a conflict or disagreement of 47%. However, the issue of conflict it not necessary completely detrimental as in the case of (c). Therefore perhaps it is just as valid to assess the statistics as follows:

- 89% of BHP anomalies coincide with either an elevated K level or a basic-type signature.
- 79% coincide with any level of elevated K and
- 68% coincide with basic-type signatures of elevated K.

Overall results show discernible improvements in both lithological discrimination and identifying potential areas of alteration using feature space data and user defined AOIs to control the classification. The method, although time consuming, allows flexibility not only in the fact that there is a choice as to which classification produces the best or desired result but also with regard to employing an additional GIS approach for problem solving.

Although basic-type signatures and those of elevated K have been identified within non-basic and basic-type signatures, these findings do not take into

Fig. 85 Spatial comparison of potassic alteration within the Birimian volcano-sedimentary zone.



account their spatial location within the landscape nor allow for their possible substantiation through the integration of other data sources. The significance of these could place a different weight upon the results observed here and as such are the subjects addressed in the following chapter.

5.7 The use of airborne magnetic data.

In large-scale reconnaissance programmes, airborne geophysics is typically used to help understand basic structure and geological composition. Consequently with a mineral like gold, which has no discernible geophysical character, exploration seeks its detection by an indirect method through attempting to identify its host lithology or structural environment. Although a variety of geophysical techniques exist airborne magnetics is reportedly a popular choice (Cowan and Crabb 1981; Isles et al. 1988) due in essence to its deep penetration and an ability not to be unduly affected by surficial material. Consequently it has been used in many regions where geology is obscured by overburden be it lateritic or glacial / till in nature as reported in Reed (1987) and Reeves (1987). Airborne magnetic surveys aim to detect minerals of magnetic character namely magnetite. Consequently rocks from basic and intermediate igneous suits have greater magnetic susceptibility than acid, whilst sedimentary are effectively non-magnetic.

Thus basalt, the major gold host within the volcano-sedimentary unit, should be discernible from surrounding Birimian sediments irrespective of the fact that some of the magnetite within the mineralised basalt zones is reportedly altered (Section 2.6.2.1; Table 2). This will allow a much-improved mapping of the volcano-sedimentary unit than is currently shown on the 1:200,000 geological map, and also the possibility of identifying new magnetic rich activity, signalling a further possible potential for Au host lithologies.

5.7.1 Airborne magnetic interpretation.

With the principal aim of helping to delineate rock type and basic structure the aeromagnetic data was imported into Erdas Imagine for image processing. The traditional method of data contouring has not been used as prior published research has shown it to be less flexible and effective at distinguishing and highlighting any subtle changes within the data (Kowalik and Glenn, 1987; Isles et al., 1988). In fact Isles et al., (1988) reported a 25% increase in geological content when magnetic data were displayed as an image.

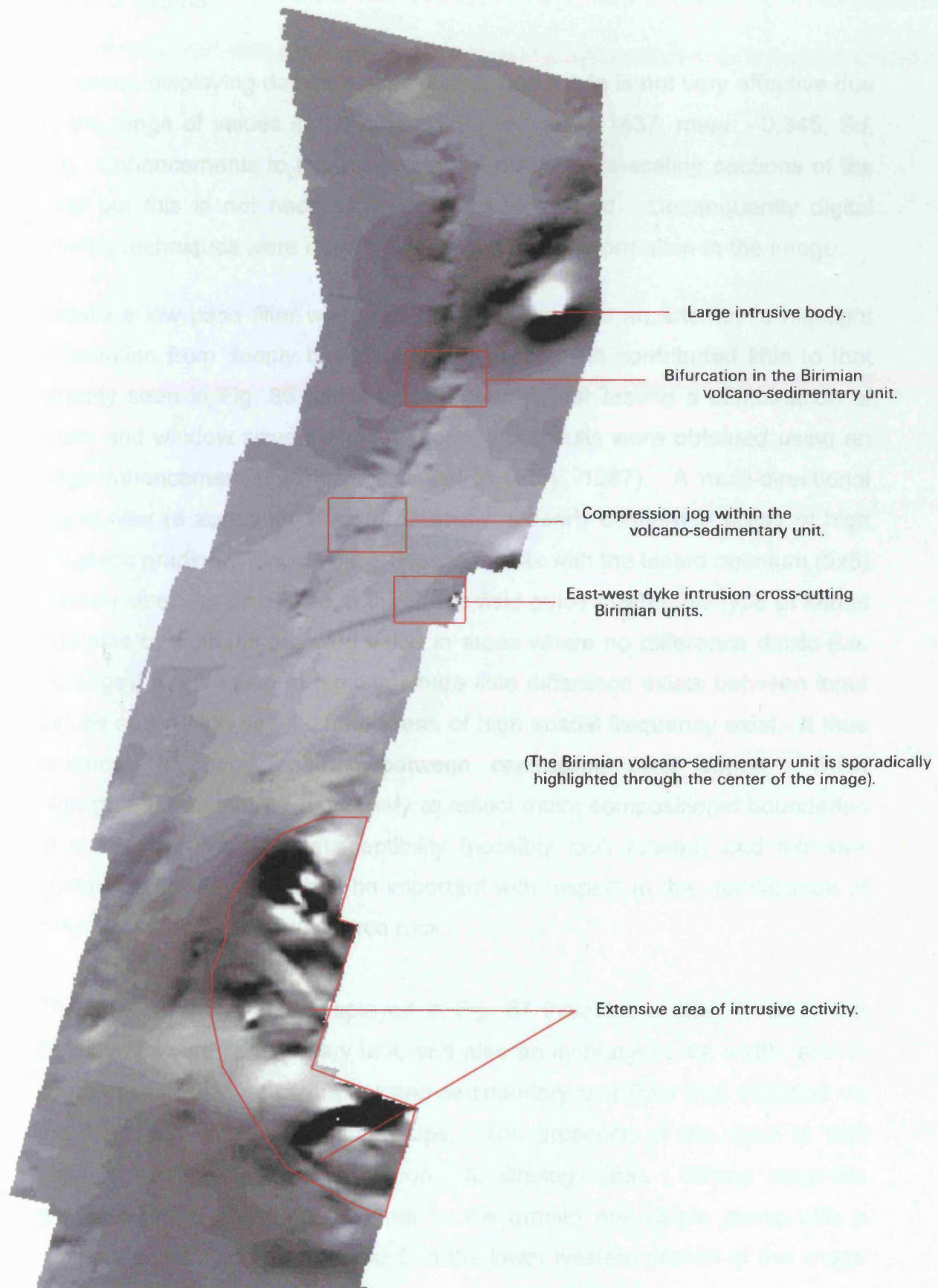
When displaying the magnetic data as a grey scale image (Fig .86), a number of interesting features are observed. Firstly there are three prominent regions exhibiting strong magnetic responses;

- (i) A large anomaly in the NE, adjacent to the Birimian.
- (ii) A small anomaly in the central eastern edge of the image showing a narrow (NE-SW) finger-like projection, crosscutting lithology (Tgr), indicative of a dyke structure.
- (iii) A collection of anomalies in the SE within and proximal to the granite (Y/Yb). Those lying beyond the known extent of the granite are not delineated on the published 1:200,000 scale geological map.

These features are all characteristic of intrusive activity. Features (i) and (ii) are new previously unmapped anomalies. Whilst the author is unsure as to whether those lying beyond the known extent of the granite in (iii) represent sub-surface granite activity buried beneath a (Tgr) cover, or separate unrelated activity, of possible basic-intermediate rather than granite composition. However the strong magnetic character exhibited in this zone, as shall be shown in Fig 88, would tend to favour the later proposition.

Also sporadically highlighted through the centre of this image is evidence of the Birimian unit. The bifurcation (as mentioned in Chapter 2) is clearly

Fig. 86 Magnetic image (data stretched).



identified in the north, accompanied with a compression jog in the shear to the south of Syama.

However, displaying data in a simple stretched mode is not very effective due to the range of values in the data (Min. -961, Max. 1437, mean -0.345, Sd. 50). Enhancements to the image can be made by re-scaling sections of the data but this is not necessarily an efficient method. Consequently digital filtering techniques were used to enhance textural information in the image.

Initially a low pass filter was applied to the image in an attempt to highlight information from deeply buried features. The result contributed little to that already seen in Fig. 86 and was dismissed. After testing a combination of filters and window sizes the most informative results were obtained using an edge-enhancement filter (as discussed in Drury, 1987). A multi-directional Sobel filter (a zero-sum 1st-order derivative) clearly delineated areas of high magnetic gradient. Fig. 87 illustrates the results with the tested optimum (5x5) window size. As discussed in the Erdas field guide (1997) this type of kernel operates by outputting a zero value in areas where no difference exists (i.e. no edge), a low value in regions where little difference exists between input values and a high value where areas of high spatial frequency exist. It thus produces a strong contrast between contrasting pixel edges. Such highlighted features are most likely to reflect major compositional boundaries of contrasting magnetic susceptibility (possibly fault related) and intrusive contacts both of which could be important with respect to the identification of potential mineral host and source rock.

The gradient information displayed in Fig. 87 indicates a clear trace to the Birimian volcano-sedimentary unit, and also an increase in the width, and in some cases position, of the volcano-sedimentary unit from that reported on the 1:200,000 scale geological maps. The presence of the dyke is well defined, trending westward through into lithology (Bs). Strong magnetic gradients associated and proximal to the granite are visible along with a similar area, previously overlooked, in the lower western portion of the image residing within lithology (Bs).

Fig. 87 Edge enhancement of magnetic data.



Image results obtained using a multi-directional Sobel (5 x 5) filter window.

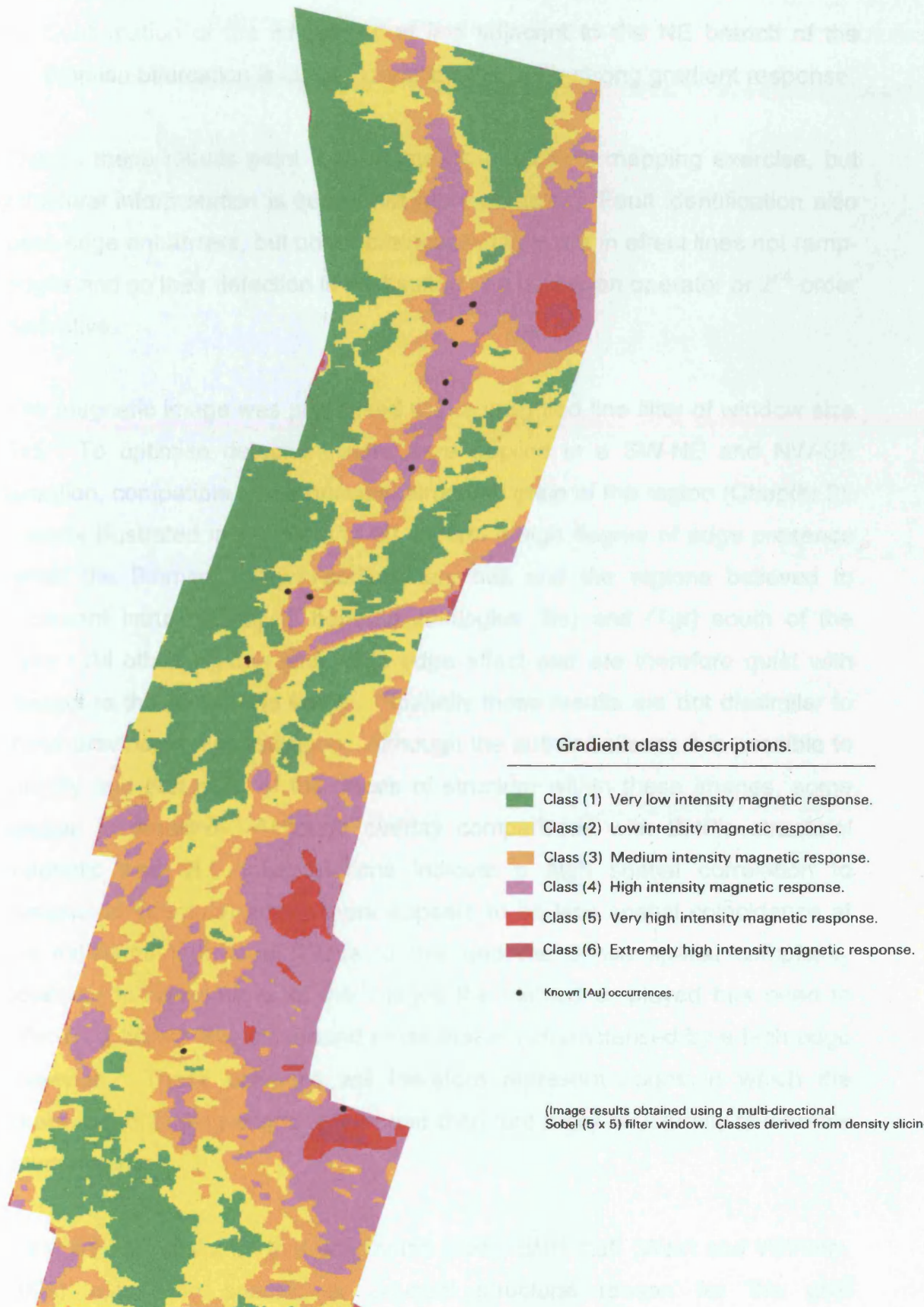
This grey scale image indicates :
Areas of high magnetic gradient as light grey - white.
Areas of low magnetic gradient as dark grey - black.

In order to better view and incorporate this magnetic gradient data into the GIS, in a user-friendly mode, the data format was changed from real to integer. This allowed it to be density sliced and classified into varying magnetic gradient intensities. The image was then median filtered to suppress sporadic noise. A median filter was chosen rather than a mean filter as it does not result in a loss of resolution and, importantly, retains step and ramp functions.

The result, illustrated in Fig. 88, shows:

- 1) Lithologies (Tgr) and (Bs) are characterised by very low magnetic gradients. Though their presence in part becomes more difficult to distinguish when approaching the higher gradients associated with the granite areas and the Birimian central zone.
- 2) The Birimian unit can be identified and traced throughout by primarily high and moderate with some intermittent lower gradients. The northern portion of the belt indicates a consistently stronger response.
- 3) The dyke trace is marked from its source in the East by a very high response decreasing to a low magnetic gradient response in the West, likely a response to increasing depth.
- 4) The regions of “extremely high” through to “high” gradient response within and surrounding the granite region infer, if granite related (as this can not be ascertained from this image), a much further sphere of influence than previously revealed on the published 1:200,000 scale geological map, due to coverage from lithology (Tgr). There is also the likelihood that some of the high intensity responses, observed in the East between the volcano-sedimentary and granite area, are in part a response to ferromagnesian minerals within inter-basic type intrusions. For within this area as indicated on the 1:200,000 scale geological map is a diorite intrusion. Possibly more exist (?), similarly it is likely the sizeable class (6 / 5) magnetic response similar to that in the NE is also of a basic-type intrusion.
- 5) There is also the indication from the high gradient responses in the West, opposite the region described in (4), that a similar potential magmatic source exists which is also covered by lithology (Bs) omitting its presence

Fig. 88 Classification of magnetic gradient intensities.



on the published geological map. This is likely the neighbouring Ivorian intrusion.

- 6) Confirmation of the intrusion that lies adjacent to the NE branch of the Birimian bifurcation is clearly identified by a very strong gradient response.

Overall these results point to a promising geological mapping exercise, but structural interpretation is somewhat more complex. Fault identification also uses edge enhancers, but unlike previously, faults are in effect lines not ramp-edges and so their detection is best suited to a Laplacian operator or 2nd-order derivative.

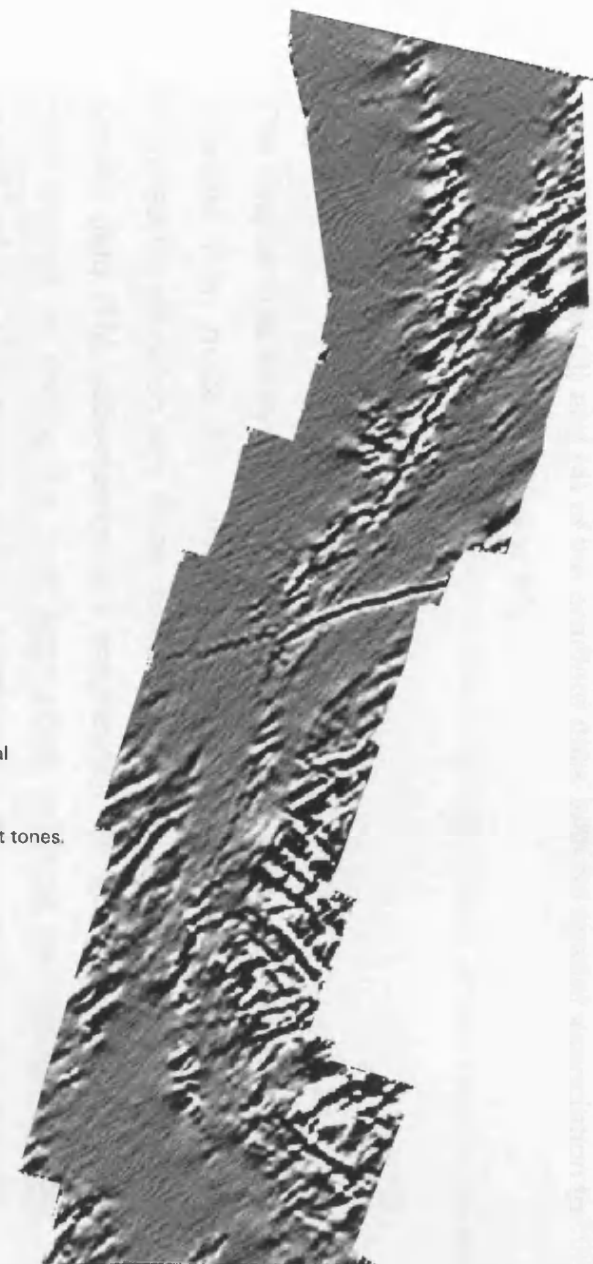
The magnetic image was processed with a weighted line filter of window size 5x5. To optimise detection filters were applied in a SW-NE and NW-SE direction, compatible to the principal structural grain of the region (Chapter 2). Results illustrated in Fig. 89 and 90 confirm a high degree of edge presence within the Birimian volcano-sedimentary belt and the regions believed to represent intrusive activity beneath lithologies (Bs) and (Tgr) south of the dyke. All other regions show little edge effect and are therefore quiet with respect to the rest of the image. Spatially these results are not dissimilar to those previously reported upon. Although the author believes it is possible to identify and plot most of the traces of structure within these images, some caution is required. Although overlay comparisons with BHP's structural magnetic and VLF interpretations indicate a high spatial correlation to designated structural areas, there appears to be less spatial coincidence at the individual fault level. Due to this and the dense spatial complexity observed in some areas of the images the method employed has been to effectively draw polygons around areas that are characterised by a high edge presence. These polygons will therefore represent zones in which the 'likelihood' of finding edges is high and therefore imply structurally favourable environments.

It should be mentioned that after some study, BHP staff (West and Witherly, 1995) report no specific or unusual structural reason for the gold concentration at Syama. However overlays of 'known' Au sites show a strong

Fig. 89 Structural directional filtering (NW - SE).



Fig. 90 Structural directional filtering (NE - SW).



Filter directions selected on compatibility to the principal structural grain of the region.

The images show :
High edge / lineament presence as contrasts between dark & light tones.
Once again the features most easily detected are :

- . - The areas of intrusive activity.
 - . - The Birimian volcano-sedimentary unit through the center of the image.
 - . - The E-W trending dyke.
 - . - The relative 'quietness' of the Bs & Tgr lithologies either side of the volcano-sedimentary unit.
- Known [Au] occurrences.

Images were processed using a Laplacian (second-order) weighted filter with a 5 x 5 window.

spatial association to those areas implying high structural favourability and primarily to class (3) and (4) of the gradient data, with no spatial association to class (1) (see Figures. 88,89 and 90).

5.8 Summary.

This chapter has analysed data from two principal sources. The first is data collected from maps from which a terrain surface was constructed and analysed for elevation and slope, whilst the second has come from remotely sensed data (TM, radiometrics and magnetics). In the later, analysis has been centred on finding the most appropriate methods for highlighting the spatial location of lithologies and the identification of potential surface mineral anomalies, as a consequence SPOT imagery has not been analysed due to its low spectral resolution and small area coverage. At present this has produced a large number of 'stand-alone' sites. However mineral exploration is also about seeking coincidences between differing data sources, in essence combining and filtering out anomalies and assessing their overall spatial location within the environment. The following chapter addresses this through the use of the data described in the summary tables (Tables 41 and 50) of Chapters 4 and 5.

Table 50 Summary of available data layers from Chapter 5.

Source data	Process results	Description
T.M data	Clay image. Iron image. Combination image.	Potential hydrothermal alteration. Potential gossan material. Potential mineralisation.
Radiometric data	Th Vs K classification. U Vs K classification. Combination image.	Confirmation of basic lithologies. Potential new basic-type lithologies Areas of potassic alteration.
Magnetic data	Gradient image. Edge-enhanced image.	Identifying lithology through mineral magnetic susceptibility. Identifying potential areas of high structural activity
Topographic map data	Terrain surface model	Dissected on the bases of altitude and slope.

CHAPTER 6

GIS INTEGRATION AND MODELING.

Contents

- 6.1 Introduction.**
- 6.2 GIS approaches in mineral exploration.**
- 6.3 Weight-of-evidence: The methodology.**
 - 6.3.1 Implementation and results of the weight-of-evidence approach.**
 - 6.3.2 Weights of evidence: discussion of results.**
- 6.4 The expert-system approach: the methodology.**
 - 6.4.1 Implementation of the expert-system approach.**
 - 6.4.2 The expert-system: discussion of results.**

6.1 Introduction.

The principal aims of this research have been to:

- 1) **Identify** and locate anomalous areas which are thought to be representative of gold mineralisation and
- 2) **Prioritise** or seek out the most important gold locations identified from (1) in order to reduce the decision risk.

The crux of any mineral exploration program is to identify mineralisation. Geochemical data, when present, are often the principal facilitator in the identification process because data collection is through surface sampling not by a remote technique and because each sample allows for the direct analysis of element(s). Consequently when seeking gold mineralisation, as objectivized by the UNDP geochemical survey, it would be appropriate to ensure that samples are analysed for gold. Identifying and locating areas that could favour gold mineralisation is best achieved through the implementation of thresholds (as explained in Chapter 4) and the mapping of their spatial distribution as illustrated in Fig. 40. Through this procedure aim (1) as reported above has, in effect, been achieved.

The prioritisation of the locations identified is in many exploration programs an important issue in helping to reduce costs and maximising the potential for returns. At the simplest level one could argue that gold classes alone reflect a priority, which they do, based on concentration. However, there can be problems with prioritising on the basis of a single data source such as gold. For example gold has a comparatively low mobility, and smaller dispersion halo (even in the cuirasse) than copper. Consequently, potential anomalies lying between sample lines may well be missed by gold but are perhaps detected by copper, a problem associated to regional sample data. Also the issue of whether a particular location is favourable because of mineralisation or whether instead it is just a reflection of either sampling or analytical error can often be addressed by comparisons with other (pathfinder) elements, based on the assumption that it is less likely that high gold concentrations would occur alone. Prioritising gold locations can also be addressed with

regard to other associate criteria such as, the lithology in which gold is most likely to be found, or if the presence of faults is significant to the location of gold, and whether the clay and iron information derived from TM data acts to collaborate a location of interest. The issue of prioritising gold locations is therefore rarely approached based upon a 'stand-alone' strategy. As indicated through the analysis of Chapters 4 and 5 modern mineral exploration employs many techniques which help to identify anomalies or areas of interest in their own right but the principal aim is to use all data as a collaborative force to substantiate those within the dataset under investigation. The overall effect is aimed at lowering the risk factor when prioritising.

In this research, gold prioritisation will be assisted by integrating the data produced from Chapters 4 and 5, with an additional dataset based upon spatial location within the landscape, as discussed in Chapter 3. The analysis is one that requires both decision making and spatial association and therefore lends itself most appropriately to a GIS.

6.2 GIS approaches in mineral exploration.

There are a number of approaches in GIS which allow data sources to be integrated. The choice of approach can be driven by the complexity of the data, but more often it is a reflection of how constraining or flexible the analysis is required to be.

Perhaps one of the most well-known and frequently used method of data integration is that described by the Boolean overlay technique. With Boolean overlay, data is first described as either 'present' ('of significance') or 'absent' ('not of significance'). By its very nature a binary decision of true/false, yes/no, present/absent, is therefore constraining as it does not allow for 'grey' areas (or 'degree', or ordinal or interval scale measurement), irrespective of the operator used to join the data sets. The choice of operator, used to execute the overlay between layers, can further exert constraint if the AND

(intersection) is selected over the more liberal flexible OR (union) operator, as discussed in Eastman (1999). Although this type of analysis does have a place in mineral exploration, its use is perhaps more appropriate in circumstances where the boundaries of data are well established or clear cut, where there are only two or three datasets to integrate, or if it is used in collaboration with another technique.

Two other principal methods for combining and analysis also exist. The first uses the location of 'known' gold deposits, assessing their spatial location against other datasets, as a way to help predict areas favourable for mineralisation. This is a probabilistic method and is known as the "weights-of-evidence" approach. The second method uses an "expert-systems" approach whereby the *user* defines or judges the importance of each input dataset. In this method the importance placed upon the input criteria can be derived from any number of sources, hence its name. The principal difference between these two is how the 'weights', in this case its correlation and therefore the importance placed upon a dataset, are calculated. The probabilistic method is in effect a hands-off technique with weights calculated purely on a mathematical spatial association to known gold deposits, whilst the expert method is hands-on. Both appear to hold great appeal as flexible methods of data integration.

6.3 Weight-of-evidence: The methodology.

A logical approach when looking for mineralisation is to go to known areas of mineralisation and see if it is possible to establish any predictor relationships to other input source data. By doing this one can help to establish a framework which suggest the most favourable conditions for gold, these conditions can then be translated to the gold data set and sites prioritised accordingly.

Work by Bonham-Carter et al., (1988), Agterberg (1989), and Bonham-Carter and Agterberg (1990) report upon the weights-of-evidence through the use of

Bayesian probability. Their method involves converting all input maps to (raster) binary layers prior to analysis. Each criterion is then overlaid with the known mineral occurrences and weights are calculated (W^+ and W^-) based upon the number of occurrences lying within or outside of the binary pattern area to total area. As the weights are mathematically derived, in essence from an occurrence-to-area calculation, it removes the necessity for any user expert judgement in their calculation. A further feature of this method is that proximity analysis can also be incorporated in the binary theme. Therefore distance buffers can be developed around criteria to establish any spatial significance. In these circumstances a range of weights result and the selection of the most appropriate cut-off (i.e. the point at which the predictive power is maximised), is determined from the point at which the contrast between W^+ and W^- is seen to be at its greatest. Once the conditional probabilities have been calculated and corresponding weights derived, an *a posteriori* probability map of gold occurrence can be calculated from the combination of the prior probability added to the summed weights, where there is a unique overlap of the binary maps.

The mathematics of this procedure, as set out below, is taken directly from Bonham-Carter et al., (1988)

- Calculation of the conditional probability is as follows:

$$\begin{aligned}
 p(j|d) &= A_{dj} / A_{dt} \\
 p(j|\bar{d}) &= (A_j - A_{dj}) / (A_t - A_{dt}) \\
 p(\bar{j}|d) &= (A_{dt} - A_{dj}) / A_{dt} \\
 p(\bar{j}|\bar{d}) &= (A_t - A_j - A_{dt} + A_{dj}) / (A_t - A_{dt})
 \end{aligned}$$

A_{dt} = Number of 1Km² units containing a deposit in the total study area.

A_{dj} = Number of 1Km² units containing a deposit in pattern j

A_j = Area of pattern j, Km²

A_t = Total study area, Km²

- Calculation of pattern weights:

$$\begin{aligned}
 W_j^+ &= \ln\{p(j|d) / p(j|\bar{d})\} \\
 W_j^- &= \ln\{p(\bar{j}|d) / p(\bar{j}|\bar{d})\}
 \end{aligned}$$

- Calculation of *a priori* odds (probability of a gold deposit occurring within a known Size, e.g. 1 Km²)

$$O_{\text{prior}} = P_{\text{prior}} / (1 - P_{\text{prior}})$$

- Calculation of the *a posteriori* odds:

$$O_{\text{post}} = \exp \{ \ln (O_{\text{prior}} + \sum_{j=1}^m W_j^k) \}$$

$$W_j^k = \left\{ \begin{array}{l} W_j^+ \text{ if pattern } j \text{ is present} \\ W_j^- \text{ if pattern } j \text{ is not present} \\ \emptyset \text{ if pattern } j \text{ is unknown} \end{array} \right\}$$

- Calculation of the *a posteriori* probability of a gold deposit occurring:

$$P_{\text{post}} = O_{\text{post}} / (1 + O_{\text{post}})$$

For further procedural information the author directs the reader to the three papers referenced at the beginning of this section.

6.3.1 Implementation and results of the weights-of-evidence approach.

As there is no current GIS software that can implement the Bonham-Carter 'weights' theory a program was developed within the ERDAS Imagine 'model-maker' language. There were a number of reasons for choosing Imagine's model-maker facility over an external stand-alone program:

- 1) To keep the analysis functioning within a GIS system, and one which is fully compatible to ArcInfo coverages. This in itself is time resourceful.
- 2) The program is developed through the use of symbols (as opposed to script) and this versatility allows greater user ease and flexibility to modify the operations.
- 3) The design of the program allows the user to browse any of the results as files, tables or images, which allows possible errors to be more easily identified and rectified.

Before the implementation of stage (1) all coverage criteria must be individually selected (i.e. to contain only one unique feature) and converted to raster format. The first stage of the weights process, as described in Fig. 91, is a method of creating a mask around the input image (the analysis window) and recoding the input image-id as to where the feature is present, is not present and outside of the analysis window. It is this recoded image which acts as the associate image coverage to be overlaid with the gold point occurrence raster image for the calculation of the weights, as set out in

Fig. 91 Stage 1. Process of selecting and masking coverage criteria to study area with a recode facility which enables new image input into Stage 2.

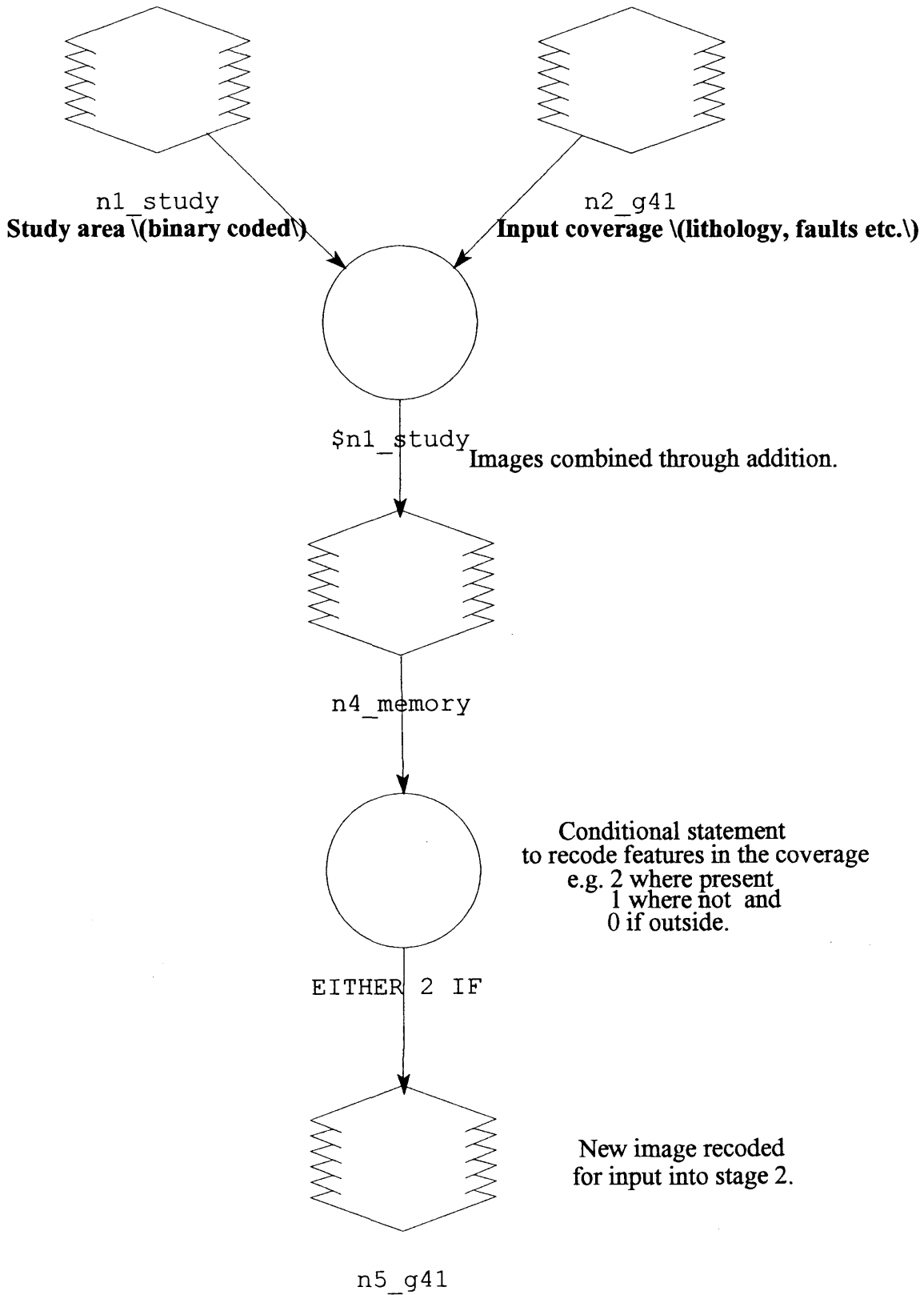


Fig. 92 Stage 2. Process for computing the weights.

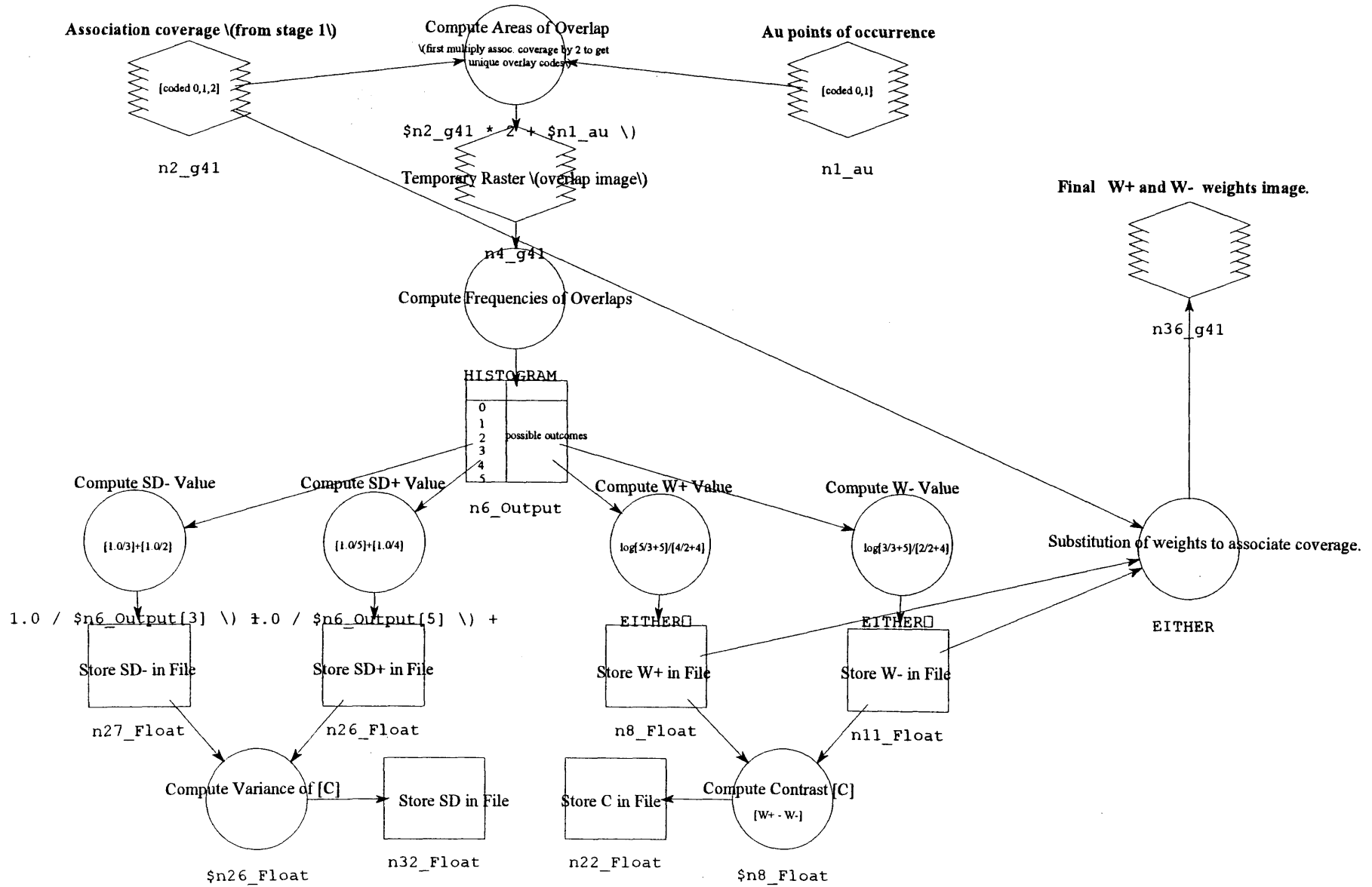
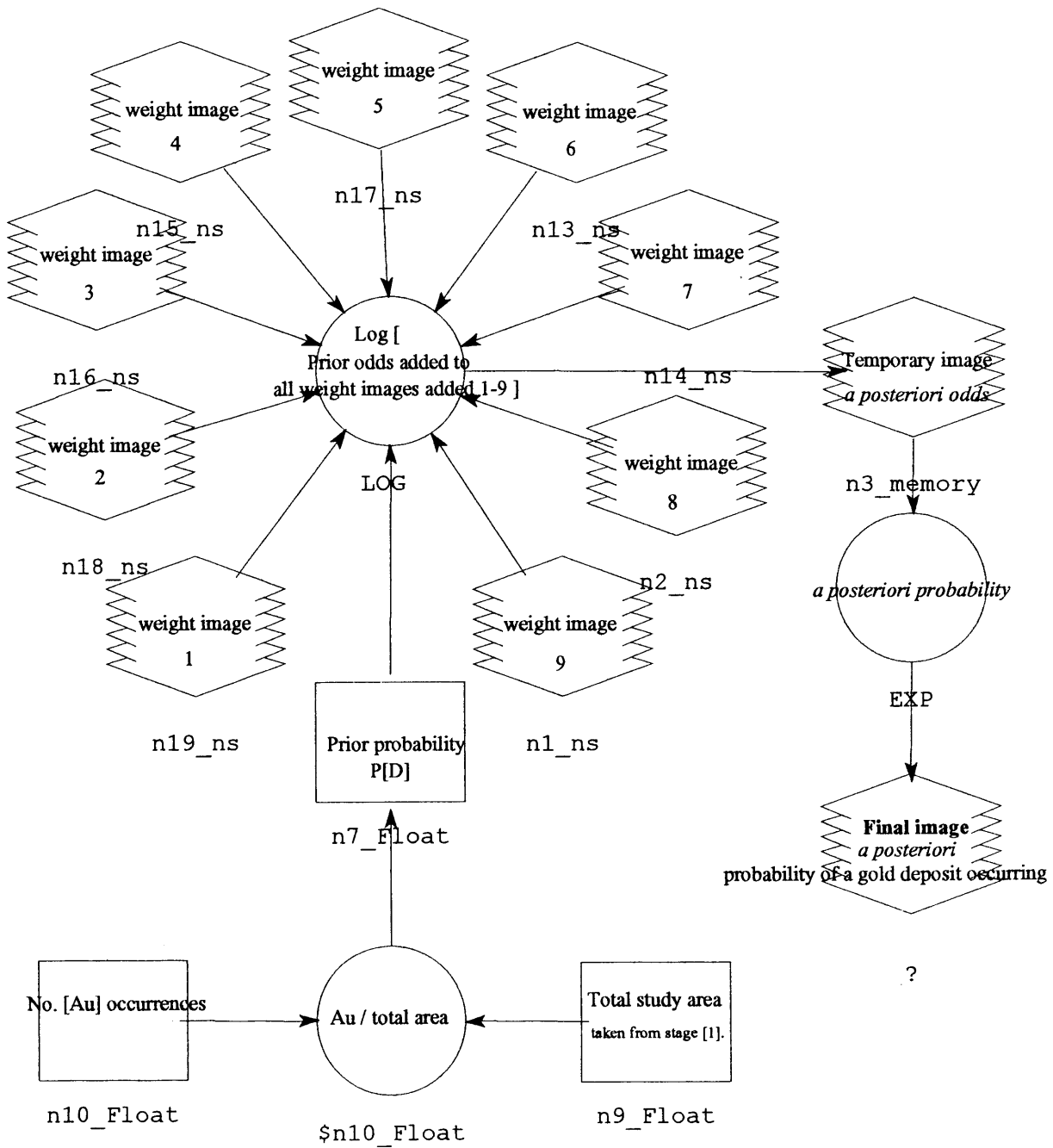


Fig. 93 Stage 3. Calculation of the a posteriori , weights combined.



Prior odds = $P[D] / 1 - P[D]$

Stage 2, Fig. 92. Stage 3, Fig. 93 represents the final construction of the Au posteriori probability map in which all unique weight conditions are accumulated into a single output image. As can be observed from these figures the retrieval of any numerical value or resultant image can be easily viewed with each of the individual file storage facilities or in the form of a raster image, where appropriate.

For the construction of the gold occurrence map, only the sites designated by the mining symbol were selected from the 1:200,000 geological map, thus no alluvial sites were included. This gave a total of 11 Au sites. However, BHP data (as revealed previously in Fig. 5 Chapter 2) indicates not only a number of other old and new sites that are not shown on the published geological map, but also a more precise spatial position of the Syama mine. This additional information raised the total to 18 Au sites (Tembelini and Baba were excluded due to some uncertainty as to whether they were mines or just mine waste). One of the advantages of using a GIS to implement this methodology is that 'new', updates, or corrections within data can be more easily managed. The key issue which therefore arises here is: how important is this additional gold information to the results? Work by Barr (1990) suggested that in his particular investigation the number of deposit occurrences made very little difference to the overall result obtained.

To test this, the first set of weight analyses were performed with lithologies selected from the geology coverage. Table 51 illustrates the results from the analysis with the original 11 sites, whilst Table 52 are the results obtained with the additional BHP sites.

Table 51 Au deposits from geology map (1:200,000) only. (Total = 11 Au deposits).

Lithology	W +	W -	C (contrast)	Sig. +	Sig. -	Sig. C (Contrast)	Au no.
Bs (g26)	1.13105	-1.03181	2.16286	0.12503	0.33334	0.45837	8
Ba (g40)	0.52251	-0.08658	0.60909	0.50007	0.11112	0.61119	2
Bv (g25)	4.03836	-0.09371	4.13207	1.00474	0.10001	1.10475	1
Bj (g41)	N/A	N/A	INF.	N/A	N/A	INF.	0
BB(g28)	N/A	N/A	INF.	N/A	N/A	INF.	0

Table 52 Au deposits taken from BHP and geology map (making additional sites total = 18 Au deposits).

Lithology	W +	W -	C (contrast)	Sig. +	Sig. -	Sig. C (contrast)	Au no.
Bs (g26)	0.95707	-0.67701	1.63408	0.09094	0.14287	0.23381	11
Ba (g40)	0.02998	-0.00369	0.03367	0.50007	0.06251	0.56258	2
Bv (g25)	3.54583	-0.05555	3.60138	1.00474	0.05883	1.06357	1
Bj (g41)	3.15469	-0.11303	3.26772	0.50160	0.06251	0.56411	* 2
BB (g28)	3.88041	-0.05601	3.93642	1.00662	0.05883	1.06545	1

NB: The results show only the lithologies for which intersection comparisons are relevant, all other lithologies showed no Au occurrence intersection and hence are not included in the tables above.

Comparisons between these two results illustrate a number of features:

- 1) By increasing the occurrence number, two new lithologies become important with respect to a weight value.
- 2) By increasing the occurrence number there is an overall reduction in the weight value from those seen in Table (51).
- 3) By increasing the occurrence number there is also a change with regard to the lithology with the highest contributing (W^+) weight, from lithology 'Bv' (undifferentiated volcano-sediment) to the basalt lithology 'BB'.

With regard to this latter point one may like to consider the reason why lithology 'BB' has a higher weight than 'Bv', even though they both have only one intersecting Au occurrence. This is because the weight, as already explained in Section 6.3, is calculated with regard to area. As the area of 'BB' is smaller than 'Bv' it produces a higher weight. This is also apparent with lithology 'Bs' (Birimian greywacke-arkose), which has a comparatively higher number of Au intersections (either 8 or 11), yet its weights are lower due to its larger area. Should that in reality make the probability of finding gold any less or more significant? This very issue reoccurs in a later weight analysis.

Another interesting feature highlighted through these results, is that of the number of Au sites intersecting with lithology 'Bj' (Birimian volcano-sedimentary unit). This unit is known through both literature reviews of neighbouring countries and those of BHP to be an important lithology with respect to hosting gold (Chapter 2). Yet the maximum number of gold

intersections here are 2 (or possibly 3 if account of omission errors due to cell size, identified by * in table 52), why so few? This time the issue is not wholly a response to the actual number of Au deposits, but more a reflection of spatial misrepresentation of 'Bj' on the 1:200,000 geological map. For example, the Syama mine is located within the Volcano-sedimentary unit. However, even accounting for its correct spatial position from current BHP maps, it still fails to intersect with this unit as it is represented on the geological map. This signifies the spatial misrepresentation of the unit. To help ascertain the impact this has upon the results shown in Table 51 and 52 a further weight was calculated for lithology 'Bj', but this time BHP's VLF structural data defined the perimeter of the unit. As illustrated in Fig.5 Chapter 2, this additional information only covers BHP's original concession area and not the full extent of the unit (for that the magnetic data could have been used). However this should not detract from the point under discussion.

Table 53 'Bj' Weight calculation accounting for extended spatial extent.

Lithology	W +	W -	C (contrast)	Sig. +	Sig. -	Sig. C (contrast)	Au no.
Results using original geol		map deposits	11 deposits.				
VLF +Bj (g41)	3.20332	-0.30731	3.51063	0.33402	0.12501	0.45903	3
Results using BHP and		geology map	18 deposits				
VLF + Bj (g41)	3.56081	-0.48136	4.04217	0.14354	0.09092	0.23446	7

Correcting for the spatial position of the 'Bj' unit has had, in the case of the 11 deposit occurrence, a significant effect compared to the previous results of Table 51. For now the volcano-sedimentary unit has not only gained a weight (unlike previously) but it also ranks second highest in its correlation to mineralisation. Similarly, with the 18 deposit occurrence the observable rise in weights and its high contrast place this lithology in the highest first rank position, above that of 'BB'. This is because the majority of 'BB' lithology resides within the new 'Bj' perimeter, especially the mineralised location. In both these case the increase observed in the 'Bj' weights can only be gained

at the expense of another lithology, this falls to the detriment of neighbouring lithology 'Bs', which has the effect of lowering the W^+ contribution seen in Table 51 and 52.

The results do show two important and fundamental points:

- 1) The importance lies not just with the number of gold deposit occurrences but also their spatial position, for these both make a difference with respect to the significance of a lithology. (Therefore subsequent analysis will use all 18 occurrences).
- 2) The results are naturally a reflection of the input data, but when the input data is incorrect the effect can be quite significant on the results. Awareness is therefore important when implementing this technique.

One of the other features that can be accounted for by this probabilistic method are 'unknown' areas. This can be a common feature in mineral exploration where a technique may have only been used within a smaller area of the total; the magnetic data is such an example. In these situations the 'unknown' (the area difference between total window of research and the new smaller area) is coded to zero, which in effect means the pattern is neither present or absent. Using this procedure on the magnetic polygon coverage, that maps the areas of high structural activity, the weights were calculated to establish if there was any spatial relationship to known mineral occurrences. Although 18 occurrences were used only 13 fall within the analysis area, with the remaining 5 lying within the 'unknown' region.

Table 54 Weights for high structural magnetic activity.

Lithology	W +	W -	C (contrast)	Sig. +	Sig. -	Sig. C (contrast)	Au no.
Magnetics --- high structural environment							
All-high-responses	0.77659	-1.37881	2.15540	0.09101	0.50007	0.59108	11
Optimum buffer 250m	0.67490	N/A	N/A	0.07701	INF	INF	13

The results of Table 54, indicate 11 out of 13 Au occurrences lie within areas described as “high structural activity”. It is also possible through visual examination of the overlay image (Fig. 92), to further categorise this result into: 8 of 11 relate to the Birimian volcano-sedimentary unit, 2 of 11 relate to the E-W dyke and 1 lies within the eastern structural mass (which is also approximately 160 m from an area denoted as a likely intrusion, Class (5), Figs. 88, 89 and 90. The other remaining two occurrences can be captured through spatial buffering, for both appear to lie within 250 m distance from the edge of areas with high responses. Both these results suggest that there is a strong spatial association (which extends to within 250 m) between known gold occurrences and areas of high structural magnetic activity.

The ability to incorporate proximity analysis, through the spatial buffer feature is of interest in mineral exploration when wanting to assess, for example, the spatial relationship of faults to mineralisation. Weight analysis was therefore conducted upon buffered faults. However, fault information was available from a number of sources. The first was that taken from the published geological maps 1:200,000 (as is shown superimposed upon the geology map of Fig. 4, Chapter 2). The second is that from the BHP in-house magnetic map (1:100,000), and the third is from BHP’s VLF analysis (1:25,000). The theme which arises here is one of scale and level of detail and the issue is therefore, “does scale and detail matter?” If so, which of these data sets is the most informative? Table 55 lists the weight analysis results.

Table 55 Fault buffering from different source data and combinations.

Faults Non-directional	W +	W -	C (contrast)	Sig. +	Sig. -	Sig. C (contrast)	Au no.
(A) Faults from geology map (1:200,000)							
Buffer 250 m	N/A	N/A	N/A	N/A	INF	INF	0
Buffer 500 m	-0.50020	0.03893	-0.53913	1.00008	0.05883	1.05891	1
Buffer 750 m	0.46605	-0.10114	0.56719	0.25005	0.07144	0.32149	4
Buffer 1000 m	0.39261	-0.11768	0.51029	0.20004	0.07693	0.27697	5
Buffer 1250 m	0.63506	-0.31923	0.95429	0.12503	0.10001	0.22504	8
Buffer 1500 m	0.67783	-0.47955	1.15738	0.10003	0.12501	0.22504	10
Buffer 1750 m	0.71176	-0.70232	1.41408	0.08336	0.16668	0.25004	12
Buffer 2000 m	0.81496	-1.33150	2.14646	0.06669	0.33334	0.40003	15

(B) Faults from BHP magnetic interpretation							
Buffer 250 m	1.62385	-0.47134	2.09519	0.16705	0.12503	0.29208	6
Buffer 500 m	1.52895	-1.08454	2.61349	0.10021	0.25004	0.35025	10
Buffer 750 m	1.19939	-1.01035	2.20973	0.10015	0.25004	0.35019	10
Buffer 1000 m	1.08260	-1.23102	2.31362	0.09103	0.33338	0.42441	11
Buffer 1250 m	0.91362	-1.16192	2.07554	0.09101	0.33338	0.42439	11
Buffer 1500 m	0.77940	-1.09354	1.87294	0.09099	0.33338	0.42438	11
Buffer 1750 m	0.75461	-1.43003	2.18464	0.08341	0.50005	0.58346	12
Buffer 2000 m	0.66145	-1.36185	2.02330	0.08341	0.50006	0.58347	12
(C) Faults from BHP magnetic and VLF.							
Buffer 250 m	1.86223	-1.13516	2.99739	0.10029	0.25004	0.35033	10
Buffer 500 m	1.49748	-1.34715	2.84463	0.09109	0.33337	0.42446	11
Buffer 750 m	1.22616	-1.27838	2.50454	0.09105	0.33337	0.42442	11
Buffer 1000 m	1.03357	-1.21263	2.24620	0.09102	0.33338	0.42440	11
Buffer 1250 m	0.87460	-1.14345	2.01805	0.09101	0.33338	0.42439	11
Buffer 1500 m	0.74684	-1.07472	1.82156	0.09099	0.33338	0.42437	11
(D) Faults from geology plus BHP map data all data combined.							
Buffer 250 m	1.35100	-1.04821	2.39921	0.10017	0.25004	2.39921	10
Buffer 500 m	0.91505	-1.16258	2.07763	0.09101	0.33338	0.42439	11
Buffer 750 m	0.62443	-0.99434	1.61877	0.09098	0.33339	0.42437	11
Buffer 1000 m	0.42524	-0.81982	1.24506	0.09097	0.33340	0.42437	11
Buffer 1250 m	0.36799	-1.04636	1.41435	0.08339	0.50008	0.58347	12
Buffer 1500 m	0.34074	-1.55895	1.89969	0.07697	1.00009	1.07706	13

Due to the aerial extent of the VLF it is analysed in conjunction with the magnetic and geology map data, as shown with results (C) and (D).

The results of these analyses are very interesting because in situation (A) there is assumed no mineral intersection (i.e. no association) within 250 m of any fault. The W^+ and contrast values then increase steadily throughout all the buffer distances, due to the fact that progressively more mineral deposits coincide, until the maximum contrast is reached at 2000 m. According to this mathematical procedure 2000 m represents the point at which the predictive power of the pattern is at its maximum. However, the question which should be asked is, "is this result reasonable, considering the low density of faults illustrated on the map?" Also, is it not possible that what this result is suggesting is in fact a negative-correlation to faults with distance?

To investigate this further the in-house BHP data were analysed, the results of which are shown by (B). Using the same number of occurrences, but with restricted area, the results are very different. This time the maximum contrast is at a substantially smaller distance from the faults than previously seen, now

at 500 m as opposed to 2000 m, and there is also Au intersection within 250 m. The principal reason for this is that, unlike in (A), this structural information shows more detail within the Volcano-sedimentary unit 'Bj', and therefore it has a closer spatial location to many of the Au sites.

This is reiterated in (C) where the combined magnetic and very detailed VLF (which this time shows an even closer spatial proximity to many of the Au sites), causes the maximum contrast to be reduced further to 250 m, although the 500 m contrast is also high with respect to this value. By the time the buffer reaches 1500 m and beyond any added benefit gained from using the VLF is lost and the results become virtually identical to those from (B).

The results of (D) reflect what happens when all map data are combined together. Once again the dominating influence upon where the maximum contrast lies is driven primarily by the incorporation of the VLF data, at 250 m.

The overall impression from these results suggests that the level of fault detail (which in this case is related to a reduction in scale) and their spatial position does project a strong influence on to which of the buffers possess the maximum weight contrast. The dilemma of selecting the most appropriate or representative result is as much an issue of whether results derived from a source at 1:25,000 scale fall within the 'regional' theme for analysis.

In Table 56 a non-geological aspect has been analysed. Here an attempt is made to see if there is any possible spatial link between gold occurrence and altitude or position within the landscape. The altitude ranges are taken from the original contour data.

Table 56 Weights according to spatial location within the landscape.

Altitude (H)	W +	W -	C (contrast)	Sig. +	Sig. -	Sig. C (contrast)	Au no.
H ≤ 320 m	N/A	N/A	INF.	N/A	N/A	INF.	0
H 321-359 m	-0.61469	0.55259	-1.16728	0.16667	0.08333	0.25000	6
H 360-399 m	1.76044	-0.83343	2.59387	0.09091	0.14286	0.23377	11
H 400-439 m	N/A	N/A	INF.	N/A	N/A	INF.	0
H ≥ 440 m	5.23860	-0.05686	5.29546	1.00040	0.05882	1.05922	1
H ≥ 360 m	1.71924	-0.97138	2.69062	0.08333	0.16667	0.25000	12

To induce some clarity these results do require some explaining. The weights suggest that the probability of finding gold at or below an altitude 320 m is none; that is all known deposits are sighted at altitudes greater than this. This is a positive result considering alluvial gold sites have been excluded. However, the results also imply that the strongest spatial association between gold occurrence and altitude resides at altitudes equal too or greater than 440 m, as this is the highest (W^*) weight. Yet this result is based upon only one occurrence. The reason for this high positive weight is because the calculation is also based upon area, as explained previously, consequently the small area produces a high weight. The altitude band 360-399 m produces the second highest weight, whilst 321-359 m is ranked third. As the 400-439 m band has no gold intersection the result implies that it is of no consequence with respect to finding gold, but this could be viewed as somewhat peculiar considering both altitude bands above and below intersect gold deposits.

Therefore it is probably more appropriate to reassess the probabilities as the probability of finding gold above or below 360 m because by doing this you are also combining areas into one maximum and removing some of the bias imposed by small areas. The last record in the table illustrates this.

Overall, the data suggests that the probability of finding gold increases (or is more likely) with attitude. The fairness of this assumption is addressed and discussed in the following section (6.3.2).

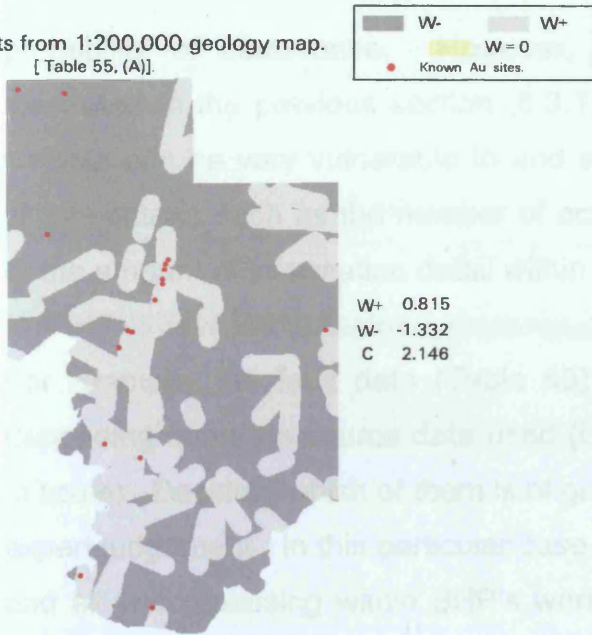
Some of these weight table results have been illustrated in Fig. 94 for visual clarity.

6.3.2 Weights of evidence: discussion of results.

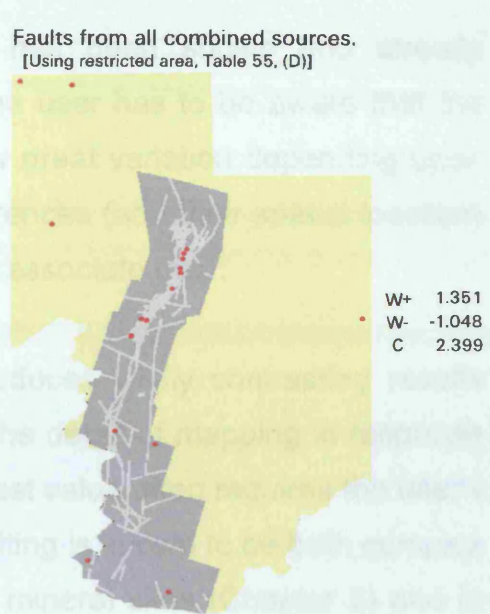
One of the principal advantages of the weights-of-evidence approach is that it removes the requirement for expert judgement in calculating the weights. However the resultant weights are the important component for they highlight both spatial correlation and are also used in an additive form as a map for the

Fig. 94 .Weight result illustrations.

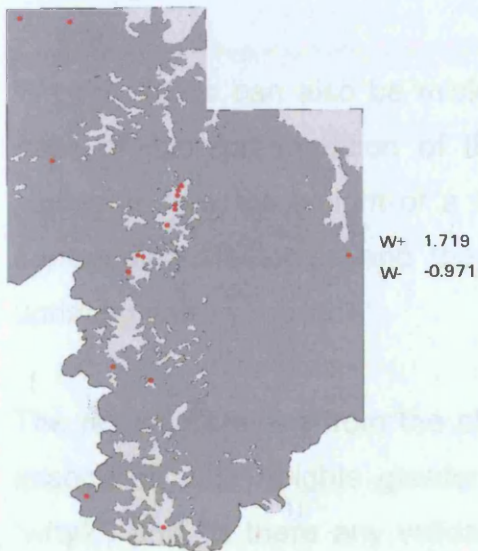
Faults from 1:200,000 geology map.
[Table 55, (A)]



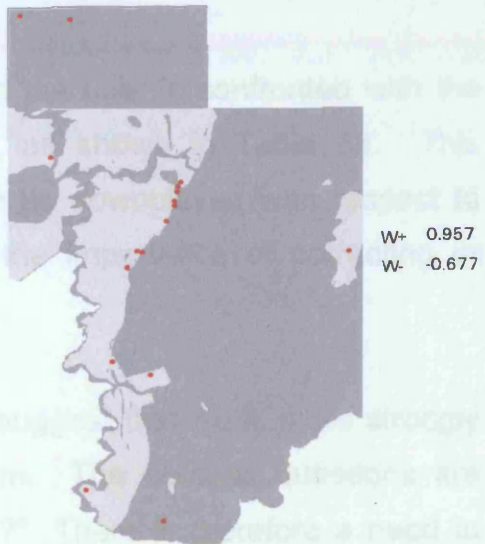
Faults from all combined sources.
[Using restricted area, Table 55, (D)]



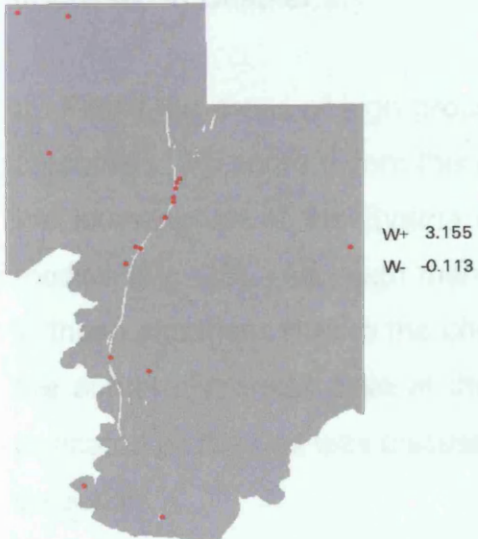
Topographic data - height ≥ 360 m
[Table 56]



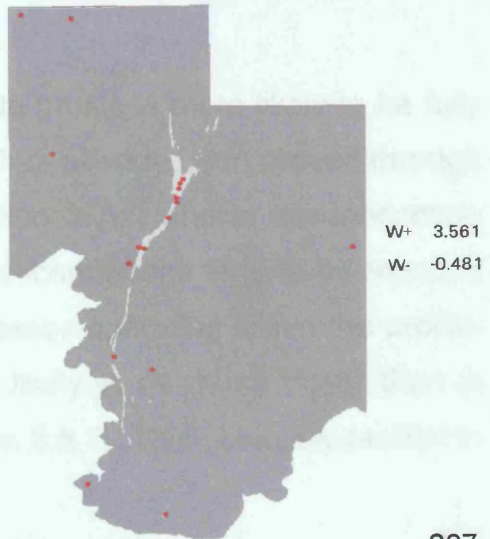
Geology - lithology 'Bs' [g26].
[Table 52]



Geology - lithology 'Bj' [g41]
[Table 52]



Geology - lithology 'Bj' [g41] updated
[Table 53]



probability of occurrence. However, as has been shown and already discussed in the previous section (6.3.1), the user has to be aware that the weights can be very vulnerable to and show great variation depending upon simple criteria such as the number of occurrences (and their spatial location) or the amount of information detail within the associate map.

For example, the fault data (Table 55) produces wildly contrasting results depending upon the source data used (i.e. the detail of mapping in response to scale). Deciding which of them is of greatest value often requires the user's expert judgement. In this particular case faulting is known to be both complex and all encompassing within BHP's worked mineral sites (Chapter 2) and in this respect the combination magnetic structure with geological map source provides a more realistic value to the results.

Weight results can also be misleading when the user is confronted with the case of misrepresentation of the lithology, as shown in Table 53. This highlights how the weight of a lithology can be downplayed with respect to surrounding lithologies and therefore sets the importance of correcting or updating data.

The results obtained from the altitude data suggest that Au is more strongly associated with heights greater than 360 m. The obvious questions are "why?", and "is there any validation for this?" There is therefore a need to assess this with regard to knowledge gained from laterite landscapes, as discussed in Chapter 3.

□ Firstly, on areas of high ground the laterite profile is more likely to be fully preserved. To some extent this assumption has already been proved through the examination of the Syama data in Section 3.7.1, and in the landscape models (Fig. 29). Although many element concentrations tend to be reduced in these situations due to the chemical processes operating within the profile, the actual dispersion halo at the surface is likely to be much larger than in truncated profiles as was discussed in Section 3.8.1. This obviously facilitates detection.

□ Secondly, other factors which can complicate mineral detection are depositional environments. These situations tend to typify low ground and especially those areas which are flat. The allochthonous mixing can weaken, or blanket the underlying signals making them hard to detect or even create a falsification. Whereas areas of high ground are reflective of an in-situ deposition environment (even to some degree on the upper slopes), and as there is little or no external mixing of source, detection is made easier. In fact, through integrating the slope data with that of height some further detail can be gained with respect to known gold occurrences:

- Of the 12 sites located at ≥ 360 m
 - 6 are located on flat land and
 - 6 are located on slopes.
- Of the 6 lying between 321-359 m:
 - 5 lie between 321-330 m on flat land and
 - 1 lies between 350-359 m on a slope position.

□ Thirdly, it should not be discounted that Au sites located at the ≥ 360 m altitude could be reflecting areas of secondary enrichment within the laterite profile, that have not been removed by erosion.

The results therefore are not suggesting that ground greater than 360 m is the only place that gold may occur, but that the chances of detection in such situations are much improved, even on the upper slopes, and this is especially so when dealing with sample spacing from regional survey programs.

The final point of issue is that concerning the number of known gold occurrences. In the example presented by Bonham-Carter et al., (1988) a total of 70 known gold occurrences were used to map spatial association, whilst Bonham-Carter and Agterberg (1990) used 68. These numbers are considerably more than the 11 and 18 tested here. But does the number of occurrences truly make a difference?

Work by Barr (1990) reported broadly similar results when buffering features and using either 35, 25, 15 or 6 occurrences, but that could also be a factor of

number of occurrences (and their spatial location) did make a difference with respect to the level of correlation or the weighted significance given to a lithology.

It is also noted here, and similarly in the work of Barr (1990), that when working with a relatively small number of known deposits occasions arise when there is neither an occurrence within the pattern, or alternatively outside. In these situations erroneous readings are produced, so how should these be treated: as either perfect correlations or as perfect anti-correlations? Similarly, using a small number of known deposits when buffering can also cause the weight contrast to “flex” i.e. increase, decrease, and then increase again. For example, if consecutive buffer distances repeatedly intersect say the same 11 occurrences, then the weight will naturally decrease because the area takes precedence. However, when there is the addition of a new known occurrence then the weight contrast increases and if, in the next buffer, another occurrence is captured then it increases yet further because the additional area becomes less significant with respect to the increasing deposit number. This is highlighted to some extent in part (D) of Table 55. There is therefore the possibility that two numerically similar weight contrasts could exist at one time! In such a case perhaps selecting on the basis of the largest W^* would suffice.

Ultimately, what the author has attempted to highlight through these worked examples is that although this method produces weights that, through their calculation, remove the requirement for expert judgement, there is still a component of expert judgement which remains fundamental (especially when dealing with so few deposits). Although the results produced are of some value the author feels that perhaps given so few deposits this method is not the most appropriate technique with respect to this research data. However, this is not to suggest that the results obtained could not be used advantageously in conjunction with the next technique, the expert-system approach.

6.4 The expert–system approach: The methodology.

The expert-system approach as discussed and used here is that of multi-criteria-evaluation implemented in the Idrisi32 GIS software. In this method of analysis the user is required to make judgemental decisions throughout all stages of the operation.

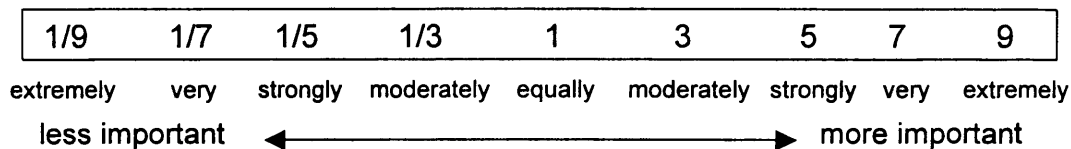
The first decision to be made is whether the nature of the objective to be achieved and the contributing input data source(s) are either singular or multiple in character. The second stage of judgemental input concerns the method of data aggregation used in order to produce a single index of evaluation or suitability. To achieve this each component contributing to an input layer (referred to as a “criterion”) is given a user-defined score. The score can range anywhere between 0-1 on a real number scale, or alternatively if using a byte scale (as adopted here) between 0-255. The implications are that the higher the score given, the more *likely* it is that the component belongs to or is important to the overall objective being sought. This type of scoring can also accommodate criteria that are thought to belong to a fuzzy set, as opposed to data that clearly form crisp sets. This feature is of use, for example, when incorporating data from proximity analyses. In these situations the user can define the membership function and the appropriate score range.

As well as providing individual criterion scores, it is also possible to develop *constraint* criteria layers. These are in effect Boolean masks (e.g. containing data with values such as yes/no, 0/1, present/absent, and so on) that act to eliminate areas from where results are not required, for whatever reason.

Once criterion scores have been established the next stage is to apply criterion weights. These are derived through a process of subjective judgement and expert opinion, which involves the pairwise comparisons of all the criteria (as developed by Saaty’s technique, see Idrisi user’s guide 1999) as to their suitability in fulfilling the stated objective. This is commonly achieved through the use of a nine-point continuous rating scale as illustrated

below in Fig. 95 with the results placed into an $n \times n$ matrix, where n is the number of criteria to be used in the analysis.

Fig. 95 Continuous rating scale for use in the pairwise comparison matrix.



A *best fit* set of weights is then computed by calculating the principal eigenvector of the pairwise comparison matrix. To accompany these weights Idrisi also produces a consistency ratio that assesses the degree of consistency used in the ratings. Provided the value is not greater than 0.10, then the probability is that the ratings were not randomly generated.

The final stage in the production of a “suitability map” is the aggregation process. The Idrisi software provides two methods for combining the individual scaled criterion scores. One approach is the Weighted Linear Combination (WLC). This multiplies and then sums all criterion scores by their associated criterion weight factor, followed by the elimination of any constraint areas using a multiplication mask. The approach can be described algebraically as shown below (taken from the Idrisi user’s guide):

$$S = \sum w_i \cdot x_i \quad \text{where} \quad \begin{array}{l} S = \text{suitability} \\ w_i = \text{weight of factor } i \\ x_i = \text{criterion score of factor } i \end{array}$$

or

$$S = \sum w_i \cdot x_i * \prod c_j \quad \text{where} \quad \begin{array}{l} c_j = \text{criterion score of constraint } j \\ \prod = \text{constraint product} \end{array}$$

The second approach is an adaptation of the first known of as the Ordered Weighted Average (OWA). In this method the order of the criterion weights is further modified within each analysis cell (pixel) allowing the final outcome to take on a bias towards either greater “risk adversity” or greater “risk acceptance” (see the Idrisi user’s guide for more detail). In this work only the weighted linear combination method has been utilised.

6.4.1 Implementation of the expert-system approach.

The first stage as explained in Section (6.4) is concerned with identifying the type of approach required to help solve the problem under investigation. As there is effectively a single objective and many contributing data layers Idrisi's "single objective–multi-criteria" decision method has been selected as the method for evaluation.

Prior to the second stage all input criterion coverages had to be converted to raster images, where necessary, and then imported into Idrisi. The Idrisi software requires that all images be of the same resolution in order to perform the WLC analysis, so some resampling was undertaken to attain the chosen resolution of 80 m. Idrisi also requires all input sources to have the same areal extent. This of course is not immediately possible with this dataset due to the smaller areal coverage of the radiometric and magnetic data compared to other inputs. Consequently, two analyses were run. The first was performed on the smaller area covered by the radiometric-magnetic region, but this could therefore incorporate all data in the analysis. The second utilised a larger area (as determined by the geochemical survey), but in this case the results would be based upon a subset of criterion inputs. Results from the later would exclude any information derived from the processing of the radiometric and magnetic data. Although procedurally this becomes lengthier, it allows for some comparison between results.

The second stage, as explained in the previous section, requires scores to be developed for each individual input criterion (and scaled between 0-255). To achieve this the 'user' must decide on the *relevance* or importance of the theme under consideration, as in this case, to the identification and prioritisation of gold. The score values are therefore based upon a judgement, the evidence for which can come from any number of sources (for example, field experiences; literature reviews; 'weights-of-evidence' probability studies, etc.). A small number of the input datasets are now used as examples, to help illustrate and discuss the theory surrounding the development of their criterion scores.

□ Example (1) The landscape model.

The review of the laterite environment in Chapter 3 revealed laterite to be composed from a number of compositionally different horizons (Fig.9). Those at the base of the profile have undergone the least weathering and are therefore the most similar compositionally to the parent rock, compared to the surface residuum which has become highly altered through prolonged and intense weathering. However, as explained in Section (3.6.4), it is the composition of the horizon which principally determines the level to which elements are retained or released. Consequently a number of key assumptions can be explained through the geochemical landscape model theory, and the discussed examples (Section 3.8.1) which are further substantiated throughout the detailed geochemical examination from Syama (Section 3.7.1). Some of these have already been touched upon in the weights discussion (Section 6.3.2).

On areas of high ground the profile is more likely to be fully preserved (as illustrated at Syama). In these situations the iron at the surface acts to subdue (through leaching) many of the element responses from mineralisation, making their detection more difficult. Therefore it can be suggested that element concentrations on high ground are of greater importance due to the assumption that element concentrations at the surface are more likely to become stronger with increasing depth.

Another important issue, as discussed in the landscape approach and allied to that discussed above, is the ability to distinguish areas of deposition and erosion or areas which represent insitu erosion/deposition from areas of allochthonous deposition. This is very much controlled by the position within the topographic landscape. The principal assumption is therefore that areas of high ground, which have little or no contributing uphill sediment source, represent most likely insitu element responses. This is contrasted with slopes from low altitude areas or flats which suggest an increased likelihood that the element signal has been progressively mixed causing a confused element signal, or possibly elimination or falsification.

The final point is concerned with halo size and detection when using data from regional sample surveys. Although fully preserved profiles indicate a decrease in element response at the surface there is however field evidence to support that this is compensated by an increase in the dispersion halo, compared to areas of lower ground. This has already been explained in the weights discussion (Section 6.3.2), where land exceeding 360 m elevation was identified as the most probable areas in which to find gold. It is not the case that gold is only present at these altitudes but just that the likelihood of detection is increased, especially when using regional sample data, due to a larger halo size and the insitu nature of the sediments. This is compared to detection in areas of lower ground, where mineral concentrations, though often stronger, are hampered by generally smaller dispersion halos and increased sediment mixing. This combination clearly increases the likelihood of evading detection when using regional data.

Both Zeegers and Butt (1992) have emphasised the importance of incorporating regolith landform data into studies, through field mapping or borehole logging. Neither of these has been available in this research. Therefore through the understanding gained in Chapter 3 and from the spatial analysis of known gold occurrences with the 'weights-of-evidence' approach, the author has attempted to incorporate these principals into the terrain model developed in Chapter 5, Section 5.2. By combining the terrain elevation and the slope image the landscape has been rudimentarily dissected into the prominent areas as suggested in Section 3.9 by Zeegers and Butt (1992):

- Areas most likely to represent full profiles and truncated profiles.
- Areas most likely to represent insitu deposition with either no or little contributing sediment mix, through to areas where overburden and mixing increase to a maximum.

The following shows the basis from which the landscape has been dissected, the designated score and its representation and landscape code.

<u>Elevation and slope combined</u>	<u>Score</u>	<u>Likely landscape representation (& code)</u>
≥350 m & flat	255	Full profile, insitu sediment. [A**(0,1)]
≥ 350 m & slope	230	Likely full profile, some semi-residual [A**(1)]
340 – 349 & flat	153	Truncated profile, insitu [B**(0/1)]
340 – 349 & slope	128	Truncated profile semi-residual [B**(1/2)]
320 – 339 & slope	89	Truncated increase semi-residual [B**(2)]
320 - 339 & flat	38	Truncated semi-residual & mixing [B**(2)]
≤ 320 & flat or slope	10	Truncated allochthonous possibly mostly transported in character. [B**(2/3)]

Consequently the highest and most significant score is given to areas where the landscape is high (i.e. the profile is full) and where the surface is flat (i.e. indicating insitu depositional environment). However, with a decrease in topography and the progressive increase in sedimentation and mixing, the score becomes further reduced. Fig 97 illustrates this result.

□ Example (2) The geology.

The scores issued to the lithologies of the geology coverage have arisen from two main sources of combined knowledge:

- Literature reviews, which have focused upon the regional and local geology, much of which was reported in Chapter 2, and
- The spatial location of known Au occurrences which were derived from the weights-of-evidence approach (Section 6.3.1).

In total there were 33 different lithologies (including alluvium) which required a criterion score to be allocated to them.

High scores were automatically given to those lithologies which were known to be gold hosts (as determined from the weights-of-evidence). However the actual value assigned also takes into account the likelihood of finding gold based upon similar geological situations from neighbouring countries.

Consequently, the following scores were given to known gold host lithologies.

<u>Lithology</u>	<u>score</u>
Birimian volcano-sedimentary (Bj)	255
Birimian undifferentiated volcano-sed (Bv)	255
Birimian basalt (BB)	242
Birimian sediments (Ba) & (Bs)	204

Thus the volcano-sedimentary unit (Bj) and the geologically similar (Bv) were given the highest score.

The next set of scores were given to those lithologies which were also known to support mineralisation (i.e. similar base metal) but not identified as gold. The assumption here being that these lithologies could be favourable for further associate mineralisation. Therefore the gabbro, peridotite and dolerites representing (Eo); (Ev); (Ep) and (Epp) were scored at 179.

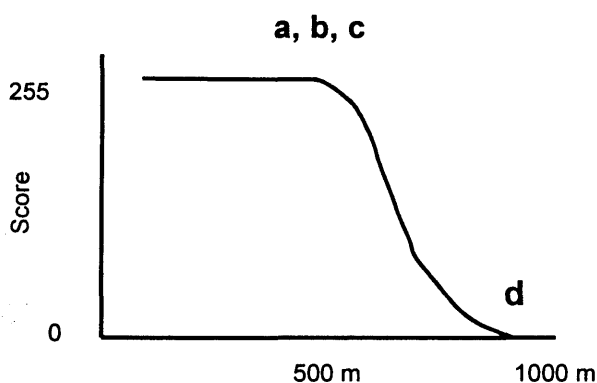
The following scores relate to all other lithologies of the area which are not currently known to be mineralised. As explained in Chapter 2 when discussing the stratigraphy of the region, difficulties arise when trying to chronologically place every lithology. Therefore what is most important is for the coding to differentiate those lithologies that were deposited or intruded around the time of the main mineralising phase against those that came after. A range of similar scores (153-100) therefore arise for lithologies such as the Tarkwaian sediments (Tcg, Tg, Tgr) and the intrusions, representing high heat source and potential fluid circulation (Eza, Ez, Euo, Y/Yb). These are contrasted with the low scores of (51-26) given to lithologies which were deposited or intruded significantly after the Birimian period of gold mineralisation. For example, the Proterozoic sandstones (Gs, Gk, Gr1), or doleritic (Vv) intrusions.

□ Example (3) Faults.

As discussed in the previous section criteria scores can be applied through a fuzzy set membership function. Such an approach has been applied to the fault data through the use of the “s-shaped” sigmoidal function. In Section 6.3.1 various levels of fault detail were investigated to establish the distance

at which known mineralisation is most strongly correlated. Although the results were somewhat conflicting, overall the weights highlighted a reduced spatial correlation with increased proximity from faults, when analysing the combined data. The most promising areas were those located within 500 m from faults, with subsequent 'flexing' of the weights with distance. The function used to model this is illustrated in Fig 96. A code of 255 is used up to the inflection point at (a,b,c) located 500 m from a fault, and thereafter is a steady decay of value significance with further distance. The maximum distance of influence was selected to be at 1000 m, with all locations exceeding this distance coded to Ø. A greater limiting distance could have been selected, due to the 'flexing' of the weights, but it was decided that this value was sufficiently far to represent the observed reduction in correlation with distance (Fig.98).

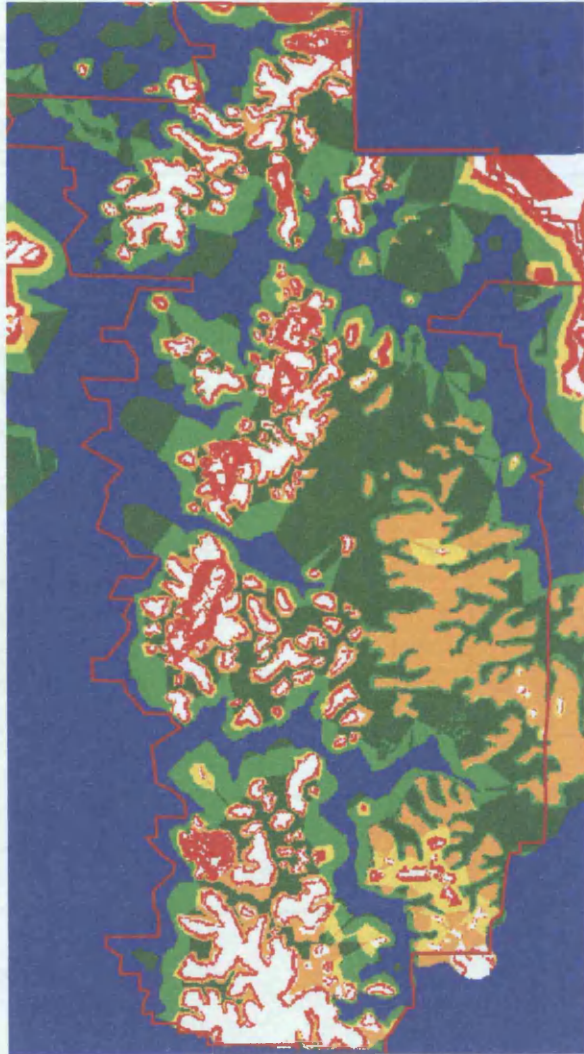
Fig. 96 Sigmoidal membership function, as applied to distance from faults.



In total, criterion scores were developed for 16 input images. The next stage involved assessing the relative importance of each criterion through the method of pairwise comparison. A pairwise comparison matrix was drawn up and a score given for each criterion's overall importance (as illustrated in Fig. 95). However, when making these comparisons the score also takes into account somewhat indirectly the overall comparative reliability of the results produced from each criterion. The matrix results are illustrated in Table 57.

Fig. 97 Criteria scores as applied to landscape.

(illustrated for total area).



- White: $\geq 350\text{m}$ & flat (255)
- Red: $\geq 350\text{m}$ & slope (230)
- Orange: 340-349m & flat (153)
- Yellow: 340-349m & slope (128)
- Green: 320-339m & slope (89)
- Dark Green: 320-339m & flat (38)
- Blue: $\leq 320\text{m}$ & flat/slope (10)

MCE process area
(determined by the geochemical sample area)



Fig. 98 Criteria scores as applied to faults.

(illustrated for total area).

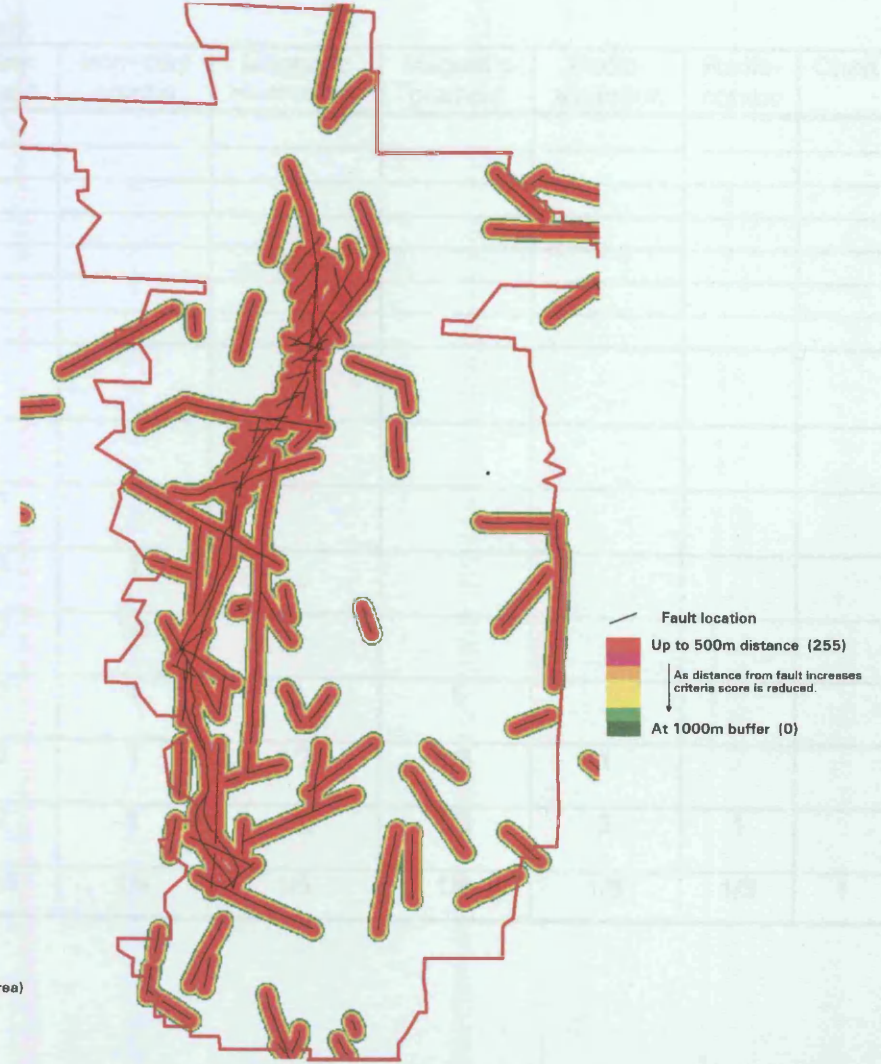


Table 57 Assessing the comparative importance of input factors through the pairwise comparison matrix.

(Rating of the row factor relative to the column factor)

R ↓ C →	Geology	Faults	Au	Cu	Ni	Zn	Pb	Geochem landscape	Iron image	Clay image	Iron+clay combo	Magnetic Hi-structural	Magnetic gradient	Radio-alteration	Radio-combo	Chert
Geology	1															
Faults	1/3	1														
Au	4	6	1													
Cu	4	6	1	1												
Ni	3	5	1/2	1	1											
Zn	2	3	1/3	1/3	1/3	1										
Pb	1/4	1/3	1/7	1/7	1/7	1/7	1									
Geochemical landscape	1	4	2	1	1	2	5	1								
Iron image (TM)	1/3	1/2	1/3	1/3	1/3	1/4	2	1/3	1							
Clay image (TM)	1/3	1/2	1/4	1/4	1/4	1/4	2	1/3	1/2	1						
Iron + clay combo (TM)	1/2	2	1	1	1	2	4	1/2	3	3	1					
Magnetic Hi-structural	2	1	1/2	1/2	1/2	2	3	1	2	2	1/3	1				
Magnetic gradient	2	3	2	1	1	2	5	1	2	3	1	2	1			
Radiometric alteration	1	4	1	1	2	3	4	1/2	3	3	1	1/2	1/3	1		
Radiometric combo(volcano)	2	5	1	1	1	2	4	1/2	2	2	1	1/2	1/3	2	1	
chert	1/3	1/5	1/3	1/3	1/3	1/3	1/2	1/4	1/5	1/5	1/4	1/5	1/5	1/5	1/5	1

The whole principle of devising scores based upon an assessment of relative importance is without doubt subjective and possibly contentious. Nevertheless, for the purpose of illustration, some of the logic or thought processes behind the scores are now discussed for a number of example cases.

The analysis of the TM data has produced two results, one showing potential iron oxide and the other hydrothermal alteration, both of which could be related to mineralisation processes. However as explained in Chapter 5, Section 5.5 and 5.5.1, laterite weathering also produces these minerals and as TM is incapable of differentiating between species a problem does arise. Also the region is vegetated, and although algorithms have been used which account for the interference of vegetation within the pixel, there still remains the possibility (even after top-slicing the data), that some intrinsic vegetation interference remains. Due to these factors, its 'remote' nature and the fact that the results are as much a derivation of landscape process, they are not considered to be as important as results derived from a direct contact method such as the geochemistry or even that from magnetic sources. These are therefore given a lower overall rating.

However, by combining the iron and clay data and seeking coincidences, many individual points are removed and what remains are areas where iron and clay are found together, which by itself could be a much stronger indication of a mineralised area. Consequently, this data set is rated comparatively higher than that from just the iron or just the clay.

Overall, the fault data has been given a relatively low rating when compared with most criteria. The logic in support of this is that the BHP staff West and Witherly (1995) report no specific or unusual structural reason for the gold concentration at Syama. Faulting is known to be present and complex within the volcano-sedimentary unit (as illustrated in Fig.5), which explains why the 'weights-of-evidence' procedure, when using 'combined data', finds strong spatial correlation close to faults (Table 55). However, are faults found within this unit a pointer towards Au mineralisation or just a reflection of differences

in rock competencies between the volcanics and sediments upon rift closure? (see discussion in Chapter 2, Section 2.4). Looking at the situation from the data available from the 1:200,000 scale geological maps it would appear that, in the case of known mineral occurrence, there is little conclusive evidence to support a high rating of faults when compared against other data criteria.

The geochemical data are important because they have been derived from a direct sampling method. Elements other than gold have been selected to help assist in the identification and prioritisation of gold anomalies, through acting as pathfinders. These elements have been selected based upon their correlation with gold which is also substantiated by the gold-sulphide mineral association reported at Syama (Chapter 2, Section 2.65). However, their individual ratings are also a response to their spatial distribution and association from within the landscape. Consequently, the poor spatial correlation observed with Pb and the observed analytical or sampling error in Zn (as reported in Chapter 4) result in lower ratings compared to the other elements, or with other criteria as shown with Pb.

From the comparative pairwise table a *best fit* set of weights is computed for both of the two analyses to be undertaken. However, because Idrisi can only perform a pairwise comparison based upon a maximum of 15 input criteria the chert data was dropped from the smaller area analysis. This input had already been established through the comparison process to be the least significant data source, not least because of its limited spatial extent.

For the small area analysis the criterion weights obtained were:

Geology	0.0549	
Faults	0.0284	
Au-geochem	0.1033	
Cu-geochem	0.1032	
Ni-geochem	0.0928	
Zn-geochem	0.0534	Consistency ratio
Pb-geochem	0.0142	0.07
Landscape	0.0981	
TM-Iron	0.0274	
TM-Clay	0.0228	

TM-combined iron & clay	0.0792
High-structural activity (magnetic)	0.0826
Magnetic gradient	0.0903
Radiometric alteration	0.0747
Radiometric combined basic-type signatures.	0.0757

For the total area the criterion weights obtained were::

Geology	0.0812	
Faults	0.0442	
Au-geochem	0.1539	
Cu-geochem	0.1489	
Ni-geochem	0.1338	
Zn-geochem	0.0867	Consistency ratio
Pb-geochem	0.0199	0.09
Landscape	0.1326	
TM-Iron	0.0421	
TM-Clay	0.0352	
TM-combined iron & clay	0.0977	
Chert	0.0237	

The maps containing criterion scores are then multiplied by their associated weights and the results summed. Once this was completed a final *constraint* criterion was applied across the data to mask out all areas represented by alluvium as identified from the geology maps. The purpose of this was to ensure the removal of any areas of transported overburden or obvious area of intense sediment mixing (as described in the landscape dispersion model) and so eliminate any potential confusion from the resultant suitability map.

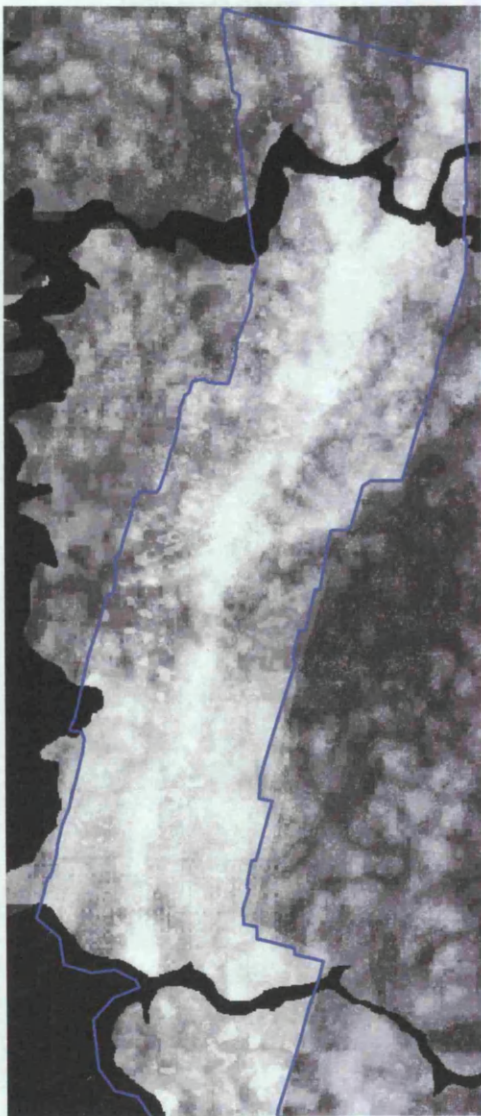
6.4.2 The expert-system discussion of results.

Figures 99 and 100 illustrate the suitability results through a grey scale image, which provides an overall impression, and more importantly by a colour image. Colour images show data from the highest 25% of all values up to the uppermost 0.5%. These 7 classes provide a priority ranking as to the most suitable areas for investigating gold, with area (1) indicating the most important of all locations. From these images it is clear that this technique has highlighted many new locations in which to explore for gold. A significant proportion of these sites lie within the trace of the Birimian volcano-sedimentary sequence, whilst others are characteristically associated with

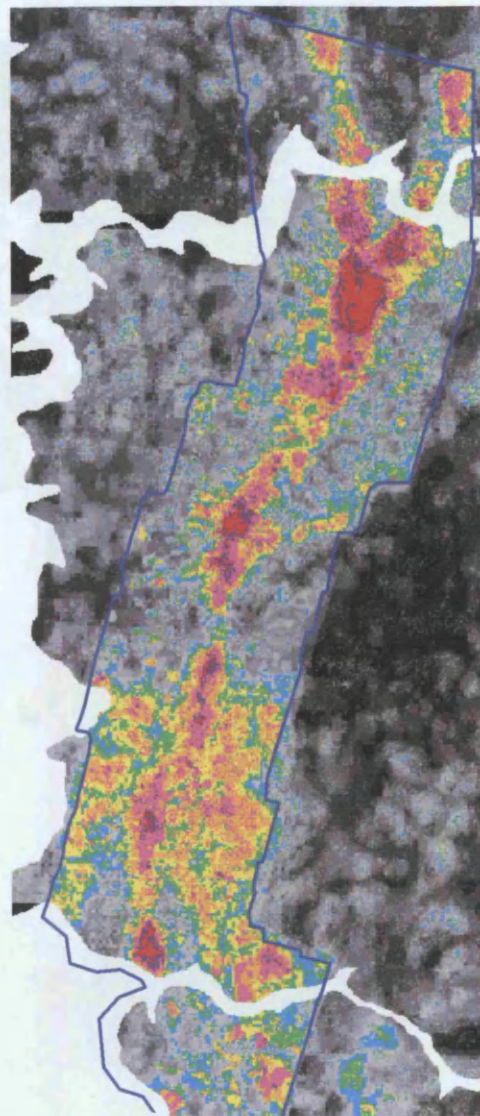
Fig. 99 MCE Results. The 'expert-system approach' .

(based on all data, restricted area)

Grey scale image.



results prioritised based upon %.



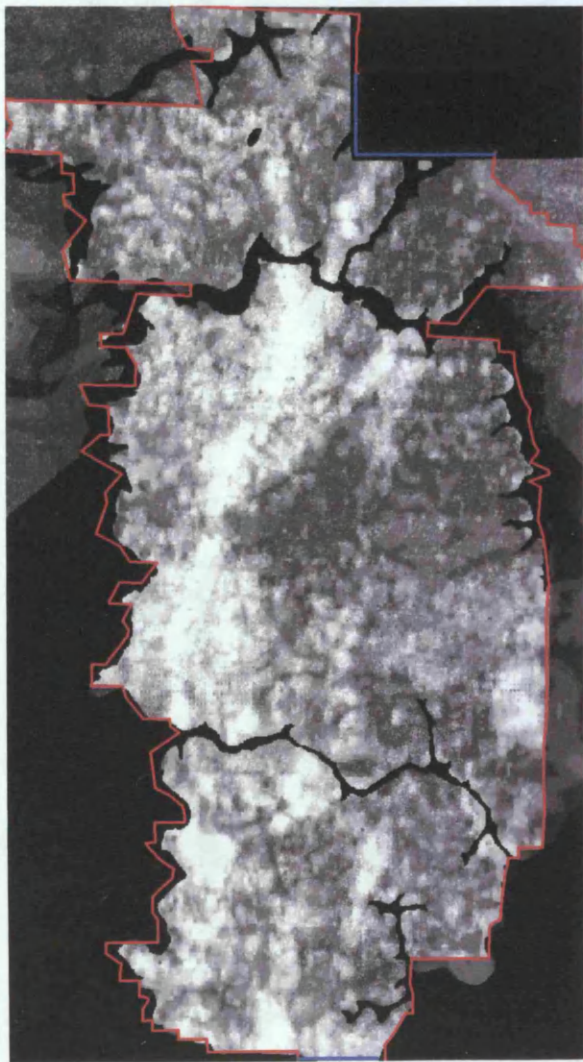
MCE process area
(determined by the radiometric/magnetic area)



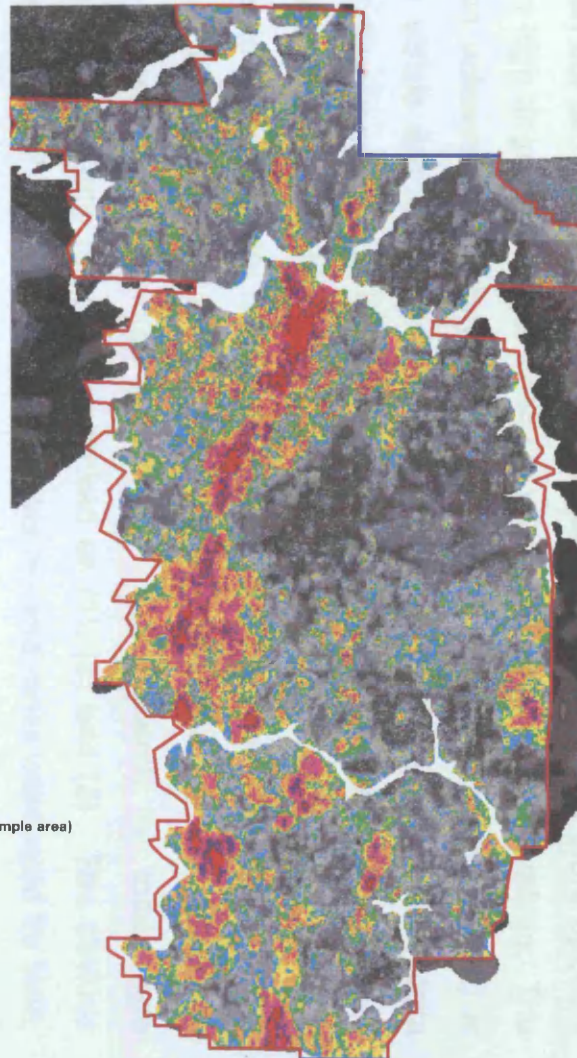
- Priority area (1) = top 0.5 % of all data.
- Priority area (2) = top 1 % of all data.
- Priority area (3) = top 5 % of all data.
- Priority area (4) = top 10 % of all data.
- Priority area (5) = top 15 % of all data.
- Priority area (6) = top 20 % of all data.
- Priority area (7) = top 25 % of all data.

Fig. 100 MCE Results. The 'expert-system approach' .
(based on partial data, total area)

Grey scale image.



results prioritised based upon %.



MCE process area
(determined by the geochemical sample area)



- Priority area (1) = top 0.5 % of all data.
- Priority area (2) = top 1 % of all data.
- Priority area (3) = top 5 % of all data.
- Priority area (4) = top 10 % of all data.
- Priority area (5) = top 15 % of all data.
- Priority area (6) = top 20 % of all data.
- Priority area (7) = top 25 % of all data.

either areas of possible basic-type intrusions and/or the Tarkwaian or Birimian formations. Visual inspection of the images also indicates far fewer areas of gold suitability lying within granite terrain.

An advantage of this display method is that visual comparisons can be made between the two results. Where the two image areas overlap there appears to be a high degree of spatial similarity within the upper 25% of values. The Birimian volcano-sedimentary unit (a known host of gold mineralisation) is clearly visible and characteristically represented by the upper 5% of data values, thus confirming its importance even when data sources are combined. However, a noticeable difference lies not in their spatial distribution but in the designation of the priority number. For example it appears that many of the areas given a priority rank (3) within the 'total' area image are on comparison only a (4) within the restricted area image. Consequently the total image highlights significantly more areas ranked as (1), (2) and (3). The obvious question is "why?" considering the same scores and ranks were used for both, and does this difference really matter?

The most likely reason for this difference is to do with the number of input criteria used in the pairwise comparison. In the small area, 15 criteria were assessed and compared, whereas in the total area only 11 were utilised. However, it is not just the number of criteria which is important, but their overall comparative contribution. The total area image does not include any of the results from the magnetic or radiometric analysis. Yet these sets of information are often placed with equal or greater comparative importance than, say, those derived from the TM data sets which (as explained in Section 6.3.1) are comparatively less important than many other criteria. The effect this has upon the total image results is to increase the overall priority weighting with respect to the geochemistry. However in the smaller area, the weight distribution is less severe because of the competing importance from the magnetic and radiometric data.

The answer to the question "does it matter?" to some extent depends upon your angle of approach. If spending extra time and resources on field

checking these sites is of no consequence, then the answer is no it does not. However, in reality that would be an unaffordable luxury.

Another approach for checking the relative validity of these results is to assess them against known Au occurrences. In both these cases all known gold occurrences (within the MCE process window) coincide with areas from within the top 10-15%. This may seem low and one may ask why they are not within the top 1% of sites, given that we know they are mineralised. On closer inspection however the results are considerably more promising, as shown:

<u>Priority area</u>	<u>Total area (restricted criteria)</u>	<u>Vs</u>	<u>Small area (all criteria)</u>
(1) red = 0.5%	9		4
(2) purple = 1%	0		2
(3) magenta = 5%	4		4
(4) orange = 10%	0		2
(5) yellow = 15%	1		0

Consequently, in the total area 13 of the 14 occurrences lie within the top 5%, whilst in the smaller area, 10 out of 12 reside within the top 5%. However this does not prove that the results from the total area are more accurate at predicting areas in which gold is most likely to occur. For, as already explained, there is some switching between the images with regard to their priority number.

It is also important to point out why a small number of these gold occurrence rank within the 10% and 15% band. Even when data have been aggregated as here, if the position of the occurrence is not highlighted or translated through into any of the accompanying data sets (e.g. the location lies between geochemical sample lines, or, in the case of the TM datasets the location is obscured by vegetation), then this location will either be "lost" or will be shown as a reduced in priority. In essence you can not highlight what was not already there within the supporting datasets.

One of the advantages of the WLC multi-criteria evaluation technique is the fact that criteria scores and pairwise comparisons can be readily changed or modified and the suitability map recomputed. This is of benefit in exploration

where often information is constantly evolving. However, presented with the results here the author's suggestion would be to use the results produced from the restricted area, based on all criteria, and outside of this area to use those from the total area, partial data.

CHAPTER 7

CONCLUSIONS, ISSUES AND FUTURE WORK.

Contents.

- 7.1 Research conclusions.**
- 7.2 Final address of issues.**
 - 7.2.1 Source quality control.**
 - 7.2.2 Database improvements.**
- 7.3 Future work.**

7.1 Research conclusions.

This research has analysed many differing data sources taken from a regional reconnaissance exploration program. The outcomes from each analysis that are reported in Chapters 4 and 5 are results which can stand-alone and be used as potential pointers to gold mineralisation or to lithologies in which gold is likely associated. However, mineral exploration is also about making decisions which are associated with minimum 'risk', e.g. the risk that the decision taken will not be wrong. This to some extent is more problematic when assumptions are based upon evidence from a single criterion. Therefore through the process of combining data and seeking coincidences the risk factor can be reduced.

With this process in mind two methods of data aggregation have been investigated and assessed, the 'weights-of-evidence' and the 'expert-system'. The former is a relatively rigid approach with weights developed purely on the spatial location of known occurrences. Although this technique has revealed some interesting results, it is perhaps the least suitable of the methods given amongst many things the small number of deposits, as discussed in Chapter 6, section 6.3.2. In contrast the expert-system approach is a very flexible technique, although it is also arguably controversial due to the subjectivity surrounding the development of the weights. This characteristic can, however, be viewed as both a strength and a weakness. The weakness lies in the requirement on the end user to have full knowledge and understanding of all input datasets, but it can also be considered as a strength when the procedure is implemented within an organisation. In this situation the knowledge base can be pooled from many "experts" operating within each of the differing fields associated with the various input datasets. For it would be foolish to assume a single person can be an expert in all. The procedure is also flexible in that the weights can be readily changed through altering the criteria or rank if additional knowledge becomes available at a later date.

Above all this technique has provided a method which has allowed the incorporation of some landscape geochemistry into the overall analysis as an

additional criteria layer, thus allowing its integration in the decision making process associated with the prioritisation of potential gold sites.

A final point should also be mentioned with regard to error and its potential to propagate when undertaking analyses within a GIS. To some extent this has already been touched upon in Chapter 4, Section 4.5.8. Nevertheless it is important to point out that within the analyses no attempt has been made to measure or quantify error possibilities. The primary reason why is because this would be a huge task, likely a PhD topic in itself. For example how would you attempt to quantify error in the geology map? It is obvious that error in this map exists simply because there is very little if any true exposure, therefore an inordinate amount of interpretation and interpolation must have occurred. To measure and quantify would require drilling many boreholes at great expense. Although this would not be practical at this late GIS stage, there does exist the possibility that if GIS activities run concurrent to active exploration activities, then drilling information could be used to update inaccuracies within the published geological maps. Alternative approaches could be to quantitatively develop either a single error parameter for each data layer used, or produce a more complex spatial error/uncertainty map, for example a raster map, in which the value of a cell is not necessarily the same as its neighbouring cell value. This later approach would be the most complex to achieve, possibly incorporating decay functions with distance from known sample point etc. Irrespective of the level of complexity, introducing quantitative error mapping into the analyses as performed in this research would required development in 'future work', Section 7.3.

7.2 Final address of issues.

Throughout this study a number of issues have come to light, these vary from quality control to data improvements as explained below. However linked to both of these and of particular relevance to this research project is the concept of GIS as an 'end-user'. For at the time that this regional reconnaissance program was undertaken GIS was never intended to be an

integral component in helping to highlight the areas deemed worthy of exploration. Therefore GIS has not been incorporated within the whole process but rather has been “added-on” at the end of the chain. An issue that arises from this is that there is a tendency as time lapses for knowledge concerning the detail of some of the data collection and preliminary processing steps to ‘disappear,’ and the concerns which are now raised regarding quality control and data improvements would needless to say not require addressing here.

7.2.1 Source quality control

There is a need with any data source for quality control, since without it results may not only be misleading but any GIS processing can easily compound the errors further. Unfortunately, there appears to have been little such control with the geochemical data collected and used here. Compromises appear to have been made from as early as the laboratory analysis stage where there is the unusual ‘common’ detection level for all elements, and then quality further degenerates to the shambolic nature of the initial computer database, which on examination proved clearly that it had never been checked. The occurrence of these sorts of errors in such an important data source is not only surprising, but also completely avoidable.

7.2.2 Database improvements

There are many ways for improving a gold exploration database, but this research has highlighted the following two. The first is a general point concerned with data formats and GIS processing whilst the latter is specific to this database.

(i) Considerable time (and money) is often spent transforming data into a format compatible for entry into GIS software. It would therefore be beneficial if there were greater standardisation between the formats of the input source data and that of commonly available GIS software.

Although GIS can accommodate both raster and vector data sources data integration is often performed within a raster system, as illustrated here by both the weights-of-evidence and the expert-system approach. This requires any vector data to be converted to raster. The reader is therefore made aware that through this conversion process and the selection of cell size commission and omission errors are inevitable.

(ii) Regional reconnaissance by its nature is geared towards large-scale low cost evaluation. However, that aside, some improvements could have been made to the database through changes or additions in the source data. For example, given the lateritic environment where clays and irons are a natural weathering phenomena TM is perhaps one of the least useful sources of remote sensing imagery at being able to distinguish between minerals of weathering and those derived from mineralising processes. Imaging spectrometers such as the Airborne Visible-Infrared Imaging Spectrometer (AVIRIS) or the Airborne Imaging Spectrometer (AIS) would have been of greater value. These have not only 224 to 128 channels allowing a continuous reflectance spectrum permitting comprehensive discrimination, but also provide improved spatial resolution of 20 m (AVIRIS) and 8 m (AIS) respectively.

- With the knowledge that gold mineralisation is accompanied by sulphides perhaps an additional geophysical technique such as an Electro-magnetic (EM) survey would also help to “home-in” on potential ore sites.
- Given the regional context of the geochemical survey it is somewhat unusual that laboratory analysis has only tested for 8 elements; in most regional surveys it is typical to find as many as 32 elements analysed. Whether in reality these extra elements exist is now relatively superfluous. However, given the geochemical nature of gold it would have been more beneficial to have had some elements more suited as gold ‘pathfinders’ (e.g. chalcophile associated pathfinders elements), rather than using the associations derived from copper, nickel, zinc, and lead. Known gold pathfinders of Arsenic (As), Antimony (Sb) and Selenium (Se), due to its

reported additional function as a potential discriminator of sulphide gossans from those of ferruginous origin (Rose et. al., 1990), would have assisted greatly in the prioritisation process.

□ Finally, an additional source of information that would have been of benefit is the location of all artisan sites. This type of information could have been easily obtained at the same time as the regional geochemical sampling. It is most likely that this would have resulted in an increase in the number of occurrences and possibly greater diversity in their spatial location, allowing for some improvement in the implementation of the weights-of-evidence as discussed earlier. Alternatively these Au site locations if known, could have been omitted from all analyses and used latter as a method to verify/check the most favourable of the Au locations resulting from the expert system approach.

7.3 Future work.

The first and most obvious suggestion for future work would be to field verify those areas with the highest ranking anomalies. This would help establish the usefulness of collectively processing data in this manner, and ascertain if it were necessary to re-weight some of the criteria codes.

A factor important in any scale study is that detail cannot be extracted beyond the scale of the input data. This is no truer than here in this regional study. For example with the TIN, the map scale and wide contour interval naturally results in the creation of a simplified surface terrain. This loss of landscape detail has prevented the analysis of slope curvature in identifying area of concavity and convexity and even the categorisation of slopes based upon angle. These additional surface features would enable a more complex landscape coding to be developed, in turn helping to locate areas where there is higher potential surface erosion and where pooling or collecting areas are at their greatest. Furthermore, a DEM supporting this level of surface detail would also benefit from a reciprocal reduction in the sampling resolution of the

geochemical data. As a consequence, any future study along these lines would by this nature alone require a move in scale from regional reconnaissance down to local /concession level.

As mentioned in Section 7.1 there has been no attempt to quantitatively analysis for error from any of the input sources. As a consequence the results observed so far are not error-less but error unknown. Future work could attempt to look at and develop appropriate methods to account for the various errors or their likelihood and thereby translate any error analyses through into the final results.

If available, future work could also attempt to spatially map profile information derived from pit or drillhole sites. If there are enough sites distributed throughout the region it may be possible to interpolate from the profile data either a 3D approach, or less complicated, a single surface criterion which could be fused with the terrain model. This would provide a more integrated geochemical–landscape approach, between the land height and profile level or truncation.

REFERENCES.

- Abrams, M. J., Ashley, R. P., Rowan, L. C., Goetz, A. F. H., and Kahle, A. B. (1977). Mapping of hydrothermal alteration in the Cuprite Mining District, Nevada, using aircraft scanner images for the spectral region 0.46 to 2.36 um. *Geology*, 5, 713.
- Ambrosi, J. P. (1984). Pétrologie et géochimie d'une séquence de profils latéritiques cuirassés ferrugineux de la région de Diouga, Burkina Faso. *PhD thesis, University of Poitiers, France*, 223p.
- Anon. (1973). *The atlas of Africa - The African continent*. Jeune Afrique, Agrégée d'Histone et de geographic: Université de Paris. 1st edition, 335p.
- Anon. (1992). North and West Africa - Mali. *Mining Journal*, London, Annual Review, p127.
- Anon. (1993). West African gold. *Mining Journal*, London. September 17th, pp198-199.
- Anon. (1995). Mali. *Mining Journal*, London, Annual Review, p127.
- Anon. (1996a). West Africa's gold potential. *African Mining*. July - August, Vol. 1, No. 4, pp26-29.
- Anon. (1996b). West African gold. *Mining Magazine*. February, pp90-99.
- Anon. (1996c). International mining companies begin looking at Mali for its gold. *Mining Engineering*. January, p23.
- Anon. (1996d). Mining in Africa. *The Northern Miner*. January 29th, ppB1-B8.
- Anon. (1996e). Exploration 1996. *The Northern Miner*. March 11th, ppD1-D28.
- Anon. (1996f). The global search for gold. *The Northern Miner*. September 2nd, ppC1-C12.
- Appiah, H., Norman, D. I. and Boadi, I. (1991). The geology of the Prestea and Ashanti goldfields: A comparative study. *Brazil Gold'91. The Economics Geology Geochemistry and Genesis of Gold Deposits*. Ladeira, E.A. (Ed), Balkema: Rotterdam, pp247-255.
- Atkinson, P. (1985). Preliminary results of the effect of resampling on thematic mapper imagery. *ACSM-ASPRS Fall convention (1985), technical papers, Falls Church Virginia*. American society for photogrammetry and remote sensing and American congress on surveying and mapping.

Baker, W. E. (1973). The role of humic acids from Tasmanian podzolic soils in mineral degradation and metal mobilisation. *Geochimica et Cosmochimica Acta*, Vol.37 pp269-281.

Baker, W. E. (1978). The role of humic acid in the transport of gold. *Geochimica et Cosmochimica Acta*, Vol.42 pp645-649.

Barker, P. E. (1968). Comparative volcanology and petrology of the Atlantic island arcs. *Bull. Volcanol.*, 32, pp189-206.

Barr, M. W. C. (1990). Pennine exploration dataset re-examined. *Remote sensing: an operational technology for the mining and petroleum industries*. Institution of Mining and Metallurgy, pp3-14.

Bassot, J. P., Meloux, J., and Traore, H. (1981). *Notice explicative de la carte géologique à 1:500,000 de la République du Mali*. DNGM: Bamako, Mali, 137p.

Benza, M. P. (1836). Memoir of the geology of the Neelgherry and Koondah mountains. *Madras Journal Lit. Science*, 4 (13), pp241-299.

Bessoles, (1977). *Géologie de l'Afrique. Le Craton ouest-africain*. Mém. BRGM, No.88. Orléans, France, 111p.

Blakemore, M. J. (1984). Generalization and error in spatial databases. *Cartographica* 21 (3 & 4) pp131-139.

Bonham-Carter, G. F., and Agterberg, F. P. (1990). Application of a microcomputer-based geographical information system to mineral-potential mapping. pp49-74. In *Microcomputers in geology. Vol. 2*, Hanley, T and Merriam, D.F (Eds). Pergamon Press: Oxford.

Bonham-Carter, G. F., Agterberg, F. P., and Wright, D. F. (1988). Integration of geological datasets for gold exploration in Nova Scotia. *Photogrammetric Engineering and Remote Sensing*. Vol. 54, No. 11, pp1585-1592.

Bowell, R. J., Foster, R. P., Gize, A. P., Hoppis, H. A., Laffoley, N., and Rex A.J. (1991). Mineralogical and chemical characteristics of a tropical weathering profile in Ghana: Implications for gold exploration. *Brazil Gold'91. The Economics Geology Geochemistry and Genesis of Gold Deposits*. Ladeira, E.A. (Ed) Balkema: Rotterdam, pp713-719.

Bowell, R. J., Afreh, E. O., Hanssen, E., Abe, S., Yao, R. K., Diallo, M., and Pohl, D. (1995). Gold and base metal distribution and exploration in tropical soils: Four contrasting case studies from West Africa. *BHP Internal report*, 45pp.

Bradshaw, P. M. D. (1975). Conceptual models in exploration geochemistry. The Canadian Cordillera and Canadian Shield. *Journal of Geochemical Exploration*, 4, 213pp.

Brown, G. R. (1997). Iamgold Corporation. *Research institutional investment report, Stockbroker publication Canaccord Capital*. June 17th 1997, pp1-11.

Buchanan, F. (1807). *A journey from Madras through the countries of Mysore, Kanara and Malabar*. Vol. 2, pp436-461, Vol. 3, p66, p89, p251, p258. East India Co.: London.

Buckingham, W. F., and Sommer, S. E. (1983). Mineralogical characterisation of rock surfaces formed by hydrothermal alteration and weathering- Applications to remote sensing. *Economic Geology*, Vol. 78, pp664-674.

Budel, J. (1982). *Climatic geomorphology*. (Trans.) Fischer, L & Busch, D. Princeton University Press: Princeton, 443pp.

Bugeco (1994). Mineral potential of Western Africa. *E&Mj*. February, pp18-21.

Bugg, S. F. (1982). Lead-zinc deposits of the coastal province of Kenya, and some exploration guidelines. *Overseas Geol. Miner. Resour.*, 59 20pp.

Burrough, P. A. (1986). *Principals of geographical information systems for land resource assessment*. Oxford University Press.

Butt, C. R. M. (1981). The nature and origin of the lateritic weathering mantle, with particular reference to Western Australia. In *Exploration in deeply weathered terrains*. Doyle, H.A., Glover, J.E & Grovers, D.I. (Eds), Geol. Dep. & Extensions Service: University of Western Australia. 6, pp11-29.

Butt, C. R. M. (1987). A basis for geochemical exploration models for tropical terrains. *Chemical Geology*, 60, pp5-16.

Butt, C. R. M. (1988a). Genesis of lateritic and supergene gold deposits in the Yilgarn Block, Western Australia. *Bicentennial Gold 88, Geological Society of Australia Inc*. No. 22, Melbourne, May 1988, pp359-364.

Butt, C. R. M. (1988b). Gold mobility in the weathering environment. 2nd *International Conference on Prospecting*. In *Arid Terrain*. Smith, B.H, Stoakes, C.A, Govey, A.L & Oates, C.J. (Eds) Publication No.18, University of Western Australia, 26-29th April 1988, pp2-5.

Butt, C. R. M. (1992). Physical weathering and dispersion. In *Handbook of Exploration Geochemistry*. Govett, G.J.S. (Ed) Vol.4, Regolith Exploration Geochemistry in Tropical and Subtropical Terrains. (Ed) Butt, C.R.M. & Zeegers, H. Elsevier, pp97-113.

Butt, C. R. M., and Nickel E. H. (1981). Mineralogy and geochemistry of the weathering of the disseminated nickel sulfide deposit at Mt. Eeith, Western Australia. *Economic Geology*, 76 pp1736-1751.

Butt, C. R. M., and Smith, R. E. (1980). (Compilers and editors) Conceptual models in exploration geochemistry, 4; Australia. Developments. *Economic Geology*, Vol.13, Elsevier: Amsterdam, 275p.

Butt, C. R. M., and Zeegers, H. (1992). Characteristics of tropical weathered terrains. *Handbook of Exploration Geochemistry*. Govett, G.J.S. (Ed), Vol.4, Regolith Exploration Geochemistry in Tropical and Subtropical Terrains. (ed) Butt, C.R.M. & Zeegers, H. Elsevier, pp3-24.

Campbell, J. M. (1917). Laterite. *Min. Mag.* 17, pp67-77, pp120-128, pp171-179 and pp220-229.

Chaplin, R., Beardsmore, S., and Hay, M. (1997). *African Gold 'North of the Limpopo'*. Stockbroker publication. T. Hoare & Co. May 1977, 94p.

Cheng, Q., Agterberg, F. P., and Ballantyne, S. B., (1994). The separation of geochemical anomalies from background by fractal methods. *Journal of Geochemical Exploration*, 51 pp109-130.

Cheng, Q., Agterberg, F. P., and Bonham-Carter, G. F., (1996). A spatial analysis method for geochemical anomaly separation. *Journal of Geochemical Exploration*, 56 pp183-195.

Chrisman, N. R. (1982). A theory of cartographic error and its measurement in digital databases. *Proc. AUTO-CARTO 5*, pp159-168.

Chrisman, N. R. (1987). Efficient digitizing through the combination of appropriate hardware and software for error detection and correction. *Inter. Journal of Geographical Information Systems*, 1 pp265-277.

Chrisman, N. R. (1989). Modelling error in overlaid categorical maps pp21-34. In *Accuracy of spatial databases*. Goodchild, M and Gopal, S (Eds). Talyor & Francis 290p.

Chrisman, N. R. (1991). The error component in spatial data pp165-174 In *Geographical Information Systems: principals and applications*. Maguire, D.J, Goodchild, M.F, Rhind, D.W (Eds). Longman: London Vol 1, 649p.

Chrisman, N. R. (1997). *Exploring Geographic Information Systems*. J. Wiley & Sons, Inc. 298p.

Chrisman, N. R., and Yandell, B. (1988). Effects of point error on area calculations. *Surveying & Mapping*, 48 pp241-246.

Clark, J. (1838). On the lateritic formation. *Madras Journal Lit. Science*. VI. 8, pp334-346

Clauer, N. (1976). Chimie isotopique du strontium des milieux sédimentaires. Application à la géochronologie du craton ouest-africain. *Thèse Univ. Strasbourg, Fr., et Mém. Soc. Géol. Fr.*, No. 45, 236p.

Cloke, P. L., and Kelly, W. C. (1964). Solubility of gold under inorganic supergene conditions. *Economic Geology*, 59 pp259-270.

Colin, F., and Lecomte, P. (1989). Dissolution features of gold particles in a lateritic profile at Dondo Mobi, Gabon. *Geoderma*, 45 pp241-250.

Colin, F., and Vieillard, P. (1991). Behaviour of gold in lateritic equatorial environment: Weathering and surface dispersion of residual gold particles, at Dondo Mobi, Gabon. *Applied Geochemistry*, 6 pp279-290.

Colin, F., Noack, Y., Delvigne, J., and Nahon, D. (1988). Petrological, mineralogical and geochemical study of the Syama gold deposit (Mali). *Inter. Report Faculté des Sciences de St-Jérôme. Case 431. Laboratoire de Géologie dynamique et de pétrologie de la surface U.A. C.N.R.S. No.132. Université d'Aix-Marseille III*, 34p.

Cowan, D. R., and Crabb, T. N. (1981). *Airborne magnetic and radiometric surveys in sequential exploration*. Geol. Dep. and extension service, University Western Australia, 6 pp127-143.

Crippen, R. E. (1989). Selection of Landsat TM band-ratio combinations to maximise lithologic information in colour composite displays. *Proceedings of the 7th Thematic Conference, Remote Sensing for Exploration Geology (ERIM). Calgary Canada, 2-6 Oct.* pp917-921.

Crist, E. P., and Cicone, R. C. (1984). Application of the Tasseled Cap concept to simulated Thematic Mapper data. *Photogrammetric Engineering & Remote Sensing*, Vol. 50, No.3 pp343-352.

Crosta, A. P., and McM. Moore, J. (1989). Enhancement of Landsat Thematic Mapper imagery for residual soil mapping in SW Minas Gerais State, Brazil: A prospecting case history in Greenstone Belt terrain. *Proceedings of the 7th Thematic Conference, Remote Sensing for Exploration Geology (ERIM). Calgary Canada, 2-6 Oct.* pp1173-1187.

Curran, P. J. (1985). *Principles of remote sensing*. Longman Scientific & Technical 282p.

Danti, K. J. and Brimhall, J. (1989). The distribution of gold in primary auriferous pyrite and two stage oxidative gold enrichment in secondary iron-oxides from the Syama gold mine, Mali, West Africa. In *Abstracts and*

programs of the Geological Society of America 1989 annual meeting St. Louis, Missouri USA. November 6-9th 1989, No.1896.

Danti, K., Brimhall, G. H., and Lewis, C, (1989). Mineralogical studies of microscopic and submicroscopic gold in primary sulphide mineralization, Mali, Ivory Coast, and Ghana: Bamako, Mali, BHP-Utah Internat., *unpub. rept.*

Darnley, A. G., and Ford, K. L. (1989). Regional airborne gamma-ray surveys: A review pp229-240. *Proceedings of Exploration' 87. Third decennial international conference on geophysical and geochemical exploration for minerals and groundwater*, Garland, D.G (Ed). Ontario Geological Survey, special vol. 3, 914pp.

Davidson, D., Bruce, B., and Jones, D. (1993). Operational remote sensing mineral exploration in a semi-arid environment: The Troodos Massif, Cyprus. *Proceedings of the 9th Thematic Conference on Geological Remote sensing, Pasadena, California, USA. 8-11th February pp845-856.*

Dickson, L. B., Fraser, S. J., and Kinsey-Henderson, A. (1996). Interpreting aerial gamma-ray surveys utilising geomorphological and weathering models. *Journal of Geochemical Exploration. 57 pp75-88.*

Dietz, R. S., and Holden, J. C. (1970). The break-up of Pangaea. *Scientific America*, 223 pp30-41.

Drury, S. A., and Hunt, G. A. (1989). Geological uses of remotely-sensed reflected and emitted data of lateritized Archaean terrain in Western Australia. *Inter. Journal of Remote Sensing*, Vol. 10, No.3 pp475-497.

Drury, S. A. (1987). *Image interpretation in geology*. Allen & Unwin, 243p.

du Bois, C. G. B., and Jeffery, P. G. (1955). Laterites on Entebbe peninsula. *Colon. Geology Mineral Resources*, 5 (4), pp387-408.

Dzigbodi-Adjimah, K. (1993). Geology and geochemical patterns of the Birimian gold deposits, Ghana, West Africa. *Jour. Of Geochemical Exploration*, 47 pp305-320.

Eastman J. R. (1999). Multi-criteria evaluation and GIS. pp 493-502, Chapter 35. In *Geographical Information Systems: principals and applications (2nd Ed)*. Maguire, D.J, Goodchild, M.F, Rhind, D.W (Eds). Longman: London Vol. 2, 580pp.

Edwards, R, and Atkinson, K (1986). *Ore deposit geology*. Chapman & Hall. London. 466p.

Elvidge, C. D., and Lyon, R. J. P. (1985). Estimation of the vegetation contribution to the 1.65/2.22um ratio in airborne thematic-mapper imagery of

the Virginia Range, Nevada. *Inter. Journal of Remote Sensing*, Vol. 6, No.1 pp75-88.

ERDAS (1994). *ERDAS Imagine Field guide. Version 8.1, 3rd edition*, ISG 660 Erdas Inc. 628p.

ERDAS (1997). *ERDAS Imagine Field guide. Version 8.3, 4th edition revised and expanded*, ISG 660 Erdas Inc. 656p.

Farrah, H. and Pickering, W. K. (1979). pH effects in the adsorption of heavy metal ions by clays. *Chem. Geology*, 25 pp317-326.

Fisher, P. F. (1989). Knowledge-based approaches to determining and correcting areas of unreliability in geographical databases pp45-54. In *Accuracy of spatial databases*. Goodchild, M and Gopal, S (Eds). Talyor & Francis 290pp.

Fisher, P. F. (1991). Spatial data sources and data problems, pp175-189 In *Geographical Information Systems: principals and applications* Maguire, D.J, Goodchild, M.F, Rhind, D.W (Eds). Longman: London Vol. 1, 649pp.

Forbes, E. A., Posner, A. M., and Quirk, J. P. (1976). The specific adsorption of divalent Cd, Co, Cu, Pb and Zn on goethite. *Journal Soil Science* 27 pp154-166.

Ford, K. L., and Carson, J. M. (1986). Application of airborne gamma-ray spectrometric surveys, Meguma terrane, Nova Scotia. *Maritime Sediments and Atlantic Geology*, Vol. 22 No. 1 pp117-135.

Fortescue, J. A. C. (1975). The use of landscape geochemistry to process exploration geochemical data. *Journal of Geochemical Exploration*, 4 pp3-13.

Fortescue, J. A. C. (1992). Landscape geochemistry: retrospect and prospect-1990. *Applied Geochemistry*. Vol. 7, pp1-53.

Fraser, S. J. (1991). Discrimination and identification of ferric oxides using satellite Thematic Mapper data: A Newman case study. *Inter. Journal of Remote Sensing*, Vol.12 No.3 pp635-641.

Fraser, S. J., and Green, A. A. (1987). A software defoliant for geological analysis of band ratios. *Inter. Journal of Remote Sensing*, Vol.8, No.3 pp525-532.

Freise, F. W. (1931). The transportation of gold by organic underground solutions. *Economic Geology* 26 pp421-431.

Freyssinet, P.h., Lawrance, L. M., and Butt, C. R. M. (1990a). Geochemistry and morphology of gold in lateritic profiles in savanna and semi-arid climates.

Geochemistry of the Earth's Surface and of Mineral Formation. 2nd International Symposium, July 2-8th 1990, France, pp61-63.

Freyssinet, P.h., Roquin, C., Muller, J. C., Paquet, H., and Tardy, Y. (1990b). Geochemistry and mineralogy of soils covering laterite and their use for gold exploration. *Geochemistry of the Earth's Surface and of Mineral Formation. 2nd International Symposium, July 2-8th 1990, France, pp58-60.*

Freyssinet, P.h., Zeegers, H., and Tardy, Y. (1989). Morphology and geochemistry of gold grains in lateritic profiles of southern Mali. *Journal of Geochemical Exploration, 32 pp17-31.*

Galbraith, J. H., and Saunders, D. F. (1983). Rock classification by characteristics of aerial gamma-ray measurements. *Journal of Geochemical Exploration, 18 pp49-73.*

Garrett, R. G., Kane, V. E., and Zeigler, R. K. (1980). The management and analysis of regional geochemical data. *Journal of Geochemical Exploration, 13 pp115-152.*

Gilbert, C. (1997). Height of uncertainty? – Sizing up the vertical in GPS. *Mapping Awareness, Vol. 11, No. 5 pp35-37.*

Gillespie, A. R., Kahle, A. B., and Walker, R. E. (1986). Colour enhancement of highly correlated images. I. Decorrelation and HSI contrast stretches. *Remote Sensing of Environment (20), pp209-235.*

Glinka, K. D. (1914). *Die typen der bodenbildung, ihre klassifikation und geographische verbreitung. (Trans.)* Borntraeger, Berlin.

Goetz, A. F. H., Billingsley, A. R., Gillespie, M. J., Abrahms, R. L., Squires, E. N., Shoemaker, I. L., and Elston, D. P. (1975). Applications of ERIS Images and image processing to regional geological problems and geologic mapping. *Northern Arizona. Pasadena, California, USA : Californian Institute of Technology, Jet Propulsion Laboratory. Technical report (32-1597), 188p.*

Goldhaber, M. B. (1983). Experimental study of metastable sulphur oxyanion formation during pyrite oxidation at pH 6-9 and 30°C. *American Journal Science, 283 pp193-217.*

Goldich, S. S. (1938). A study in rock weathering. *Journal of Geology, 46 pp17-58.*

Goleva, G. A., Krivenkov, V. A., and Gutz, Z. G. (1970). Geochemical trends in the occurrence and migration forms of gold in natural water. *Geochem. Int. 7 (3) pp518-529.*

Goodchild, M. F. (1988). The issue of accuracy in global databases pp31-48. In *Building databases for global science*. Mounsey, H (Ed), Tomlinson, R (General Ed.). Taylor & Francis pp419.

Gosselin, R. (1997) *Company portfolio*. Oxford Resources Inc.

Goudie, A. (1973). Duricrusts in tropical and subtropical landscapes. *Oxford Research Studies in Geography*. Oxford University Press: London. 174p.

Graham, D. F., and Bonham-Carter, G. F. (1993). Airborne radiometric data a tool for reconnaissance mapping using a GIS. pp 43-52. *Proceedings of the 9th Thematic Conference on Geological Remote Sensing, Pasadena California, USA*. 8-11th February 1993.

Gray, D. J., Butt, C. R. M., and Lawrance, L. M. (1992). The geochemistry of gold in lateritic terrains. In *Handbook of Exploration Geochemistry*. Govett, G.J.S. (Ed) Vol.4, Regolith Exploration Geochemistry in Tropical and Subtropical Terrains. (ed) Butt, C.R.M. & Zeegers, H. Elsevier, pp461-482.

Green, A. A., and Huntington, J. F. (1987). Remote sensing for surface mineralogy. pp213-227. *Proceedings of Exploration' 87. Third decennial international conference on geophysical and geochemical exploration for minerals and groundwater*, Garland, D.G (Ed). Ontario Geological Survey, special vol. 3, 914p.

Hanssen, E. (1995). Exploration potential for oxide ore in the Syama district. *BHP internal report*, December 1995

Hanssen, E., Guindo, A., Winer, N., Pohl, D., Olson, S., Abe, S. D., and Ford, C. R. B. (1991). Exploration history and geological setting of gold mineralisation in the Syama-Bundiali belt (Southern Mali). *Brazil Gold'91. The Economics Geology Geochemistry and Genesis of Gold Deposits*. Ladeira, E.A. (Ed).Balkema, Rotterdam, pp817-819.

Harris, J. R. (1989). Clustering of gamma-ray spectrometer data using a computer image analysis system. *Statistical Applications in the Earth Sciences*. Agterberg, F. P and Bonham-Carter, G.F (ed). Geological survey of Canada, paper 89-9.

Harrison, J. B., and Reid, K. D. (1910). The residual earths of British Guiana and commonly termed 'laterite', Vol. III, IV and V. *Geol. Mag.* 47,pp439-452, pp488-495, and pp553-562.

Hastings, D. A. (1982). On the tectonics and metallogenesis of West Africa: A model incorporating new geophysical data. *Geoexploration*, 20 pp295-327.

Hodgkinson, E (1994). Economy. *Africa south of the Sahara*. Europa Publications Ltd. 23rd edition, pp543-559.

Howarth, R. J., and Sinding-Larsen, R. (1983). Multivariate analysis. In *Handbook of Exploration Geochemistry*. Govett, G.J.S.(Ed) Vol.2, Statistics & Data Analysis in Geochemical Prospecting. (Ed) Howarth, R.J. Elsevier, pp207-289.

Hutchinson, M. F., and Gallant, J. C. (1999). Representation of terrain. pp105-124. In *Geographical Information Systems: principals and applications (second edition)*. Maguire, D.J, Goodchild, M.F, Rhind, D.W (Eds).. Longman: London Vol. 1, 580p.

Iamgold (1997). Company portfolio, Iamgold Corp.

IDRISI (1999). *Idrisi 32 for windows, Guide to GIS and image processing*. Vol.2. Idrisi production, Clark University. 170pp.

Isles, D. J., Harman, P. G., and Cunneen, J. P. (1988). Aeromagnetism and the Yilgarn Gold rush. pp 259-264. *Proceedings of the Bicentennial Gold 88, Melbourne, Australia, May 1988*. Geological Society of Australia Inc. Abstract No. 22.

Jackson, M. L., Tyler, A. S., Willis, A. L., *et al* (1948). Weathering sequence of clay-size minerals in soils and sediments. *Journal Phys. Chemistry*, 52 pp1237-1260.

Jimenez-Espinosa, R., Sousa, A. J., and Chica-Olmo, M. (1993). Identification of geochemical anomalies using principal component analysis and factorial kriging analysis. *Journal of Geochemical Exploration*, 46 pp245-256.

Jones, H (1990). *Population geography*. Paul Chapman Pub. Ltd. 2nd edition, 330p.

Kinniburgh, D. G., Jackson, M. L., and Syers, J. K. (1976). Adsorption of alkaline earth, transition and heavy metal cations by hydrous oxide gels of iron and aluminum. *Soil Sci. Society American Journal* 40 pp796-799.

Kootnikoff, L. (1997). Oliver sets exploration pace in Mali. *The Northern Miner, Africa*. February, 3rd 1997, ppC1-C16.

Kowalik, W. S., and Glenn, W. E. (1987). Image processing of aeromagnetic data and integration with Landsat images for improved structural interpretation. *Geophysics* Vol. 52, No. 7 pp 875-884.

Krauskopf, K. B. (1951). The solubility of gold. *Economic Geology*, 46 pp858-870.

Kühnel, R. A. (1987). The role of cationic and anionic scavengers in Laterites. *Chemical Geology*, 60 pp31-40.

Kusnir, L. Keita, N. D., and Diallo, M. (1987). *Kadiolo, Notice Explicative De La Carte Geologique Au 1/200,000 (Feuille NC-30-XIII Nielle)*. Ministere du Developpement Industriel et du Tourisme, Direction Nationale de la Geologie et des Mines, Republic du Mali, 16p.

Lakin, H. W., Curtin, G. C., Hubert, A. E., Schacklette, H. T., and Doxtader, K. G. (1974). Geochemistry of gold in the weathering cycle. U.S. Geological Survey Bulletin, 1330, 80pp.

Larsen, E. S., and Gottfried, D. (1960). Uranium and thorium in selected suites of igneous rocks. *American Journal Science*, 258-A pp151-169.

Lawrance, L. M. (1988a). Behaviour of gold in the lateritic weathering profile of the Yilgarn Block, Western Australia. In *Advances in understanding Precambrian gold deposits, (II)*. Ho, S E and Groves, D I. (Eds) Geology Department and University Extensions, University Western Australia, Publi. 12.

Lawrance, L. M. (1988b). The morphology and geochemistry of supergene gold at Hannan South gold mine, Western Australia. In *Bicentennial Gold 88.*, Goode, A D T, Smyth, E L, Birch, W D and Bosma, L I, (Eds). Vol. 1, Extended abstracts, poster programme. Geol. Society Australia Inc., Abstract No.23 pp360-364.

Lecomte, P. (1988). Stone line profiles: importance in geochemical exploration. *Journal of Geochemical Exploration*, 30 pp35-61.

Lecomte, P., and Colin, F. (1989). Gold dispersion in a tropical weathering profile at Dondo Mobi, Gabon. *Journal of Geochemical Exploration*, 34 pp285-301.

Lecomte, P., and Zeegers, H. (1992). Humid Tropical Terrains. In *Handbook of Exploration Geochemistry*. Govett, G.J.S.(Ed) Vol.4, Regolith Exploration Geochemistry in Tropical and Subtropical Terrains. (Eds) Butt, C.R.M. & Zeegers, H. Elsevier, pp241-294.

Ledru, P., Milesi, J. P., Vinchon, C., Ankrah, P. T., and Marcoux, E. (1991). The geology of the Lower Proterozoic succession of Ghana. *Proc. Of the Inter. Conference on the geology of Ghana with special emphasis on gold. Geological Society of Ghana*, Vol.3(M), pp1-33.

Lemoine, S., Tempier, P., Bassot, J. P., Cahen-Vachette, M., Vialette, Y., Wenmenga, U., Toure, S. (1985). The Burkinian, an orogenic cycle, precursor of the Eburnean of West Africa. *13th Colloquium of African geology, St-Andrews, Scotland. 10-13th September 1985. Occasional publication 1985/3. CIFEG, Paris.*

Levinson, A. A., Bradshaw, P. M. D., and Thomson, I. (1987). The influence of geology and geography in determining thresholds, Colorado, USA. *Practical Problems in Exploration Geochemistry*. Applied publishing Ltd. 269p.

Liégeois, J. P. (1986). Rapport sur les mesures des isotopes du Nd des roches du Sud Mali. Rapp. Ined. Mus. R. Afr. Centrale Tervuren, Belg., 3p.

Liégeois, J. P., Claessens, W., Camara, D., and Klerkx, J. (1991). Short-lived Eburnian orogeny in southern Mali. Geology, tectonics, U-Pb and Rb-Sr geochronology. *Precambrian Research*, 50 pp111-136.

Lillesand, T. M., and Kiefer, R. W. (1994). *Remote Sensing and Image Interpretation (Third edition)*. J. Wiley & Sons Inc. 750p.

Listova, L. P., Vainshtein, A. Z., and Ryabinina A. A. (1968). Dissolution of gold in media forming during oxidation of some sulphides. *Chem. Abstracts*, 68 88967h.

Loughlin, W. P. (1991). Principal component analysis for alteration mapping. *Photogrammetric Engineering & Remote Sensing*, Vol. 57, No. 9 pp1163-1169.

Lovering, T. G., and McCarthy, J. H. (1978). Conceptual models in exploration geochemistry - The Basin and Range province of Western United States and Northern Mexico. *Journal of Geochemical Exploration*, 9 pp113-276.

Lucas, Y., and Chauvel, A. (1992). Soil formation in tropically weathered terrains. In *Handbook of Exploration Geochemistry*. Govett, G.J.S. (Ed) Vol.4, Regolith Exploration Geochemistry in Tropical and Subtropical Terrains. (Eds) Butt, C.R.M. & Zeegers, H. Elsevier, pp57-77.

Mackay, R. A. (1944). The purity of native gold as a criterion in secondary enrichment. *Economic Geology*, 39 pp56-68.

Maclaren, M. (1906). On the origin of certain laterites. *Geol. Mag*, 43, pp536-547.

Maignien, R. (1978). *Review of Research on Laterites*. *Natural Resources Research, IV*. United Nations Educational Scientific and Cultural Organisation, Paris, 148pp.

Mann, A. W. (1984a). Redistribution of gold in the oxidized zone of some Western Australian deposits. In *The Australian I.M.M. Perth and Kalgoorlie Branches, Regional Conference on "Gold mining , Metallurgy and Geology"*. October 1984, pp447-458.

Mann, A. W. (1984b). Mobility of gold and silver in lateritic weathering profiles: some observations from Western Australia. *Economic Geology*, Vol.79, pp38-49.

Marcelin, J., and Serre, J. C. (1971). *Notice explicative de la carte géologique au 1:200,000 Banfora-Sindou-Mangodara*. BRGM, Paris, 35p.

Matheis, G. (1981). Trace-element patterns in lateritic soils applied to geochemical exploration. *Journal of Geochemical Exploration*, 15, pp471-480.

Mather, P. M. (1989). *Computer processing of remotely-sensed images – An introduction*. J. Wiley & Sons, 352p.

McFarlane, M. J. (1971). Lateritisation and landscape development in Kyagwe, Uganda. *Quart. Journal Geol. Soc. London*, 126, pp501-539.

McFarlane, M. J. (1976). *Laterite and Landscape*. Academic Press 151p.

Millot, G. (1983). Planation of continents by intertropical weathering and pedogenetic processes. In *Lateritisation Processes*. Melfi, A J and Carvalho, A.(Eds) University of Sao Paulo Press, Sao Paulo, pp53-63.

Moore, J. McM., Guo, L. J., Copp, D. L., and Youngs, K. (1993). Mineral discrimination by directed band difference techniques using TM and ATM image data. *Proceedings of the 9th Thematic Conference on Geological Remote sensing, Pasadena, California, USA*. 8-11th February pp821-830.

Murray, J. W. (1975). The interaction of metal ions at the manganese dioxide-solution interface. *Geochim. Cosmochim. Acta* 39 pp505-520.

Nahon, D., and Tardy, Y. (1992). The ferruginous laterites. In *Handbook of Exploration Geochemistry*. Govett, G.J.S. (Ed) Vol.4, Regolith Exploration Geochemistry in Tropical and Subtropical Terrains. (Eds) Butt, C.R.M. & Zeegers, H. Elsevier, pp41-55.

O'Connor, E. A. (1993). Mapping metamorphism with Landsat TM in the Arabian Shield, Eastern Egypt. *Proceedings of the 9th Thematic Conference on Geological Remote sensing, Pasadena, California, USA*. 8-11th February p687.

O'Donoghue, M. (1994). *The colour dictionary of gemstones & minerals*. Black Cat imprint, Little Brown and Company, 159 pp.

Oberthür, T., Vetter, U., Schwartz, M. O., Weiser, T. H., Amanor, J., Gyapong, W. (1991). Gold mineralization at the Ashanti mine, Obuasi, Ghana: Preliminary mineralogical and geochemical data. In *Brazil Gold'91. The Economics Geology Geochemistry and Genesis of Gold Deposits*. Ladeira, E.A.(Ed). Balkema: Rotterdam, pp533-537.

Olson, S. F., Diakite, A., Guindo, A., Ford, C. R. B., Winer, N., Hanssen, E., Lay, N., and Bradley, R. (1991). Geology of the Syama gold mine, Mali, West Africa. In *Brazil Gold'91. The Economics Geology Geochemistry and Genesis of Gold Deposits*. Ladeira, E.A.(Ed). Balkema: Rotterdam, pp593-599

Olson, S. F., Kassoum, D., Lawrence, O., Guindo, A., Ford, C. R. B., Winer, N., Hanssen, E., Lay, N., Bradley, R., and Pohl, D. (1992). Regional setting, structure, and descriptive geology of the Middle Proterozoic Syama gold deposit, Mali, West Africa. *Economic Geology*, Vol.87, pp310-331.

Ong, H. L., and Swanson, V. E. (1969). Natural organic acids in the transportation, deposition and concentration of gold. *Quart. Colorado School Mines*, 64 pp395-425.

Openshaw, S. (1989). Learning to live with errors in spatial databases pp263-276. In *Accuracy of spatial databases*. Goodchild, M and Gopal, S (Eds). Taylor & Francis 290p.

Parfitt, R. L. (1980). Chemical properties of variable charged soils. In *Soils of Variable Charge*, Theng, B K G.(Ed). New Zealand Society of Soil Science, pp167-194.

Park, S. K., and Schowengerdt, R. A. (1983). Image reconstruction by parametric cubic convolution. *Computer Vision Graphics and Image Processing*, 23 pp258-272.

Parks, G. A. (1967). Aqueous surface chemistry of oxides and complex oxide minerals. In *Equilibrium Concepts in Natural Waters*, Gould, R F (Ed). *Advances in Chemistry*, 67 pp121-159.

Parks, G. A., and De Bruyn, P. J. (1962). The zero point charge of oxides. *Journal Phys. Chemistry*, 66 pp967-973.

Pedro, G. (1966). Essai sur la caractérisation géochimique des différents processus zonaux résultant de l'altération superficielle. *C. R. Acad. Sci.*, Paris, 262D: 1828-1830.

Pedro, G. (1984). La genèse des argiles pédologiques, ses implications minéralogiques, physico-chimiques et hydriques. *Sci. Geology Bulletin*, 37 (4) pp333-347.

Peters, W. C. (1987). *Exploration and mining geology*. J. Wiley & Sons. Inc. 2nd Ed. 685p.

Petersen, E. U. (1990). Syama petrology and alteration. *BHP inter. Report* 10p.

Podwysocki, M. H., Segal, D. B., and Abrams, M. J. (1983). The use of multispectral scanner images for assessment of hydrothermal alteration in the Marysvale, Utah, mining area. *Economic Geology*, 78 675.

Pohl, D., Olson, S., Guindo, A., Hanssen, K., Grant, J. A., and Krogh, T. E. (1991). Distribution and timing of Au mineralization in the 2.0-2.2 Ga. Birimian supergroup of Southern Mali, West Africa. (abs.): *Geol. Assoc. Canada-Mineralogical Assoc. Canada, joint annual, meeting with Society Economic Geologists. Program with abstracts*, May 27-29, 1991, Toronto, Canada, V16 pA100.

Prescott, J. A., and Pendleton, R. L. (1952). Laterite and lateritic soils. *Commonwealth Bur. Soil Sci.*, Technical communications. No.47.

Raghavan, V., Masumoto, S., Koike, K., and Nagano, S. (1995). Automatic lineament extraction from digital images using a segment tracing and rotation transformation approach. *Computers & Geosciences*, Vol.21, No.4, pp555-591.

Reed, L. E. (1987). Geophysics in gold exploration-some examples. pp 473-485. *Proceedings of Exploration' 87. Third decennial international conference on geophysical and geochemical exploration for minerals and groundwater*, Garland, D.G (Ed). Ontario Geological Survey, special vol. 3, 914p.

Reeves, C. V. (1987). Geophysical mapping of Precambrian granite-greenstone terranes as an aid to exploration. pp 254-266. *Proceedings of Exploration' 87. Third decennial international conference on geophysical and geochemical exploration for minerals and groundwater*, Garland, D.G (Ed). . Ontario Geological Survey, special vol. 3, 914p.

Rhind, D., and Clark, P. (1988). Cartographic data inputs to global databases pp79-104. In *Building databases for global science*. Mounsey, H (Ed), Tomlinson, R (General Ed.). Taylor & Francis p419.

Ringwood, A. E. (1974). The petrological evolution of island arc systems. *Journal of Geological Society*, London, 130 pp183-204.

Robertson, I. D. M. (1996). Ferruginous lag geochemistry on the Yilgarn Craton of Western Australia; Practical aspects and limitations. *Journal of Geochemical Exploration*, 57 pp139-151.

Roquin, C., Dandjinou, T., Freyssinet, P. H., & Pion, J. C. (1989). The correlation between geochemical data and SPOT satellite imagery of lateritic terrain in southern Mali. *Journal of Geochemical Exploration*, 32 pp149-168.

Roquin, C., Freyssinet P.H., Zeegers, H., & Tardy, Y. (1990). Element distribution patterns in laterites of southern Mali: consequence for

geochemical prospecting and mineral exploration. *Applied Geochemistry*, Vol.5, No.3, pp303-315.

Rose, A. W., and Wright, R. J. (1980). Geochemical exploration models for sedimentary uranium deposits. *Journal of Geochemical Exploration* 13, pp153-179.

Rose, A. W., Hawkes, H. E., and Webb, J. S. (1990). *Geochemistry in Mineral Exploration*. 2nd edition, Academic Press Inc., 657p.

Rothery, D. A. (1987). Improved discrimination of rock units using Landsat Thematic Mapper imagery of the Oman ophiolite. *Journal of the Geological Society, London*. Vol. 144, pp587-597.

Roy, D. P., and Dikshit, O. (1994). Investigation of image resampling effects upon the textural information content of a high spatial resolution remotely sensed image. *Inter. Journal Remote Sensing*, Vol.15, No.5 pp1123-1130.

Ruffini, A. (1997). Gold targets overshadow Mali's geological diversity. *The Northern Miner, Africa*. February 3rd 1997, pB7

Russell, I. C. (1889). Sub-aerial decay of rocks and origin of red colour in certain formations. *US. Geological Society Bulletin* No.52.

Séa, F., Tanguay, M. G., Trudel, P., and Perrault, G. (1990). Résultats préliminaires d'une étude sur la dispersion de l'or en milieu latéritique autour de l'indice aurifère de Misséni, au Mali. *Canadian Journal of Earth Science*, 27 pp1686-1698.

Shaw, D. M. (1961). Element distribution laws in geochemistry. *Geochim. Cosmochim. Acta*, 23 pp116-134.

Siegel, F. R., Roach, N. M., Yang, W., and Viterito, A. (1993). Stream suspensates for Au and base metal exploration, in metavolcanic felsic rocks, eastern Piedmont, Georgia, USA. *Journal of Exploration Geochemistry*, 47, n.1-3, pp235-249.

Simpson, E. S. (1912). Notes on laterite in Western Australia. *Geol.Mag.*, 49, pp399-406.

Sinclair A. J. (1983). Univariate analysis. In *Handbook of Exploration Geochemistry*. Govett, G.J.S.(Ed) Vol.2, Statistics & Data Analysis in Geochemical Prospecting. (Eds) Howarth, R.J. Elsevier, pp59-81.

Sinclair, A. J. (1974). Selection of threshold values in geochemical data using probability graphs. *Journal of Geochemical Exploration*, 3 pp129-149.

Smith, R. E. and Hunt, R. J. (1985). Solubilisation of gold by *Chromobacterium violaceum*. *Journal of Chem. Technol. Biotechnol.*, 35B: pp 110-116.

Smith, R. E. (1996). Regolith research in support of mineral exploration in Australia. *Journal of Geochemical Exploration*, 57 pp159-173.

Stanley, C. R., and Sinclair, A. J. (1987). Anomaly recognition for multi-element geochemical data – A background characterisation approach. *Journal of Geochemical Exploration*, 29 pp333-353.

Stoop, W. A. (1980). Ion adsorption mechanisms in oxidic soils; replication for zero point charge determinations. *Geoderma*, 23 pp303-314.

Tanaka, S. M., and Segal, D. B. (1990). Integrated remote sensing/vector-based GIS technology for Gold exploration, Round Mountain District, Nevada, USA. *Proceedings of the 23rd International Symposium on Remote Sensing of Environment. Bangkok, Thailand, 18-25th April* pp747-753.

Tanré, D., Deroo, C., Duhaut, P., Herman, M., Morcrette, J. J., Perbos, J., and Deschamps, P. Y. (1986). *Simulation of the satellite signal in the solar spectrum ("5s")*. Laboratoire d'Optique Atmosphérique, Université des Sciences et Techniques de Lille, 59655, Villeneuve D'Ascq Cedex, France/Centre Spatiale de Toulouse, 31055 Toulouse Cedex France.

Tardy, Y., Melfi, A. J., & Valetton, I. (1988). Climats et paléoclimats tropicaux périatlantiques. Rôle des facteurs climatiques et thermodynamiques: température et activité de l'eau, sur la répartition et la composition minéralogique des bauxites et des cuirasses ferrugineuses au Brésil et en Afrique. *C.R. Acad. Sci.*, Paris , 306 pp289-295.

Teillet, P. M., and Fedosejevs, G. (1995). On the dark target approach to atmospheric correction of Remotely sensed data. *Canadian Journal of Remote Sensing*, Vol.21, No.4 pp374-386.

The Times (1994). *Times World map and database. ON CD-Rom.*

Thomas, A., Crow, B., Frenz, P., Hewitt, T., Kassam, S., and Treagust, S. (1994). *Third World Atlas*. Open University Press: Buckingham, 2nd edition 80p.

Thomas, M. F. (1974). *Tropical Geomorphology - A study of weathering and landform developments in warm climates*. MacMillan: London, 332pp.

Thomas, P. (1997). *Iamgold*. Stockbroker publication, Griffiths McBurney & Partners. March 14th 1997, pp1-15.

Thornber, M. R. (1992). The chemical mobility and transport of elements in the weathering environment. In *Handbook of Exploration Geochemistry*. Govett, G.J.S.(Ed). Vol.4, Regolith Exploration Geochemistry in Tropical and Subtropical Terrains. (Eds) Butt, C.R.M. & Zeegers, H. Elsevier, pp79-96.

Thornber, M. R., and Taylor, G. F. (1992). The mechanisms of sulphide oxidation and gossan formation. In *Handbook of Exploration Geochemistry*. Govett, G.J.S.(Ed). Vol.4, Regolith Exploration Geochemistry in Tropical and Subtropical Terrains. (Eds) Butt, C.R.M. & Zeegers, H. Elsevier, pp119-138.

Tilling, R. I., and Gottfried, D. (1969). Distribution of thorium, uranium and potassium in igneous rocks of the Boulder Batholith Region, Montana, and its bearings on radiogenic heat production and heat flow. *USGS. Paper 614-E*, 29pp.

Timofeyev, B. V. (1989). Formation and physical state of leached ferrallitic savanna soils of Mali. (*Trans.*) *Pochvovedeniye*, No.3:5-14, pp8-17.

Tobler, W. R. (1988). Resolution, resampling, and all that, pp129-137. In *Building databases for global science* Mounsey, H (Ed), Tomlinson, R (General Ed.). Taylor & Francis p419.

Trendall, A. F. (1962). The formation of apparent peneplains by a process of combined lateritisation and surface wash. *Z. Geomorphic. (NS)*, 6, (2), pp183-197.

Trescases, J. J. (1992). Chemical Weathering. In *Handbook of Exploration Geochemistry*. Govett, G.J.S.(Ed). Vol.4, Regolith Exploration Geochemistry in Tropical and Subtropical Terrains. (Eds) Butt, C.R.M. & Zeegers, H. Elsevier, pp25-40.

Tsai, V. J. D. (1993). Delaunay triangulations in TIN creation: an overview and a linear-time algorithm. *Inter. Journal of Geographical Information Systems*, Vol. 7, No.6 pp501-524.

Veregin, H. (1989). Error modeling for the map overlay operation pp3-18. In *Accuracy of spatial databases* Goodchild, M and Gopal, S (Eds)..Talyor & Francis. pp290.

Vickers, G. (1965). *The art of judgement*. Chapman and Hall: London pp228.

Webster, J. G. (1984). Thioisulphate complexing of gold and silver during the oxidation of a sulphide-bearing carbonate lode system, Upper Ridges Mine, P.N.G. *The Australian I.M.M Perth and Kalgoorlie branches, regional conference on "Gold-Mining, Metallurgy and Geology", October 1984*, pp437-445.

Webster, J. G. (1986). The solubility of gold and silver in the system Au-Ag-S-O₂-H₂O at 25°C and 1 atm. *Geochimica et Cosmochimica Acta*. Vol.50, pp1837-1845.

Webster, J. G., and Mann, A. W. (1984). The influence of climate, geomorphology and primary geology on the supergene migration of gold and silver. *Journal of Geochemical Exploration*, 22 pp21-42.

West, D., and Witherly, K. (1995). Geophysical exploration for gold in deeply weathered terrains; two tropical cases. *Exploration Geophysics*, 26 pp124-130.

Whitelaw, O. A. L. (1929). Geological and mining features of the Tarkwa-Aboso goldfield, Gold Coast *Geological survey, Mem. No.1*.

Whitfield, J. N., Rogers, J. J. W., and Adams, J. A. S. (1959). The relationship between the petrology and the thorium and uranium contents of some granitic rocks. *Geochim. Cosmochim. Acta*. 17, pp248-271.

Whitten, D. G. A., and Brooks, J. R. V. (1983). *The Penguin Dictionary of Geology*. Penguin Books, 520p.

Whyte, J. (1997). Sadiola Hill mine makes golden progress. *The Northern Miner*, Vol.83, No.14 June 2nd.

Wilson, A. (1981). The economic significance of non-hydrothermal transport of gold, and of the accretion of large gold nuggets in lateritic and other weathering profiles in Australia. *International conference for Applied Mineralogy, Johannesburg S. Africa, 1981*, pp1-15.

Wright, B. J., Hasting, D. A., Jones, W. B., and Williams, H. R. (1985). *Geology and mineral resources of West Africa*. Allen and Unwin: London. 187p.

WWW. (1997a). World Wide Web access point;
<http://www.yahoo.com/Regional/Countries/Mali/>

WWW. (1997b). World Wide Web access point;
http://www.sas.upenn.edu/Africa_Studies/Country-Specific/Mali.html

WWW. (1997c). World Wide Web access point;
<http://www.odci.gov/cia/publications/nsolo/factbook/ml.htm>

WWW. (1997d). World Wide Web access point;
<http://www.interknowledge.com/mali/index.html>

WWW. (1997e). World Wide Web access point;
<http://www.goldsheet.simplenet.com/geo4.htm#Mali>

WWW. (1997f). Company World Wide Web access point Alpine Exploration Corp.; <http://www.stockgroup.com/axc.html>

WWW. (1997g). Company World Wide Web access point Ste-Genevieve Group (EAG); <http://www.eagold.com> or <http://www.sgv.com>

WWW. (1997h). Company World Wide Web access point Leo Shield Exploration NL; <http://www.leoshield.com.au/>

WWW. (1997i). Company World Wide Web access point Oxford Resources Inc.; <http://www.oxford.qc.ac> or <http://www.oasis.ca/explocto/112.htm>

WWW. (1997j). Company World Wide Web access point Mink International Resources Corp.; <http://www.mink.com/>

WWW. (1997k). Company World Wide Web access point lamgold Corp.; <http://www.lamgold.com/index.html>

WWW. (1997L). Company World Wide Web access point Pacific Galleon Mining Corp.; <http://www.pacificgalleon.com/>

WWW. (1997m). Company World Wide Web access point Randgold Resources; <http://www.btimes.co.za/96/1103/comp/comp6.htm>

WWW. (1997n). Company World Wide Web access point BHP; http://www.yahoo.com/business_and_economy/companies/mining_and_mine ral_exploration/Brocken_Hill_Proprietary_Company_Limited/

WWW. (1997o). Company World Wide Web access point Ashanti Goldfields Corp.; <http://www.mbendi.co.za/cymky.htm>

WWW. (1997p). Company World Wide Web access point JCI Ltd.; <http://www.jci.co.za/> or <http://www.mbendi.co.za/cymky.htm>

WWW. (1997q). Company World Wide Web access point Ashton Mining Ltd.; <http://www.ashton.net.au/index.html>

Zeegers, H. (1987). Remaniements de surface et prospection géochimique de l'or. *Chron. Rech. Min.*, 488, pp55-61.

Zeegers, H., and Butt, C. R. M. (1992). Summary and procedural recommendations. In *Handbook of Exploration Geochemistry*. Govett, G.J.S.(Ed). Vol.4, Regolith Exploration Geochemistry in Tropical and Subtropical Terrains. (Eds) Butt, C.R.M. & Zeegers, H. Elsevier, pp499-512.

Zeegers, H., and Lecomte, P. (1992). Seasonally humid and tropical terrains (savannas). In *Handbook of Exploration Geochemistry*. Govett, G.J.S.(Ed). Vol.4, Regolith Exploration Geochemistry in Tropical and Subtropical Terrains. (Eds) Butt, C.R.M. & Zeegers, H. Elsevier, pp203-240.

APPENDIX

CD-ROM index of headings

contents

Geochemistry

Descriptive statistics (Au, Cu, Zn, Pb, Ni, Mo, Li Cr)
Descriptive statistics-log (Au, Cu, Zn, Pb, Ni, Mo, Li Cr)
Scatterplots (Au, Cu, Zn, Pb, Ni, Mo, Li Cr)
Scatterplots-log (Au, Cu, Zn, Pb, Ni, Mo, Li Cr)
R-Mode cluster analysis

Radiometric

FORTRAN import program

Remote-sensing

Lineament program